Logical Control over Biomaterial Properties through Boolean Responsive Linkers

Barry Alick Badeau

A dissertation

submitted in partial fulfillment of the

requirements for the degree of

Doctor of Philosophy

University of Washington

2019

Reading Committee:

Cole DeForest, Chair

Elizabeth Nance

Buddy Ratner

Program Authorized to Offer Degree:

Chemical Engineering

University of Washington

Abstract

Logical Control over Biomaterial Properties through Boolean Responsive Linkers

Barry Alick Badeau

Chair of the Supervisory Committee:
Assistant Professor Cole DeForest
Department of Chemical Engineering

Medicine is fundamentally constrained by our ability to manipulate the levers and gears of biology—cells, genes, and proteins. Typical approaches, including systemic therapeutic administration and surgery, lack the precision required to effectively treat certain diseases. Biomaterials that dynamically sense and respond to critical aspects of their environment could enable new possibilities in targeted drug delivery, diagnostics, cell culture and regenerative medicine. However, there is not yet a framework for creating materials responsive to multiple inputs in a well-defined manner. This dissertation details the development of a modular biomaterial platform that can integrate multiple biochemical inputs to provide a functional output through Boolean computation. The connectivity and architecture of multiple stimuli-labile groups incorporated into a single linker determines its behavior upon the environmentally triggered cleavage of combinations of these moieties. To validate this framework, we employed light, reductant, and enzyme as inputs to create seventeen unique logically degradable hydrogels. The Boolean linkers were then used to govern the release of pendant proteins, small molecules, and therapeutics from non-degradable hydrogels. Finally, we exploited this system to enable logic-triggered activation of cell-penetrating peptides to regulate the cellular uptake of proteins.

This modular platform offers unprecedented control over biomaterial performance in complex biological environments. By enabling the creation of materials tailored to application-specific needs, it could unlock new possibilities in science and medicine.

TABLE OF CONTENTS

LIST OF FIGURES

ACKNOWLEDGEMENTS

First and foremost, I am indebted to all scientists past and present. Science is a collective project, thousands of people's dedicated work laid the foundation of this research. I am constantly inspired by the brilliance and determination that has led to our understanding of the world and the efforts to make it a better place.

Thank you Cole DeForest for all of your enthusiasm, mentorship, and knowledge that you provided over the past 5.5 years. I appreciate that you took a chance on me when starting up the lab, it was a great experience to be a part of. Thank you for all of the time you put into helping me to develop and grow as a researcher.

Thank you to my labmates and collaborators. I am so grateful to have worked with and learned from such an amazing group of people. You have been an incredible source of both scientific support and friendship over the years. Thank you for all of the support and for making day-to-day work exciting, even through the tedious times.

Thank you to all of my ChemE peers and colleagues. I am so fortunate to have joined this wonderful community filled with enthusiasm, passion, and curiosity. You have been a huge source of inspiration and have helped balance and ground me throughout the ups and downs of grad school.

Thank you to all my friends, roommates, and teammates for making Seattle a special place and a wonderful experience. I am especially grateful to all of you with shared non-academic interests for getting me out of lab.

DEDICATION

To Mom, Dad, Sydney, and Gage:

Your constant love, support, and encouragement made this possible

CHAPTER 1: INTRODUCTION AND BACKGROUND

Adapted from: Programming Stimuli-Responsive Behavior into Biomaterials
Annual Review of Biomedical Engineering, **21**, 241-265 (2019)[1]

1.1 Abstract

Stimuli-responsive materials undergo triggered changes when presented with specific environmental cues. These dynamic systems can leverage biological signals found locally within the body as well as exogenous cues administered with spatiotemporal control, providing powerful opportunities in next-generation diagnostics and personalized medicine. Here, we review the synthetic and strategic advances used to impart diverse responsiveness to a wide variety of biomaterials. Categorizing systems on the basis of material type, number of inputs, and response mechanism, we examine past and ongoing efforts toward endowing biomaterials with customizable sensitivity. We draw an analogy to computer science, whereby a stimuli-responsive biomaterial transduces a set of inputs into a functional output as governed by a user-specified logical operator. We discuss Boolean and non-Boolean operations, as well as the various chemical and physical modes of signal transduction. Finally, we examine current limitations and promising directions in the ongoing development of programmable stimuli-responsive biomaterials.

1.2 Introduction

The past several decades have seen substantial progress in our ability to understand, design, and synthesize materials that interact with living systems to guide biological processes in a predictable and controlled manner. Through advances in synthetic chemistry, monomer availability, and enhanced processing techniques, the biomaterials community has evolved beyond its initial reliance on commercial precursors to develop novel systems exhibiting application-

specific properties. This transition has permitted a shift from static to dynamic materials that respond on demand to specific inputs, forming the basis of the stimuli-responsive biomaterials field[2–5]. Such stimuli sensitivity can be encoded into various types of materials, including physically assembled nanoparticles, supramolecular hydrogels, and covalent polymer networks.

Synthetic flexibility has yielded dynamic biomaterials that respond to a diverse set of stimuli[6]. These constructs can be characterized by their environmental triggers and the sources from which they are presented. Bioresponsive systems react to intrinsic cues provided by the physiological environment, whereas externally responsive systems react to extrinsically administered cues (**Figure 1.1a**). Bioresponsive systems are most commonly triggered by enzymes, pH, redox conditions, or hydrolysis. Materials that autonomously respond to cues characteristic of specific tissues or diseases (e.g., acidic conditions in the stomach, reductive environment of tumors) can enrich bioresponsive behavior at bodily locations that are encoded into the material design. Alternatively, materials that respond to light, ultrasound, temperature, or magnetic fields, stimuli typically absent from living systems, can be remotely triggered in 4D with spatial and temporal control.

Although stimuli-responsive biomaterials have found utility in bio-sensing, 3D cell culture, tissue regeneration, and other biomedical applications, their primary niche remains in targeted drug delivery[7]. So-called smart carrier vehicles that are designed to degrade, swell, or dissociate from a therapeutic in response to a given stimulus can be used to confine drug release to specific cells, tissues, or organs within the body. Such site-specific therapeutic delivery can reduce or eliminate adverse effects arising from off-target distribution, enhancing the efficacy of conventional drugs

(e.g., chemotherapies) while potentially rescuing the use of otherwise-flawed compounds with systemic toxicity, poor solubility, or untenable pharmacokinetics. Building on the early success of materials responsive to a single stimulus for enriching local delivery, recent efforts have focused on the development of materials that can respond to more than one cue[8–10]. Compared with singly responsive systems, those that respond to either of two inputs are sensitive to a broader set of environments, while those that require two inputs to invoke a response can further increase delivery specificity.

As the field moves towards materials that are sensitive to different input combinations, we have elected to describe the manner in which multiple inputs are transduced into a functional output by using the Boolean logical operators of computer science (**Figure 1.1b**). When a single input induces a material response, this is denoted as a YES gate; when either of two inputs elicits a complete material response, this is denoted as an OR gate; when two different inputs are both required to invoke a material response, this represents an AND gate[11]. To depict stimuli-responsive modalities that are not fully Boolean, we also introduce the concepts of sequential and cumulative response. A sequential response requires order-specific presentation of inputs to elicit a functional change. A cumulative response exhibits differential responses to each relevant cue, where complete response is triggered by the combination of both relevant cues. We find that describing stimuli-responsiveness through these programmable operations serves as a useful framework to highlight the current and future efforts of our community.

The chapter seeks to summarize our understanding of stimuli-responsive materials in a systematic and structured framework. First, we discuss biomedically relevant chemical and

physical signals used as material triggers along with the corresponding chemistries and the processes by which they actuate material properties. Second, we describe the mechanisms and strategies that combine different functionalities into multi-responsive systems, organized by the class of material and mode of response. Third, we summarize the available tool kit, highlighting the most successful strategies and providing design considerations for tailoring biomaterial response. Finally, we critically examine the successes and shortcomings of current efforts and speculate on future opportunities for programming stimuli sensitivity into synthetic biomaterials.

1.3 Single-input-responsive biomaterials

The simplest dynamic biomaterials are engineered to undergo response to a single cue, which can be biologically presented or externally administered. When such a material exhibits a binary response, it acts as a YES gate. Other systems may exhibit a proportional response wherein the magnitude of the input determines the magnitude of the output state. In this section, we describe these diverse input classes and the chemistries most commonly employed to translate response (**Figure 1.2**).

1.3.1 *Bioresponsive material inputs*

Systems that exploit chemical signals presented heterogeneously by biology can be exploited to control where material response occurs in a biologically dictated manner. Here, we discuss material both the strategies and the specific chemistries utilized to make materials sensitive to water, pH, enzymes, redox condition, small molecules, and shear forces.

Hydrolysis

Polymers that undergo hydrolysis, or water-induced degradation, are some of the most fundamental and well-studied classes of stimuli-responsive materials. As water constitutes 70-80%

of most tissues, hydrolytic materials in biological environments spontaneously exhibit dynamic behavior. A key limitation of hydrolytically degradable biomaterials is that the presence of water in nearly all tissues precludes usage for site-specific delivery. Hydrolysable materials provide a useful platform for applications ranging from bioresorbable medical implants and cell scaffolds to temporal control over therapeutic delivery.

Hydrolytically sensitive materials contain functional groups that covalently cleave upon reaction with water. Esters are the most commonly utilized moiety, cleaving to form an acid and an alcohol. Other well-explored water-labile groups include carbonates and ureas.

The ester-rich poly(lactic-*co*-glycolic acid) (PLGA) is one of the best-characterized stimuli-responsive materials and is both biocompatible and approved by the US Food and Drug Administration for use in a variety of medical applications. Key characteristics of PLGA, including its degradation rate and mechanical properties, may be tuned by varying its co-polymer ratio, stereochemistry, molecular weight, and morphology[12–14]. As the polymer degradation rate dictates the release of its encapsulated payload, the ability to tune PLGA degradation time from a few weeks to several months enables user-defined control over the rate of therapeutic release or implant degradation[14,15].

The ester-containing poly(ε-caprolactone) (PCL) is another popular hydrolytic polymer used in biomaterials. Owing to its increased hydrophobicity relative to PLGA, PCL exhibits an extended in vivo degradation time, persisting as long as several years. PCL is more elastic and

pliable than PLGA, but is also mechanically weaker. Despite these limitations, PCL is often utilized as the basis for tissue engineering both hard and soft tissues[16].

Hydrolytically degradable systems have additional factors that must be considered when designing translational materials. The release rate of the encapsulated payloads is governed by the simultaneous processes of material degradation and molecular diffusion. Furthermore, degradation can take place homogeneously throughout the material (i.e., bulk degradation) or from the surface inward; the latter mechanism dominates in hydrophobic materials through which water poorly penetrates. Practically, both surface and bulk erosion occur simultaneously but in varying proportions[13,17].

pH

Physiological environments contain significant heterogeneities in local pH values. Compared with normal extracellular environments, which have a pH of 7.4, endosomes and lysosomes have an acidic environment, with a pH of 5-6.5. Similarly, the extracellular tumor microenvironment is more acidic than healthy tissue (pH = 6.5-7.2), a property also associated with inflammation and chronic wounds[18]. As such, pH-responsive therapeutic carriers have been employed to achieve tumor- or intracellular-specific delivery[19].

pH-responsive behavior can be imparted to materials through the incorporation of acid-labile bonds within the carrier (e.g., hydrazones, imines, acetals, ketals). Triggering bond cleavage can induce carrier breakdown or degradation. This is demonstrated in a microgel platform in which three benzacetal linkers, each with different acid sensitivities, can be used to tune the degradation kinetics of cell-loaded microgels over the pH range of 4.5-7.4[20]. Alternatively, acid-labile bonds

can link a therapeutic with a carrier to enable targeted release[21]. Finally, pH-cleavable linkers can anchor a protective stealth layer on the surface of a nanoparticle that, upon exposure to acid, is shed to enable drug-carrier uptake[22].

pH-responsive materials may also undergo a dynamic response to their environment through a protonation/deprotonation mechanism. The charge state of ionizable functional groups (e.g., carboxylic acids, amines) incorporated within the material can be altered upon exposure to relevant acidic or basic environments. Materials may be tuned by matching the functional group's pK_a to the pH of the targeted microenvironment. pH-induced charge alteration can yield either swelling or breakdown of the carrier. For example, a poly(methacrylic acid-graft-ethylene glycol) (PMAA-*g*-PEG) hydrogel formulated for oral insulin delivery remained protonated and collapsed in the stomach, protecting its payload; upon reaching the intestines, the neutral pH induced deprotonation of the carboxylic acids, triggering material swelling and subsequently insulin delivery[23]. Changes in pH may also be used to alter polymer charge so as to disrupt electrostatic carrier-drug binding, for example, between cationic doxorubicin (DOX) and a pH-dependent anionic polymeric nanoparticle[24]. Another novel application exploiting pH-triggered ionization was the development of pH (low) insertion peptide (pHLIP) technologies. These cell-penetrating peptides become activated in acidic environments to facilitate cellular internalization of cargo[25].

Enzymes

Similar to pH, enzymes are heterogeneously distributed within a biological environment. Owing to their specificity in both location and function, enzymes have been used as triggers in targeted drug delivery and tissue engineering platforms. Otherwise stable functional groups may be incorporated into biomaterials, where enzymatic degradation induces bond cleavage. Common

enzymatic classes exploited in stimuli-responsive biomaterials are proteases, lipidases, and oxidoreductases[26,27], which respectively cleave proteins, lipids, and catalyze electron transfer.

The most common class of enzyme used to trigger biomaterial responses are proteases, in particular matrix metalloproteases (MMPs)[28]. MMPs, a family of proteases that degrade the extracellular matrix (ECM), are associated with a host of diseases, including tumor metastasis and invasion. MMPs recognize specific amino acid sequences and cleave an amide bond of the oligopeptide substrate. Nagase & Fields[29] examined the kinetics of many MMPs on a wide variety of peptide sequences, providing a blueprint for tuning biomaterial kinetic response by choosing the substrate sequence. MMP-labile oligopeptides have been incorporated within hydrogels to create bioactive synthetic materials that permit cell-mediated ECM remodeling for tissue engineering applications[30], as well as to deliver a therapeutic MMP-inhibitor to tumors[31]. In another approach, MMP-labile peptides enabled enzyme-triggered cell-penetrating peptide activation of nanocarriers for tumor-targeted MRI contrast agents[32].

Beyond MMPs, many other proteases have served as inputs for stimuli-responsive biomaterials, including cathepsins, phospholipidases, thrombin, and azoreductase. Another mechanism by which enzymes can induce stimuli-responsive behavior is by linking a therapeutic to a material via a stimuli-labile bond. In one demonstration, heparin bound to a PEG hydrogel through a thrombin-labile peptide was cleaved in response to thrombin; the released heparin subsequentially inactivated thrombin to induce an autoregulated anti-coagulation cascade[33]. In another system, azobenzene was incorporated between hydrophilic and hydrophobic blocks of an

amphiphilic polymer. This polymer spontaneously formed micelles that enzymatically degraded upon exposure to azoreductase found in the colon[34].

Redox conditions

Differences in redox potential characterize several important microenvironmental targets for drug delivery. Glutathione (GSH) and its corresponding oxidized species, glutathione disulfide, represent the most common redox pair in biology. The concentration of GSH in intracellular environments (0.5-10 mM) is approximately 1,000-fold greater than in extracellular environments (2-20 μM)[35]. Similarly, the GSH concentration in mouse tumors is at least four-times higher than in healthy tissues[36]. The high levels of reactive oxygen species (ROS) in sites of inflammation and tissue injury[37] indicate that they may be targets for delivery from oxidation-responsive materials.

The disulfide bond, ubiquitous in biology, is also the redox-sensitive chemical functionality most commonly exploited by biomaterials. Disulfide bonds cleave in the presence of reducing conditions to yield two free thiols. As with other stimuli-labile linkers, disulfide bonds may be incorporated into materials in several ways to improve tumor-specific delivery or aid endosomal escape for intracellular delivery. Disulfide bonds have been used to achieve redox-mediated carrier breakdown and drug release through incorporation into hydrogel crosslinkers[38] and between the two regions of an amphiphilic block-copolymer micelle[39]. Drugs have also been linked to dendrimers through a disulfide bond to achieve intracellular release[40]. Reduction of hydrophobic 2-nitroimidazoles to hydrophilic 2-aminoimidazoles has also been exploited to increase the rate of DOX release[41].

Oxidative-labile linkers, including thioketals, thioethers, arylborinic esters, and aryloxylates, can be triggered by ROS such as hydrogen peroxide, superoxide, or hydroxyl radicals. For example, oral delivery of a therapeutic targeted sites of intestinal inflammation by complexation with polymeric nanoparticles containing thioketals. In a mouse model, the oral formulation of small interfering RNA (siRNA) was able to reach the inflamed colon tissue to protect against ulcerative colitis[42]. In another system, amphiphilic block copolymers between the hydrophilic PEG and hydrophobic poly(propylene sulfide) (PPS) formed polymersome vesicles. Upon exposure to H_2O_2, the sulfides of PPS domain oxidized into sulfoxides, converting the PPS domain from hydrophobic to hydrophilic to disrupt the carrier and release its cargo[43].

Small molecules

Significant advances have been made in creating bioresponsive materials sensitive to many small molecules, including glucose, adenosine triphosphate (ATP), and nucleic acids.

Glucose

Diabetes is characterized by the inability of the body to properly regulate its blood glucose levels. Managing diabetes is a burdensome and cyclic process involving the self-monitoring of glucose levels and intravenous injections of exogenous insulin. To ease this process and improve patient compliance, glucose-responsive biomaterials have been engineered to both auto-regulate insulin release and enable oral delivery.

A glucose-responsive hydrogel was engineered to be crosslinked through dynamic covalent bonding between phenyl-boronic acid (PBA) and poly(vinyl alchohol) (PVA). Glucose has affinity for PBA; its presence interrupts the hydrogel network, triggering the release of encapsulated

proteins[44]. An alternative methodology for enabling glucose-responsive delivery employed the enzyme glucose oxidase (GOx), which catalyzes the conversion of glucose to gluconic acid. Here, both insulin and GOx-loaded nanocapsules were loaded into chitosan microgels that swell in an acidic environment. These particles convert glucose to gluconic acid, lowering the local pH to enable gel swelling and insulin delivery in a glucose concentration-dependent manner[45].

ATP

ATP is a ubiquitous biomolecule that facilitates the energy transfer necessary to carry out cellular functions. Intracellular ATP concentration (1-10 mM) is approximately 1,000-fold greater than in the extracellular environment (<5 μM)[46], making ATP an attractive candidate for intracellular-targeted drug delivery.

ATP has been used as a competitive binding partner to trigger material response. In one case, DOX was loaded into an ATP-binding DNA aptamer; ATP–aptamer binding induced a DNA conformational change, selectively releasing DOX[47]. In another system, PBA–siRNA complexes have been engineered such that ATP binds to the PBA, triggering intracellular siRNA delivery[48]. Other ATP-responsive materials have repurposed ATP's native biological function to drive reactions within a dynamic material. In one system, ATP hydrolysis provides the energy needed to induce a conformational change in protein-based tubular nanocarriers, resulting in therapeutic payload release[49].

Nucleic acids

Nucleic acids (i.e., RNA, DNA) remain relatively underexplored as triggers for stimuli-responsive biomaterials. Given their highly specific binding mechanism, nucleic acids may

provide a route to targeted delivery. In one system, a gold nanoparticle assembly was linked together with single-stranded DNA (ssDNA). Hybridization with complementary ssDNA chains altered nanoparticle configuration. These changes in the nanoparticle cluster structure hide or expose folic acid moieties to influence cell-particle interactions[50]. A mesoporous silica nanoparticle (MSNP) loaded with a DOX payload was engineered such that its pores were capped with a DNA hybrid complex responsive specifically to a microRNA that is upregulated in cancers. Exposure of the MSNP to the tumor environment, and subsequent binding of miR-21, removed the pore gatekeeper and triggered drug release[51].

Shear forces

Partially obstructed blood vessels and healthy capillaries are sites of high shear stresses that can be leveraged to enable targeted delivery. For example, micro-aggregates of nanoparticles were engineered to break up under pathophysiological shear forces. By coating the aggregates with a therapeutic, researchers were able to dissolve blood clots in an otherwise-fatal embolism mouse model[52]. Another mechanism for targeting obstructed blood vessels employs platelet-like nanoparticles with an enhanced ability to adhere under high shear stress to target damaged sites[53].

1.3.2 *Externally responsive biomaterial inputs*

Systems whose properties can be exogenously regulated enable user-defined 4D control of biomaterial response. Here, we describe synthetic approaches and the specific chemistries utilized to make materials sensitive to temperature, light, ultrasound, and magnetic fields.

Temperature

Thermoresponsive polymers are one of the oldest and most widely explored classes of stimuli-responsive materials[54]. As the temperature of a human body is relatively homogeneous,

thermoresponsive biomaterials can be selectively modulated when heated upon the application of an external field (e.g., light, magnetic field, ultrasound).

A unique aspect of these materials is their ability to undergo a phase transition at a distinct temperature—typically a lower critical solution temperature (LCST). Below their LCST, polymers are hydrophilic and water-soluble; above their LCST, polymers become hydrophobic and water insoluble, exhibiting gel-like behavior[55]. The critical solution temperature is determined by the polymer concentration and identity.

The first and most widely utilized thermoresponsive polymers is poly(N-isopropylacrylamide) (PNIPAM). The LCST of PNIPAM, 32 °C, is near physiological temperature and may be further tuned through the incorporation of a copolymer[56]. PNIPAM has been explored as an injectable hydrogel, owing to its liquid-like behavior at room temperature and rapid gelation in the body[57]. PNIPAM also exhibits temperature-dependent swelling, which has been exploited to culture cell sheets for tissue engineering, whereby cells can be lifted from PNIPAM surfaces following cooling of the system from 37 to 20 °C. This approach preserves cell-cell junctions that would be destroyed by proteolytic surface removal, enabling cell sheets to remain intact for tissue assembly[58].

PNIPAM has some limitations, including potential cytotoxicity of the residual monomer and phase-transition hysteresis. To circumvent these drawbacks, a vast number of other thermoresponsive polymers have been developed[55]. Some promising alternatives are elastin-like polypeptides (ELPs), biopolymers with a LCST that can be varied from at least 30°C to 80°C by

tuning the sequence and length[59]. The inherent biocompatibility of ELPs positions this as a useful platform for tissue engineering[60].

Light

Light, particularly near-infrared (IR) wavelengths, can penetrate human tissue to modulate subcutaneous biomaterials[61]. Photo-sensitive biomaterials often incorporate photoscissile moieties that covalently cleave upon exposure to specific wavelengths of light. *Ortho*-nitrobenzyl ester (*o*NB) is frequently used, owing to its ease of synthesis and susceptibility to cytocompatible near-ultraviolet (UV) light. In one example, vitronectin was attached to a human mesenchymal stem cell–laden PEG hydrogel via an *o*NB-containing linker[62]. Multiphoton lithography enabled precise control over vitronectin presentation, affording 4D control over cell fate. Coumarin represents another popular photolabile functional group, degrading under UV light as well as multiphoton activation in the near-IR region[63].

Photo-responsive materials have also been engineered by exploiting functional groups that undergo a conformational change in response to light. Azobenzene undergoes a reversible *trans*-to-*cis* conformational change under UV exposure, and a *cis*-to-*trans* reversion in the dark or in the presence of visible light, a phenomenon that has been leveraged to generate macroscopic material responses. For example, azobenzene-containing block copolymer-based vesicles have been engineered such that the photoisomerization of azobenzene disrupts the amphiphilic character of the drug carrier, triggering payload release[64]. Spiropyran (SP), a hydrophobic closed-ring functional group, converts to the hydrophilic open-ring merocyanine (MC) group upon exposure to UV light or the dark. MC reverts to its SP state upon exposure to visible light. SPs have been exploited to enable photoresponsive delivery of a payload from nanocapsules[65].

Ultrasound

Ultrasound is energy in the form of acoustic waves and may be controlled with high precision and tissue penetration. Focused ultrasound can induce hyperthermia and/or cavitation to locally disrupt nanocarriers with spatiotemporal control[66]. Ultrasound has been demonstrated to induce cavitation in DOX-loaded micelles and nanodroplets, thereby enhancing drug transport both into the cell and the nucleus[67]. Microbubbles ranging from 1 to 10 μm in diameter are composed of a gas core with a stabilizing shell (e.g., polymer, protein, lipid). Microbubbles are particularly attractive as ultrasound-sensitive materials, owing to their cavitation susceptibility. In one system, PLA-shell microbubbles loaded with DOX were used to treat a rat tumor model, with ultrasound focused on the cancerous tissue. The microbubbles underwent destructive cavitation at the tumor site, and the polymer shards enhanced DOX uptake[68].

Magnetic fields

Similar to ultrasound, magnetic fields are an attractive option for facilitating triggered drug release as they can be spatiotemporally presented to living organisms. Magnetically responsive materials may be engineered such that an applied magnetic field can guide carrier accumulation or induce disruption, leading to payload delivery. Nanoparticles consisting of a magnetic iron oxide core and a polymer shell can be manipulated by magnetic fields to guide their distribution and accumulation in vivo. The polymeric shell can be engineered to carry genes or drugs, enabling non-invasive magnetic targeting[69]. An alternating magnetic field (AMF) can be applied to induce heating in a magnetic nanoparticle, which in turn can trigger payload delivery. In one example,

MSNPs were capped with a lipid bilayer and loaded with iron oxide nanoparticles and a model therapeutic. The application of an AMF heated the particle, increasing the porosity of the lipid bilayer to permit payload delivery[70].

1.4 Two-input-responsive biomaterials

Although single-stimulus responsive biomaterials have been successfully created for many inputs and exploited for a variety of applications, investigators have devoted increasing efforts to developing systems that respond to more than one cue. The use of additional inputs enables the use of materials with a greater range of response types, as well as improved specificity. By simply incorporating different combinations of stimuli-responsive moieties within a single biomaterial, one can create a nearly limitless number of material systems can be created to undergo a wide variety of responses (i.e., swelling, degradation, cargo release) via several modalities (i.e., OR gate, AND gate, cumulative triggering, sequential triggering). Here, we categorize two-input platforms on the basis of their material type, focusing on nanoparticles that are physically assembled or based on mesoporous silica, supramolecular hydrogels, and covalent networks.

1.4.1 *Physically assembled nanoparticles*

Physically assembled nanoparticles are stabilized by intermolecular forces that arise from the amphiphilic nature of the constituent polymers. In aqueous biological environments, polymers self-assemble such that the hydrophilic domains are on the surface of the nanoparticle and the hydrophobic domains are buried in the micellar core. Similar phenomena can be exploited to create responsive bilayer structures (e.g., polymersomes, vesicles), which can be further crosslinked to improve stability. Here, we characterize dually sensitive materials on the basis of their response

mechanism, including whether the stimuli change the polymer polarity, induce bond cleavage, or act through a combination of these mechanisms (**Figure 1.3a**).

Dual regulation of hydrophobic/hydrophilic polarity

In physically assembled systems, stimuli-responsive groups may be incorporated within the constituent polymers such that a signal triggers the conversion of one domain from hydrophobic to hydrophilic, or vice versa. This change disrupts the supramolecular interactions that provide the nanostructure, inducing carrier breakdown and/or swelling, and subsequent payload release.

One example of such a material arises from diblock copolymers forming "schizophrenic" micelles that undergo stimuli-triggered inversion. Each polymer block is responsive to a separate stimulus capable of independently controlling its polarity. The polymer self-assembles into micelles when blocks are oppositely charged, but becomes a unimer when its blocks display the same polarity. Poly(acrylic acid) (PAA) was incorporated into the block copolymer PAA-*b*-PNIPAM, which exhibits such behavior: thermoresponsive PNIPAM is hydrophobic at 37 °C and hydrophilic at 25 °C, wheras the pH-responsive PAA is deprotonated/hydrophilic at pH < 4 and protonated/hydrophobic at a neutral pH. This system can reversibly transition between a PNIPAM-core micelle (37°C, pH 7), a unimer (25°C, pH 7), and a PAA-core micelle (25°C, pH 3)[71]. In a similar approach, the Fe^{3+}-responsive poly[sodium 2-(acrylamido)-2-methylpropanesulfonate] (PAMPS) was incorporated into the block copolymer PAMPS-*b*-PNIPAM. This system can

reversibly convert between a PNIPAM-core micelle (45°C, no Fe^{3+}), a unimer (25°C, no Fe^{3+}), and a PAMPS-core micelle (25°C, Fe^{3+})[72].

The two stimuli-responsive groups can also exist within the same block copolymer domain. A block copolymer synthesized from hydrophilic PEG and hydrophobic poly[2-(diethylamino)ethyl methacrylate-co-(2,2,2-trifluoro)ethyl methacrylate] (DEA-*co*-FMA) was self-assembled into nanovesicles. CO_2/DEA binding introduced a positive charge, leading to a vesicle-micelle transition and particle shrinking, while O_2/FMA binding increased segment hydrophilicity to yield vesicle swelling[73]. Finally, a block copolymer containing a hydrophilic PEG segment and a hydrophobic poly[(2-tetrahydrofuranyloxy)ethyl methacrylate-co-DEA] segment responded to DEA-protonating acid OR structure-disrupting ultrasound, either of which induces vesicle shrinkage and drug release[74].

Dual regulation via cleavable bonds

Cleavable bonds also provide a stimuli-responsive handle for biomaterial systems. Bond cleavage can be used to unlink a drug from the material, cleave two polymer domains, degrade a polymer, or irreversibly switch domain polarity. For example, micelles were created from ABA block copolymers containing hydrophilic PEG domains flanking a hydrophobic region containing both disulfide and *o*NB moieties; exposure to either reducing conditions OR light severed the hydrophobic domain, leading to material breakdown and payload delivery[75]. In another system, micelles were formed from hydrophobic DOX linked to a hydrophilic PEG via a disulfide bond. The hydrophobic core was stabilized by Cu^{2+}, which dimerizes DOX at neutral pH but not under acidic conditions. These nanoparticles exhibited a cumulative release profile in which a reductant or an acidic environment elicited partial delivery, but maximal release occurred in the combined

environment[76]. In yet another system, a hydrophobic polymer containing a thioether solubility switch and an acid-labile ketal group was formulated into a sequentially triggered nanoparticle. This hydrophobic polymer resists acid-catalyzed hydrolytic degradation until the thioether is oxidized into a thioketal, permitting material degradation only after H_2O_2 and acid are sequentially presented[77].

In other systems, stimuli-labile crosslinks are used to stabilize micelles. Hydrophilic polyethylenimine modified with hydrophobic *o*NB groups self-assembled into micelles and were further stabilized with disulfide-containing crosslinks. Particles persisted until both crosslinks were reduced AND *o*NB was photoremoved[78]. Similarly, the hydrophilic biopolymer chitosan was modified with *o*NB side chains, self-assembled into micelles, and subsequently crosslinked with species containing acid-labile imine bonds. A hydrophobic anticancer drug, camptothecin, was released upon nanoparticle breakdown cumulatively triggered by exposure to both reducing and acidic conditions[79]. In another demonstration, micelles containing DOX bound to PEG-*b*-PMAA via an acid-labile hydrazone bond were crosslinked with a disulfide-containing species; maximal drug release was achieved upon exposure to both acid and reductant[80].

Multi-component materials, in which each portion is sensitive to a different stimulus, have also been created. For instance, payload-containing nanocapsules synthesized from the pH-responsive polyaniline polymer were electrostatically modified with gold nanoparticles whose surfaces were functionalized with a second payload through a reductive-labile gold–sulfur bond. Delivery of each of the two payloads was independently triggered by basic pH (12.4) and reductant[81].

Dual regulation via both cleavable bond and physical mechanism

The two primary mechanisms to enable stimuli-sensing behavior—reversing domain polarity and bond cleavage—can also be combined to generate multi-stimuli-responsive materials. For example, PEG and cyclic RGD side chains were grafted to a poly(β-amino ester) (BAE) backbone via disulfide bonds, and subsequently self-assembled into micelles with a PEG corona and a BAE core. DOX payload release could be triggered by two independent mechanisms: Disulfide reduction severs the link between hydrophobic and hydrophilic domains, and acidic environments protonate the basic BAE residues and polarize the core[82]. In another example, block copolymers synthesized from PEG and PNIPAM domains were linked through an enzyme-labile peptide sequence; micelles assembled upon heating above the LCST, but were disrupted upon proteolytic cleavage of the PEG corona[83]. In a recent example, hydrogels were formed by crosslinking thermoresponsive liposomes with polyacrylamide chains through DNA susceptible to enzymatic cleavage. Liposome contents were released upon heating, while hydrogels were degraded by the restriction enzyme EcoRI[84].

1.4.2 *Mesoporous silica nanoparticles*

Many stimuli-responsive biomaterials have been created by decorating MSNPs with an environmentally responsive polymer layer. MSNPs have pores, ranging from 2-30 nm, into which drugs can be loaded. Polymers grafted to the particle surface serve as selective gatekeepers, permitting therapeutic release only upon an environmentally triggered change to the polymer physics or chemistry[85].

Significant efforts have been dedicated to the creation of MSNP drug delivery platforms that release their payload in response to multiple stimuli. Those sensitive to both temperature and pH have been engineered with surface-grafted PNIPAM-*co*-PMAA, where polymer-shell collapse

above the LCST or at low pH cumulatively triggers the delivery of a small-molecule payload[86,87]. In another system, PAA attached to the surface of an MSNP via a disulfide bond afforded payload delivery in the presence of GSH or an acidic environment (pH 5)[88]. Alternatively, OR-gated cargo release was achieved under acidic OR reducing conditions for dextran grafted to MSNPs via an acid-labile imine bond and crosslinked with reducible disulfide bonds[89].

Other MSNP drug delivery platforms have been developed in which sequential exposure to two different cues triggers payload delivery. In one example, PCL was polymerized in the core of DOX-loaded MSNPs, which were then coated with PAA. The PAA disassociated from the particle in an acidic environment (pH 5.5), enabling PCL to be degraded by esterases or through hydrolysis[90]. In an example exploiting stepwise pH responsiveness, a surface-grafted PEG stealth layer can be shed under mildly acidic conditions (pH 6.5) characteristic of the tumor microenvironment, presenting a positive charge to facilitate cellular uptake; the more acidic intracellular environment (pH 5) cleaves a boronate ester bond to remove the polymer gatekeeper and trigger payload delivery[91]. Another system, sequentially responsive to pH and light, was created by attaching a cucubit[6]uril nanovalve to the surface of the MSNP through either an acid- or base-labile manner, wherein the MSNP pores remain capped until the relevant pH is achieved. Through further functionalization of the pores with an azobenzene-based nanoimpeller that undergoes a photoreversible *cis–trans* isomerization, a light-induced wagging motion is required to actuate payload release[92].

1.4.3 *Supramolecular hydrogels*

Hydrogelators, which are typically small molecules or polymers, are amphiphiles that spontaneously self-assemble into fiber-like structures and, subsequently, bulk hydrogels on the basis of their hydrophobic/hydrophilic intermolecular interactions. Hydrogelators can be readily

engineered such that their structure and subsequent hydrogel properties respond to environmental signals. To date, supramolecular hydrogel systems have yielded some of the most complex responses programmed into multi-stimuli-responsive biomaterials. Here, we describe and characterize systems formed through physical associations, covalent bonds, or guest-host interactions.

Physically responsive supramolecular hydrogels

Supramolecular gels are stabilized through physical interactions that can undergo stimuli-triggered rearrangement to reversibly respond to their environment. In one system, a supramolecular hydrogelator was built with a hydrophilic ion-sensitive phosphate headgroup and a hydrophobic tail containing a photoresponsive olefinic bond. Introduction of cationic species such as Ca^{2+} and H^{+} ions strengthened the resultant hydrogel network, while the trans-to-cis UV-induced photoisomerization event destroyed supramolecular hydrogel assemblies; a variety of logical behaviors were achieved with different initial conditions and inputs[93]. Another hydrogelator system was created with amphiphilic phenylalanine and photoresponsive azobenzene moieties; deviations from neutral pH OR photoswitching of azobenzene isomerization yielded reversible gel degradation[94].

Supramolecular gels may also employ guest-host chemistry, in which two counterreactive functional groups form strong non-covalent intermolecular bonds material components, which give rise to a unique class of shear-thinning injectable hydrogels. In one system, cadmium sulfide quantum dots were functionalized with β-cyclodextran and mixed with a thermoresponsive block copolymer end-functionalized with azobenzene [azo-(PDMA-*b*-PNIPAM)]. The azobenzene forms non-covalent bonds with the β-CD quantum dots (QDs) to yield a hybrid inclusion complex

with a QD core and PNIPAM corona. Upon heating above the LCST, the PNIPAM chains aggregate to form a supramolecular hydrogel, which degrades upon cooling OR in the presence of competitive binders to the guest-host system (i.e., adamantane, α-cyclodextran)[95].

Covalently responsive supramolecular hydrogels

Supramolecular hydrogels may also exhibit irreversible phase transitions when the gelator undergoes covalent modification in response to external signals. Ikeda et al.[96] have developed stimuli-sensitive amphiphilic gelators in which the hydrophobic head group was cleaved upon exposure to oxidative conditions. Encapsulation of oxidases that produce hydrogen peroxidase in response to a variety of analytes (i.e., glucose, sarcosine, choline, uric acid) underwent irreversible degradation triggered by small molecules. Encapsulation of multiple enzymes within a single gel permitted formation of OR- and AND-gated materials. In one example, materials containing choline oxidase and a hydrolase that converts acetylcholine to choline generated degradation-inducing H_2O_2 in the presence of either acetylcholine or choline. Alternatively, materials containing both redox- and electron-responsive nanofibers, respectively containing nitroreductase and glucose oxidase, required inputs of both nicotinamide adenine dinucleotide AND glucose to induce complete material degradation. In another approach, an ABC triblock copolymer platform was created in which the A block was either an oxidative-sensitive PPS or hydrolytic PCL or PLGA, B was hydrophilic poly(*N*,*N*-dimethylacrylamide) (PDMA), and C was the thermoresponsive PNIPAM. At room temperature, the particle formed micelles, which assembled

into supramolecular hydrogels at 37 °C. These gels degrade upon cooling OR upon exposure to either oxidative or hydrolytic conditions on the basis of the A-block composition[97].

1.4.4 *Covalently assembled systems*

Stimuli-responsive biomaterials have also been created through covalent interactions. Since these materials are generally more stable than physical assemblies and may be formulated into a wider range of sizes and shapes, these systems may be preferable over physically assembled systems for certain applications. Here, we discuss both single and interpenetrating polymer networks (IPNs), as well as covalently assembled nanoparticles (Figure 1.3b).

Single covalent polymer networks

Multi-stimuli-responsive hydrogels have been engineered by incorporating multiple stimuli-labile moieties within a single polymer network. For example, gels formed from the ECM protein hyaluronic acid crosslinked via disulfide bonds underwent an OR-gated gel-sol transition upon exposure to either hyaluronidase or reducing conditions[98]. Additionally, PEG/PAMAM hydrogel constructs incorporating both acetal and disulfide bonds underwent degradation in the presence of acidic OR reducing conditions to deliver DOX[99]. Another step-growth PEG network was engineered with peptide-based crosslinkers that contained the photolabile *o*NB group and an MMP-labile peptide sequence, permitting degradation through user-directed laser light OR cell-secreted enzymes for the creation of custom endothelialized vasculature[100].

Interpenetrating polymer networks

IPNs are composed of two independent polymer networks that are interlaced at the molecular scale. If these networks are orthogonally labile, both environmental signals are required for full material degradation. In the case of an interpenetrating network between gelatin and

dextran, exposure to both α-chymotrypsin AND dextranase is required to release encapsulated lipid microspheres that serve as drug reservoirs[101].

IPNs may also be exploited to control material swelling in response to multiple environmental stimuli. An IPN between pH-responsive PMAA and thermoresponsive PNIPAM polymers exhibited tunable swelling. At low pH (< 5.5), the PMAA acid side chains are protonated, inducing network collapse; at higher pH values, the PMAA side chains become charged, and the gel swells due to electrostatic repulsion. The PNIPAM network was significantly swollen below its LCST (32 °C) and collapsed above this temperature[102]. A similar IPN of PAA and PNIPAM has been formulated as hollow-core nanogels; these materials can be loaded with cargo in their swollen state at room temperature, shrunk at 37 °C, and then reswollen upon acidic treatment for pH-targeted drug delivery[103].

Covalent nanoparticle carrier systems

Several novel nanoparticle carriers have been developed such that material response is triggered through exposure to multiple external stimuli. In one creative example, the small protein capsid of the adeno-associated virus is decorated with small peptide-based "locks" that inhibit transportation across the cell membrane. These locks are removed upon treatment with MMP-7 and MMP-9, enabling AND-gated gene delivery and cell transduction[104]. Similarly, DNA nanocapsules have been engineered to contain two DNA-based "clasps" and "locks", such that exposure to both relevant aptamer "keys" unlocked the carriers to trigger AND-gated delivery of antibody fragments[105].

1.5 Multi-stimuli-responsive biomaterials

While biomaterials sensitive to two unique environmental cues can exhibit complex environmentally defined responses, further specificity and control can be gained by building sensitivity to additional stimuli. With each additional stimulus, an exponential increase in the number of possible material states gives rise to systems that exhibit even more complex responses. Despite this immense potential, materials engineered to respond to three or more environmental signals remain relatively underexplored. In this section, we describe some exciting examples of multi-stimuli-responsive biomaterials based on physically assembled nanoparticles, supramolecular hydrogels, and covalent networks.

1.5.1 *Physically assembled nanoparticles*

Amphiphilic polymer systems can self-assemble into supramolecular nanostructures including micelles and polymerasomes. As discussed in Chapter 1.3.1 and 1.3.2, stimuli-responsive functionalities can be used to control the swelling, degradation, or payload release from such nanoparticles. Multi-input materials in this category build on this existing framework by incorporating three or more stimuli-responsive moieties.

Three-input responsive nanoparticles

The most common multi-stimuli-sensitive nanoparticles can incorporate information from three different environmental inputs. To date, the majority of these systems combine thermal responsiveness about an LCST with two other stimuli. In one example, an amphiphilic copolymer was created from disulfide-linked PNIPAM and tetrahydropyran (THP)-protected 2-hydroxyethyl methacrylate (HEMA) blocks[106]. Acidic conditions removed the THP, converting the HEMA domain from hydrophobic to hydrophilic; raising the temperature above the LCST converted the

PNIPAM domain from hydrophilic to hydrophobic; reducing conditions severed the disulfide linkage between the two domains. In each case, the encapsulated guest molecule was released from the micelle, effectively creating a double OR gate. In another example, multi stimuli-sensitive star-polymer aggregates were built from PEG, PCL, PAA, and PNIPAM[107]. These micelles are destabilized above their LCST (37 °C), leading to DOX release. Reducing conditions removed the PAA-DOX chains, while acidic conditions disrupted the DOX-PAA electrostatic interaction; both stimuli cumulatively triggered DOX release, though maximal release was achieved in the combined environment. In a final example, micelles were created from amphiphilic copolymer poly(NIPAM-*co*-SP)[108]. Micellar disruption occurred above their LCST (35 °C) as PNIPAM was converted from hydrophilic to hydrophobic. Micelles could also degrade when the hydrophobic SP was converted to the hydrophilic MC group in the presence of light or the hydrophilic MCH^+ group in the presence of acid; maximal payload release occurred when the materials were treated with both light and acid.

Triply responsive nanoparticles that do not rely on an LCST transition have also been created. For example, a polyanionic polymer containing charged head groups attached to its backbone via disulfide bonds, upon complexation with a cationic surfactant, formed a micelle-like assembly[109]. Particles disassembled in the presence of a reductant OR acidic conditions OR high-ionic-strength environments. In another example, a DNA-intercalating agent was tethered to the surface of a MSNP and capped with double stranded DNA[110]. The pore-loaded calcein payload was released following reductant-mediated release of the intercalating agent, OR when the DNA was cleaved by a DNase OR converted to ssDNA upon heating. The intercalating agent was

released upon exposure to reducing conditions AND either heat OR DNase in a complex Boolean response.

Four- and five-input responsive nanoparticles

Several investigators have created nanoparticles that respond to more than three environmental stimuli. In one example, the triblock copolymer SP-*b*-NIPAM-*b*-AMPS self-assembled into micelles with an SP core, PNIPAM shell, and an AMPS corona[111]. Upon exposure to UV light, SP solubility increases causing particle expansion, which is reversed upon exposure to visible light. Heating the particles increases the hydrophobicity of the PNIPAM-shell, shrinking the particle. Fe^{3+} ions bind to the sulfonate groups on the AMPS, decreasing its solubility and shrinking the particle. Exposure to acid increases the hydrophilicity of the SP group, swelling the particle. In another example, the diblock copolymer poly(2-nitrobenzyl methacrylate)-SS-poly(dimethylaminoethyl methacrylate) (PNBM-SS-PDMAEMA) self-assembles into micelles[112]. The hydrophobic PNBM core irreversibly becomes less hydrophobic upon UV cleavage of the *o*NB groups, and the disulfide linker is cleaved in reducing conditions. The PDMAEMA corona is responsive to both temperature and pH; at elevated T and pH the micelle shrinks, while in acidic conditions (pH = 3) the micelle swells. Combinations of acid/UV or acid/dithiothreitol are able to fully degrade the micelles to enable nile red delivery. Finally, quintuple-stimuli responsive micelles have been formed from the block copolymer PMAEFe-*o*NB-PDMAEMA with BBAC crosslinking of the PDMAEMA-shell[113]. The ferrocene containing core swelled in the presence of H_2O_2-triggered oxidation of Fe^{2+} to Fe^{3+}, releasing much of the NR payload. UV-induced *o*NB photodegradation separated the two domains and induced micelle breakdown if the BBAC crosslinker was also cleaved with reducing conditions. The PDMAEMA corona is sensitive to

temperature and pH, causing micelle swelling in acidic conditions and shrinking when heated above the LCST.

1.5.2 *Supramolecular polymer networks*

The framework used for creating two-input-responsive supramolecular hydrogels (Chapter 1.3.3) can be extended to generate systems responsive to three or more inputs simply by incorporating additional stimuli-responsive functionalities within the hydrogelators. In an example of such a supramolecular material triply sensitive to light, temperature, and pH, microgels formed from PNIPAM modified with SP were formed that collapse above the polymer's LCST[114]. SP is highly hydrophobic after visible light exposure, and reversibly converts to a less hydrophobic MC species in the dark state or upon UV exposure. Visible light exposure increases the gel hydrophobicity, thus decreasing the LCST and leading to gel collapse. Residual amine groups were partially ionized at a neutral pH, but deprotonated in basic conditions (pH = 10), leading to gel shrinkage. In another example, in which the material is sensitive to temperature, pH, and glucose, P(NIPAM-*co*-MAAmBO) was synthesized with different ratios of boronic acid side chains, which dimerize with glucose[115]. The PNIPAM component of these polymers imparts an LCST to the system, yielding temperature responsiveness. Glucose binds to the MAAmBO chains, increasing the hydrophilicity of the system and their LCST. P(NIPAM-*st*-MAAmBO) can be mixed with a glycopolymer to form a crosslinked gel in basic conditions (pH = 13); these gels are glucose sensitive because competitive binding induces gel degradation.

Guest-host chemistries have also been used to create triple-stimuli-responsive supramolecular gels. One study used a two-polymer system consisting of: 1) a BCD dimer linked via disulfide bonds and 2) PNIPAM with azobenzene side chains[116]. Reducing conditions severed

the crosslinkers and resulted in gel degradation. UV light induced an azobenzene isomerization that inhibited its guest-host binding to BCD; this process was reversed upon isomerization induced by visible light. Finally, the gels were hydrated and swollen below their LCST and underwent a volume phase transition into a collapsed state above their LCST.

A quadruple-stimuli-responsive supramolecular gelator was engineered with a naphthalene-based salicylideneaniline and a sorbitol moiety[117]. This molecule can interact with four unique environmental stimuli—Cu^{2+}, light, pH, and temperature—which influence the presence and properties of its supramolecular assemblies. Cu^{2+} ions complexed with two naphthalene moieties to enable supramolecular fiber assembly. Similarly, the phenol group can be deprotonated in basic conditions, and the salicylideneaniline group reversibly tautomerizes under UV light (reversed by visible light), which can influence system assembly. Finally, these materials exhibit thermosensitive behavior. Ultimately, these different stimuli can have complex cooperative or competitive combined effects on whether hydrogels form; several logic-gated systems were defined by specifying the initial conditions and variable inputs.

1.5.3 *Covalently polymer networks*

On the basis of the frameworks presented in Section 1.3.4, efforts have been made to generate covalent polymer networks sensitive to three or more environmental inputs through the inclusion of additional stimuli-responsive functional groups within a material. In one example, a crosslinked zwitterionic hydrogel network comprised of glutamic acid and lysine residues was found to deliver DOX in response to three inputs[118]. This hydrogel is enzymatically digested by trypsin. Furthermore, this hydrogel swells as the pH deviates from 6 or the ionic strength of its buffer increases, owing to the change of charge states of its ionizable side chains. Crosslinked

copolymers of NIPAM with phenylalanine and/or valine containing embedded Fe_3O_4 nanoparticles also exhibited triple-stimuli-responsive delivery[119]. DOX binds electrostatically to the carboxylic acid side chains of the hydrogel network, and this binding is disrupted at elevated temperature and sensitive to pH. Application of an external AMF induces heating, also stimulating DOX release. In another example, stimuli-triggered expansile nanogels were formulated by crosslinking a copolymer of PNIPAM/PEG/PDA[120]. Under reducing conditions, acidic conditions, and elevated temperature, these particles expanded in volume up to 1,000-fold. The copolymer P(DMAEMA-*co*-AAPBA) was crosslinked into a hydrogel network[121]. This system exhibited pH- and temperature-responsive swelling, owing to its PDMAEMA domain. The boronic acid component of AAPBA binds with glucose to modify the thermoresponsive behavior of the system. At physiological pH and temperature, environmental glucose induced hydrogel swelling to increase the rate of encapsulated bovine serum albumin release.

Almost every extant triple-stimuli-responsive hydrogel system undergoes responses primarily via physical mechanisms, resulting in complex behaviors when multiple stimuli are present. More predicable behaviors can be engineered by incorporating only stimuli-labile groups within hydrogel crosslinkers, enabling a true off/on material degradation in response to multiple cues. For example, step-growth polymer networks were polymerized from four-arm PEG macromers such that each crosslink contained a photolabile *o*NB group, a redox-responsive arylthiol-based thioether succinimide, and a hydrolytically sensitive ester[122]. This double OR-gated system was responsive to light, reducing conditions, or water, with degradation rates spanning three orders of magnitude depending on the mode of cleavage.

1.6 Looking forward

In this chapter, we describe a diverse range of synthetic and strategic approaches used to create stimuli-responsive biomaterials. Categorizing systems on basis of the number of inputs, material type, and response mechanism, we have examined how functional moieties that undergo predictable chemical or physical changes toward a specific stimulus can be combined to create multi-stimuli-sensitive constructs. Materials that respond to biologically presented and externally administered signals could transform the fields of drug delivery, biosensing, and regenerative medicine. The central objective of this thesis seeks to establish a modular approach to enable the rational design of multi-stimuli-responsive biomaterials from a common framework.

1.7 Figures

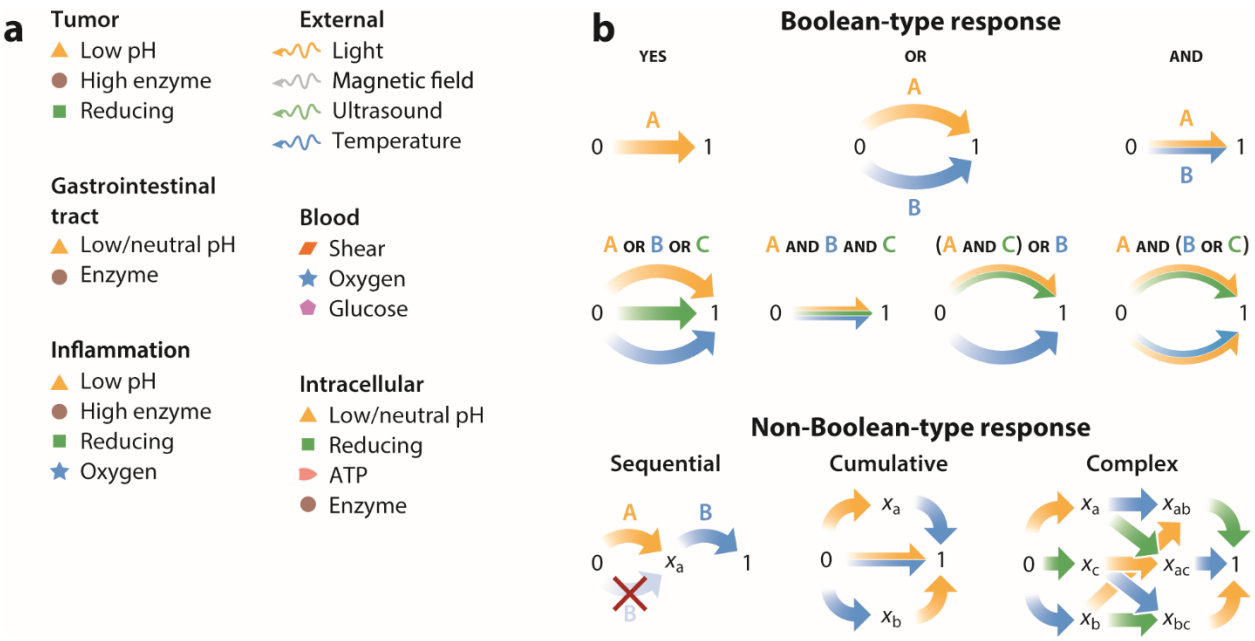

Figure 1.1: An overview of common biomaterial stimuli and response types.
(a) An overview of the locations of commonly used biological and external triggers. (b) A schematic representation of recurring stimuli-responsive modalities.

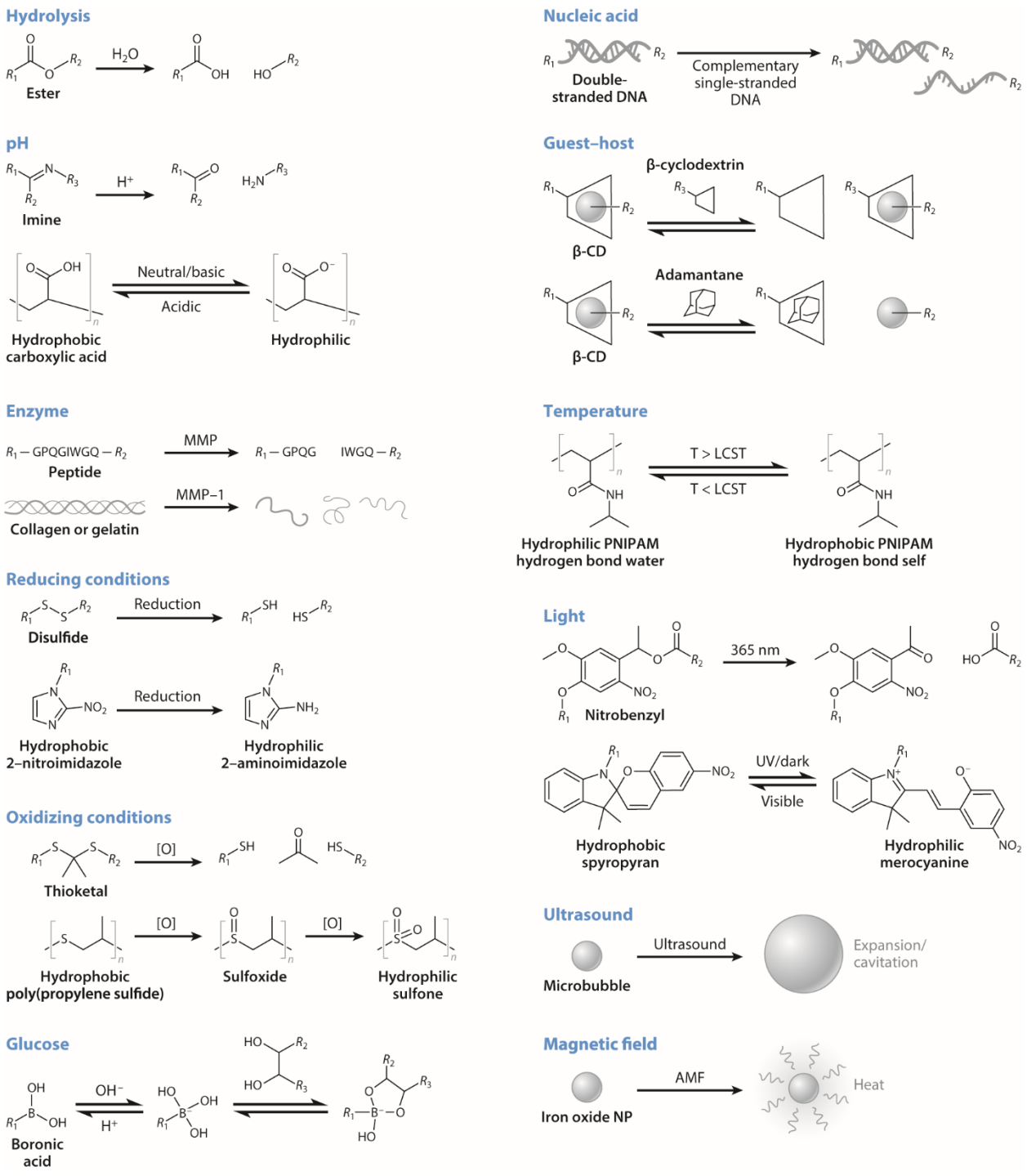

Figure 1.2: A summary of common stimuli-sensitive chemical functionalities employed in biomaterials.

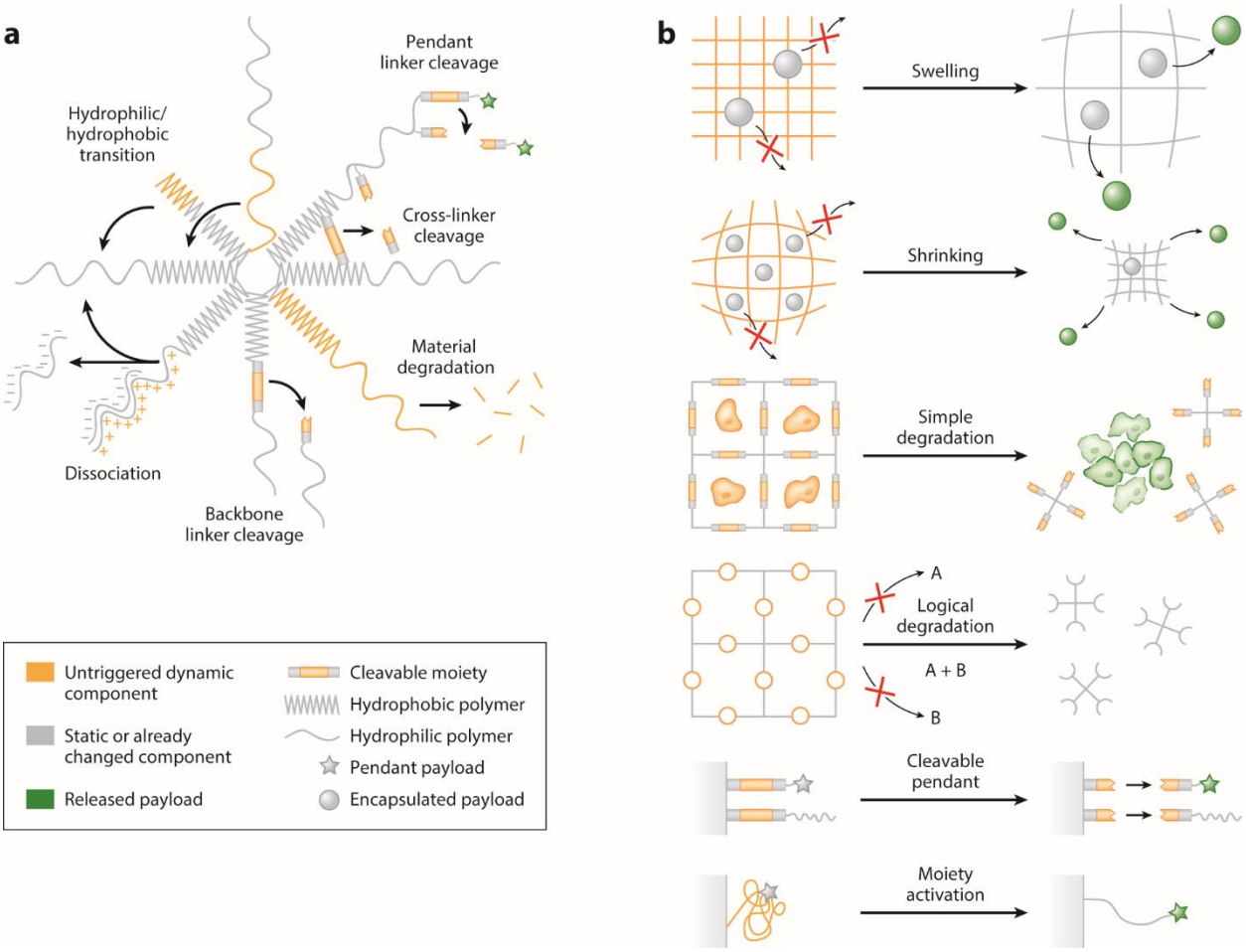

Figure 1.3: An overview of the mechanisms and strategies that enable functional material responses.

From (**a**) physically assembled systems and (**b**) covalent networks.

CHAPTER 2: THESIS OBJECTIVES

Biology is the world's most complex machine; its constitutive elements—cells, genes, and proteins—coordinate in a dynamic and intricate synchrony. The tools available to modify these components fundamentally constrain our ability to perform both medicine and biological research. Systemic drug administration and surgery are crude techniques that lack the precision necessary to achieve certain desired outcomes. Stimuli-responsive biomaterials are capable of dynamically sensing and interacting with critical components within living systems. Despite their extensive development, there is not yet a modular approach for generating materials capable of integrating multiple environmental signals to yield a precise, well-defined response. Biomaterials that can respond to subtle differences in complex, multi-factor biological environments may enable unprecedented possibilities in tissue engineering and targeted drug delivery.

The central objective of this research dissertation is to develop a modular biomaterial platform that can provide a tailorable and well-defined response profile towards complex, multi-signal environments. In Chapter 3, we hypothesize that we can build Boolean-responsive degradable hydrogels by creating crosslinkers with multiple stimuli-labile groups in a controlled molecular architecture. There, we will establish a generalizable framework for predicting material behavior on the basis of linker structure and develop a synthetic approach for generating such linkers. We then explore the capabilities of this system and its applications for environmentally controlled hydrogel degradation, therapeutic delivery, and cell delivery. In Chapter 4, we apply the logical linkers to a clinically relevant activatable cell-penetrating peptide system in order to control the cellular internalization of functional proteins. By combining the logical linkers with

site-specific sortase-based protein modification, we develop a unique approach to overcoming transport barriers for targeted delivery applications.

CHAPTER 3: ENGINEERING MODULAR BIOMATERIAL LOGIC GATES FOR ENVIRONMENTALLY TRIGGERED THERAPEUTIC DELIVERY

As published in *Nature Chemistry*, **10**, 251-258 (2018)[123]

3.1 Abstract

The successful transport of drug- and cell-based therapeutics to diseased sites represents a major barrier in the development of clinical therapies. Targeted delivery can be mediated through degradable biomaterial vehicles that utilize disease biomarkers to trigger payload release. Here, we report a modular chemical framework for imparting hydrogels with precise degradative responsiveness by using multiple environmental cues to trigger reactions that operate user-programmable Boolean logic. By specifying the molecular architecture and connectivity of orthogonal stimuli-labile moieties within material crosslinkers, we show selective control over gel dissolution and therapeutic delivery. To illustrate the versatility of this methodology, we synthesized seventeen distinct stimuli-responsive materials that collectively yielded all possible YES/OR/AND logical outputs from input combinations involving enzyme, reductant, and light. Using these hydrogels we demonstrate the first sequential and environmentally stimulated release of multiple cell lines in well-defined combinations from a material. We expect these platforms will find utility in several diverse fields including drug delivery, diagnostics, and regenerative medicine.

3.2 Main text

Recent innovations in therapeutic development and cell engineering have yielded powerful tools to combat an increasing number of debilitating and life-threatening diseases. Despite these advances, several barriers to clinical translation remain, including the significant challenge of

limiting therapeutic deployment to sites of disease that can be widespread and unknown[2,8,10,124]. Targeted delivery strategies that exploit disease-related biomarkers improve treatment efficiency and efficacy by reducing dosage requirements and adverse off-target effects[4,6,8,11,125]. Most typically, these methods employ polymer-based vehicles to facilitate delivery and protect therapeutic cargo from immune recognition, clearance, and non-specific cellular uptake. Cell-based therapies further necessitate that these vehicles recapitulate critical aspects of native tissue to ensure sustained cell viability and function. Hydrogels offer promise in each of these regards, as they are robust material platforms whose biochemical and biophysical properties can be tuned to preserve and promote specific cell fates, are readily formulated into a variety of shapes and stiffnesses to control transport to and within tissues, and can be engineered to degrade in response to locally presented cues to facilitate therapeutic release[3,126].

Smart materials have been engineered to leverage pathophysiology for targeted delivery by integrating functional groups that cleave or change conformation in response to an external stimulus (e.g., enzyme, pH, temperature, redox conditions, small molecules), allowing them to sense and respond to disease-associated biochemical hallmarks[8,10,11]. Though materials sensitive to single factors can enrich therapeutic delivery to sites of disease, individual biomarkers are rarely unique to these locations, leading to suboptimal selectivity. For example, cancer microenvironments have been targeted through their extensive matrix metalloproteinase (MMP) activity, reducing conditions, and subphysiological pH; however, these characteristics are respectively shared by healthy joints[28], the intracellular milieu[8], and the stomach. To improve site-specificity of payload release, materials that degrade only when presented with multiple cues have been developed[10,90,93,96,98,105,127–129]. While previous approaches have enabled therapeutic delivery

in response to two environmental factors, they lack a generalizable framework to exploit additional input stimuli to further refine release specificity. Moreover, the uniqueness of each previously reported responsive platform necessitates a complete material redesign – one that is generally not synthetically tractable due to inherent constraints on material composition and vehicle geometry – in order to alter the response profiles or utilize different biochemical triggers. Further, the subset of degradable materials demonstrated for live cell release has been limited to single biological inputs[20,63,130,131], confining next-generation cellular therapeutics to simple delivery platforms.

To address these technological limitations and enable unprecedented specificity over controlled therapeutic release, we sought to develop a versatile chemistry-based approach to create multi-stimuli responsive hydrogel platforms that are: 1) able to perform biocomputation, 2) modular in design, and 3) fully cytocompatible. Biocomputation represents the ability to simultaneously sense multiple biologically presented inputs and follow a user-programmed Boolean logic-based algorithm to provide a functional output[11], demonstrated here in the form of material degradation and therapeutic delivery. System modularity allows both the inputs and the logical functions to be changed and combined to generate a theoretically limitless number of novel materials, each with unique and user-specified release characteristics. Furthermore, exploitation of cytocompatible bioorthogonal chemistries permits responsive material platforms to be formed and degraded on demand in the presence of live cells, representing a major improvement over existing cell delivery strategies.

In our rational design-based approach, stimuli-sensitive components are incorporated into discrete, monodisperse, synthetic crosslinkers that, upon reaction with polymer macromers, form

hydrogels of well-defined molecular architecture. Information governing the environmental-responsiveness of the resulting material is embedded within the crosslinker domain; when the linker is covalently cleaved, the material degrades and simultaneously releases any encapsulated or tethered payload. The simplest Boolean logical function, the YES-gate, is implemented when a single stimuli-labile moiety is included in the linker. We hypothesized that more advanced logical operations could be built through the controlled connectivity of additional cleavable groups within a crosslinker. When two degradable units are connected in series, the cleavage of either moiety causes material dissolution, forming an OR-gate (denoted with logic symbol ∨); when two degradable units are connected in parallel, the cleavage of both moieties is required for material dissolution, forming an AND-gate (denoted by logic symbol ∧). These concepts can be expanded hierarchically, combining multiple gates into a logical circuit to engineer complex responses to additional dynamic stimuli (**Figure 3.1**). Formalizing the relationship between crosslinker architecture and hydrogel degradability provides a template for creating materials that are structurally simple yet functionally complex.

3.3 Results

3.3.1 *Synthesis of logic-based responsive crosslinkers*

Implementation of the outlined biocomputational strategy requires precise control over crosslinker functionality and architecture. We used peptide-based crosslinkers due to the efficiency of solid-phase peptide synthesis in generating monodisperse macromolecules that contain a range of functional groups with sequence-defined order and connectivity. Peptides, which possess intrinsic biocompatibility, can be chemically modified to introduce non-canonical functionality, connectivity (e.g., branching, cyclization, intramolecular stapling), and degradability. As a

demonstration of this logic-based approach, three chemically orthogonal stimuli-labile moieties from different reaction classes were employed: 1) the enzymatically degradable oligopeptide sequence, GPQG↓IWGQ, which cleaves in the presence of MMPs and allows for cell- and disease-triggered response[29], 2) disulfide bonds, which degrade under reducing conditions present both intracellularly and in disease states, and 3) an *ortho*-nitrobenzyl ester (*o*NB), which undergoes photoscission upon cytocompatible near-UV light exposure ($\lambda = 365$ nm), thereby facilitating user-defined spatiotemporal control over material properties[132] (**Figure 3.1e**). Exhaustively spanning all hierarchical YES/OR/AND combinations of these three stimuli-labile moieties, we synthesized seventeen distinct crosslinkers that each exhibited a unique logical output (Methods A1-A21). Each crosslinker was flanked with two reactive azide moieties to enable formation of nearly ideal step-growth hydrogel networks *via* a strain-promoted, azide-alkyne cycloaddition (SPAAC) reaction[133] with four-arm poly(ethylene glycol) tetrabicyclononyne (PEG-tetraBCN, Method A22). SPAAC click chemistry rapidly produces homogenous hydrogels in a bioorthogonal fashion, thereby permitting encapsulation of bioactive therapeutics and living cells[62,134,135]. Moreover, an extensive toolbox of SPAAC-compatible modifications allows for uniform network functionalization with moieties ranging from small molecules to full-length proteins[62,136–138]. Such tunability further enables the design of complex delivery vehicles, for example, through the inclusion of targeting moieties, instructive cues to guide encapsulated cell fate and function, or tethered therapeutics to be released upon material dissolution.

3.3.2 *Assessing solution-based crosslinker degradation in response to environmental stimuli*

To demonstrate that crosslinkers degrade as engineered in response to environmental cues and that stimuli-responsive reactions are chemically orthogonal, we treated each of the one- and two-input linkers with every possible combination of MMP enzyme ($_E$), reducing components ($_R$),

and light ($_P$) (Methods A23 & A24). Reaction products were characterized using matrix-assisted laser desorption/ionization time-of-flight mass spectrometry (MALDI-TOF). Detected masses were in excellent agreement with those of the expected reaction products (**Figures 3.2** & A1-A9), indicating that the linkers respond as designed on a molecular level. To further investigate, the enzyme AND photo linker (E∧P) was pretreated with different combinations of enzyme and light, added to a stoichiometrically defined amount of PEG-tetraBCN, and characterized by *in situ* oscillatory rheology to monitor evolution of material properties (Methods A22 & A25). Untreated E∧P yielded robust gels, demonstrating the first successful use of a cyclic or stapled peptide for material crosslinking. Final storage moduli of samples containing the untreated linker (G' = 1660 ± 170 Pa) were similar to that of the linkers subjected to either enzyme or light (G' = 1580 ± 130 Pa and 1540 ± 110 Pa, respectively), while the linker treated with both enzyme and light did not form a gel (G' = 200 ± 30). All samples had a final loss modulus (G") of ~ 50 Pa. Consistent with rubber elasticity theory where shear moduli scales with crosslinking density[139] and calculations that distances between network branch points increase ≤ 3% upon cleavage of a single arm of AND-gated linkers (Method A26), this data suggests that the mechanical properties of these materials depend only on the final logical state of the Boolean linker.

3.3.3 *Logic-based hydrogel degradation in response to environmental stimuli*

After validating linker behavior on the molecular level, we sought to characterize the logic-based stimuli-responsiveness of bulk materials. Each crosslinker was reacted independently with Alexa568®-labeled PEG-tetraBCN to form seventeen different types of fluorescent hydrogels. For each type, responsiveness to all eight input combinations involving reducing agents, light, and enzyme were evaluated. Hydrogel degradation was quantified by measuring supernatant fluorescence at non-kinetically limited endpoints following treatment (**Figures 3.3** & A10-A11,

Methods A27 & A28). Each of the YES-gated materials (E, R, and P) behaved as expected, degrading only when the programmed cue was present. The high selectivity (>10-fold over non-specific release) again demonstrates the orthogonality of the employed stimuli-labile chemistries. The OR-gated materials (R∨E, E∨P, R∨P) also responded as expected, degrading fully when either of the relevant cues was present. The AND-gated materials (R∧E, E∧P, R∧P) also functioned properly, fully degrading only when both programmed cues were present. The observed release selectivity (>7-fold) is as or more specific than the most successful dual-input degradable materials previously reported[90,93,96,105]. Of the three-input materials containing two logic gates, six of eight [i.e., E∨(R∧P), P∨(R∧E), R∧(E∨P), P∧(R∨E), R∨E∨P, R∨(E∧P)] behaved fully as designed, degrading with high selectivity only when the respective cues were present. The conditions $[E\wedge(R\vee P)]_{EP}$ and $(R\wedge E\wedge P)_{REP}$ did not fully degrade, which we attribute to known decreased proteolytic cleavage kinetics for strained MMP-degradable substrates[140], in this case due to internal ring strain. These higher-order, three-input crosslinkers are the most complex logical operators ever used to control material degradation. This generalizable approach proves robust as 132 of the 136 treatment conditions yielded engineered degradation (defined as either complete degradation or <30% nonspecific release). The exhaustive synthesis and testing of each possible material demonstrates that complex biomaterial computation can be achieved with high fidelity through the hierarchical combination of simple YES/OR/AND logic gates. Given the initial success of this modular framework, we expect to be able to substitute the chosen stimuli-labile groups with any number of other chemically orthogonal moieties sensitive to pH, additional proteases, visible light, temperature, or ultrasound.

3.3.4 *Disease-associated delivery of doxorubicin to an in vitro cancer model*

To demonstrate the ability to deliver functional therapeutics in response to precise combinations of pathophysiological stimuli, we tethered a BCN-tagged doxorubicin (DOX) chemotherapeutic into RΛE gels that degrade with high specificity to cancer microenvironmental cues (**Figure 3.4**, Method A29). Extent of hydrogel functionalization was chosen such that solution DOX concentration following full material degradation (44 μM) would yield population-wide apoptotic death of plated cervical cancer-derived HeLa cells (**Figure 3.4c**). Following treatment by each relevant input combination (i.e., $_{N}$, $_{E}$, $_{R}$, $_{RE}$), cells were incubated in hydrogel supernatants for 48 hours prior to quantitative analysis of double-stranded DNA (dsDNA) content, indicative of the total number of viable cells. In the absence of treatment, or that with just reductant or MMP, normal proliferation was observed (95 ± 3%, 97 ± 2%, and 76 ± 5%, respectively, relative to non-treated controls lacking gels). The slight decrease in total dsDNA content following enzymatic treatment is attributed to secondary effects of the MMP treatment, rather than to non-specific DOX release (Method A29). In stark contrast to treatments with a single input, treatment with both inputs resulted in complete cell eradication (1.8 ± 0.2% dsDNA content relative to controls), as designed. These results highlight the unique capacity of this approach to control release of functional small molecule therapeutics through logic-based gel degradation, enabling precise regulation of cell fate in response to disease-defined combinations of external cues.

3.3.5 *Logic-based delivery of live cells from stimuli-responsive hydrogels*

To illustrate the biocomputational response of these engineered materials to a combination of spatially defined as well as environmental cues, we formulated a multifunctional hydrogel comprised of three distinct logical regions (RΛP, P, RVP), each labeled with a different fluorophore

(**Figure 3.5**). These hydrogels were sequentially exposed to masked UV light and reducing conditions, and imaged *via* fluorescent confocal microscopy (Method A30). Each region responded to external cues as engineered, degrading only when the proper set of input conditions had been presented. To demonstrate cytocompatible gelation and multi-stimuli-responsive degradation, an analogous experiment was performed with each region containing encapsulated hS5 bone marrow-derived stromal cells that constitutively express a different fluorescent protein. Cells were released from gels following sequential masked light exposure, reducing conditions, and flood illumination, harvested after each treatment, and analyzed by flow cytometry. Each treatment yielded a distinct cell collection matching the expected color composition (Method A31). Encapsulated cells were also shown to be viable when released through each stimulus, demonstrating whole process cytocompatibility (Figure A12). This material system, which yields sequential and environmentally triggered release of multiple cell lines in well-defined combinations, represents the most advanced live-cell delivery platform to date.

3.4 Discussion

Although we have first implemented our logic-gated approach to control biomaterial degradation using SPAAC-based PEG hydrogels that respond to reductant, enzyme, and light inputs, these general methodologies should be readily extendable to different stimuli-labile moieties, polymer compositions, and gelation chemistries. We hypothesize that these logic-based strategies can be extended to covalently tether other small molecules, peptides, proteins, polysaccharides, and nucleic acids to a non-degradable hydrogel *via* a stimuli-responsive linker, affording precise biochemical presentation through environmentally triggered controlled release of bioactive species.

Another potential benefit of our approach stems from the ability to tailor the "propagation delay"—the time required to transduce input signals into the appropriate functional output—of the Boolean operator for different therapeutic applications. For these logic-based materials, gate delay is governed by the susceptibility of each labile region to its relevant input, overall construct size/geometry, and the concentrations of the environmental cues triggering degradation. The degradation rate of a linkage to a given input may be tuned over several orders of magnitude, for example by modifying substituents on photodegradable groups or substituting single amino acids within enzyme-labile peptide sequences[29,141–143]. The propagation delay can be further decreased by formulating materials into geometries where response is reaction-limited rather than diffusion-limited. Careful choice of construct geometry and stimuli-labile group identity enables user-specified control over material response rates.

Capitalizing on this platform's unique capacity to govern material properties in response to combinations of both exogenous user-specified spatiotemporal cues (e.g., light) and endogenous cell-produced signals (e.g., enzymes, reductants) may enable new advances in 3D cell culture and tissue engineering. In one envisioned application, user-specified material photodegradation can be performed within E∨P gels to generate customizable vasculature[100] within a synthetic environment that supports enzyme-mediated matrix remodeling and long-term cell survival. In another, cells encapsulated within a photopatterned E∧P material will only undergo cell-mediated spreading within user-defined gel regions; we anticipate that such combined user and cellular control over the culture microenvironment will provide unique opportunities towards directing 4D stem cell differentiation[62,144,145].

Here we have introduced the first modular approach to engineer materials with tailored, user-specified, logic-based responsiveness to environmental cues. By controlling the molecular architecture and connectivity of multiple stimuli-labile moieties within discrete peptide-based crosslinkers, we have endowed biomaterials with unprecedented computational capacity through hierarchical combinations of Boolean YES/OR/AND gates. Having exhaustively synthesized crosslinkers that are each uniquely sensitive to combinations of three orthogonal inputs (i.e., enzyme, reduction, light), we have shown that constructs exhibit expected behavior spanning molecular and macroscopic scales. We have utilized these platforms to demonstrate the first sequential and spatiotemporally varied delivery of multiple cell lines from a single gel, as well as the controlled release of a functional chemotherapeutic in response to disease-associated cues. We expect that these platforms will find great utility in targeted drug delivery, where release of therapeutics, proteins, and cells can be confined to sites of disease with high selectivity, as well for applications in diagnostics, tissue engineering, and regenerative medicine.

3.5 Methods

3.5.1 *Synthesis and characterization logical crosslinkers*

For complete details of all logical crosslinker syntheses and characterization, see Methods A1-A21. Briefly, peptides were generated by standard microwave-assisted Fmoc solid-phase peptide synthesis (CEM Liberty 1) and purified using reversed-phase high-pressure liquid chromatography (RP-HPLC, Dionex Ultimate 3000, C18 column). Peptide-based crosslinkers were characterized *via* MALDI-TOF mass spectrometry (Bruker AutoFlex II).

3.5.2 *Assessing solution-based crosslinker degradation in response to external stimuli*

Each crosslinker species (40 nmol) was dissolved in MMP buffer (110 μL, 200 mM sodium chloride, 50 mM tris, 5 mM calcium chloride, 1 μM zinc chloride, pH adjusted to 7.5 with hydrochloric acid) and exposed to each unique combination of enzyme, reductive, and light.

Samples receiving the reductive input ($_R$) were treated with tris(2-carboxyethyl)phosphine hydrochloride (TCEP·HCl, 200 nmol) and all samples were incubated overnight (37 °C). To quench any unreached TCEP, these samples were further treated with hydroxyethyl disulfide (HEDS, 500 nmol) and incubated (4 hr, 37 °C). Samples receiving the enzyme input ($_E$) were then treated with MMP-8 (5 μL, 0.2 mg mL^{-1} in MMP buffer) and all samples were incubated overnight (37 °C). Samples receiving the light input ($_P$) were subsequently exposed to UV light (λ = 365 nm, 10 mW cm^{-2} incident light, 60 minutes). All samples were diluted with acetonitrile/water (80:20, 100 μL) containing trifluoroacetic acid (0.1%) and characterized by MALDI-TOF; mass-to-charge ratios (m/z) of treated species were compared to expected products (Figures A1-A9). Complete experimental detail is provided in Method A24.

3.5.3 *In situ rheology of hydrogel formation*

Oscillatory rheological analysis (Anton Paar MCR301) was performed with a cone and plate geometry (25 mm diameter, 1° cone) at 25 °C and 25 Hz with a 1% strain (conditions identified to be in the viscoelastic region). The E∧P crosslinker was pre-treated with each combination of MMP ($_E$) and/or light ($_P$), as described above. A hydrogel precursor solution of PEG-tetraBCN (2 mM) and pre-treated E∧P crosslinker (4 mM) in MMP buffer was reacted *in*

situ, G' and G" were monitored for 120 minutes. Complete experimental detail is provided in Method A25.

3.5.4 *Logic-based hydrogel degradation in response to sequential stimuli*

Fluorescent hydrogels (10 μL) were formulated in microcentrifuge tubes from a precursor solution of PEG-tetraBCN-AF568 (2 mM) and a logical peptide crosslinker (4 mM) in MMP buffer (reacted 60 minutes, 25 °C). Hydrogels were washed in MMP buffer. Every logical material was treated with each unique input combination in experimental triplicate, as described above. The extent of gel degradation was assessed through supernatant fluorescence quantification (SpectraMax M5, excitation: 570 nm, emission: 610 nm, emission cut-off filter: 590 nm). Complete experimental detail is provided in Method A27.

3.5.5 *In vitro cellular response to environmentally triggered degradation of a doxorubicin containing hydrogel*

Hydrogels (15 μL) were formulated with DOX (1 mM) from a precursor solution of PEG-tetraBCN (2 mM) and the RΛE-DOX linker (4 mM, Method A29) in a 4-(2-hydroxyethyl)-1-piperazineethanesulfonic acid) (HEPES) buffer (5 mM HEPES, 3 mM $CaCl_2$, 5 μM $ZnCl_2$). Gels were washed with HEPES buffer and treated with each set of relevant inputs in experimental triplicate. Hydrogel supernatant was collected and diluted (1:1) with 2x Dulbecco's Modified Eagle's medium. HeLa cells were cultured in this mixture (170 μL) in a 96-well plate for 48 hours (beginning 24 hours after HeLa seeding at 2 x 10^3 cells $well^{-1}$), upon which cellular double-stranded DNA content was quantified with a PicoGreen® Assay (ThermoFisher). Complete experimental detail is provided in Method A29.

3.5.6 *Multi-logic hydrogel treatment and visualization*

Hydrogels (130 μm thickness) were formulated with three distinct logically degradable regions, each labeled with a unique fluorophore: 1) R∧P crosslinker with AF568, 2) P crosslinker with FAM, and 3) R∨P crosslinker with Cyanine5.

Hydrogels were imaged *via* fluorescent confocal microscopy. Preformed tri-color gels were exposed to UV light (λ = 365 nm, 10 mW cm^{-2} incident light, 10 minutes) through a slitted photomask (alternating 200 μm wide lines and spaces) and imaged. Gels were subsequently treated with 2-mercaptoethanol [BME, 0.25 mM in 50 mL phosphate-buffered saline (PBS), 45 minutes, 25 °C] and imaged. Complete experimental detail is provided in Method A30.

3.5.7 *Hydrogel-encapsulated cell release studies*

Hydrogels (130 μm thickness) were formulated with three distinct logically degradable regions, each encapsulating an hS5 cell line (40 x 10^6 cells mL^{-1}) that stably expresses a unique fluorescent protein: 1) R∧P crosslinker with hS5-$mCherry^+$, 2) P crosslinker with hS5-GFP^+, and 3) R∨P crosslinker with hS5-BFP^+. Cell-laden hydrogels were incubated overnight in media (RPMI-1640, 10% fetal bovine serum, 1% Penicillin-Streptomycin). Hydrogels were treated sequentially with light and reducing conditions, and imaged as described above.

Following each degradative step, released cells were collected and fixed (4% formaldehyde). Flow cytometry was performed on released cell populations (BD Biosciences LSR II Flow Cytometer). Forward scattering, side scattering, and the fluorescence corresponding to

each protein were recorded for each event. Complete experimental and analytical details are provided in Method A31.

3.5.8 *Cell viability following hydrogel encapsulation and triggered release*

hS5 cells (40 x 10^6 cells mL^{-1}) were encapsulated within each single-input responsive hydrogel (130 μm thick, either R, E, or P) in experimental triplicate, and stored in media for one hour. To induce gel degradation, R gels were treated with BME (0.25 mM in PBS, 37 °C, 45 minutes); P gels were exposed to UV light (λ = 365 nm, 10 mW cm^{-2}, 10 minutes); E gels were treated with MMP-8 (0.20 nM in RPMI, 37 °C, 60 minutes). Cells were collected, stained with a Live/Dead® assay (Invitrogen), and imaged (Nikon Eclipse TE2000-U). Cell viability was determined by standard image analysis. Complete experimental detail is provided in Figure A12.

3.6 Figures

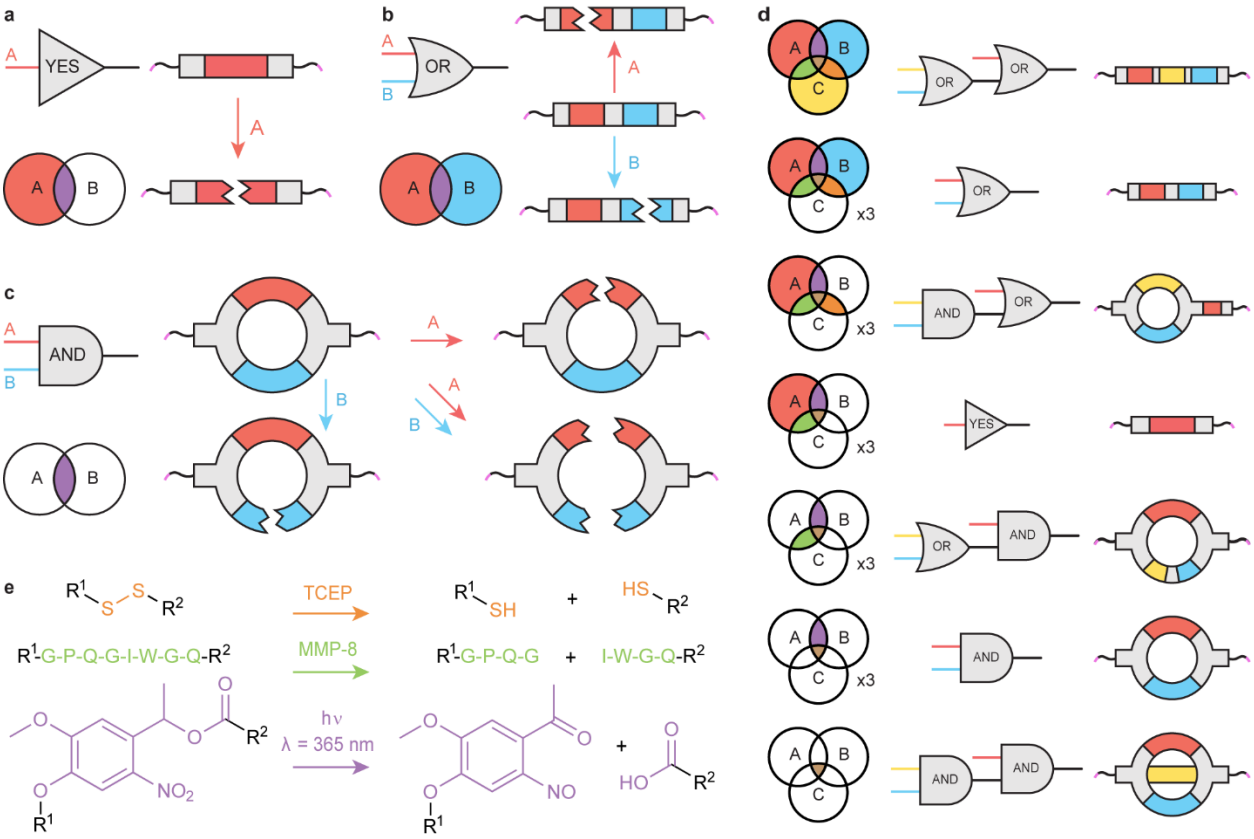

Figure 3.1: Rationally designed crosslinker architecture enables logic-based material degradation.

(**a**) The YES-gate material crosslinker contains a single stimuli-labile moiety (red). Presence of the corresponding chemical input cleaves this moiety, breaking covalent linkage between molecular endpoints (pink) to yield material degradation. Each region of the Venn diagram corresponds to a unique combination of inputs and indicates whether the material is expected to degrade (colored) or remain intact (white). (**b**) The OR-gate crosslinker contains two different stimuli-labile moieties (red and blue) connected in series. The presence of either relevant input cleaves the crosslinker, resulting in material degradation. (**c**) The AND-gate crosslinker contains two different stimuli-labile moieties (red and blue) connected in parallel. The presence of a single programmed input cleaves one linker arm but does not fully sever the crosslink, leaving material crosslinking density and mechanical properties unchanged. (**d**) Logic gates can be hierarchically combined to generate higher-order logical responses. Seventeen unique materials can be generated by combining three logic gates (YES, OR, AND) with three distinct inputs. (**e**) Reactions depicting cleavage of the stimuli-labile groups: disulfide bonds (orange) are reduced into free thiols, the proteolytically sensitive peptide sequence GPQG↓IWGQ (green) is enzymatically cleaved by MMP, and the *o*NB moiety (purple) undergoes photoscission in the presence of near-UV light (λ = 365 nm).

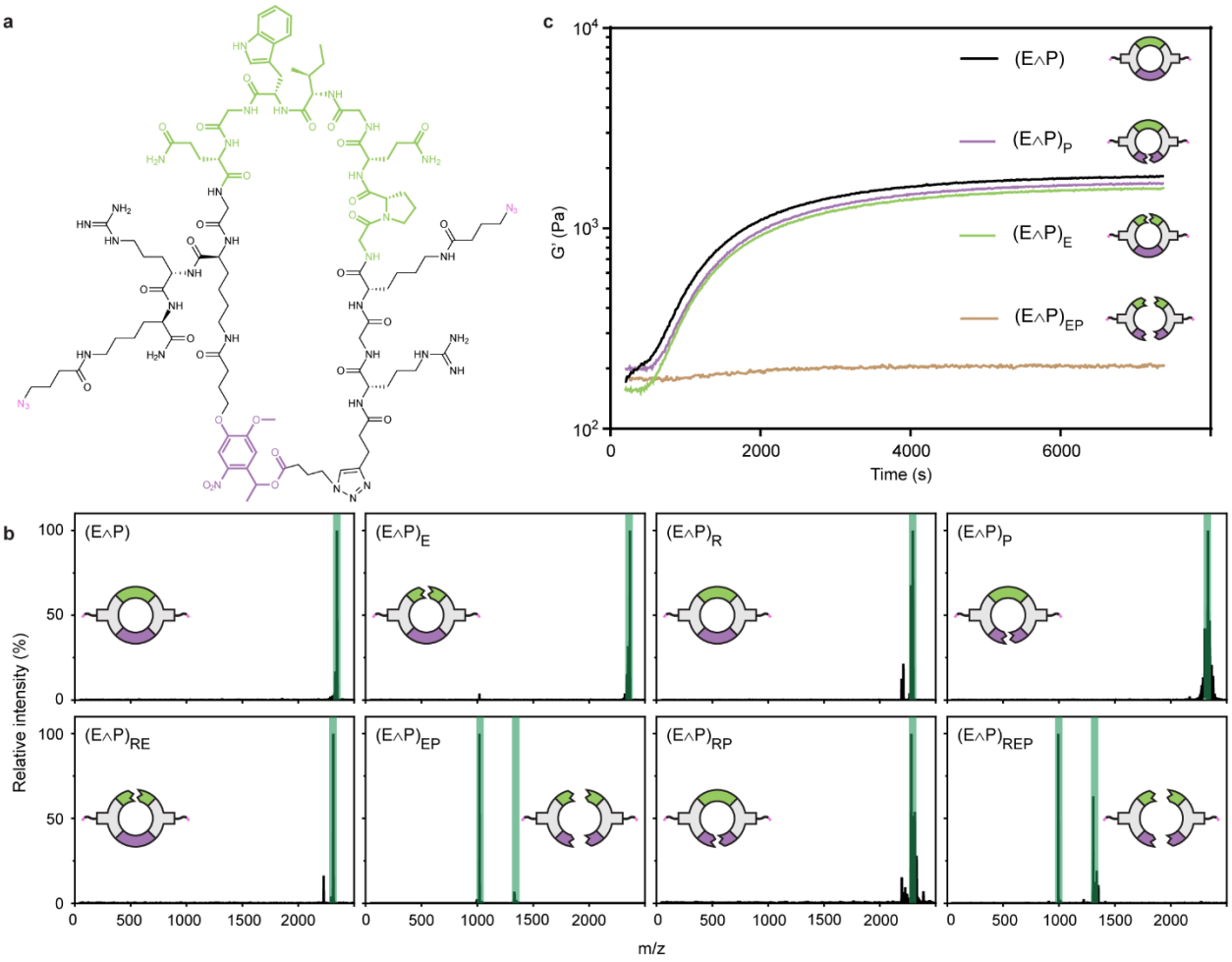

Figure 3.2: Engineered crosslinkers respond to environmental input combinations on the molecular level.

(**a**) The chemical structure of the E∧P crosslinker includes an MMP-degradable peptide sequence (green), a photolabile *o*NB moiety (purple), and two flanking azides (pink) for SPAAC-based hydrogel crosslinking. (**b**) The MALDI-TOF spectra of the E∧P crosslinker after treatment with all unique combinations of enzyme ($_E$), reductive species ($_R$), and light ($_P$) demonstrates correct molecular response followed each input combination. Expected product masses are highlighted in green. (**c**) *In situ* oscillatory rheological analysis of hydrogels crosslinked using treated E∧P demonstrates that AND-gated materials require treatment by both relevant inputs to yield changes in bulk material properties.

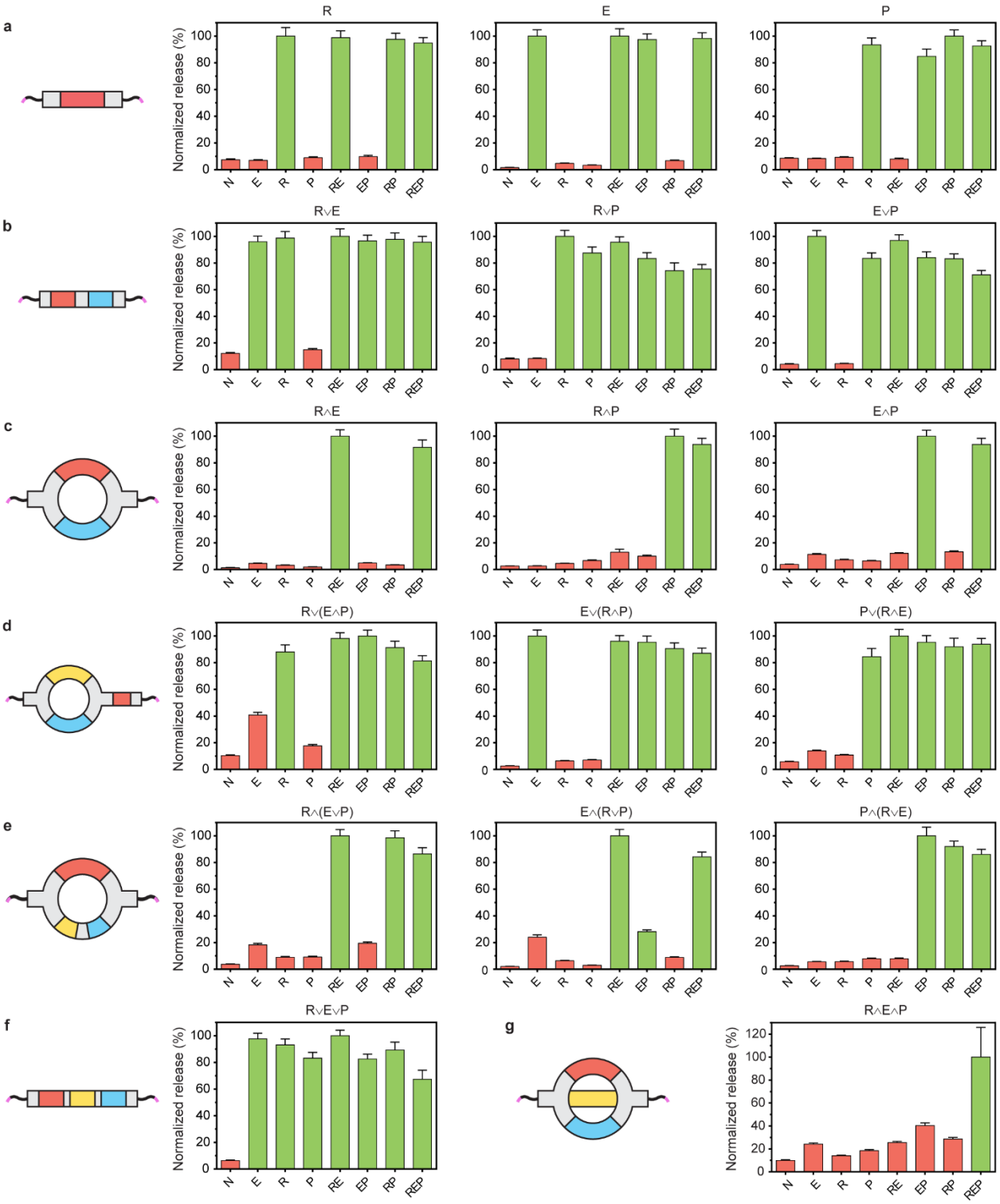

Figure 3.3: Logic-gated biomaterials exhibit programmable degradation in response to environmentally presented input combinations.

(**a**) The response profiles of the single-input YES-gated materials. The response profiles of the two-input (**b**) OR-gated materials and (**c**) AND-gated materials. The response profiles of the

higher-order, three-input (**d**) OR/(AND)-, (**e**) AND/(OR)-, (**f**) OR/OR-, and (**g**) AND/AND-gated materials. Plot titles correspond to crosslinker identity, with x-axis labels indicating material treatment conditions ($_N$ is no treatment, $_E$ is MMP enzyme, $_R$ is a chemical reductant, $_P$ is UV light). Green bars signify conditions expected to result in material degradation; red bars indicate conditions expected not to yield material degradation. Error bars correspond to ± 1 standard deviation about the mean with propagated uncertainties for n = 3 experimental replicates.

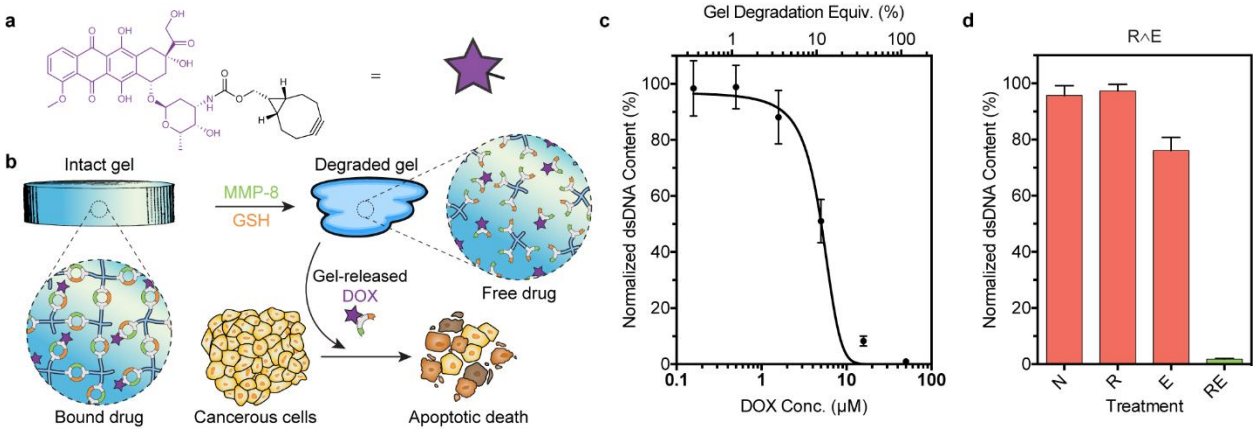

Figure 3.4: Logic-based doxorubicin delivery enhances specificity of HeLa cell death in presence of multiple disease-state hallmarks.

(**a**) The chemical structure of doxorubicin functionalized at the amino group with BCN. (**b**) R∧E hydrogel degradation is triggered in the presence of pathophysiological cues associated with tumor microenvironments: reducing conditions and MMPs. Liberated DOX induces apoptosis in cervical cancer-derived HeLa cells. **(c)** Dose-response curve of HeLa cells following treatment with R∧E-DOX conjugate. (**d**) Normalized dsDNA content after culturing HeLa with released hydrogel components following varying treatments. X-axis label indicates material treatment conditions ($_N$ is no treatment, $_R$ is a chemical reductant, $_E$ is MMP enzyme). Green bars signify conditions expected to result in DOX release though material degradation; red bars indicate conditions expected not to yield material degradation. Error bars correspond to ± 1 standard deviation about the mean for n = 3 experimental replicates.

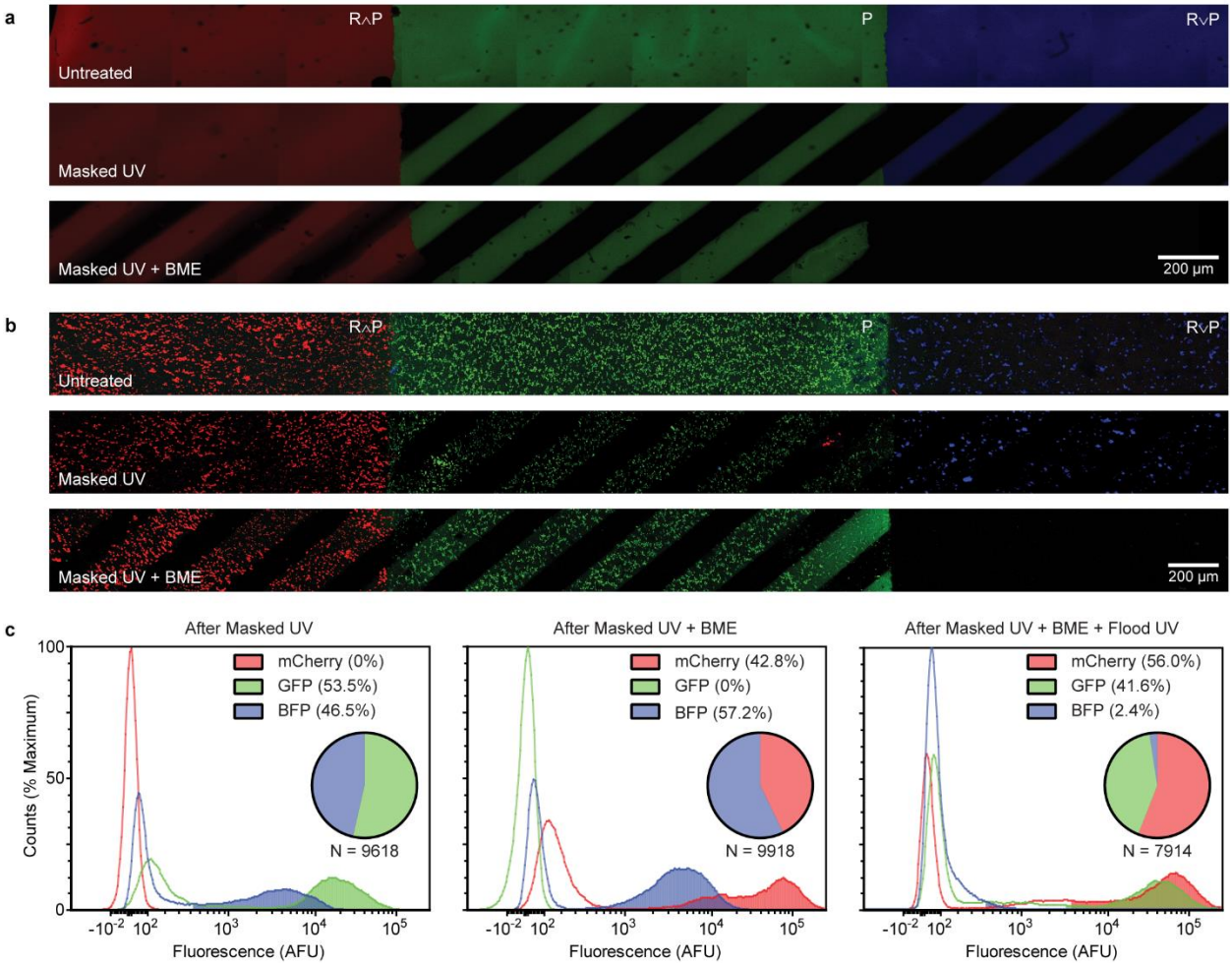

Figure 3.5: Sequential and spatiotemporally varied delivery of small molecules and cells from gels following logic-based response to environmental cues.

(**a**) Spatially segregated regions of fluorescently labeled RΛP (red), P (green), and RVP (blue) were formulated and imaged *via* confocal microscopy following sequential treatments of photomasked light and reducing conditions (β-mercaptoethanol, BME). Each region responded to the cues as engineered, degrading only in the presence of the proper set of input conditions. Scale bar, 200 μm. (**b**) The experiment in panel A was repeated with encapsulated fluorescent cells [hS5 stably transfected to produce mCherry, Green Fluorescent Protein (GFP), and Blue Fluorescent Protein (BFP), respectively replacing the small molecule fluorophores]. Scale bar, 200 μm. (**c**) The cells released from gels in panel B following sequential exposure to photomasked UV light, reducing conditions, and UV light flood exposure were quantified using flow cytometry. Histograms present fluorescence intensity for channels corresponding to each cell line with the shaded regions indicating positively gated cells.

CHAPTER 4: BOOLEAN ENVIRONMENTALLY TRIGGERED ACTIVATION OF CELL-PENETRATING PEPTIDES FOR TARGETED PROTEIN DELIVERY

A manuscript in preparation

4.1 Introduction

Systemically administered therapeutic and imaging agents must cross multiple barriers to reach their biological target, including cell membranes which tightly regulate transcellular transport. Cell-penetrating peptides (CPPs) are short oligopeptide domains that readily facilitate the cellular internalization of attached cargo, including small molecules, proteins, nucleic acids, and nanoparticles[146–148]. While CPPs are small, relatively non-toxic, and exhibit low immunogenicity, their main obstacle to clinical translation is their potent and non-specific cellular uptake which leads to off-target delivery and adverse side-effects[148,149].

While many strategies have been developed to harness CPP activity, the most common approach inhibits CPP activity by appending the construct with bulky polymer chains through stimuli-labile linkers[149–156]. When exposed to a stimulus that cleaves the linker, the polymer chain is selectively released to recover CPP activity. A more elegant alternative, known as the "activatable cell-penetrating peptide" (ACPP), consists of a polycationic CPP domain conjugated to a complementary polyanionic domain through a stimuli-labile linker[32]. When the linker is intact, the polyanionic domain electrostatically associates with the CPP, blocking its activity. Only upon linker cleavage do the two regions dissociate to activate the CPP to induce cellular uptake (**Figure 4.1a**). Compared to the steric approach, ACPPs exhibit superior performance since cargo transport and linker activation are uninhibited by a bulky polymer.

Protease-ACCPs have can selectively partition into tumor and stroke *in vivo* models to enable multi-modal imaging and aide in surgical resection[157–160]; photo-ACPPs permit user-triggered cellular uptake of small molecules, proteins, and nanoparticles[161]; thrombin-ACPPs enable targeted ultrasound contrast agents for the detection of acute thrombosis[162]; oxidative-ACPPs have been developed to detect and image disease-associated reactive oxygen species[163]. All previously reported ACPP systems are responsive only to a single input; however, as single environmental factors are rarely unique to sites of disease, multi-factor control over CPP activation could enhance delivery selectivity[6,8,28]. To achieve this, we employed logical linkers that can integrate multiple environmental signals and perform a Boolean computation to dictate behavior[123]. In this framework, linkers containing two stimuli-labile groups in series function as an OR-gate, activating the CPP in the presence of either cue (**Figure 4.1b**).

Therapeutic proteins are a powerful tool plagued by low delivery efficiency and selectivity, positioning them to maximally leverage ACPP technology[146]. While full-length proteins are conventionally modified using stochastic chemical approaches, site-specifically modified proteins exhibit enhanced and homogenous bioactivity. Since the Boolean logic gate approach can utilize non-natural stimuli-labile groups (e.g. *o*NB) and complex linker architectures, we seek a generalizable strategy for installing any arbitrary ACPP-linker, preferably onto a protein terminus to minimize loss of native protein activity.

Towards this, we identified *Staphylococcus aureus* sortase A, a catalase widely used for post-translational chemoenzymatic protein modification[164]. The transpeptidase heptamutant Sortase A (SrtA-7M, Methods B1-B2) recognizes the sorting peptide motif, “LPETG” and cleaves

between the threonine and glycine residues to form an acyl-enzyme intermediate. A probe containing an N-terminal polyglycine sequence will nucleophilically displace the acyl-enzyme bond, forming a stable amide bond ligating the probe to the protein-of-interest. The site-specific nature of this approach ensures that only the C-terminus is modified with a logical linker and polyanionic domain, completing the ACPP hairpin configuration. Because sortagging permits the installation of arbitrary stimuli-labile moieties, including non-natural functionalities and cyclic architectures, complex Boolean linkers can be employed to control multi-stimuli CPP activation and, subsequently, cellular uptake[165].

4.2 Results

ACPPs were generated by sortagging a protein-of-interest containing a C-terminal polyarginine-LPETG-6xHis domain to a peptide-of-interest containing an N-terminal polyglycine, a central Boolean degradable linker, and a C-terminal polyglutamic acid domain (**Figure 4.1c**). This appends the protein with a C-terminal ACPP with activation governed by a user-defined logical function programmed into the peptide. Superfolder Green Fluorescent Protein (sfGFP) was used as a proof-of-concept so that its native fluorescence could be used to visualize and quantify environmentally triggered cellular uptake and distribution.

Two stimuli-labile chemistries were utilized in the ACPP linkers: *ortho*-nitrobenzyl ester (*o*NB, Method B3), which cleaves upon exposure to near-UV light ($\lambda = 365$ nm) to allow for user-controlled spatiotemporal control[132], and the oligopeptide sequence, GPQG↓IWGQ, which cleaves in the presence of matrix metalloproteases (MMPs) to enable cell- and disease-triggered responsiveness[29] (**Figure 4.1d**). Sortaggable Boolean probes were synthesized using solid-phase peptide synthesis (Methods B4-B7). The single-input YES gate linkers contain one labile group

and activate upon exposure to the relevant stimulus; G_4-*o*NB-E_9 and G_4-GPQGIWGQG-E_9 were denoted ACCP(P) and ACPP(M), respectively. The OR-gate linker contains the two labile groups in series and activates in the presence of either input; G_4-*o*NB-GPQGIWGQG–E_9 is denoted ACPP(MVP). Each peptide construct was used to generate an sfGFP-ACPP through a sortase-mediated reaction (Method B8).

Each sfGFP-ACPP construct was treated with all four relevant environmental conditions—MMP, light, neither, and both—exposed to a culture of HeLa cells, and imaged using confocal microscopy (Methods B9-B10). Cells treated with activated sfGFP-ACPP exhibited homogenous GFP fluorescence throughout their volume (with a nuclear shadow from DAPI), demonstrating intracellular protein transport and distribution (**Figure 4.2a)**. Confocal image analysis (ImageJ) was then used to quantify uptake for each sfGFP-ACPP construct under each treatment condition; CellTracker™ Red was used to map cell boundaries, which were used to measure the mean cellular GFP fluorescent intensity. The enzyme responsive YES-gate exhibited a 2- to 3- fold increase in uptake versus the untreated control when exposed to MMP (p-values = 5×10^{-6} and 5×10^{-7} for the E & EP treated samples, 0.13 for the P treated sample) (**Figure 4.2b**). The photo responsive YES-gate exhibited a 1.5-fold increase in uptake versus the untreated control when exposed to light (p-values = 8×10^{-4} and 2×10^{-6} for the P & EP treated samples, 0.10 for the E treated sample). Photobleaching did not play a significant role in this system (Method B11). These YES-gate constructs validate the ACPP domain's ability to dictate environmentally triggered protein uptake. This result compares with the only other reported protein-ACPP construct, which reported a 2-fold enhancement of avidin uptake when triggered by light[161]. The OR-gate sfGFP-ACPP exhibited a 1.1- to 1.7-fold uptake enhancement upon treatment with light and/or enzyme. While the

enhancement in the MMP treatment condition was statistically significant (p-value = 0.001), the enhancement in the other treatment conditions was not (p-values = 0.43 and 0.19 for the P & EP conditions). The lower selectivity of the OR-gate linker was attributed to its longer length which enabled greater dissociation between the two charged domains, resulting in greater "off-state" uptake. This phenomenon was first predicted during by Tsien et. al. in their rigorous development and optimization of this electrostatic ACPP approach[158].

After successfully validating the Boolean ACPPs with a model fluorescent protein, we sought to apply this technology to a biologically active protein. We identified the chicken anemia virus-derived apoptin, which induces a caspase-mediated apoptosis when localized in the nucleus of cells[166–168]. Apoptin is a promising anti-cancer therapeutic due to its enhanced nuclear localization in cancerous cells compared normal cells and a requisite threshold concentration to induce a cellular response, which minimizes induced apoptosis in healthy cells[168,169]. Furthermore, it has been shown that fusing a CPP to apoptin is effective at transfecting cells and does not hinder its nuclear localization or native bioactivity[169,170].

The still-preliminary protein construct, 10xHis-DSB-Apoptin-R_9-LPETG, was recombinantly expressed and purified (Methods B1-B2) prior to sortase-mediated ligation to generate apoptin-R_9-LPETGGG and apoptin-ACPP(P) (Method B8). Apoptin-R_9-LPETGGG was incubated with HeLa cells at various concentrations for 48 hours, and cell viability was quantified using PicoGreen™ (**Figure 4.3a**). The viability curve shows a dose-dependent apoptin-induced apoptosis, though optimization of initial cell density and treatment time will enhance the range of biological outcomes. Apoptin-ACPP(P) was synthesized on a small scale, in which the final

concentration was unknown but < 0.12 mg/mL. Compared to controls, HeLa cells treated with both the unexposed and photoexposed apoptin-ACPP(P) constructs exhibited reduced viability (66 ± 4 % and 56 ± 3 %; p-values = 3 x 10^{-7} and 4 x 10^{-9}, respectively) (**Figure 4.3b**). Importantly, there is a significant enhancement in cellular uptake and biological activity of environmentally activated apoptin in the triggered state compared to the untriggered state (p-value = 0.03). However, the untriggered, "off-state" apoptin-ACPP showed significant biological activity and cell-death. Optimization of this system, including treatment concentrations and linker identity, could achieve a more Boolean response profile.

4.3 Conclusions

In this chapter, we apply Boolean responsive linkers to enable the environmentally triggered cellular uptake of proteins. By linking a cationic cell-penetrating peptide domain to an anionic "cage" via a Boolean degradable linker, the bioactivity of the CPP domain is recovered upon the stimuli-triggered linker cleavage. A hybrid approach of protein engineering and peptide synthesis enabled site-specific ACPP installation onto the C-terminus of the protein-of-interest. We created three unique Boolean responsive ACPP domains: a YES-gate responsive to MMP, a YES-gate responsive to light, and the OR-gate responsive to both. Environmentally triggered activation was validated and quantified using sfGFP, demonstrating up to a 3-fold enhancement in cell uptake in the triggered state. Apoptin-ACPP, which requires nuclear localization to induce cell death, also exhibited increased biological activity and apoptosis upon environmentally triggered linker cleavage. These methods could provide a blueprint for harnessing the potent CPPs to enable modular, environmentally triggered therapeutic protein delivery.

4.4 Figures

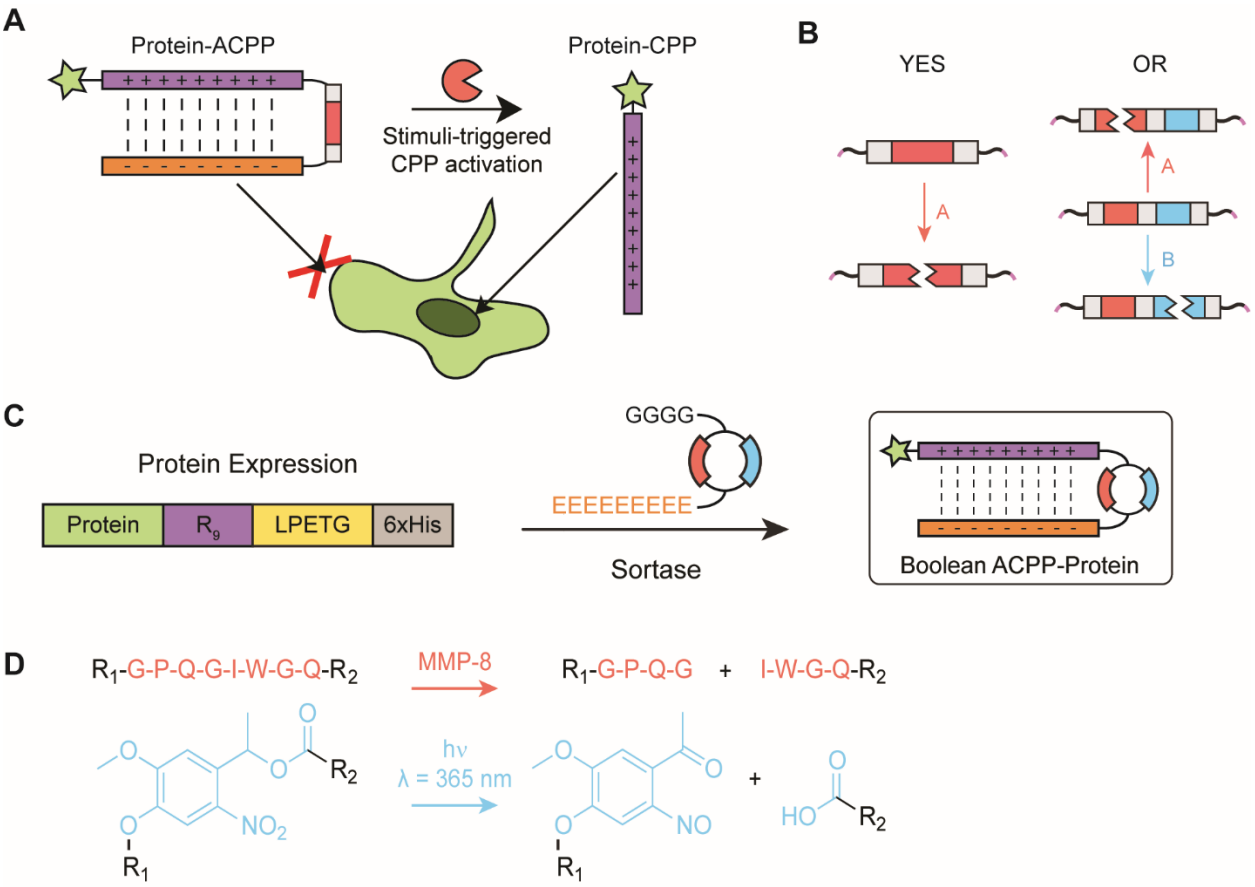

Figure 4.1: An overview of proteins with logically activated activatable cell-penetrating peptides to enable environmentally triggered cellular uptake.
(a) The ACPP-protein construct cannot undergo CPP-mediated cellular internalization until the linker (red) is cleaved by environmental signals, liberating the CPP (purple) from its electrostatic shield (orange). **(b)** The arrangement of stimuli-labile groups (red, blue) within the linker architecture dictates the Boolean function and can generate YES and OR logic gates. **(c)** ACPP-protein constructs are generated when a recombinant protein and logically degradable peptide are fused with a sortase-mediated ligation. **(d)** Reactions depicting cleavage of the stimuli-labile groups: the proteolytically sensitive peptide sequence GPQG↓IWGQ (red) is enzymatically cleaved by MMP, and the oNB moiety (blue) undergoes photoscission in the presence of near-UV light ($\lambda = 365$ nm).

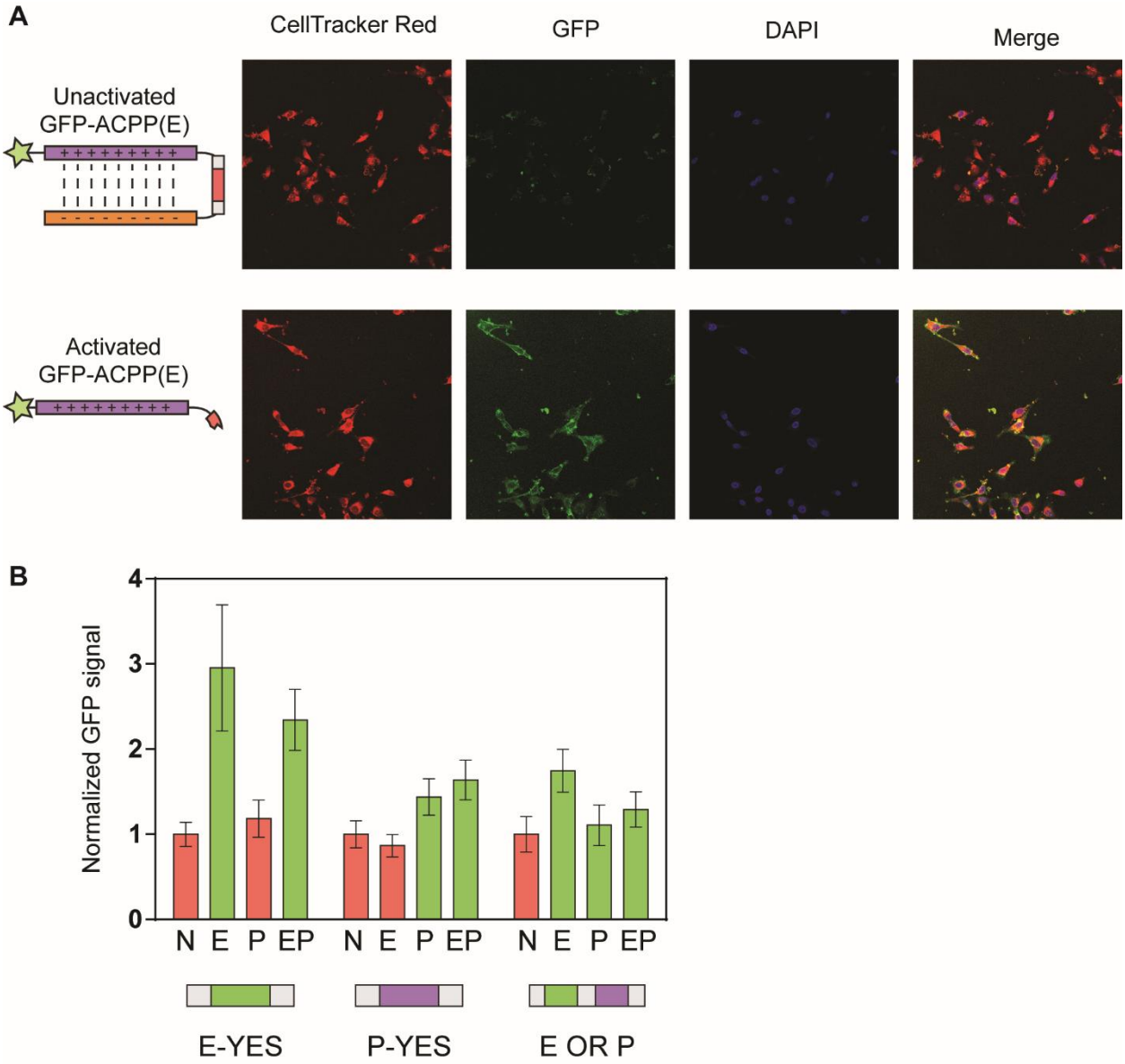

Figure 4.2: ACPP constructs enable Boolean control over protein uptake in response to light and enzyme

(a) Confocal microscopy images of HeLa cells treated with sfGFP-ACPP(E), with and without exposure to MMP. The red, green, and blue channels correspond respectively to CellTracker Red™, sfGFP, and DAPI. **(b)** Quantification of sfGFP uptake for each linker/treatment combination. The data was normalized such that the uptake in the non-treated condition is 1, to show the fold enhancement in each condition. Green bars correspond to treatments expected to yield CPP activation; red bars correspond to conditions expected to not yield CPP activation. Error bars correspond to the standard error of mean (n = 9).

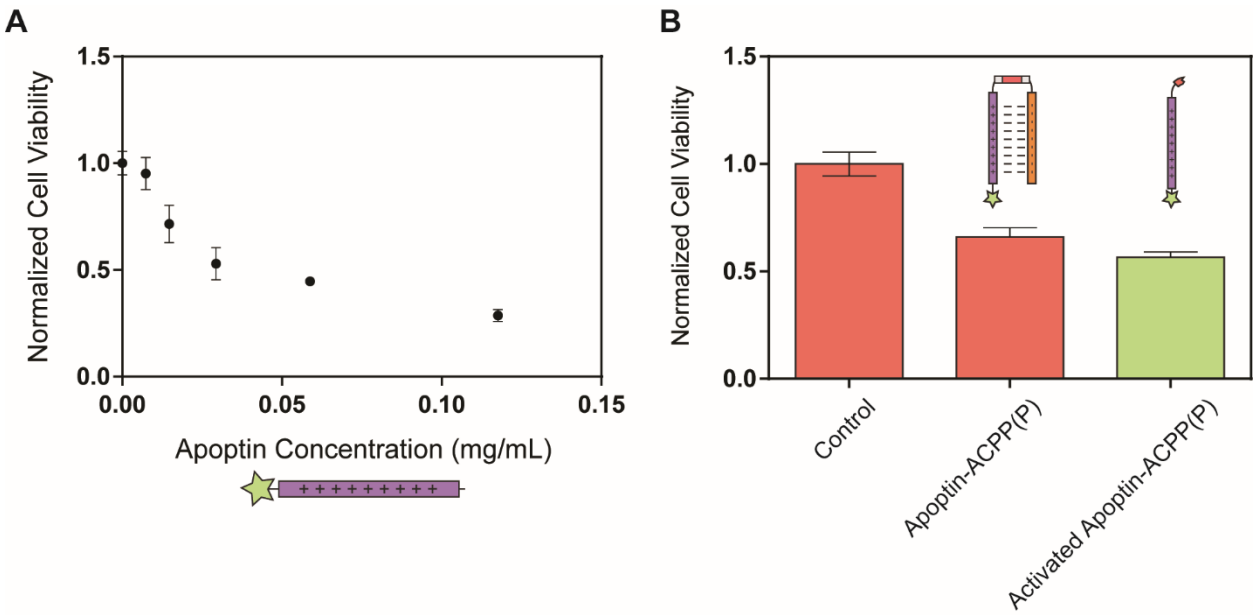

Figure 4.3: Environmentally triggered activation of ACPP-apoptin enhances cellular uptake and cell death

(a) A dose-response curve of HeLa cells treated with apoptin-R_9. Error bars correspond to the standard deviation (n = 3). **(b)** Quantification of cell viability for unactivated and activated apoptin-ACPP(P). Green bar corresponds to treatment expected to yield CPP activation and cell death; red bars correspond to conditions expected to not yield CPP activation or induce cell death. Error bars correspond to the standard deviation (n = 3).

CHAPTER 5: CONCLUSIONS AND FUTURE DIRECTIONS

5.1 Conclusions

Amidst the staggering complexity of biology, our understanding of living systems is constantly growing and evolving. Molecular biology, biochemistry, and genetics are providing unprecedented insight into the fundamental aspects of biological systems, reshaping the underlying framework from which we understand biology and medicine. An emerging mechanistic view of biology, rooted in its constitutive elements—specific cells, genes, proteins, and biochemicals—seeks to understand the complex interactions between these components and suggests vast, unrealized opportunities in medicine.

Successful medical intervention requires a treatment to induce a causal transformation to a living organism. Without biomaterials, our ability to interact with biological systems is quite narrow in scope and precision. Pharmacological compounds are typically administered in a temporally discrete and spatially global manner; *in vivo* drugs are delivered by intravenous injection or oral formulation while *in vitro* cell cultures are homogeneously treated. While surgery allows for some degree of spatial control, it offers limited precision and potentially deleterious side-effects.

Biomaterials enable medical intervention with improved precision, complexity, and nuance. Stimuli-responsive biomaterials can dynamically sense and respond to specific biochemical or biophysical signals. These systems exhibit a reciprocal causation whereby the material simultaneously changes, and is changed by, critical aspects of its biological environment.

A mechanistic understanding of the interactions between biomaterials and biology enables rational design of novel materials that could advance both science and medicine.

This thesis began by recognizing the limitations of existing multi-stimuli-responsive biomaterials. As such systems increase in functional complexity, their ability to respond to complex, multi-stimuli environments sharply decreases. Therefore, we sought to develop a modular framework for creating biomaterials that can sense and integrate multiple environmental signals using Boolean logic to provide a binary output.

In Chapter 3 we formalized this concept by outlining how the structure of a degradable linker is related to its stimuli-responsive behavior[123]. The simplest logical function, the YES gate, is created by including a single stimuli-labile functionality in a linker. We hypothesized that Boolean operations can be built by including a second stimuli-labile group. When these two units are connected in series, the cleavage of either moiety breaks the linker, which functions as an OR-gate; when these two units are connected in parallel, the cleavage of both moieties is required to break the linker, which functions as an AND-gate.

Building these linkers required an advanced synthetic approach to create molecules with many functional groups in a well-defined architecture. Solid-phase peptide synthesis enabled the construction of monodisperse macromolecules with sequence-defined topological connectivity. Stimuli-responsive crosslinkers with two azides would react with a four-arm PEG tetra-BCN via SPAAC click reaction to rapidly generate logically degradable hydrogels in a cytocompatible manner.

Three orthogonal stimuli-labile moieties, each responsive to a different type of environmental factor, were used in this proof-of-concept: 1) the peptide sequence -GPQG↓IWGQ- which is cleaved by the protease, MMP; 2) disulfide bonds, which are broken in a reducing environment; and 3) the *o*NB group, which degrades under UV light. Synthetic methodologies were developed and used to synthesize all nine possible YES, OR, or AND crosslinkers. We subsequently generated and tested degradable hydrogels from each linker, finding that their behavior in these complex environments agrees with our Boolean logical framework. We extended the system to all eight possible three-input, two-operator linkers. These higher-order logical systems also behaved as expected, highlighting the generalizability and modularity of this approach.

Extending this approach beyond degradable hydrogels, we delivered the bioactive chemotherapeutic drug, DOX, from an AND-gated gel responsive to two signals characteristic of the tumor microenvironment. This system shows unprecedented ability to limit drug delivery to environments only with multiple specific cues *in vitro*. Additionally, cells were encapsulated into heterogeneous multi-region logical hydrogels. Living cells were delivered following exposure to relevant combinations of chemical factors, demonstrating the potential for implementation in tissue engineering and cell delivery.

The Boolean degradable linker concepts were adopted by two DeForest group master's thesis students to enable logically triggered release of pendant molecules from non-degradable hydrogels. In both cases, the synthetic strategies developed in Chapter 3 were exploited to generate

OR- and AND- gate logic gates sensitive to combinations of MMP, reductant, and light. In one instance, fluorescein was used as a model hydrophobic small molecule and drug analog; when tethered to a stable hydrogel through a Boolean linker, it exhibited logically triggered release[171]. In another paper, model fluorescent proteins were site-specifically modified with a Boolean degradable linker[165]. These proteins released from the material as expected, demonstrating utility for targeted protein delivery or for cell culture platforms with dynamically tunable biochemical environments.

In Chapter 4, we employed these stimuli-responsive logic-based linkers to harness the potent but mercurial CPPs to facilitate selective, intracellular cargo delivery[32]. In the ACPP framework, a cationic CPP domain is linked to a complementary anionic domain via a stimuli labile linker. CPP activity is electrostatically blocked by the negatively charged region, which dissociates upon linker cleavage to liberate a bioactive CPP. We hypothesized that using Boolean logical linkers could enhance the specificity of the ACPP-mediated cargo delivery.

We created logically responsive protein-ACPP constructs using a sortase-mediated conjugation of a recombinantly expressed protein-R_9-LPETG construct with a peptide containing an N-terminal triglycine attached through a Boolean degradable linker to a C-terminal E_9. Using a model fluorescent protein as our proof-of-concept, we synthesized sfGFP-ACPP constructs that were activated by either MMP or light, as well as the two input OR-gate. These sfGFP-ACPPs exhibited enhanced cellular uptake in the presence of the relevant environmental cues in the first reported demonstration of multi-stimuli-responsive ACPPs.

5.2 Future work: Fundamental

This thesis outlines the development of a multi-stimuli-responsive Boolean logical biomaterial platform and its application to delivery, tissue engineering, and sensing. Given its initial successes, we will speculate about its future here. We suggest how this system could be improved, better characterized, and expanded, and follow with a discussion of promising opportunities for these logical linkers in both science and medicine.

Peptides were a practical choice for the basis of the proof-of-concept logical linkers; the maturation of SPPS technology has led to widespread commercialization of equipment and reagents, providing a flexible platform for rapid linker prototyping. While peptides are expedient for laboratory scale synthesis and research, other systems should be explored for medical and industrial applications. Peptides are inherently bioactive and may exhibit unintended reactivity in living systems. Other polymers, including peptoids or synthetics, may allow for more stable linkers *in vivo.* Alternative platforms might also prove more scalable or economical.

The logical linkers presented in Chapter 3 respond to combinations of enzyme, reductant, and light. However, these are just a few of the stimuli-labile bonds used in biomaterials. Other commonly used triggers include: water (and by proxy, time), various wavelengths of light, pH, oxidation, reduction, and additional enzymes such as thrombin, phospholipidases, and cathepsins. Logical materials responsive to alternative inputs could be created simply by substituting different labile groups within the framework of the logical molecular structures. However, for some of the more advanced linkers containing certain stimuli-sensitive moieties, it may prove challenging to find tractable synthetic routes. Complex molecular architectures require a long series of reactions;

at each step the inherently unstable labile groups can potentially break down. Realizing certain linkers may require some ingenuity in their design and synthesis.

The scope and performance of our logical material platform is fundamentally limited by the availability of stimuli-labile groups. To use an environmental input as a trigger requires a corresponding functional group that will cleave in response to this cue. Even then, its implementation into logical materials depends on the chemistry's orthogonality towards other native biochemicals, sensitivity towards its environmental trigger, and degradation kinetics. Despite extensive development, the catalog of existing chemistries captures only a small subset of important environmental signals. If stimuli-labile chemistries could target specific signals from biology—aspects of the genome, transcriptome, and proteome—they could enable unprecedented user-control over *in vivo* materials. One can also imagine labile groups capable of sensing the magnitude of a biochemical signal, and using this non-binary information to further refine the material response. However, there is no obvious path to drastically improve the state of stimuli-labile chemistry; to achieve this aim we may need to revisit underlying assumptions and explore unconventional bonds and cascade reactions.

Thus far, we have described the molecular logic gates using a reductionist approach that does not describe critical dynamic and non-ideal behaviors. Stimuli-labile cleavage events are the underlying mechanism by which environmental signals are transduced and encoded into a binary material state. These bonds store the system's "memory" and perform a Boolean computation in accordance with the linker structure (**Figure 5.1**). The analog-to-digital conversion is dependent on: 1) the magnitude of the relevant stimulus; 2) the length of exposure to the stimulus; and 3) the

local chemical environment. Electrical engineers model the analog-to-digital conversion using transfer functions, which mathematically describe the binary digital state as a function of the analog inputs.

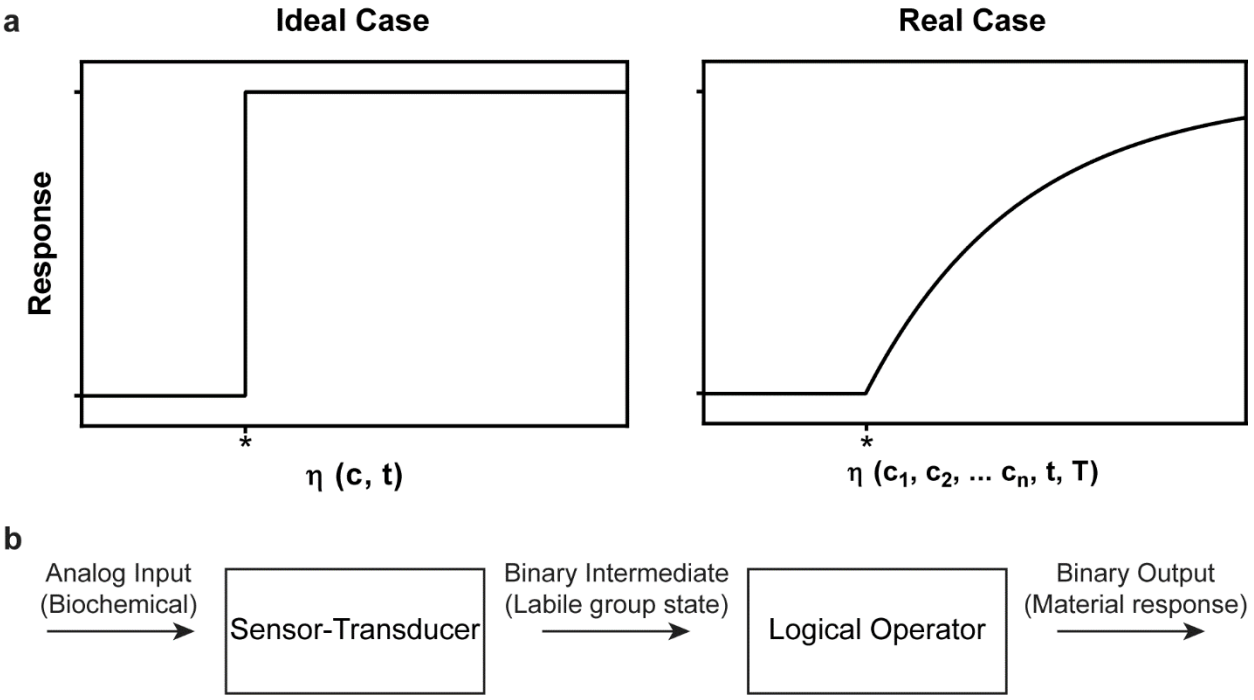

Figure 5.1: Using transfer functions to model the dynamic and non-ideal behaviors of stimuli-responsive biomaterials.
(**a**) A comparison of ideal and real system behaviors, where η is a non-dimensional function of all physically meaningful variables. In the ideal case, the response is triggered instantaneously upon stimulus presentation (denoted as *); in the real case, the response depends upon the input concentrations (c_n), reaction time (t), temperature (T), and any other relevant variables. (**b**) The analog input signal is sensed, transduced, and stored as a binary intermediate in the labile-bonds of the linker. These intermediate values are operated on in accordance with the linker architecture to provide a binary material output.

Transfer functions should be informed by the underlying molecular phenomena, including kinetics and transport. Crude models may only describe how the linker state changes with trigger concentration and exposure time. More advanced models may capture side-reactions, diffusion limitations, or how the chemical environment influences reaction kinetics. By using transfer

functions to model linker dynamics, we might better predict their behavior in complex biological environments. With commensurate advances in sensor miniaturization and data analytics, advanced modeling could enable unprecedented *in silico* tools for designing and validating biomaterials tailored for specific medical applications.

While semiconductors are far better suited to perform complex computations than stimuli-labile peptides, we might draw on the more mature field for useful analogies and inspiration. There are sixteen unique two-input logic functions; a subset of these functions that can be combined to yield all others is known as "functionally complete"[172,173]. The set of YES/OR/AND-gates developed in Chapter 3 can be made functionally complete with the inclusion of the NOT-gate, a logical inverter that converts a signal from "true" to "false", and vice versa. While previous gates were built exclusively with bond breaking, the NOT-gate would require a stimuli-triggered bond forming reaction. A promising strategy for implementing a NOT-gate would be adapting a spontaneous ligation reaction between heterogeneous reaction partners, in which one component is caged to prevent the ligation until a stimulus-induced liberation event. We identified the native chemical ligation between an N-terminal cysteine and a C-terminal thioester as a promising candidate owing to its high yield, favorable kinetics, and absence of byproducts[174–176].

Our efforts to implement logical NOT-gates elucidated many of the limitations inherent to material-based computation. Unlike digital circuits, which can be infinitely and reversibly cycled through their states, the logical linkers do not revert back to their null state upon removal of the stimulus—once a labile bond is cleaved, it typically cannot reform. This physical hysteresis might, for example, cause an AND-gate to trigger upon sequential exposure to environments each

presenting only one of the relevant inputs. Additionally, while digital logic gates respond to stimuli in picoseconds, their mechanical counterparts' response requires seconds to hours depending on the labile group, stimulus magnitude, and material geometry. To build NOT-gates, the workhorse ligation reaction must be both bioorthogonal and have favorable kinetics under native biological conditions. Finally, *in vivo* NOT-gate systems could be rapidly dispersed prior to activation and ligation, preventing material formation from ever occurring. While NOT-gates could be carefully engineered to function in highly idealized abiological environments, given these limitations, we believe their continued development to be quixotic and devoid of practical utility.

Over the course of this thesis, Boolean linkers were used to connect a variety of molecules: polymer-polymer for degradable hydrogels, protein-peptide for modulating CPP activity, and polymer-pendant for hydrogel-based delivery of proteins, fluorophores, and small molecules. All evidence supports the hypothesis that the linkers perform as expected regardless of what they connect. Here we will discuss some of the nearly limitless potential linker configurations. Linkers can be attached to cells to enable dynamic cell-cell or cell-material attachment for tissue engineering applications. Degradable hydrogels could be created from a heterogeneous mixture of degradable and non-degradable linkers, further refining user-directed control over material stiffness. Multiple pendants could be attached to a material, each through a different logical linker, to offer a highly tunable biochemical environment for tissue engineering, or as complex multi-stage delivery vehicles.

5.3 Future work: Translational

Our logical stimuli-responsive biomaterial platform is just a novel curiosity until it meaningfully advances the state of medicine or our understanding of fundamental biological processes. In this section, we will discuss how this technology might be applied towards these aims.

The most obvious translational potential of this system is as a targeted delivery platform for therapeutics and imaging agents. Many of our initial demonstrations—hydrogel degradation, pendant release, and CPP activation—validate mechanisms and behaviors relevant to targeted delivery. The AND-gates offer a flexible and modular route to creating materials that deliver a payload only in the presence of multiple environmental signals, enabling the selective targeting of disease-specific environments. This could improve therapeutic efficiency and efficacy by reducing dosage requirements and reducing unwanted off-target effects.

To enable the systemic circulation necessary for targeted delivery, we must develop methodologies to formulate these materials as nanogels. We are actively working to adapt existing methods for generating step-growth nanogels through emulsion polymerization. Next, animal studies should be undertaken to test and validate the performance of logically responsive nanomaterials *in vivo*. Two of the signals used in the development of this platform are upregulated in the tumor microenvironment—reducing conditions and MMP. A murine tumor model could be used to compare the efficacy of: 1) free DOX, 2) DOX tethered to an MMP-degradable nanogel, 3) DOX tethered to a reductive-degradable nanogel, and 4) DOX tethered to an MMP- AND

reductive-degradable gel. This study will illuminate how these materials perform in a complex biological systems rather than highly controlled *in vitro* environments.

Perhaps more interestingly, these experiments could elucidate the intrinsic value and potential of multi-stimuli-responsive biomaterials. Given this vast dedication of academic labor and resources to developing such materials, the field has yielded surprisingly few successes *in vivo*. Since our AND-gated materials represent the most precise and selective multi-stimuli-responsive system to date, its application to an animal model will be important regardless of the outcome. While a successful *in vivo* result could pave the way towards improvements in targeted delivery, a poor result would demonstrate the diminishing returns gained from targeting multiple stimuli and enable redirection of future resources towards more relevant technologies.

These systems may also find utility in cell culture, both for tissue engineering and fundamental biological studies. Our logically degradable linkers enable unprecedented dynamic control over biomechanical and biochemical properties. The most relevant inputs in this context include light, which allows for user-directed spatiotemporal control, and enzymes, which enable cell-mediated reshaping of their local environment. In tissue engineering, this platform would allow for simultaneous spatiotemporal and biological control over material stiffness, degradation, and biochemical functionalization—critical factors for directing cell fate and function. It could also enable new opportunities to probe underlying biological mechanisms to better understand how dynamic aspects of the local cellular environment influence cell behavior.

Ultimately, the true power and broad potential of this system lies in its modularity. While we can speculate about the ways and applications it might be used, we must also acknowledge its utility in ways we cannot yet envision. The potential of this technology will be realized by biologists and clinicians with specialty expertise, who may find it to be the missing ingredient they need to tackle an open challenge or question. While we anticipate further developing this platform, science is a collective process and we are excited to work with the broader scientific community to achieve its full potential.

CHAPTER 6: BIBLIOGRAPHY

1. Badeau, B. A. & Deforest, C. A. Programming stimuli-responsive behavior into biomaterials. *Annu. Rev. Biomed. Eng.* **21,** 241–265 (2019).

2. Burdick, J. A. & Murphy, W. L. Moving from static to dynamic complexity in hydrogel design. *Nat. Commun.* **3,** 1269 (2012).

3. DeForest, C. A. & Anseth, K. S. Advances in bioactive hydrogels to probe and direct cell fate. *Annu. Rev. Chem. Biomol. Eng.* **3,** 421–444 (2012).

4. Tibbitt, M. W., Rodell, C. B., Burdick, J. A. & Anseth, K. S. Progress in material design for biomedical applications. *Proc. Natl. Acad. Sci.* **112,** 14444–14451 (2015).

5. Li, J. & Mooney, D. J. Designing hydrogels for controlled drug delivery. *Nat. Rev. Mater.* **1,** 16071 (2016).

6. Lu, Y., Aimetti, A. A., Langer, R. & Gu, Z. Bioresponsive materials. *Nat. Rev. Mater.* **2,** 16075 (2016).

7. Hoffman, A. S. Hydrogels for biomedical applications. *Adv. Drug Deliv. Rev.* **64,** 18–23 (2012).

8. Mura, S., Nicolas, J. & Couvreur, P. Stimuli-responsive nanocarriers for drug delivery. *Nat. Mater.* **12,** 991–1003 (2013).

9. Guragain, S., Bastakoti, B. P., Malgras, V., Nakashima, K. & Yamuauchi, Y. Multi-stimuli-responsive polymeric materials. *Chem. Eur. J.* **21,** 13164–13174 (2015).

10. Knipe, J. M. & Peppas, N. A. Multi-responsive hydrogels for drug delivery and tissue engineering applications. *Regen. Biomater.* **1,** 57–65 (2014).

11. Evans, A. C., Thadani, N. N. & Suh, J. Biocomputing nanoplatforms as therapeutics and diagnostics. *J. Control. Release* **240,** 387–393 (2016).

12. Gentile, P., Chiono, V., Carmagnola, I. & Hatton, P. V. An overview of poly(lactic-co-glycolic) acid (PLGA)-based biomaterials for bone tissue engineering. *Int. J. Mol. Sci.* **15,** 3640–3659 (2014).

13. Brannigan, R. P. & Dove, A. P. Synthesis, properties and biomedical applications of hydrolytically degradable materials based on aliphatic polyesters and polycarbonates. *Biomater. Sci.* **5,** 9–21 (2017).

14. Makadia, H. K. & Siegel, S. J. Poly lactic-co-glycolic acid (PLGA) as biodegradable controlled drug delivery carrier. *Polym.* **3,** 1377–1397 (2011).

15. Mirakabad, F. S. T. *et al.* PLGA-based nanoparticles as cancer drug delivery systems. *Asian Pacific J. Cancer Prev.* **15,** 517–535 (2014).

16. Abedalwafa, M., Wang, F., Wang, L. & Li, C. Biodegradable poly-epsilon-caprolactone (PCL) for tissue engineering applications: A review. *Rev. Adv. Mater. Sci.* **34,** 123–140 (2013).

17. Engineer, C., Parikh, J. & Raval, A. Review on hydrolytic degradation behavior of biodegradable polymers from controlled drug delivery system. *Trends Biomater. Artif. Organs* **25,** 79–85 (2011).

18. Schmaljohann, D. Thermo- and pH-responsive polymers in drug delivery. *Adv Drug Deliv Rev* **58,** 1655–1670 (2006).

19. Kanamala, M., Wilson, W. R., Yang, M., Palmer, B. D. & Wu, Z. Mechanisms and biomaterials in pH-responsive tumour targeted drug delivery: A review. *Biomaterials* **85,** 152–167 (2016).

20. Steinhilber, D. *et al.* A microgel construction kit for bioorthogonal encapsulation and pH-controlled release of living cells. *Angew. Chemie Int. Ed.* **52,** 13538–13543 (2013).

21. Bae, Y., Fukushima, S., Harada, A. & Kataoka, K. Design of environment-sensitive supramolecular assemblies for intracellular drug delivery: Polymeric micelles that are responsive to intracellular pH change. *Angew. Chemie - Int. Ed.* **42,** 4640–4643 (2003).

22. Poon, Z., Chang, D., Zhao, X. & Hammond, P. T. Layer-by-layer nanoparticles with a pH-sheddable layer for in vivo targeting of tumor hypoxia. *ACS Nano* **5,** 4284–4292 (2011).

23. Lowman, A. M., Morishita, M., Kajita, M., Nagai, T. & Peppas, N. A. Oral delivery of insulin using pH responsive complexation gels. *J. Pharm. Sci.* **88,** 933–937 (1999).

24. Shalviri, A. *et al.* pH-dependent doxorubicin release from terpolymer of starch, polymethacrylic acid and polysorbate 80 nanoparticles for overcoming multi-drug resistance in human breast cancer cells. *Eur. J. Pharm. Biopharm.* **82,** 587–597 (2012).

25. Weerakkody, D. *et al.* Family of pH (low) insertion peptides for tumor targeting. *Proc. Natl. Acad. Sci.* **110,** 5834–5839 (2013).

26. de la Rica, R., Aili, D. & Stevens, M. M. Enzyme-responsive nanoparticles for drug release and diagnostics. *Adv. Drug Deliv. Rev.* **64,** 967–978 (2012).

27. Hu, Q., Katti, P. S. & Gu, Z. Enzyme-responsive nanomaterials for controlled drug delivery. *Nanoscale* **6,** 12273–12286 (2014).

28. McCawley, L. J. & Matrisian, L. M. Matrix metalloproteinases: Multifunctional contributors to tumor progression. *Mol. Med. Today* **6,** 149–156 (2000).

29. Nagase, H. & Fields, G. B. Human matrix metalloproteinase specificity studies using

collagen sequence-based synthetic peptides. *Pept. Sci.* **40,** 399–416 (1996).

30. Park, Y., Lutolf, M. P., Hubbell, J. A., Hunziker, E. B. & Wong, M. Bovine primary chondrocyte culture in synthetic matrix metalloproteinase-sensitive poly(ethylene glycol)-based hydrogels as a scaffold for cartilage repair. *Tissue Eng.* **10,** 515–522 (2004).

31. Purcell, B. P. *et al.* Injectable and bioresponsive hydrogels for on-demand matrix metalloproteinase inhibition. *Nat. Mater.* **13,** 653–661 (2014).

32. Jiang, T. *et al.* Tumor imaging by means of proteolytic activation of cell-penetrating peptides. *Proc. Natl. Acad. Sci.* **101,** 17867–17872 (2004).

33. Maitz, M. F. *et al.* Bio-responsive polymer hydrogels homeostatically regulate blood coagulation. *Nat. Commun.* **4,** 2168 (2013).

34. Rao, J. & Khan, A. Enzyme sensitive synthetic polymer micelles based on the azobenzene motif. *J. Am. Chem. Soc.* **135,** 14056–14059 (2013).

35. Wu, G., Fang, Y.-Z., Yang, S., Lupton, J. R. & Turner, N. D. Glutathione metabolism and its implications for health. *J. Nutr.* **134,** 489–492 (2004).

36. Kuppusamy, P. *et al.* Noninvasive imaging of tumor redox status and its modification by tissue glutathione levels. *Cancer Res.* **62,** 307–312 (2002).

37. Mittal, M., Siddiqui, M. R., Tran, K., Reddy, S. P. & Malik, A. B. Reactive oxygen species in inflammation and tissue injury. *Antioxidants Redox Signal.* **20,** 1126–1167 (2014).

38. Nguyen, D. H., Choi, J. H., Joung, Y. K. & Park, K. D. Disulfide-crosslinked heparin-pluronic nanogels as a redox-sensitive nanocarrier for intracellular protein delivery. *J. Bioact. Compat. Polym.* **26,** 287–300 (2011).

39. Wen, H.-Y. *et al.* Rapidly disassembling nanomicelles with disulfide-linked PEG shells for glutathione-mediated intracellular drug delivery. *Chem. Commun.* **47,** 3550–3552 (2011).

40. Kurtoglu, Y. E. *et al.* Poly(amidoamine) dendrimer-drug conjugates with disulfide linkages for intracellular drug delivery. *Biomaterials* **30,** 2112–2121 (2009).

41. Thambi, T. *et al.* Hypoxia-responsive polymeric nanoparticles for tumor-targeted drug delivery. *Biomaterials* **35,** 1735–1743 (2014).

42. Wilson, D. S. *et al.* Orally delivered thioketal nanoparticles loaded with TNF-α-siRNA target inflammation and inhibit gene expression in the intestines. *Nat. Mater.* **9,** 923–928 (2010).

43. Napoli, A., Valentini, M., Tirelli, N., Müller, M. & Hubbell, J. A. Oxidation-responsive polymeric vesicles. *Nat. Mater.* **3,** 183–189 (2004).

44. Yang, T., Ji, R., Deng, X.-X., Du, F.-S. & Li, Z.-C. Glucose-responsive hydrogels based on dynamic covalent chemistry and inclusion complexation. *Soft Matter* **10,** 2671–2678 (2014).

45. Gu, Z. *et al.* Glucose-responsive microgels integrated with enzyme nanocapsules for closed-loop insulin delivery. *ACS Nano* **7,** 6758–6766 (2013).

46. Mo, R., Jiang, T. & Gu, Z. Enhanced anticancer efficacy by ATP-mediated liposomal drug delivery. *Angew. Chemie Int. Ed.* **53,** 5815–5820 (2014).

47. Mo, R., Jiang, T., DiSanto, R., Tai, W. & Gu, Z. ATP-triggered anticancer drug delivery. *Nat. Commun.* **5,** 3364 (2014).

48. Naito, M. *et al.* A phenylboronate-functionalized polyion complex micelle for ATP-triggered release of siRNA. *Angew. Chemie Int. Ed.* **51,** 10751–10755 (2012).

49. Biswas, S. *et al.* Biomolecular robotics for chemomechanically driven guest delivery fuelled by intracellular ATP. *Nat. Chem.* **5,** 613–620 (2013).

50. Ohta, S., Glancy, D. & Chan, W. C. W. DNA-controlled dynamic colloidal nanoparticle systems for mediating cellular interaction. *Science* **351,** 841–845 (2016).

51. Zhang, P. *et al.* DNA-hybrid-gated multifunctional mesoporous silica nanocarriers for dual-targeted and microRNA-responsive controlled drug delivery. *Angew. Chemie* **126,** 2403–2407 (2014).

52. Korin, N. *et al.* Shear-activated nanotherapeutics for drug targeting to obstructed blood vessels. *Science* **337,** 738–742 (2012).

53. Anselmo, A. C. *et al.* Platelet-like nanoparticles: Mimicking shape, flexibility, and surface biology of platelets to target vascular injuries. *ACS Nano* **8,** 11243–11253 (2014).

54. Heskins, M. & Guillet, J. E. Solution properties of poly(N-isopropylacrylamide). *J. Macromol. Sci. A* **2,** 37–41 (1968).

55. Roy, D., Brooks, W. L. A. & Sumerlin, B. S. New directions in thermoresponsive polymers. *Chem. Soc. Rev.* **42,** 7214–7243 (2013).

56. Kim, Y.-J. & Matsunaga, Y. T. Thermo-responsive polymers and their application as smart biomaterials. *J. Mater. Chem. B* **5,** 4307–4321 (2017).

57. Bai, X. *et al.* Self-reinforcing injectable hydrogel with both high water content and mechanical strength for bone repair. *Chem. Eng. J.* **288,** 546–556 (2016).

58. Matsuda, N., Shimizu, T., Yamato, M. & Okano, T. Tissue engineering based on cell sheet technology. *Adv. Mater.* **19,** 3089–3099 (2007).

59. Meyer, D. E. & Chilkoti, A. Purification of recombinant proteins by fusion with

thermally-responsive polypeptides. *Nat. Biotechnol.* **17,** 1112–1115 (1999).

60. Nettles, D. L., Chilkoti, A. & Setton, L. A. Applications of elastin-like polypeptides in tissue engineering. *Adv. Drug Deliv. Rev.* **62,** 1479–1485 (2010).

61. Ruskowitz, E. R. & DeForest, C. A. Photoresponsive biomaterials for targeted drug delivery and 4D cell culture. *Nat. Rev. Mater.* **3,** 17087 (2018).

62. DeForest, C. A. & Tirrell, D. A. A photoreversible protein-patterning approach for guiding stem cell fate in three-dimensional gels. *Nat. Mater.* **14,** 523–531 (2015).

63. de Garcia Lux, C. *et al.* Short soluble coumarin crosslinkers for light-controlled release of cells and proteins from hydrogels. *Biomacromolecules* **16,** 3286–3296 (2015).

64. Wang, Y. *et al.* Photocontrolled self-assembly and disassembly of block ionomer complex vesicles: A facile approach toward supramolecular polymer nanocontainers. *Langmuir* **26,** 709–715 (2010).

65. Achilleos, D. S., Hatton, T. A. & Vamvakaki, M. Light-regulated supramolecular engineering of polymeric nanocapsules. *J. Am. Chem. Soc.* **134,** 5726–5729 (2012).

66. Sirsi, S. R. & Borden, M. A. State-of-the-art materials for ultrasound-triggered drug delivery. *Adv. Drug Deliv. Rev.* **72,** 3–14 (2014).

67. Mohan, P. & Rapoport, N. Doxorubicin as a molecular nanotheranostic agent: Effect of doxorubicin encapsulation in micelles or nanoemulsions on the ultrasound-mediated intracellular delivery and nuclear trafficking. *Mol. Pharm.* **7,** 1959–1973 (2010).

68. Cochran, M. C. *et al.* Disposition of ultrasound sensitive polymeric drug carrier in a rat hepatocellular carcinoma model. *Acad. Radiol.* **18,** 1341–1348 (2011).

69. Chertok, B., David, A. E. & Yang, V. C. Polyethyleneimine-modified iron oxide nanoparticles for brain tumor drug delivery using magnetic targeting and intra-carotid administration. *Biomaterials* **31,** 6317–6324 (2010).

70. Bringas, E. *et al.* Triggered release in lipid bilayer-capped mesoporous silica nanoparticles containing SPION using an alternating magnetic field. *Chem. Commun.* **48,** 5647–5649 (2012).

71. Bastakoti, B. P., Guragain, S., Nakashima, K. & Yamauchi, Y. Stimuli-induced core-corona inversion of micelle of poly(acrylic acid)-block-poly(N-isopropylacrylamide) and its application in drug delivery. *Macromol. Chem. Phys.* **216,** 287–291 (2015).

72. Guragain, S., Bastakoti, B. P., Yusa, S. & Nakashima, K. Stimuli-induced core-corona inversion of micelles of water-soluble poly(sodium 2-(acrylamido)-2-methyl propanesulfonate-b-N-isopropylacrylamide). *Polymer (Guildf).* **51,** 3181–3186 (2010).

73. Zhang, Q. & Zhu, S. Oxygen and carbon dioxide dual responsive nanoaggregates of

fluoro- and amino-containing copolymer. *ACS Macro Lett.* **3,** 743–746 (2014).

74. Chen, W. & Du, J. Ultrasound and pH dually responsive polymer vesicles for anticancer drug delivery. *Sci. Rep.* **3,** 2162 (2013).

75. Han, D., Tong, X. & Zhao, Y. Block copolymer micelles with a dual-stimuli-responsive core for fast or slow degradation. *Langmuir* **28,** 2327–2331 (2012).

76. Bai, L., Wang, X., Song, F., Wang, X. & Wang, Y. "AND" logic gate regulated pH and reduction dual-responsive prodrug nanoparticles for efficient intracellular anticancer drug delivery. *Chem. Commun.* **51,** 93–96 (2015).

77. Mahmoud, E. A., Sankaranarayanan, J., Morachis, J. M., Kim, G. & Almutairi, A. Inflammation responsive logic gate nanoparticles for the delivery of proteins. *Bioconjug. Chem.* **22,** 1416–1421 (2011).

78. Huang, Q. *et al.* Light and reductive dual stimuli-responsive PEI nanoparticles: 'AND' logic response and controllable release. *J. Mater. Chem. B* **2,** 3333–3339 (2014).

79. Meng, L. *et al.* Chitosan-based nanocarriers with pH and light dual response for anticancer drug delivery. *Biomacromolecules* **14,** 2601–2610 (2013).

80. Wei, C., Guo, J. & Wang, C. Dual stimuli-responsive polymeric micelles exhibiting 'AND' logic gate for controlled release of adriamycin. *Macromol. Rapid Commun.* **32,** 451–455 (2011).

81. Lv, L.-P., Landfester, K. & Crespy, D. Stimuli-selective delivery of two payloads from dual responsive nanocontainers. *Chem. Mater.* **26,** 3351–3353 (2014).

82. Chen, J. *et al.* pH and reduction dual-sensitive copolymeric micelles for intracellular doxorubicin delivery. *Biomacromolecules* **12,** 3601–3611 (2011).

83. de Graaf, A. J. *et al.* Thermosensitive peptide-hybrid ABC block copolymers obtained by ATRP: Synthesis, self-assembly, and enzymatic degradation. *Macromolecules* **45,** 842–851 (2012).

84. Lyu, D., Chen, S. & Guo, W. Liposome crosslinked polyacrylamide/DNA hydrogel: a smart controlled-release system for small molecular payloads. *Small* **14,** 170439 (2018).

85. Wang, Y. *et al.* Mesoporous silica nanoparticles in drug delivery and biomedical applications. *Nanomedicine Nanotechnology, Biol. Med.* **11,** 313–327 (2015).

86. Liu, X. *et al.* A dual responsive targeted drug delivery system based on smart polymer coated mesoporous silica for laryngeal carcinoma treatment. *New J. Chem.* **38,** 4830–4836 (2014).

87. Chang, B. *et al.* Thermo and pH dual responsive, polymer shell coated, magnetic mesoporous silica nanoparticles for controlled drug release. *J. Mater. Chem.* **21,** 9239–

9247 (2011).

88. Wang, Y. *et al.* Redox and pH dual-responsive mesoporous silica nanoparticles for site-specific drug delivery. *Appl. Surf. Sci.* **356,** 1282–1288 (2015).

89. Chen, C. *et al.* Functional polymeric dialdehyde dextrin network capped mesoporous silica nanoparticles for pH/GSH dual-controlled drug release. *RSC Adv.* **8,** 20862–20871 (2018).

90. Chen, X. *et al.* Dual bioresponsive mesoporous silica nanocarrier as an "AND" logic gate for targeted drug delivery cancer cells. *Adv. Funct. Mater.* **24,** 6999–7006 (2014).

91. Chen, H. *et al.* Dual-pH-sensitive mesoporous silica nanoparticle-based drug delivery system for tumor-triggered intracellular drug release. *J. Mater. Sci.* **53,** 10653–10665 (2018).

92. Angelos, S., Yang, Y.-W., Khashab, N. M., Stoddart, J. F. & Zink, J. I. Dual-controlled nanoparticles exhibiting AND logic. *J. Am. Chem. Soc.* **131,** 11344–11346 (2009).

93. Komatsu, H. *et al.* Supramolecular hydrogel exhibiting four basic logic gate functions to fine-tune substance release. *J. Am. Chem. Soc.* **131,** 5580–5585 (2009).

94. Liu, G.-F., Ji, W. & Feng, C.-L. Installing logic gates to multiresponsive supramolecular hydrogel co-assembled from phenylalanine amphiphile and bis(pyridinyl) derivative. *Langmuir* **31,** 7122–7128 (2015).

95. Liu, J., Chen, G., Guo, M. & Jiang, M. Dual stimuli-responsive supramolecular hydrogel based on hybrid inclusion complex (HIC). *Macromolecules* **43,** 8086–8093 (2010).

96. Ikeda, M. *et al.* Installing logic-gate responses to a variety of biological substances in supramolecular hydrogel-enzyme hybrids. *Nat. Chem.* **6,** 511–518 (2014).

97. Gupta, M. K., Martin, J. R., Dollinger, B. R., Hattaway, M. E. & Duvall, C. L. Thermogelling, ABC triblock copolymer platform for resorbable hydrogels with tunable, degradation-mediated drug release. *Adv. Funct. Mater.* **27,** 1704107 (2017).

98. Choh, S.-Y., Cross, D. & Wang, C. Facile synthesis and characterization of disulfide-cross-linked hyaluronic acid hydrogels for protein delivery and cell encapsulation. *Biomacromolecules* **12,** 1126–1136 (2011).

99. Patil, S. S., Shinde, V. S. & Misra, R. D. K. pH and reduction dual-stimuli-responsive PEGDA/PAMAM injectable network hydrogels via aza-Michael addition for anticancer drug delivery. *J. Polym. Sci. A Polym.* doi:10.1002/pola.29168 (2018). doi:10.1002/pola.29168

100. Arakawa, C. K., Badeau, B. A., Zheng, Y. & DeForest, C. A. Multicellular vascularized engineered tissues through user-programmable biomaterial photodegradation. *Adv. Mater.* **29,** 1703156 (2017).

101. Kurisawa, M. & Yui, N. Dual-stimuli-responsive drug release from interpenetrating polymer network-structured hydrogels of gelatin and dextran. *J. Control. Release* **54,** 191–200 (1998).

102. Zhang, J. & Peppas, N. A. Synthesis and characterization of pH- and temperature-sensitive poly(methacrylic acid)/poly(N-isopropylacrylamide) interpenetrating polymeric networks. *Macromolecules* **33,** 102–107 (2000).

103. Xing, Z. *et al.* Dual stimuli responsive hollow nanogels with IPN structure for temperature controlling drug loading and pH triggering drug release. *Soft Matter* **7,** 7992–7997 (2011).

104. Judd, J. *et al.* Tunable protease-activatable virus nanonodes. *ACS Nano* **8,** 4740–4746 (2014).

105. Douglas, S. M., Bachelet, I. & Church, G. M. A logic-gated nanorobot for targeted transport of molecular payloads. *Science* **335,** 831–834 (2012).

106. Klaikherd, A., Nagamani, C. & Thayumanavan, S. Multi-stimuli sensitive amphilic block copolymer assemblies. *J. Am. Chem. Soc.* **131,** 4830–4838 (2009).

107. Miao, K., Liu, H. & Zhao, Y. Thermo, pH and reduction responsive coaggregates comprising AB2C2 star terpolymers for multi-triggered release of doxorubicin. *Polym. Chem.* **5,** 3335–3345 (2014).

108. Chen, S., Jiang, F., Cao, Z., Wang, G. & Dang, Z.-M. Photo, pH, and thermo triple-responsive spiropyran-based copolymer nanoparticles for controlled release. *Chem. Commun.* **51,** 12633–12636 (2015).

109. Ghosh, S., Yesilyurt, V., Savariar, E. N., Irvin, K. & Thayumanavan, S. Redox, ionic strength, and pH sensitive supramolecular polymer assemblies. *J. Polym. Sci. A Polym.* **47,** 1052–1060 (2008).

110. Zhou, S., Du, X., Cui, F. & Zhang, X. Multi-responsive and logic controlled release of DNA-gated mesoporous silica vehicles functionalized with intercalators for multiple delivery. *Small* **10,** 980–988 (2014).

111. Guragain, S., Bastakoti, B. P., Ito, M., Yusa, S. & Nakashima, K. Aqueous polymeric micelles of poly[N-isopropylacrylamide-b-sodium 2-(acrylamido)-2-methylpropanesulfonate] with a spiropyran dimer pendant: quadruple stimuli-responsiveness. *Soft Matter* **8,** 9628–9634 (2012).

112. Cao, Z., Wu, H., Dong, J. & Wang, G. Quadruple-stimuli-sensitive polymeric nanocarriers for controlled release under combined stimulation. *Macromolecules* **47,** 8777–8783 (2014).

113. Zhang, K. *et al.* Synthesis of temperature, pH, light and dual-redox quintuple-stimuli-responsive shell-crosslinked polymeric nanoparticles for controlled release. *Mater. Sci. Eng. C* **87,** 1–9 (2018).

114. Garcia, A. *et al.* Photo-, thermally, and pH-responsive microgels. *Langmuir* **23,** 224–229 (2007).

115. Kotsuchibashi, Y., Agustin, R. V. C., Lu, J.-Y., Hall, D. G. & Narain, R. Temperature, pH, and glucose responsive gels via simple mixing of boroxole- and glyco-based polymers. *ACS Macro Lett.* **2,** 260–264 (2013).

116. Guan, Y., Zhao, H.-B., Yu, L.-X., Chen, S.-C. & Wang, Y.-Z. Multi-stimuli sensitive supramolecular hydrogel formed by host–guest interaction between PNIPAM-Azo and cyclodextrin dimers. *RSC Adv.* **4,** 4955–4959 (2014).

117. Fan, K., Yang, J., Wang, X. & Song, J. Rational construction of gel-based supramolecular logic gates by using a functional gelator with multiple-stimuli responsive properties. *Soft Matter* **10,** 8370–8375 (2014).

118. Ma, G. *et al.* Development of ionic strength/pH/enzyme triple-responsive zwitterionic hydrogel of the mixed l-glutamic acid and l-lysine polypeptide for site-specific drug delivery. *J. Mater. Chem. B* **5,** 935–943 (2017).

119. Casolaro, M. *et al.* Long-term doxorubicin release from multiple stimuli-responsive hydrogels based on α-amino-acid residues. *Eur. J. Pharm. Biopharm.* **88,** 424–433 (2014).

120. He, H., Cattran, A. W., Nguyen, T., Nieminen, A.-L. & Xu, P. Triple-responsive expansile nanogel for tumor and mitochondria targeted photosensitizer delivery. *Biomaterials* **35,** 9546–9553 (2014).

121. Wang, L., Liu, M., Gao, C., Ma, L. & Cui, D. A pH-, thermo-, and glucose-, triple-responsive hydrogels: Synthesis and controlled drug delivery. *React. Funct. Polym.* **70,** 159–167 (2010).

122. Kharkar, P. M., Kiick, K. L. & Kloxin, A. M. Design of thiol- and light-sensitive degradable hydrogels using Michael-type addition reactions. *Polym. Chem.* **6,** 5565–5574 (2015).

123. Badeau, B. A., Comerford, M. P., Arakawa, C. K., Shadish, J. A. & DeForest, C. A. Engineered modular biomaterial logic gates for environmentally triggered therapeutic delivery. *Nat. Chem.* **10,** 251–258 (2018).

124. Hoffman, A. S. Stimuli-responsive polymers: Biomedical applications and challenges for clinical translation. *Adv. Drug Deliv. Rev.* **65,** 10–16 (2013).

125. O'Neill, H. S. *et al.* Biomaterial-enhanced cell and drug delivery: Lessons learned in the cardiac field and future perspectives. *Adv. Mater.* **28,** 5648–5661 (2016).

126. Li, J. & Mooney, D. J. Designing hydrogels for controlled drug delivery. *Nat. Rev. Mater.* **1,** 16071 (2016).

127. Liu, G.-F., Ji, W. J. & Feng, C.-L. Installing logic gates to multiresponsive supramolecular

hydrogel co-assembled from phenylalanine amphiphile and bis(pyridinyl) derivative. *Langmuir* **31,** 7122–7128 (2015).

128. Motornov, M. *et al.* "Chemical transformers" from nanoparticle ensembles operated with logic. *Nano Lett.* **8,** 2993–2997 (2008).

129. Kharkar, P. M., Kiick, K. L. & Kloxin, A. M. Design of thiol- and light-sensitive degradable hydrogels using Michael-type additon reactions. *Polym. Chem.* **6,** 5565–5574 (2015).

130. Roche, E. T. *et al.* Comparison of biomaterial delivery vehicles for improving acute retention of stem cells in the infarcted heart. *Biomaterials* **35,** 6850–6858 (2014).

131. Griffin, D. R. & Kasko, A. M. Photodegradable macromers and hydrogels for live cell encapsulation and release. *J. Am. Chem. Soc.* **134,** 13103–13107 (2012).

132. Kloxin, A. M., Tibbitt, M. W. & Anseth, K. S. Synthesis of photodegradable hydrogels as dynamically tunable cell culture platforms. *Nat. Protoc.* **5,** 1867–1887 (2010).

133. Agard, N. J., Prescher, J. A. & Bertozzi, C. R. A strain-promoted [3 + 2] azide-alkyne cycloaddition for covalent modification of biomolecules in living systems. *J. Am. Chem. Soc.* **126,** 15046–15047 (2004).

134. DeForest, C. A. & Anseth, K. S. Cytocompatible click-based hydrogels with dynamically tunable properties through orthogonal photoconjugation and photocleavage reactions. *Nat. Chem.* **3,** 925–931 (2011).

135. DeForest, C. A., Polizzotti, B. D. & Anseth, K. S. Sequential click reactions for synthesizing and patterning three-dimensional cell microenvironments. *Nat. Mater.* **8,** 659–664 (2009).

136. Madl, C. M., Katz, L. M. & Heilshorn, S. C. Bio-orthogonally crosslinked, engineered protein hydrogels with tunable mechanics and biochemistry for cell encapsulation. *Adv. Funct. Mater.* **26,** 3612–3620 (2016).

137. Jiang, Y., Chen, J., Deng, C., Suuronen, E. J. & Zhong, Z. Click hydrogels, microgels and nanogels: Emerging platforms for drug delivery and tissue engineering. *Biomaterials* **35,** 4969–4985 (2014).

138. Das, R. K., Gocheva, V., Hammink, R., Zouani, O. F. & Rowan, A. E. Stress-stiffening-mediated stem-cell commitment switch in soft responsive hydrogels. *Nat. Mater.* **15,** 318–25 (2016).

139. Hiemenz, P. C. & Lodge, T. P. *Polymer Chemistry*. (CRC Press, 2007).

140. Flynn, B. P. *et al.* Mechanical strain stabilizes reconstituted collagen fibrils against enzymatic degradation by mammalian collagenase matrix metalloproteinase 8 (MMP-8). *PLoS One* **5,** e12337 (2010).

141. Huo, M., Yuan, J. & Wei, Y. Redox-responsive polymers for drug delivery: From molecular design to applications. *Polym. Chem.* **5,** 1519–1528 (2014).

142. Zhu, C., Ninh, C. & Bettinger, C. J. Photoreconfigurable polymers for biomedical applications: Chemistry and macromolecular engineering. *Biomacromolecules* **15,** 3474–3494 (2014).

143. Uhrich, K. E., Cannizzaro, S. M., Langer, R. S. & Shakesheff, K. M. Polymeric systems for controlled drug release. *Chem. Rev.* **99,** 3181–3198 (1999).

144. Khetan, S. & Burdick, J. A. Patterning network structure to spatially control cellular remodeling and stem cell fate within 3-dimensional hydrogels. *Biomaterials* **31,** 8228–8234 (2010).

145. Khetan, S. *et al.* Degradation-mediated cellular traction directs stem cell fate in covalently crosslinked three-dimensional hydrogels. *Nat. Mater.* **12,** 458–65 (2013).

146. Bolhassani, A., Jafarzade, B. S. & Mardani, G. In vitro and in vivo delivery of therapeutic proteins using cell penetrating peptides. *Peptides* **87,** 50–63 (2017).

147. Guidotti, G., Brambilla, L. & Rossi, D. Cell-penetrating peptides: From basic research to clinics. *Trends Pharmacol. Sci.* **38,** 406–424 (2017).

148. Dissanayake, S., Denny, W. A., Gamage, S. & Sarojini, V. Recent developments in anticancer drug delivery using cell penetrating and tumor targeting peptides. *J. Control. Release* **250,** 62–76 (2017).

149. Huang, Y. *et al.* Curb challenges of the 'Trojan Horse' approach: Smart strategies in achieving effective yet safe cell-penetrating peptide-based drug delivery. *Adv. Drug Deliv. Rev.* **65,** 1299–1315 (2013).

150. Mok, H., Bae, K. H., Ahn, C. H. & Park, T. G. PEGylated and MMP-2 specifically DePEGylated quantum dots: Comparative evaluation of cellular uptake. *Langmuir* **25,** 1645–1650 (2009).

151. Zhu, L., Kate, P. & Torchilin, V. P. Matrix metalloprotease 2-responsive multifunctional liposomal nanocarrier for enhanced tumor targeting. *ACS Nano* **6,** 3491–3498 (2012).

152. Harris, T. J. *et al.* Protease-triggered unveiling of bioactive nanoparticles. *Small* **4,** 1307–1312 (2008).

153. Kuai, R. *et al.* Efficient delivery of payload into tumor cells in a controlled manner by TAT and thiolytic cleavable PEG co-modified liposomes. *Mol. Pharm.* **7,** 1816–1826 (2010).

154. Hansen, M. B. *et al.* Constrained and UV-activatable cell-penetrating peptides for intracellular delivery of liposomes. *J. Control. Release* **164,** 87–94 (2012).

155. Sawant, R. M. *et al.* 'SMART' drug delivery systems: Double-targeted pH-responsive pharmaceutical nanocarriers. *Bioconjug. Chem.* **17,** 943–949 (2006).

156. Kale, A. A. & Torchilin, V. P. Enhanced transfection of tumor cells in vivo using 'Smart' pH-sensitive TAT-modified pegylated liposomes. *J. Drug Target.* **15,** 538–545 (2007).

157. Aguilera, T. A., Olson, E. S., Timmers, M. M. & Tsien, R. Y. Systemic in vivo distribution of activatable cell penetrating peptides is superior to that of cell penetrating peptides. *Integr. Biol.* **1,** (2009).

158. Olson, E. S. *et al.* In vivo characterization of activatable cell penetrating peptides for targeting protease activity in cancer. 382–393 (2009).

159. Scadeng, M. *et al.* Surgery with molecular fluorescence imaging using activable cell-penetrating peptides decreases residual cancer and improves survival. *Proc. Natl. Acad. Sci.* **107,** 4317–4322 (2010).

160. Malone, C. D. *et al.* Tumor detection at 3 Tesla with an activatable cell penetrating peptide dendrimer (ACPPD-Gd), a T1 magnetic resonance (MR) molecular imaging agent. *PLoS One* **10,** 1–15 (2015).

161. Lin, Y. *et al.* Activatable cell-biomaterial interfacing with photo-caged peptides. *Chem. Sci.* **10,** 1158–1167 (2019).

162. Lux, J. *et al.* Thrombin-activatable microbubbles as potential ultrasound contrast agents for the detection of acute thrombosis. *ACS Appl. Mater. Interfaces* **9,** 37587–37596 (2017).

163. Weinstain, R., Savariar, E. N., Felsen, C. N. & Tsien, R. Y. In vivo targeting of hydrogen peroxide by activatable cell-penetrating peptides. *J. Am. Chem. Soc.* **136,** 874–877 (2014).

164. Guimaraes, C. P. *et al.* Site-specific C-terminal and internal loop labeling of proteins using sortase-mediated reactions. *Nat. Protoc.* **8,** 1787–1799 (2013).

165. Gawade, P. G., Badeau, B. A., Shadish, J. A. & DeForest, C. A. Logic-based delivery of site-specifically modified proteins from environmentally responsive hydrogel biomaterials. **In Prep.* (2019).

166. Zhuang, S. M. *et al.* Apoptin, a protein derived from chicken anemia virus, induces p53-independent apoptosis in human osteosarcoma cells. *Cancer Res.* **55,** 486–489 (1995).

167. Danen-van Oorschot, A. A. A. M. *et al.* Importance of nuclear localization of apoptin for tumor-specific induction of apoptosis. *J. Biol. Chem.* **278,** 27729–27736 (2003).

168. Los, M. *et al.* Apoptin, a tumor-selective killer. *Biochim. Biophys. Acta - Mol. Cell Res.* **1793,** 1335–1342 (2009).

169. Rollano Peñaloza, O. M. *et al.* Apoptins: Selective anticancer agents. *Trends Mol. Med.*

20, 519–528 (2014).

170. Guelen, L. *et al.* TAT-apoptin is efficiently delivered and induces apoptosis in cancer cells. *Oncogene* **23,** 1153–65 (2004).

171. Ruskowitz, E. R., Comerford, M. P., Badeau, B. A. & DeForest, C. A. Logical stimuli-triggered delivery of small molecules from hydrogel biomaterials. *Biomater. Sci.* (2018).

172. Enderton, H. *A mathematical introduction to logic*. (2001).

173. Wittgenstein, L. *Tractatus logico-philosophicus*. (1921).

174. Bracher, P. J., Snyder, P. W., Bohall, B. R. & Whitesides, G. M. The relative rates of thiol– thioester exchange and hydrolysis for alkyl and aryl thioalkanoates in water. *Orig. Life Evol. Biosph.* **41,** 399–412 (2011).

175. Wang, C., Guo, Q. & Fu, Y. Theoretical analysis of the detailed mechanism of native chemical ligation reactions. *Chem. Asian J.* **6,** 1241–1251 (2011).

176. Johnson, E. C. B. & Kent, S. B. H. Insights into the mechanism and catalysis of the native chemical ligation reaction. *J. Am. Chem. Soc.* **6,** 6640–6646 (2006).

177. Goddard-Borger, E. D. & Stick, R. V. An efficient, inexpensive, and shelf-stable diazotransfer reagent: Imidazole-1-sulfonyl azide hydrochloride. *Org. Lett.* **9,** 3797–3800 (2007).

178. Chapman, R., Jolliffe, K. A. & Perrier, S. Synthesis of self assembling cyclic peptide-polymer conjugates using click chemistry. *Aust. J. Chem.* **63,** 1169–1172 (2010).

179. Dommerholt, J. *et al.* Readily accessible bicyclononynes for bioorthogonal labeling and three-dimensional imaging of living cells. *Angew. Chemie - Int. Ed.* **49,** 9422–9425 (2010).

180. Palavalli, L. H. *et al.* Analysis of the matrix metalloproteinase family reveals that MMP8 is often mutated in melanoma. *Nat Genet* **41,** 518–520 (2009).

181. Zhang, S. *et al.* A novel strategy for MALDI-TOF MS analysis of small molecules. *J. Am. Soc. Mass Spectrom.* **21,** 154–160 (2010).

182. Sarver, A., Scheffler, N. K., Shetlar, M. D. & Gibson, B. W. Analysis of peptides and proteins containing nitrotyrosine by matrix-assisted laser desorption/ionization mass spectrometry. *J. Am. Soc. Mass Spectrom.* **12,** 439–448 (2001).

183. Strohalm, M., Kodíček, M. & Pechar, M. Tryptophan modification by 2-hydroxy-5-nitrobenzyl bromide studied by MALDI-TOF mass spectrometry. *Biochem. Biophys. Res. Commun.* **312,** 811–816 (2003).

184. Faucher, A.-M. & Grand-Maître, C. tris(2-carboxyethyl)phosphine (TCEP) for the

reduction of sulfoxides, sulfonylchlorides, N-oxides and azides. *Synth. Commun.* **33,** 3503–3511 (2003).

185. Walba, D. M. *et al.* Self-assembled monolayers for liquid crystal alignment: simple preparation on glass using alkyltrialkoxysilanes. *Liq. Cryst.* **31,** 481–489 (2004).

186. Godula, K., Rabuka, D., Nam, K. T. & Bertozzi, C. R. Synthesis and microcontact printing of dual end-functionalized mucin-like glycopolymers for microarray applications. *Angew. Chemie - Int. Ed.* **48,** 4973–4976 (2009).

187. Iwata, M., Torok-Storb, B., Wayner, E. A. & Carter, W. G. CDCP1 identifies a CD146 negative subset of marrow fibroblasts involved with cytokine production. *PLoS One* **9,** 1–11 (2014).

APPENDIX A: SUPPLEMENTARY INFORMATION FOR CHAPTER 3

General synthetic information

Chemical reagents and solvents were purchased from either Sigma-Aldrich or Fisher Scientific and used as received. Peptide synthesis reagents were purchased from either ChemPep or Chem-Impex and used as received. Deionized water (dH_2O) was generated by a U.S. Filter Corporation Reverse Osmosis System with a Desal membrane. Synthetic chemical reactions were performed under a nitrogen atmosphere in oven-dried glassware and stirred with a Teflon-coated magnetic stir bar unless otherwise noted. Solvents were removed *in vacuo* with a Büchi Rotovapor R-3 equipped with a V-700 vacuum pump and V-855 vacuum controller and a Welch 1400 DuoSeal Belt-Drive high vacuum pump. ^{1}H and ^{13}C nuclear magnetic resonance (NMR) data was collected at 298 K on Bruker instruments and chemical shifts are reported relative to tetramethylsilane (TMS, $\delta = 0$). Microwave-assisted peptide synthesis was performed on a CEM Liberty 1. Semi-preparative reversed-phase high-pressure liquid chromatography (RP-HPLC) was performed on a Dionex Ultimate 3000 equipped with a variable multiple wavelength detector, automated fraction collector, and Thermo 5 µm Synchronis silica 250 x 21.2 mm C18 column. Lyophilization was performed on a LABCONCO FreeZone 2.5 Plus freeze-dryer equipped with a LABCONCO rotary vane 117 vacuum pump. Matrix-assisted laser desorption/ionization time of flight (MALDI-TOF) mass spectrometry was performed in reflectron positive ion mode on a Bruker AutoFlex II using a matrix of α-cyano-4-hydroxycinnamic acid:2,5-dihydroxy benzoic acid (2:1). High-resolution mass spectrometry (HRMS) was performed on a Thermo Linear Trap Quadrupole Orbitrap Xcalibur 2.0 DS. The light source for the photochemical cleavage was a Lumen Dynamics OmniCure S1500 Spot UV Curing system with an internal 365 nm filter and an external 360 nm cut-on longpass filter. Light intensity was measured using a Cole-Parmer Radiometer (Series 9811-50, $\lambda = 365$ nm). Fluorescence readings were acquired on a SpectraMax M5 spectrometer using Thermo Scientific Nunc black polypropylene 96-well plates. Rheological measurements were performed on an Anton Paar MCR301 equipped with a C-PTD200 Peltier plate and a CP25-1 cone and plate geometry. Fluorescent microscopy was performed on a Nikon Eclipse TE2000-U. Confocal microscopy was performed at the University of Washington Keck Microscopy Center on a Leica SP8X. Polymerase chain reaction (PCR) was performed in a Bioer LifeECO thermal cycler. Protein expression was performed in a Thermo Scientific MaxQ 4000 shaker incubator. Cells were lysed using a Fisher Scientific Model 505 Sonic Dismembrator. Mammalian cell culture was performed in a NuAire LabGard ES NU-437 Class II Type A2 Biosafety Cabinet. Cells were maintained in a Sanyo inCu saFe® MCO-17AC incubator at 37 °C and 5% CO_2. Flow cytometry was performed at the University of Washington Pathology Flow Cytometry Core Facility on a BD Biosciences LSR II Flow Cytometer.

Method A1: Synthesis of 2,5-dioxopyrrolidin-1-yl 4-azidobutanoate (N_3-OSu)

4-azidobutanoic acid (N_3-COOH) was synthesized following a published synthetic route[134], and used as a synthetic precursor for 2,5-dioxopyrrolidin-1-yl 4-azidobutanoate (N_3-OSu).

Synthesis of ethyl 4-azidobutanoate:

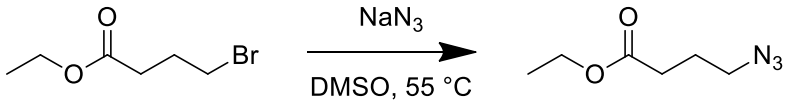

Ethyl-4-bromobutyrate (49.6 g, 254 mmol) and sodium azide (24.7 g, 378 mmol, 1.5x) were dissolved in dimethyl sulfoxide (DMSO, 375 mL) and reacted at 55 °C overnight under a nitrogen atmosphere. The reaction mixture was diluted with water (250 mL) and extracted into diethyl ether (3 x 250 mL). The organic layer was washed with water (250 mL) and brine (250 mL), dried over $MgSO_4$, filtered, and concentrated *in vacuo* to give the intermediate ethyl-4-azidobutanoate (37.7 g, 240 mmol, 94.5% yield) as a clear liquid. ^{1}H NMR (300 MHz, $CDCl_3$) δ 4.17 (q, *J* = 7.1 Hz, 2H), 3.38 (t, *J* = 6.7 Hz, 2H), 2.43 (t, *J* = 7.2 Hz, 2H), 1.94 (p, *J* = 7.1 Hz, 2H), 1.29 (t, *J* = 7.1 Hz, 3H).

Synthesis of 4-azidobutanoic acid (N_3-COOH):

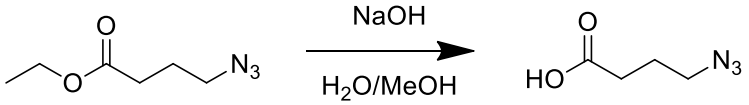

Ethyl-4-azidobutanoate (37.66 g, 240 mmol) was dissolved in aqueous sodium hydroxide (1 M, 250 mL). Methanol was added to homogenize the solution (175 mL) and the reaction mixture was stirred at room temperature for 3 hr. The methanol was removed *in vacuo* and aqueous hydrochloric acid was added dropwise to the reaction mixture until the pH became 1. The product was extracted into diethyl ether (3 x 250 mL), dried over magnesium sulfate ($MgSO_4$), filtered, and concentrated on a rotary evaporator to give 4-azidobutanoic acid (denoted N_3-COOH) as a faint yellow liquid (30.7 g, 237 mmol, 98.8% yield). ^{1}H NMR (300 MHz, $CDCl_3$) δ 8.64 (br s, 1H), 3.41 (t, *J* = 6.7 Hz, 2H), 2.50 (t, *J* = 7.2 Hz, 2H), 2.01 – 1.88 (m, 2H). These spectral data matched those previously reported[134].

Synthesis of 2,5-dioxopyrrolidin-1-yl 4-azidobutanoate (N_3-OSu):

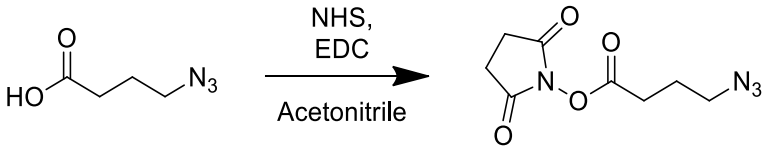

N_3-COOH (5.00 g, 38.7 mmol), N-hydroxysuccinimide (5.79 g, 50.3 mmol, 1.3x), and 1-ethyl-3-(3-dimethylaminopropyl)carbodiimide hydrochloride (EDC·HCl 9.65 g, 50.3 mmol, 1.3x) were combined in a flame-dried flask and purged with nitrogen. Dry acetonitrile (50 mL) added *via* syringe to solubilize the reagents. The reaction mixture was stirred overnight at room temperature. The acetonitrile was removed *in vacuo* and the reaction products were dissolved in

dichloromethane (DCM, 100 mL), washed with water (3 x 100 mL), dried over $MgSO_4$, filtered, and concentrated *via* rotary evaporation to give the pure 2,5-dioxopyrrolidin-1-yl 4-azidobutanoate product (denoted N_3-OSu) as a white solid (7.98 g, 35.3 mmol, 91% yield). ^{1}H NMR (300 MHz, $CDCl_3$) δ 3.45 (t, J = 6.6 Hz, 2H), 2.85 (s, 4H), 2.74 (t, J = 7.2 Hz, 2H), 2.09 – 1.96 (m, 2H).

Method A2: Synthesis of 2,5-dioxopyrrolidin-1-yl 4-(4-(1-((4-azidobutanoyl)oxy)ethyl)-2-methoxy-5-nitrophenoxy)butanoate (N_3-*o*NB-OSu)

The synthesis of N_3-*o*NB-OSu was based on a published synthetic route[134] involving the reaction of 4-(4-(1-hydroxyethyl)-2-methoxy-5-nitrophenoxy)butanoic acid[132] and N_3-COOH (Method A1) with minor modifications.

Synthesis of ethyl 4-(4-acetyl-2-methoxyphenoxy)butanoate:

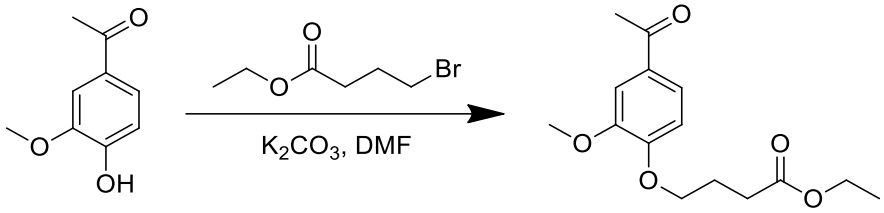

Acetovanillone (30.0 g, 180 mmol) and ethyl-4-bromobutyrate (42.3 g, 217 mmol, 1.2x) were dissolved in dimethylformamide (DMF, 150 mL) in a flame-dried flask. Potassium carbonate (37.4 g, 271 mmol, 1.5x) was added, and the reaction mixture was stirred overnight at room temperature under a nitrogen atmosphere. The reaction mixture was slowly poured into stirring water (1.5 L), and stirring was continued at room temperature for 2 hours. The mixture was stored overnight at 4 °C to precipitate the product. The product was vacuum filtered and lyophilized to give the intermediate, ethyl 4-(4-acetyl-2-methoxyphenoxy)butanoate, as a yellow solid (49.29 g, 175.8 mmol, 97.4% yield). ^{1}H NMR (300 MHz, $CDCl_3$) δ 7.54 (m, 2H), 6.89 (d, *J* = 8.2 Hz, 1H), 4.20 – 4.09 (m, 4H), 3.91 (s, 3H), 2.60 – 2.48 (m, 5H), 2.18 (p, *J* = 6.8 Hz, 2H), 1.26 (t, *J* = 7.1 Hz, 3H).

Synthesis of ethyl 4-(4-acetyl-2-methoxy-5-nitrophenoxy)butanoate:

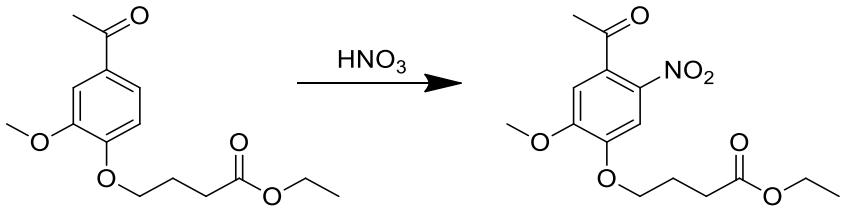

Nitric acid (140 mL) was cooled in an ice bath in a round bottom flask (1 L). Ethyl 4-(4-acetyl-2-methoxyphenoxy)butanoate (48.65 g, 173.6 mmol) was added in small portions to the continually stirred solution, allowing for full dissolution before subsequent additions (approximately 40 minutes to dissolve the product). The reaction mixture was stirred while in the ice bath, and progress was monitored *via* thin-layer chromatography (TLC, hexanes/ethyl acetate/acetic acid, 50:50:1, product R_f ~ 0.5). Upon reaction completion (~40 minutes), the reaction mixture was added dropwise to continually stirred ice-cold water (1.5 L). This mixture was further agitated at room temperature for 1 hour, after which the crude product was precipitated overnight at 4 °C. The precipitate was filtered, rinsed with ice-cold water, and lyophilized to give a yellow-brown solid. The solid was dissolved in 65 °C ethanol (700 mL), cooled to room temperature, and recrystallized overnight at 4 °C. The product was vacuum filtered, rinsed with -20 °C ethanol, and dried to give the intermediate, ethyl 4-(4-acetyl-2-methoxy-5-nitrophenoxy)butanoate, as a yellow solid (33.90 g, 104.2 mmol, 60.0% yield). ^{1}H NMR (300 MHz, $CDCl_3$) δ 7.60 (s, 1H), 6.74 (s, 1H), 4.20 – 4.11

(m, 4H), 3.95 (s, 3H), 2.54 (t, *J* = 7.2 Hz, 2H), 2.49 (s, 3H), 2.19 (p, *J* = 6.7 Hz, 2H), 1.26 (t, *J* = 7.1 Hz, 3H).

Synthesis of ethyl 4-(4-(1-hydroxyethyl)-2-methoxy-5-nitrophenoxy)butanoate:

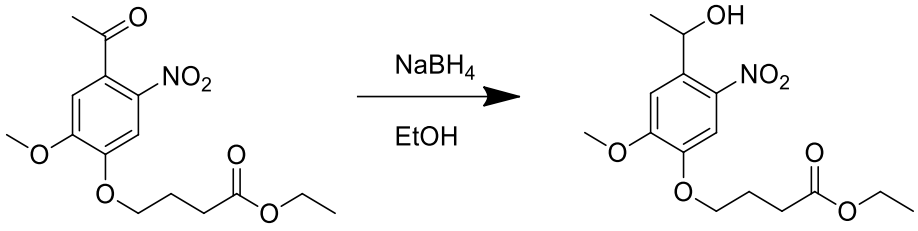

Ethyl 4-(4-acetyl-2-methoxy-5-nitrophenoxy)butanoate (47.12 g, 144 mmol) was dissolved in anhydrous ethanol (700 mL), purged with nitrogen, and heated to 38 °C. Sodium borohydride (5.33 g, 141 mmol, 0.97x) was added to the reaction mixture in equal portions every 5 minutes over a 40 minute period. The mixture was purged with nitrogen and stirred overnight at 38 °C. The reaction mixture was added to water (7 L), stirred 1 hour at room temperature, and the product was precipitated overnight at 4 °C. The suspension was filtered, rinsed with ice-cold water, and lyophilized to yield the intermediate, ethyl 4-(4-(1-hydroxyethyl)-2-methoxy-5-nitrophenoxy)butanoate, as a dark yellow solid (37.84 g, 115.6 mmol, 80% yield). ^{1}H NMR (300 MHz, DMSO) δ 7.53 (s, 1H), 7.36 (s, 1H), 5.48 (d, *J* = 4.4 Hz, 1H), 5.33 – 5.19 (m, 1H), 4.17 – 3.99 (m, 4H), 3.91 (s, 3H), 2.48 (m, 2H), 1.99 (p, *J* = 6.8 Hz, 2H), 1.37 (d, *J* = 6.2 Hz, 3H), 1.19 (t, *J* = 7.1 Hz, 3H).

Synthesis of 4-(4-(1-hydroxyethyl)-2-methoxy-5-nitrophenoxy)butanoic acid:

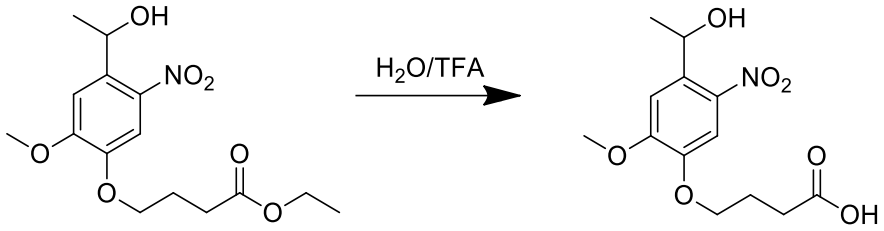

Ethyl 4-(4-(1-hydroxyethyl)-2-methoxy-5-nitrophenoxy)butanoate (37.84 g, 115.6 mmol) was added to a solution of water (1 L) and trifluoroacetic acid (TFA, 96 mL) in a round-bottomed flask (2 L). The reaction mixture was stirred and heated to 90 °C. After 6 hours, additional TFA (48 mL) was added to the reaction mixture. After another 18 hours, additional TFA (48 mL) was added to the reaction mixture. After another 6 hours, the reaction mixture was filtered to remove the black solid. The filtrate was cooled to room temperature, upon which the precipitate was dissolved in minimal aqueous sodium hydroxide (1 M, 150 mL) and acidified to a pH of 1 *via* dropwise addition of hydrochloric acid. The precipitated product was vacuum filtered, washed, and lyophilized to give 4-(4-(1-hydroxyethyl)-2-methoxy-5-nitrophenoxy)butanoic acid as a yellow solid (20.08 g, 93.6 mmol, 81.0% yield). ^{1}H NMR (300 MHz, DMSO) δ 12.18 (s, 1H), 7.55 (s, 1H), 7.37 (s, 1H), 5.50 (m, 1H), 5.27 (m, 1H), 4.07 (t, *J* = 6.5 Hz, 2H), 3.92 (s, 3H), 2.40 (t, *J* = 7.3 Hz, 2H), 1.96 (p, *J* = 6.8 Hz, 2H), 1.37 (d, *J* = 6.2 Hz, 3H). These spectral data matched those previously reported[132].

Synthesis of 4-(4-(1-((4-azidobutanoyl)oxy)ethyl)-2-methoxy-5-nitrophenoxy)butanoic acid (N_3-*o*NB-COOH):

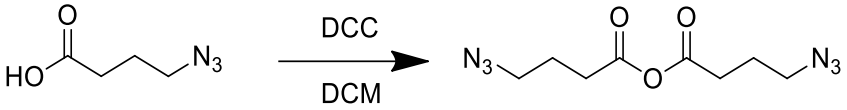

N_3-COOH (Method A1, 64.6 g, 500 mmol) and N,N'-Dicyclohexylcarbodiimide (33.0 g, 160 mmol) were combined in a flame-dried flask, purged with nitrogen, dissolved in anhydrous DCM (400 mL), and reacted at room temperature for 60 minutes. The reaction mixture was filtered to remove the dicyclohexylurea byproduct, concentrated *in vacuo*, and filtered. The crude product was repeatedly redissolved in anhydrous DCM (~90 mL), concentrated, and filtered until urea formation ceased.

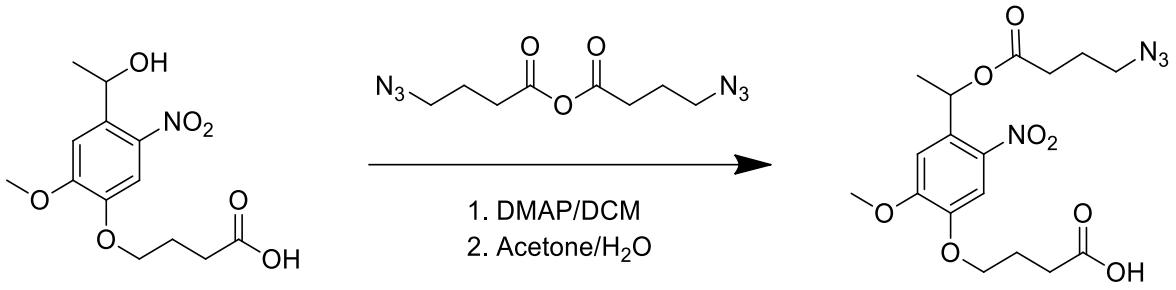

4-(4-(1-hydroxyethyl)-2-methoxy-5-nitrophenoxy)butanoic acid (10.0 g, 33.4 mmol), 4-dimethylaminopyridine (DMAP, 205 mg, 1.67 mmol) were added to the crude anhydride and dissolved in minimal DCM (250 mL). Pyridine (2.69 mL, 33.4 mmol) was added to the reaction and stirred at room temperature overnight under a nitrogen atmosphere. The reaction mixture was washed with saturated aqueous sodium carbonate (250 mL), 1 M hydrochloric acid (250 mL), and concentrated *in vacuo*. The intermediate was dissolved in water/acetone (50:50, 1400 mL) and stirred at room temperature overnight. The acetone was removed *in vacuo* and the product was extracted into DCM (3 x 300 mL). The organic layer was washed with 1 M hydrochloric acid, brine, dried over $MgSO_4$, filtered, and concentrated *in vacuo*. The crude mixture was purified on a silica flash column (20-40% Ethyl acetate in hexanes with 1% acetic acid) and concentrated to give 4-(4-(1-((4-azidobutanoyl)oxy)ethyl)-2-methoxy-5-nitrophenoxy)butanoic acid (denoted N_3-*o*NB-COOH) as a yellow solid (11.59 g, 28.24 mmol, 85% yield). ^{1}H NMR (500 MHz, DMSO) δ 12.08 (s, 1H), 7.57 (s, 1H), 7.10 (s, 1H), 6.21 (q, J = 6.4 Hz, 1H), 4.07 (t, J = 6.4 Hz, 2H), 3.93 (s, 3H), 3.32 (t, J = 6.8 Hz, 2H), 2.43 (t, J = 7.3 Hz, 2H), 2.38 (t, J = 7.3 Hz, 2H), 1.95 (p, J = 6.8 Hz, 2H), 1.76 (p, J = 7.1 Hz, 2H), 1.58 (d, J = 6.5 Hz, 3H). These spectral data matched those previously reported[134].

Synthesis of 2,5-dioxopyrrolidin-1-yl 4-(4-(1-((4-azidobutanoyl)oxy)ethyl)-2-methoxy-5-nitrophenoxy)butanoate (N_3-*o*NB-OSu):

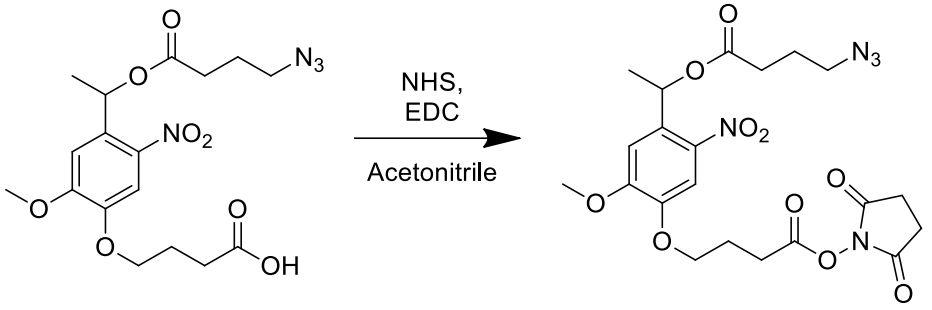

N_3-*o*NB-COOH (5.51 g, 13.4 mmol), N-hydroxysuccinimide (2.01 g, 17.5 mmol, 1.3x), and 1-ethyl-3-(3-dimethylaminopropyl)carbodiimide hydrochloride (EDC·HCl 3.35 g, 17.5 mmol, 1.3x) were combined in a flame-dried flask and purged with nitrogen. Dry acetonitrile (50 mL) added *via* syringe to solubilize the reagents. The reaction mixture was stirred overnight at room temperature. The acetonitrile was removed *in vacuo* and the reaction mixture was dissolved in DCM (100 mL), washed with water (3 x 100 mL), dried over $MgSO_4$, filtered, and concentrated *in vacuo* to give the product (denoted N_3-*o*NB-OSu) as a yellow solid (6.69 g, 13.2 mmol, 98% yield). ^{1}H NMR (500 MHz, $CDCl_3$) δ 7.62 (s, 1H), 7.03 (s, 1H), 6.52 (q, J = 6.4 Hz, 1H), 4.20 (t, J = 6.0 Hz, 2H), 4.00 (s, 3H), 3.42 – 3.31 (m, 2H), 2.91 (t, J = 7.3 Hz, 2H), 2.88 (s, 4H), 2.55 – 2.42 (m, 2H), 2.32 (p, J = 6.7 Hz, 2H), 1.93 (p, J = 6.9 Hz, 2H), 1.65 (d, J = 6.4 Hz, 3H).

Method A3: Synthesis of (*R*)-2-((((9H-fluoren-9-yl)methoxy)carbonyl)amino)-6-azido-hexanoic acid (Fmoc-Lys(N_3)-OH)

Imidazole-1-sulfonyl azide hydrochloride (Stick's reagent) and (*R*)-2-((((9H-fluoren-9-yl)methoxy)carbonyl)amino)-6-azidohexanoic acid (Fmoc-Lys(N_3)-OH) were synthesized following known synthetic routes[177,178] with minor modifications.

Synthesis of imidazole-1-sulfonyl azide hydrochloride:

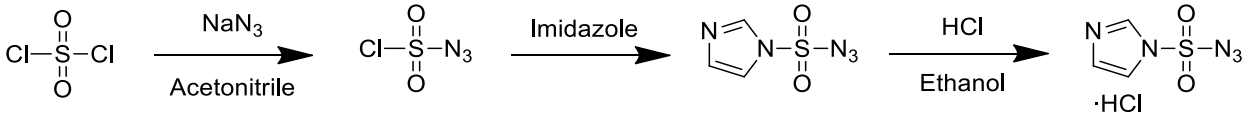

Sulfuryl chloride (27.0 g, 16.2 mL, 200 mmol) was added dropwise to a suspension of sodium azide (13.0 g, 200 mmol) in acetonitrile (200 mL, 0 °C), and the reaction was stirred overnight at room temperature. The mixture was cooled in an ice bath, and imidazole (25.9 g, 380 mmol) was added in small portions to the stirred reaction mixture. The reaction mixture was brought to room temperature and stirred for 3 hours. The reaction mixture was diluted with ethyl acetate (400 mL), washed with water (2 x 400 mL), washed with saturated aqueous sodium carbonate (2 x 400 mL), dried over $MgSO_4$, and filtered. Hydrochloric acid in ethanol [formulated under a nitrogen atmosphere by dropwise addition of acetyl chloride (23.5 g, 300 mmol) into ice-cold anhydrous ethanol (75 mL)] was added dropwise to the stirring filtrate. The product was precipitated in an ice bath and filtered. The filter cake was washed with ice-cold ethyl acetate (3 x 100 mL) to yield the pure product, imidazole-1-sulfonyl azide hydrochloride [Stick's reagent[177]], as a white powder (25.86 g, 123.4 mmol, 61.7% yield). ^{1}H NMR (300 MHz, D_2O) δ 9.45 – 9.42 (m, 1H), 8.06 – 8.01 (m, 1H), 7.65 – 7.60 (m, 1H); ^{13}C-NMR (75 MHz, D_2O) δ = 137.7, 123.3, 120.1. These spectral data matched those previously reported[177].

Synthesis of (*R*)-2-((((9H-fluoren-9-yl)methoxy)carbonyl)amino)-6-azidohexanoic acid (Fmoc-Lys(N_3)-OH):

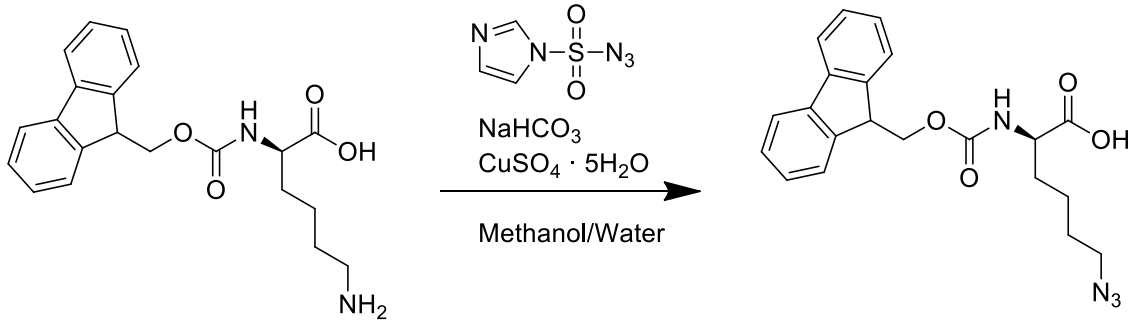

Fmoc-Lys-OH (11.00 g, 29.86 mmol) was dissolved in water (30 mL) with hydrochloric acid (aqueous 37%, 2.47 mL, 1x). A solution of water/methanol (1:2, 130 mL), imidazole-1-sulfonyl azide hydrochloride (7.50 g, 35.8 mmol, 1.2x), sodium bicarbonate (16.22 g, 193.1 mmol, 6.5 x), and aqueous $CuSO_4 \cdot 5H_2O$ (74.6 mg in 2 mL dH_2O, 0.299 mmol, 0.01x) were added, in order, to the reaction mixture and stirred for 17 hours at room temperature. The methanol was removed *in vacuo*, and the mixture was diluted with water (300 mL) and adjusted to a pH of 2 with hydrochloric acid. The crude product was extracted into ethyl acetate (3 x 150 mL), dried over

$MgSO_4$, filtered, and concentrated on a rotary evaporator. The crude product was purified on a silica column with a mobile phase of toluene/ethyl acetate/acetic acid (85:10:5) and concentrated to give the pure product [(*R*)-2-((((9H-fluoren-9-yl)methoxy)carbonyl)amino)-6-azidohexanoic acid, denoted Fmoc-Lys(N_3)-OH], as a light-yellow solid (10.82 g, 27.4 mmol, 92% yield). ^{1}H NMR (300 MHz, $CDCl_3$) δ 9.93 (s, 1H), 7.79 (d, J = 7.5 Hz, 2H), 7.63 (d, J = 7.0 Hz, 2H), 7.39 (dt, J = 26.7, 7.2 Hz, 4H), 5.43 (d, J = 8.2 Hz, 1H), 4.65 – 4.34 (m, 3H), 4.25 (t, J = 6.8 Hz, 1H), 3.38 – 3.14 (m, 2H), 2.04 – 1.35 (m, 6H). These spectral data matched those previously reported[178].

Method A4: Fmoc solid-phase peptide synthesis

Automated microwave-assisted Fmoc solid-phase peptide synthesis was performed on a CEM Liberty 1 (0.5 mmol scale). Fmoc deprotections were performed in 20% piperidine (v/v) in DMF with 0.1 M 1-hydroxybenzotriazole (HOBt) at 90 ^{o}C for 90 seconds. Amino acids (except arginine and cysteine) were coupled to resin-bound peptides upon treatment (75 ^{o}C for 5 minutes) with Fmoc-protected amino acid (2 mmol, 4x), 2-(1H-benzotriazol-1-yl)-1,1,3,3-tetramethyluronium hexafluorophosphate (HBTU, 2 mmol, 4x), and *N*,*N*-diisopropylethylamine (DIEA, 2 mmol, 4x) in a mixture of DMF (9 mL) and *N*-Methyl-2-pyrrolidone (NMP, 2 mL). Cysteine couplings were performed using the same reagents as above but the reaction was performed at 50 ^{o}C for 30 minutes. Arginine couplings were performed using the same reagents as above but the reaction was performed at 25 ^{o}C for 45 minutes, drained, and repeated at 75 ^{o}C for 5 minutes.

Method A5: Enzymatic "YES" degradable crosslinker synthesis (E)

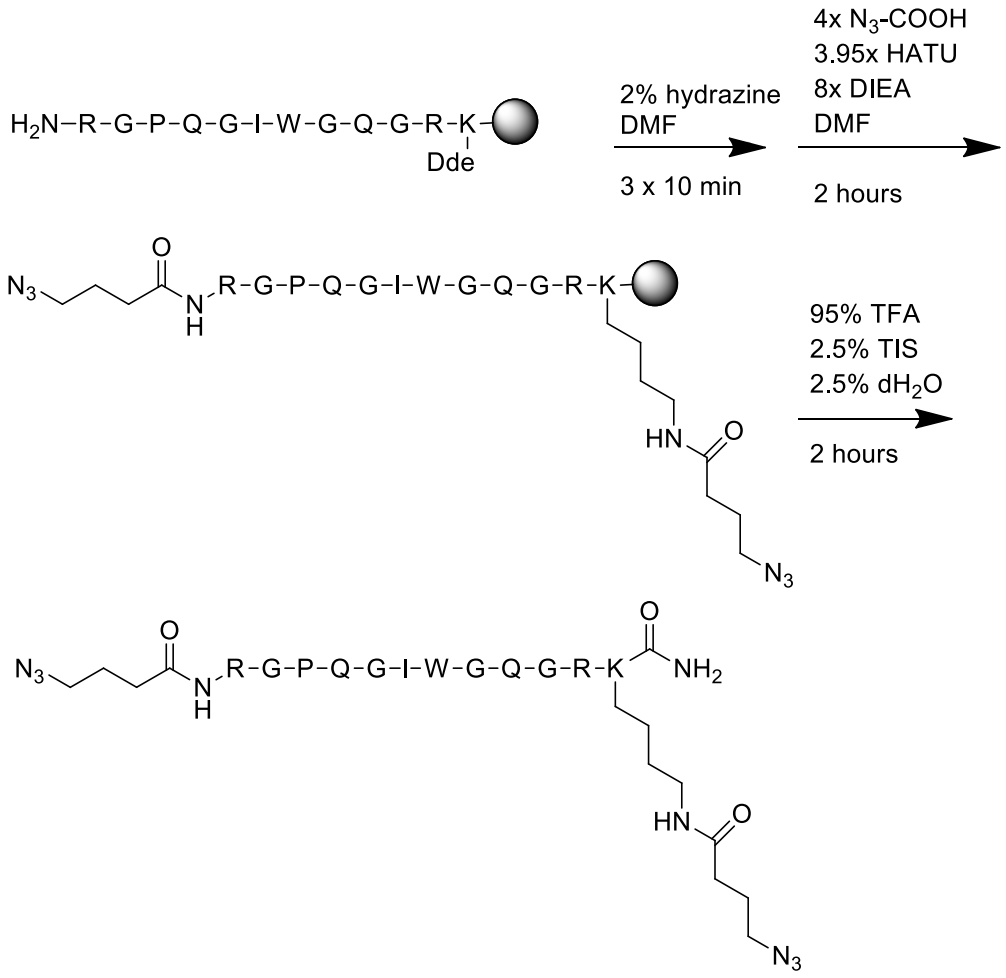

The resin-bound peptide H-RGPQGIWGQGRK(Dde)-NH_2 was synthesized by microwave-assisted Fmoc solid-phase peptide synthesis (SPPS, Method A4) on Rink amide resin (0.5 mmol scale). The resin was treated with hydrazine monohydrate (2%) in DMF (3 x 10 min) to remove the N-(1-(4,4-dimethyl-2,6-dioxocyclohexylidene)ethyl) (Dde) protecting group. N_3-COOH (0.517 g, 4.0 mmol, 4x, Method A1) was pre-activated upon reaction with 1-[Bis(dimethylamino)methylene]-1H-1,2,3-triazolo[4,5-b]pyridinium 3-oxid hexafluorophosphate (HATU, 1.502 g, 3.95 mmol, 3.95x) and DIEA (1.034 g, 8.0 mmol, 8x) in minimal DMF for 5 minutes and then reacted with the resin for 90 minutes to functionalize the N-terminus and the ε-amino group of the lysine with an azide. The peptide was simultaneously deprotected and cleaved from resin upon treatment with TFA/triisopropylsilane (TIS)/dH_2O (95:2.5:2.5, 30 mL) for 2 hours, and the crude peptide was precipitated in and washed with ice-cold diethyl ether (2x). The crude peptide was purified using RP-HPLC operating with a 55 minute linear gradient (5–100%) of acetonitrile in water containing TFA (0.1%); lyophilization yielded the final product (N_3-RGPQGIWGQGRK(N_3)-NH_2, denoted E) as a yellow solid (222.0 mg, 0.142 mmol, 28.4% overall yield). Peptide purity was confirmed using MALDI-TOF: calculated for $C_{66}H_{106}N_{29}O_{16}^+$ [M + $^1H]^+$, 1560.8; observed 1560.9.

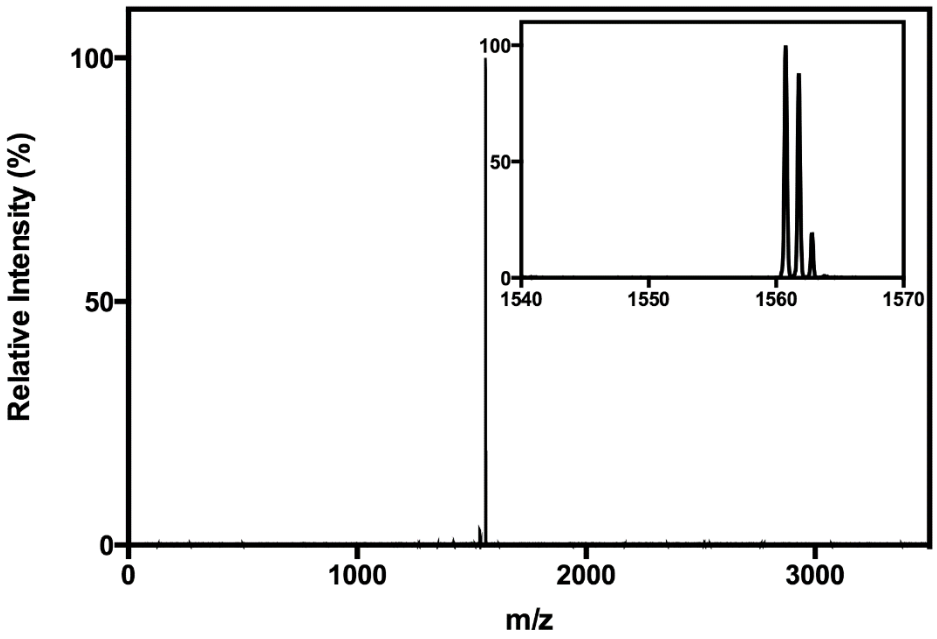
Relative Intensity (%)
100
50
0
0
1000
2000
3000
m/z
100
50
0
1540
1550
1560
1570

Method A6: Reductive "YES" degradable crosslinker synthesis (R)

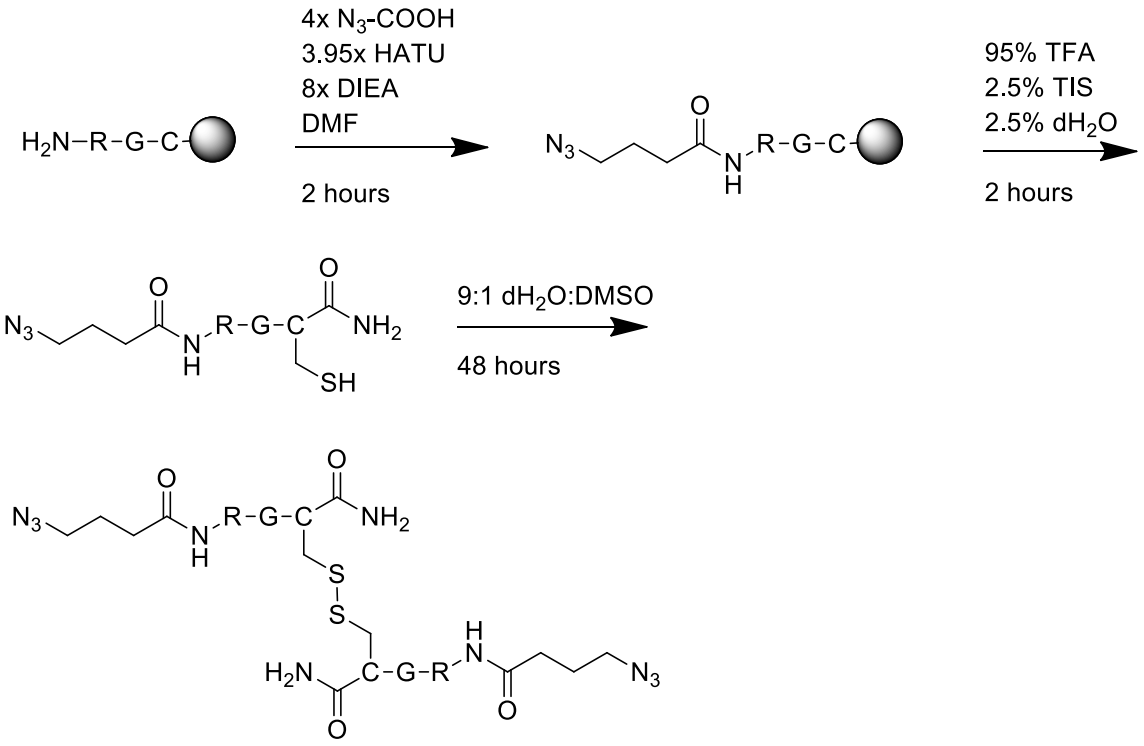

The resin-bound peptide H-RGC-NH_2 was synthesized by microwave-assisted Fmoc SPPS (Method A4) on Rink amide resin (1.0 mmol scale). N_3-COOH (Method A1, 0.517 g, 4.0 mmol, 4x) was pre-activated upon reaction with HATU (1.502 g, 3.95 mmol, 3.95x) and DIEA (1.034 g, 8.0 mmol, 8x) in minimal DMF for 5 minutes and then reacted with the resin for 90 minutes to functionalize the N-terminus with an azide. The peptide was simultaneously deprotected and cleaved from resin upon treatment with TFA/TIS/dH_2O (95:2.5:2.5, 30 mL) for 2 hours, and the crude peptide was precipitated in and washed with ice-cold diethyl ether (2x). The crude peptide was dissolved in a dH_2O/DMSO (90:10) solution (100 mL) and reacted at room temperature for 48 hours. The peptide was concentrated and purified using RP-HPLC operating with a 55 minute linear gradient (5–100%) of acetonitrile in water containing TFA (0.1%); lyophilization yielded the final product (N_3-RG<u>C</u>(N_3-RG<u>C</u>-NH_2)-NH_2 dimerized *via* <u>disulfide bond</u>, denoted R) as a yellow solid (139.5 mg, 0.1572 mol, 31.5% overall yield). Peptide purity was confirmed using MALDI-TOF: calculated for $C_{30}H_{55}N_{20}O_8S_2^+$ $[M + {}^1H]^+$, 887.4; observed 887.4.

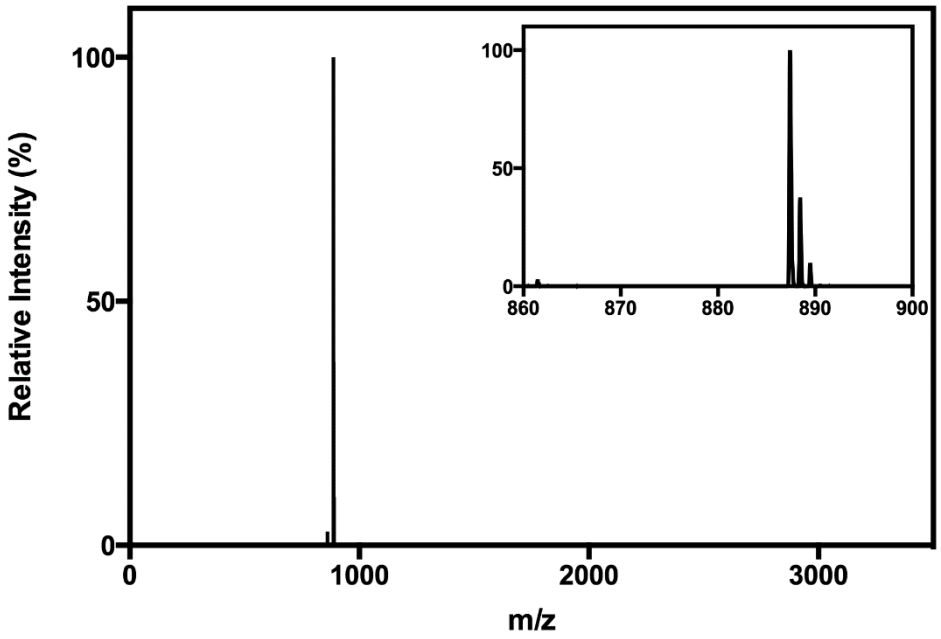
Relative Intensity (%)
100
50
0
0
1000
2000
3000
m/z
100
50
0
860
870
880
890
900

Method A7: Photo "YES" degradable crosslinker synthesis (P)

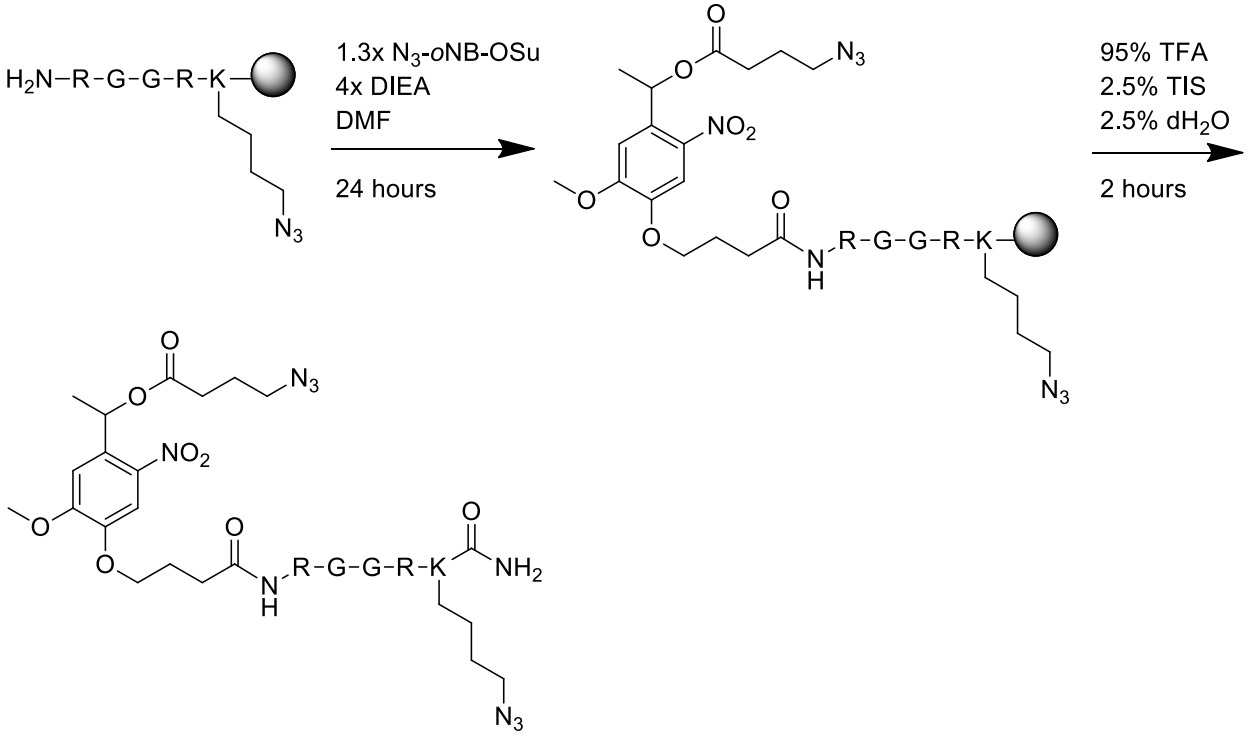

The resin-bound peptide H-RGGRK(N_3)-NH_2 was synthesized by microwave-assisted Fmoc SPPS (Method A4) on Rink amide resin (0.5 mmol scale) using a C-terminal Fmoc-Lys(N_3)-OH (Method A3). Resin was subsequently treated with N_3-*o*NB-OSu (Method A2, 0.65 mmol, 330 mg) and DIEA (2.0 mmol, 258 mg) in minimal DMF to introduce *o*NB functionality to the N-terminus. The peptide was simultaneously deprotected and cleaved from resin upon treatment with TFA/TIS/dH_2O (95:2.5:2.5, 30 mL) for 2 hours, and the crude peptide was precipitated in and washed with ice-cold diethyl ether (2x). The crude peptide was purified using RP-HPLC operating with a 43.4 minute linear gradient (20–100%) of acetonitrile in water containing TFA (0.1%); lyophilization yielded the final product (N_3-*o*NB-RGGRK(N_3)-NH_2, denoted P) as a yellow solid (147.4 mg, 0.1488 mol, 29.8% overall yield). Peptide purity was confirmed using MALDI-TOF: calculated for $C_{39}H_{64}N_{19}O_{12}^+$ $[M + {}^1H]^+$, 990.5; observed 990.4.

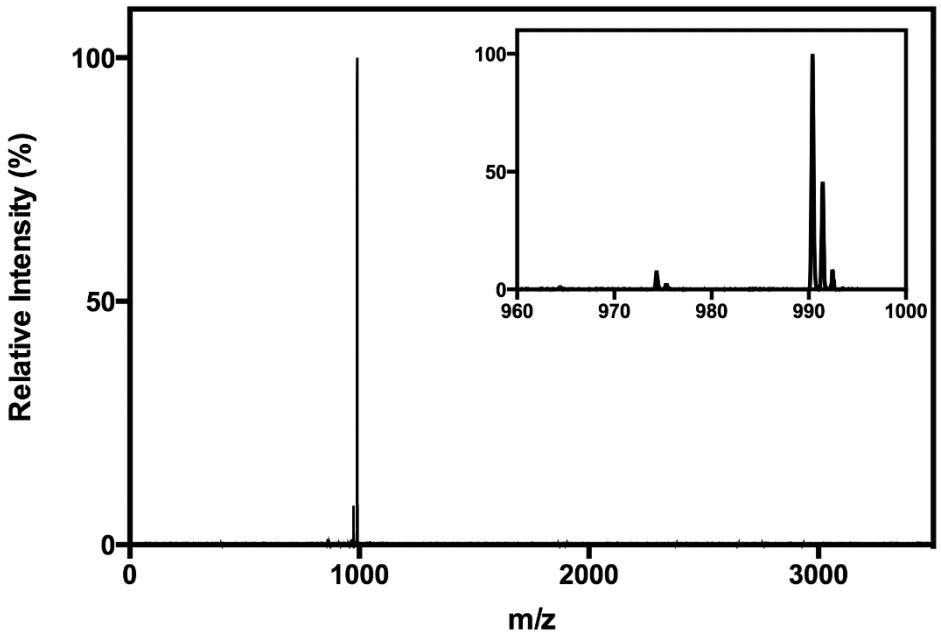
Relative Intensity (%)
100
50
0
0
1000
2000
3000
m/z
100
50
0
960
970
980
990
1000

Method A8: Reductive "OR" Enzymatic degradable crosslinker synthesis (RVE)

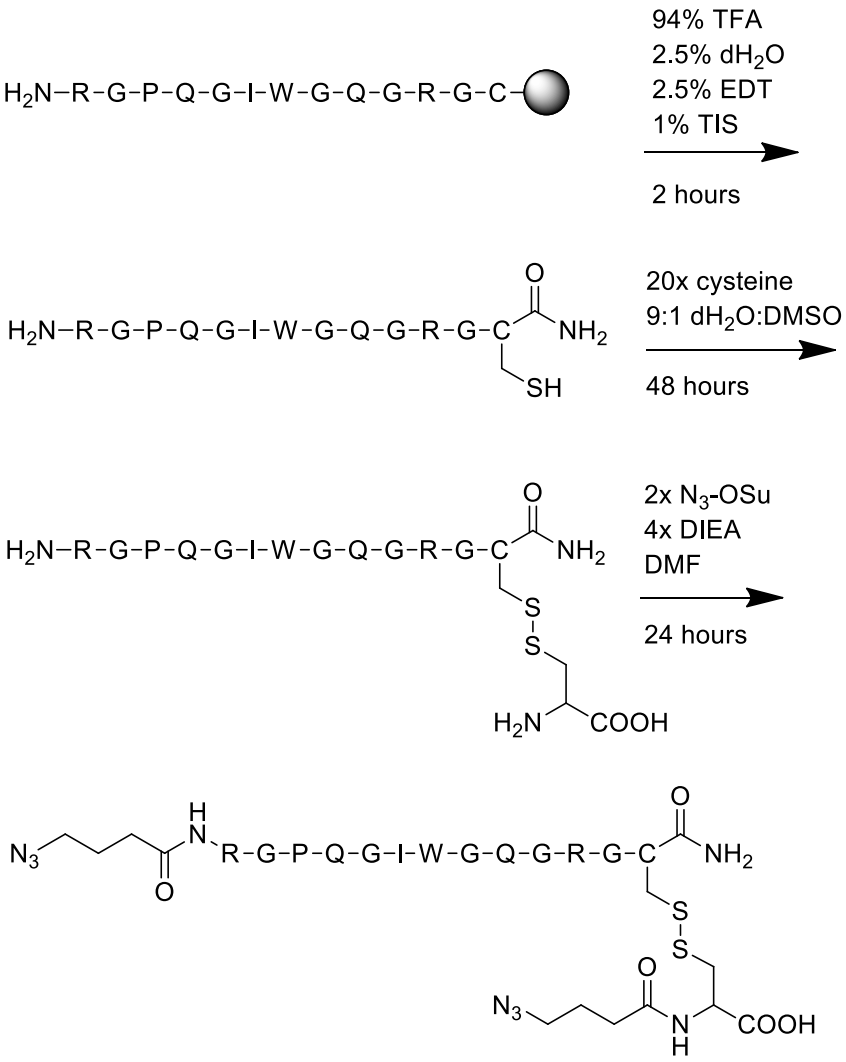

The resin-bound peptide H-RGPQGIWGQGRGC-NH_2 was synthesized by microwave-assisted Fmoc SPPS (Method A4) on Rink amide resin (0.5 mmol scale). The peptide was simultaneously deprotected and cleaved from resin upon treatment with TFA/dH_2O/1,2-ethanedithiol (EDT)/TIS (94:2.5:2.5:1, 30 mL) for 2 hours, and the crude peptide was precipitated in and washed with ice-cold diethyl ether (2x). The crude peptide was purified using RP-HPLC operating with a 55 minute linear gradient (5–100%) of acetonitrile in water containing TFA (0.1%); lyophilization yielded the pure intermediate (H-RGPQGIWGQGRGC-NH_2) as a white solid (417.4 mg, 0.305 mmol). The purified peptide and cysteine (0.74 g, 6.1 mmol, 20x) were dissolved in a dH_2O/DMSO (90:10) solution (50 mL) and stirred at room temperature for 48 hours. Product was filtered, concentrated *in vacuo*, and purified using RP-HPLC operating with a 55 minute linear gradient (5–100%) of acetonitrile in water containing TFA (0.1%); lyophilization yielded the pure intermediate (H-RGPQGIWGQGRGC(H-C-OH)-NH_2 with cysteines linked *via* disulfide bond) as a white solid (241.4 mg, 0.162 mmol). To introduce azide functionalities requisite for hydrogel crosslinking, N_3-OSu (Method A1, 146.6 mg, 0.648 mmol, 2x) was dissolved in minimal DMF

with DIEA (167.5 mg, 1.30 mmol, 4x) and reacted with the peptide overnight at room temperature. The peptide was purified using RP-HPLC operating with a 55 minute linear gradient (5–100%) of acetonitrile in water containing TFA (0.1%); lyophilization yielded the final product (N_3-RGPQGIWGQGRGC(N_3-C-OH)-NH_2 with cysteines linked *via* disulfide bridge, denoted RVE) as a white solid (89.8 mg, 0.0525 mmol, 10.5% overall yield). Peptide purity was confirmed using MALDI-TOF: calculated for $C_{68}H_{107}N_{30}O_{19}S_2^+$ $[M + {}^1H]^+$, 1711.7; observed 1711.5.

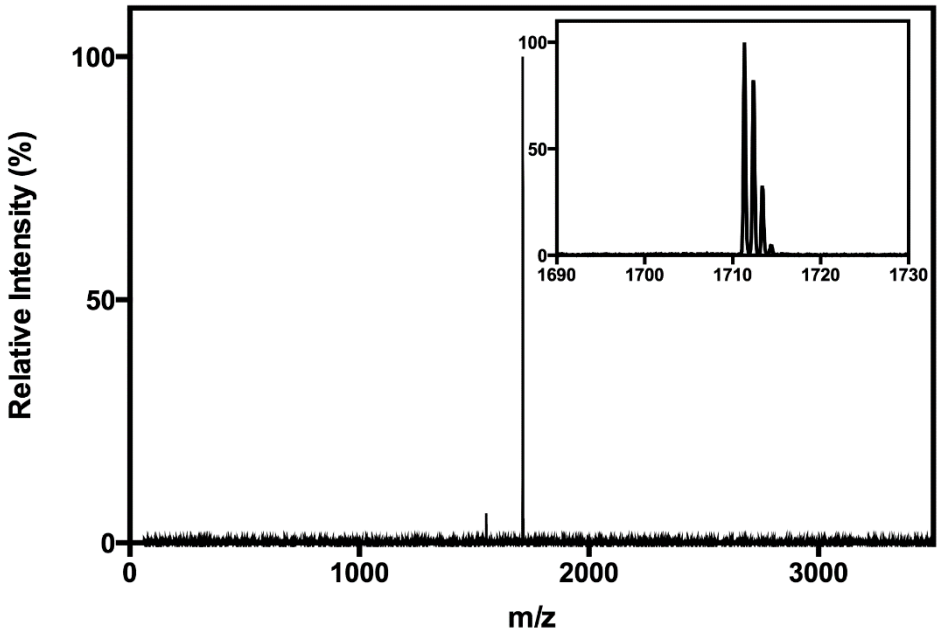

Method A9: Enzymatic "OR" Photo degradable crosslinker synthesis (EVP)

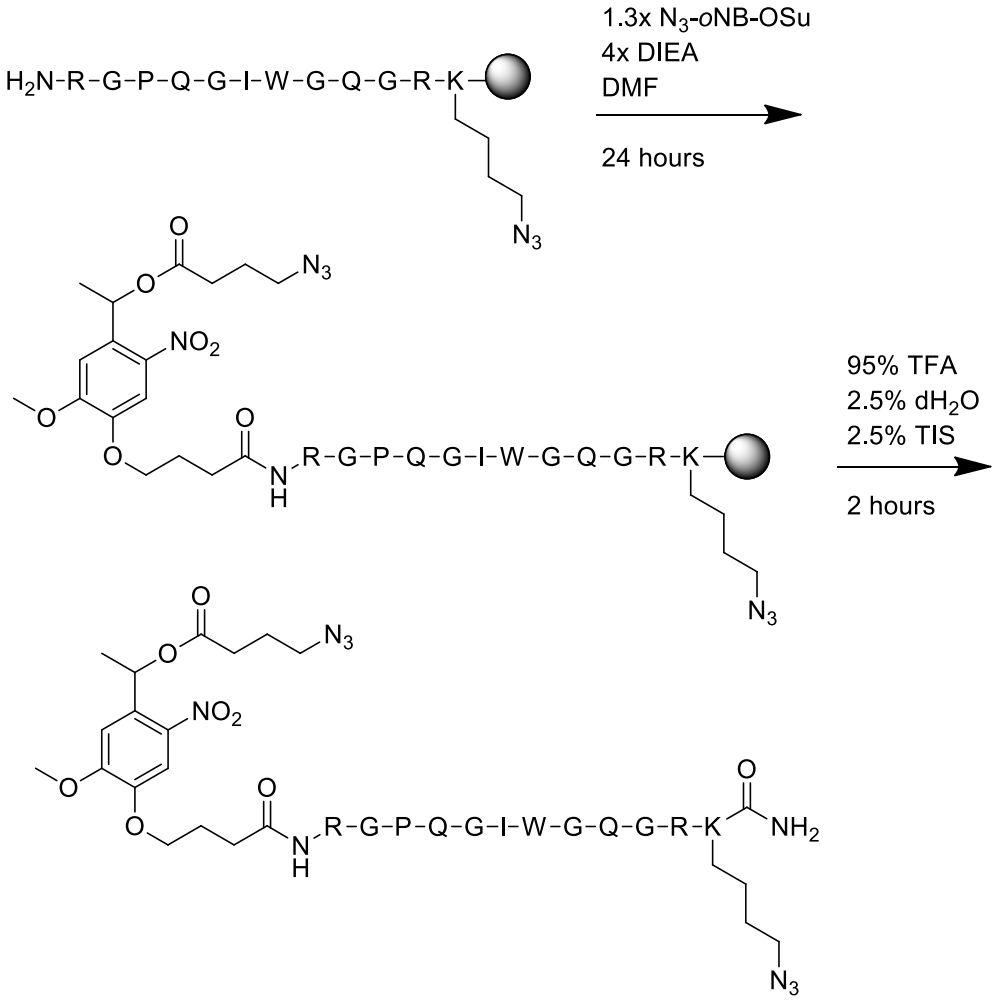

The resin-bound peptide H-RGPQGIWGQGRK(N_3)-NH_2 was synthesized by microwave-assisted Fmoc SPPS (Method A4) on Rink amide resin (0.5 mmol scale) using a C-terminal Fmoc-Lys(N_3)-OH (Method A3). Resin was subsequently treated with N_3-*o*NB-OSu (Method A2, 0.65 mmol, 330 mg) and DIEA (2.0 mmol, 258 mg) in minimal DMF to introduce *o*NB functionality to the N-terminus. The peptide was simultaneously deprotected and cleaved from resin upon treatment with TFA/TIS/dH_2O (95:2.5:2.5, 30 mL) for 2 hours, and the crude peptide was precipitated in and washed with ice-cold diethyl ether (2x). The crude peptide was purified using RP-HPLC operating with a 43.4 minute linear gradient (20–100%) of acetonitrile in water containing TFA (0.1%); lyophilization yielded the final product (N_3-*o*NB-RGPQGIWGQGRK(N_3)-NH_2, denoted EVP) as a yellow solid (159.9 mg, 0.0910 mmol, 18.2% overall yield). Peptide purity was confirmed using MALDI-TOF: calculated for $C_{75}H_{114}N_{29}O_{21}^+$ $[M + {}^1H]^+$, 1756.9; observed 1756.9.

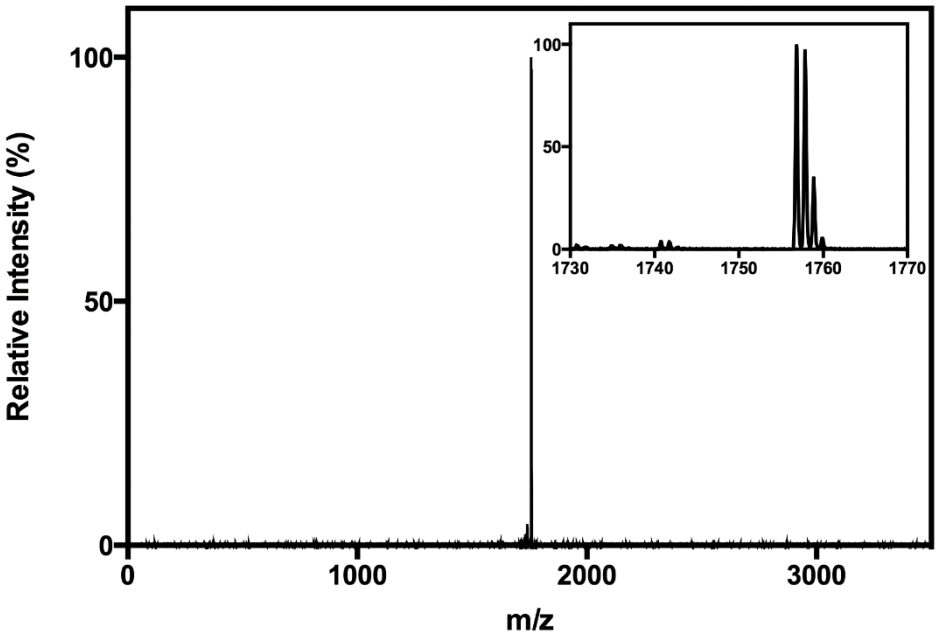
Relative Intensity (%)
100
50
0
0
1000
2000
3000
m/z
100
50
0
1730
1740
1750
1760
1770

Method A10: Reductive "OR" Photo degradable crosslinker synthesis (RVP)

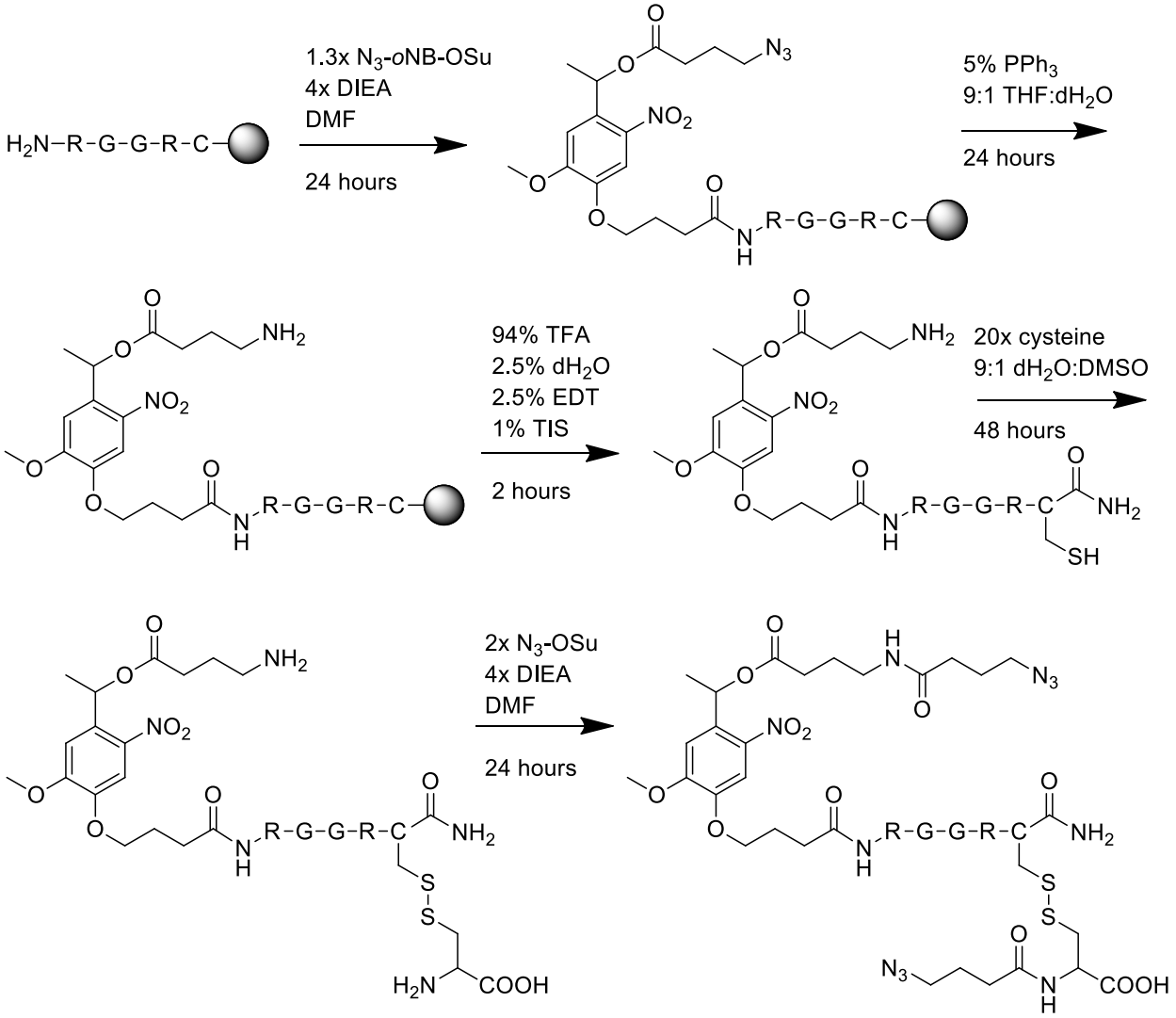

The resin-bound peptide H-RGGRC-NH_2 was synthesized by microwave-assisted Fmoc SPPS (Method A4) on Rink amide resin (0.5 mmol scale). Resin was subsequently treated with N_3-*o*NB-OSu (Method A2, 0.65 mmol, 330 mg) and DIEA (2.0 mmol, 258 mg) in minimal DMF to introduce *o*NB functionality to the N-terminus. The N-terminal azide was reduced to an amine by a Staudinger reduction; resin was washed with tetrahydrofuran (THF)/H_2O (90:10, 3 x 20 mL), followed by reaction with 5 wt% triphenylphosphine in THF/H_2O (90:10, 30 mL) for 18 hours. The peptide was simultaneously deprotected and cleaved from resin upon treatment with TFA/dH_2O/EDT/TIS (94:2.5:2.5:1, 30 mL) for 2 hours, and the crude peptide was precipitated in and washed with ice-cold diethyl ether (2x). The crude peptide was purified using RP-HPLC operating with a 43.4 minute linear gradient (20–100%) of acetonitrile in water containing TFA (0.1%); lyophilization yielded the pure intermediate (H-*o*NB-RGGRC-NH_2) as a yellow solid (146.4 mg, 0.160 mmol). The purified peptide and cysteine (0.39 g, 3.2 mmol, 20x) were dissolved in a dH_2O/DMSO (90:10) solution (50 mL) and stirred at room temperature for 48 hours. The peptide was filtered, concentrated *in vacuo*, and purified using RP-HPLC operating with a 43.4

minute linear gradient (20–100%) of acetonitrile in water containing TFA (0.1%); lyophilization yielded the pure intermediate (H-*o*NB-RGGRC(H-C-OH)-NH_2 with cysteines linked *via* disulfide bond) as a yellow solid (120.8 mg, 0.117 mmol). N_3-OSu (Method A1, 121 mg, 0.468 mmol, 2x) was dissolved in minimal DMF with DIEA (167.5 mg, 0.963 mmol, 4x) and reacted with the peptide overnight at room temperature. The peptide was purified using RP-HPLC operating with a 43.4 minute linear gradient (20–100%) of acetonitrile in water containing TFA (0.1%); lyophilization yielded the final product (N_3-*o*NB-RGGRC(N_3-C-OH)-NH_2 with cysteines linked *via* disulfide bond, denoted RVP) as a yellow solid (32.2 mg, 0.0257 mmol, 5.1% overall yield). Peptide purity was confirmed using MALDI-TOF: calculated for $C_{47}H_{76}N_{21}O_{16}S_2^+$ $[M + {}^1H]^+$, 1254.5; observed 1254.6.

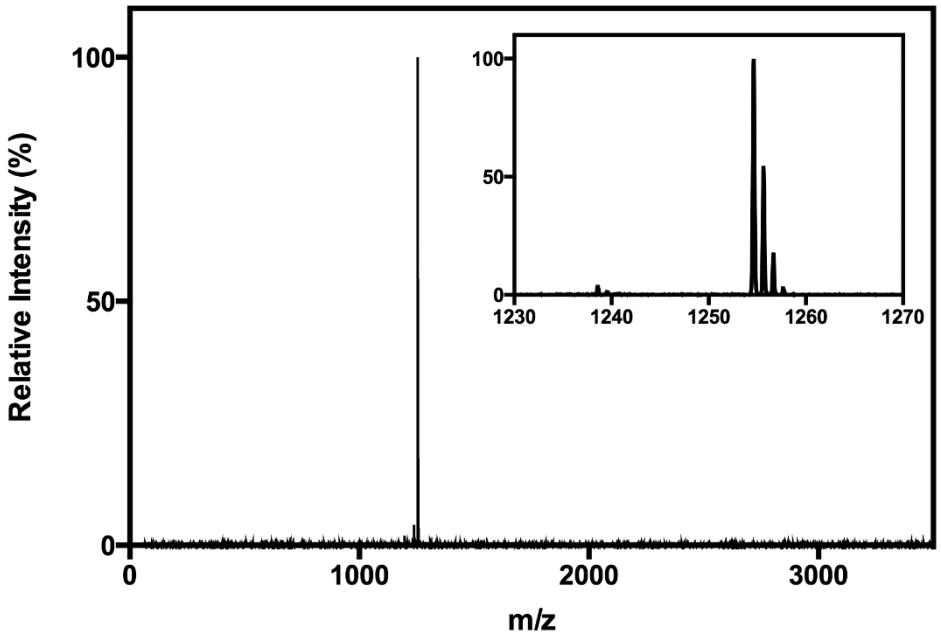

Method A11: Reductive "AND" Enzymatic degradable crosslinker synthesis (R∧E)

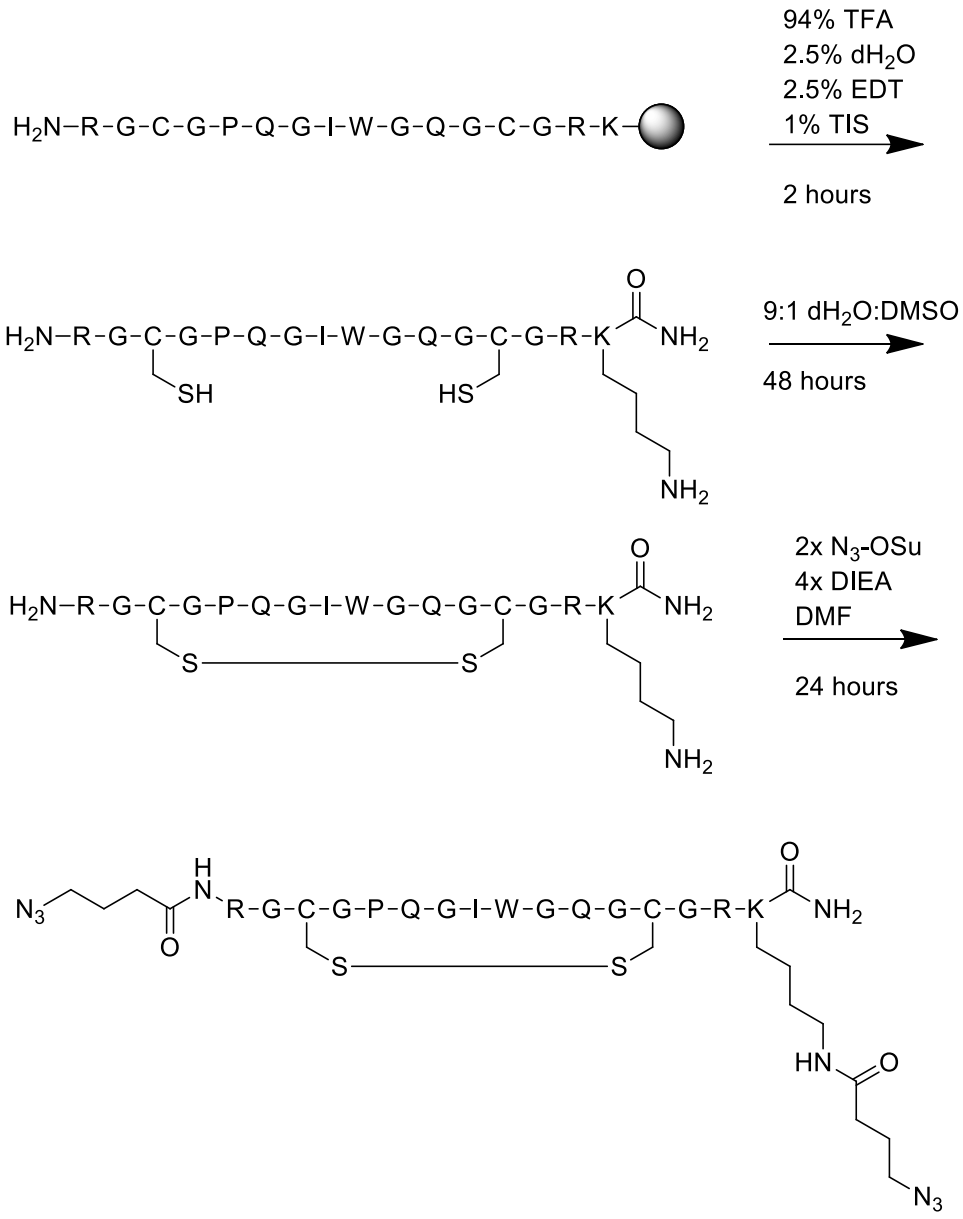

The resin-bound peptide H-RGCGPQGIWGQGCGRK-NH_2 was synthesized by microwave-assisted Fmoc SPPS (Method A4) on Rink amide resin (1.0 mmol scale). The peptide was simultaneously deprotected and cleaved from resin upon treatment with TFA/dH_2O/EDT/TIS (94:2.5:2.5:1) for 3 hours and the crude peptide was precipitated in and washed with ice-cold diethyl ether (2x). The crude peptide was purified using RP-HPLC operating with a 55 minute linear gradient (5–100%) of acetonitrile in water containing TFA (0.1%); lyophilization yielded the pure intermediate (H-RGCGPQGIWGQGCGRK-NH_2) as a white solid (531.0 mg, 0.320 mmol). To promote disulfide-mediated intramolecular stapling, the purified peptide was dissolved at 0.5 mM in a dH_2O/DMSO (90:10) solution (700 mL) and reacted at room temperature with no agitation for 48 hours. Stapled product was concentrated *in vacuo* and purified using RP-HPLC

operating with a 55 minute linear gradient (5–100%) of acetonitrile in water containing TFA (0.1%); lyophilization yielded the pure intermediate (H-RGCGPQGIWGQGCGRK-NH_2 with intramolecular stapling *via* cysteine-cysteine disulfide bond) as a white solid (489 mg, 0.295 mmol). To introduce azide functionalities requisite for hydrogel crosslinking, N_3-OSu (Method A1, 267 mg, 1.18 mmol, 2x) was dissolved in minimal DMF with DIEA (305 mg, 2.36 mmol, 4x) and reacted with the peptide overnight at room temperature. Stapled peptide was purified using RP-HPLC operating with a 55 minute linear gradient (5–100%) of acetonitrile in water containing TFA (0.1%); lyophilization yielded the final product (N_3-RGCGPQGIWGQGCGRK(N_3)-NH_2 with intramolecular stapling *via* cysteine-cysteine disulfide bond, denoted R∧E) as a white solid (197 mg, 0.105 mmol, 10.5% overall yield). Peptide purity was confirmed using MALDI-TOF: calculated for $C_{76}H_{120}N_{33}O_{20}S_2^+$ $[M + {}^1H]^+$, 1878.9; observed 1879.0.

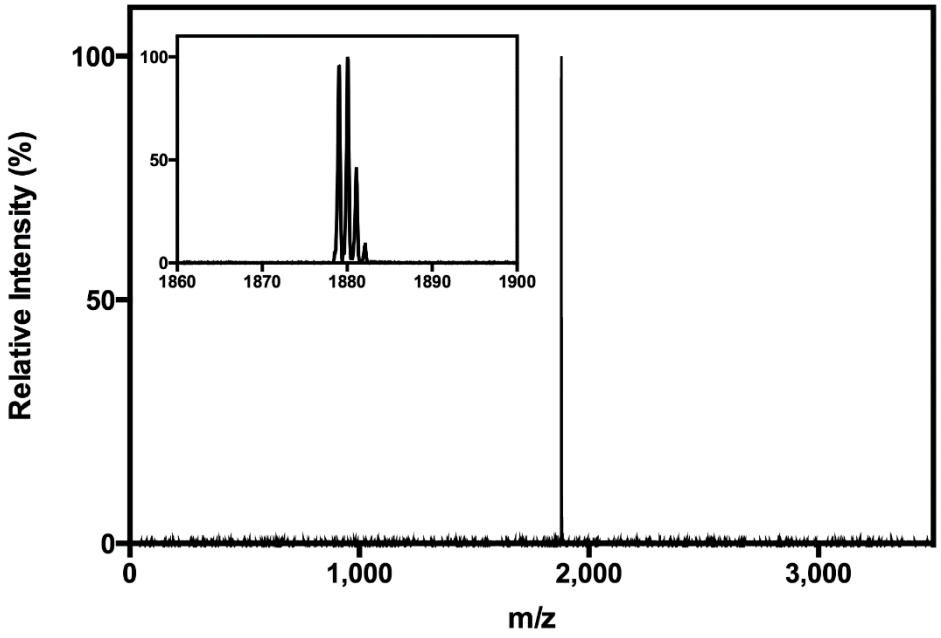

Method A12: Enzymatic “AND” Photo degradable crosslinker synthesis (E∧P)

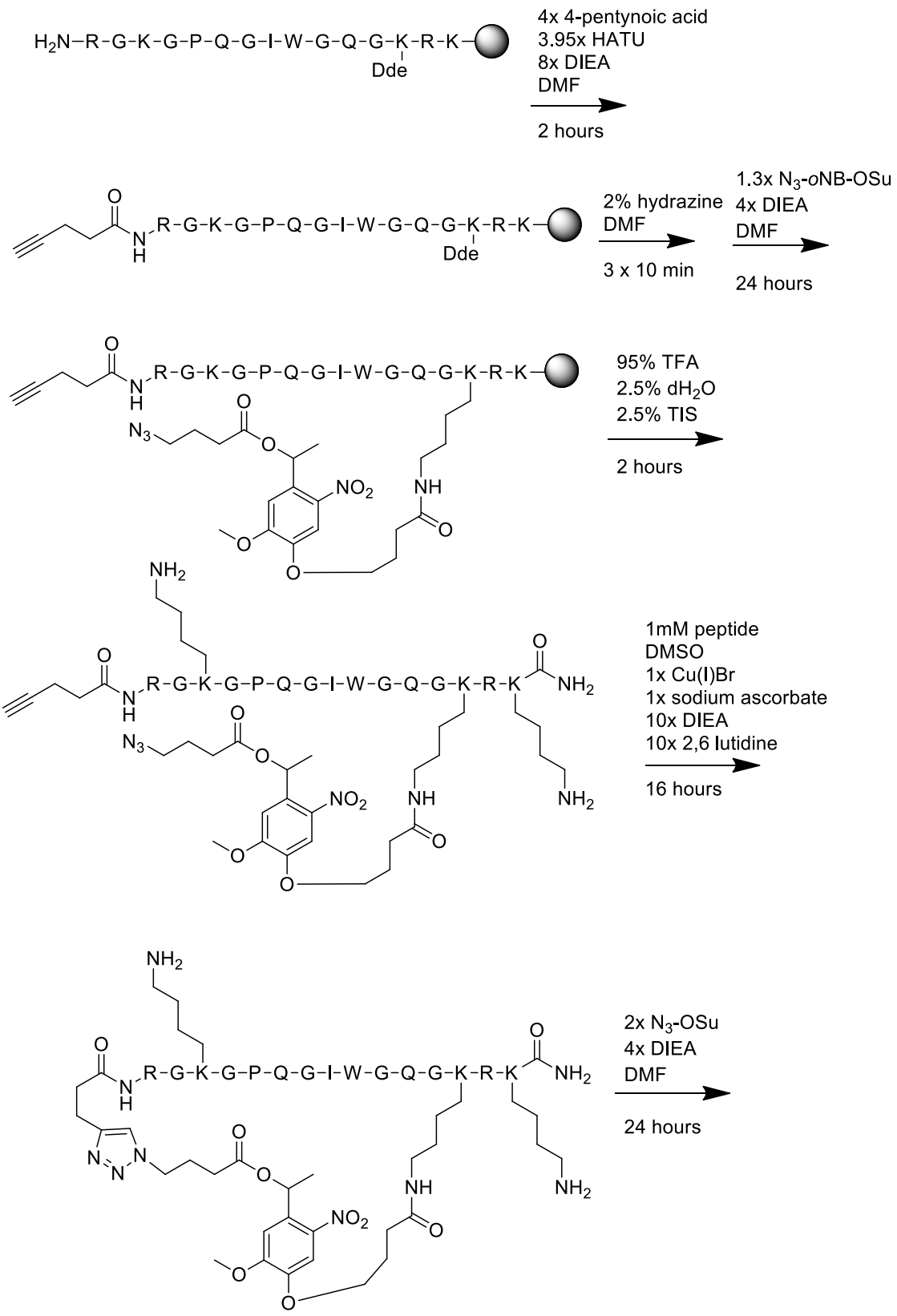
H2N–R–G–K–G–P–Q–G–I–W–G–Q–G–K–R–K
Dde
4x 4-pentynoic acid
3.95x HATU
8x DIEA
DMF
2 hours
2% hydrazine
DMF
3 x 10 min
1.3x N3-oNB-OSu
4x DIEA
DMF
24 hours
95% TFA
2.5% dH2O
2.5% TIS
2 hours
1mM peptide
DMSO
1x Cu(I)Br
1x sodium ascorbate
10x DIEA
10x 2,6 lutidine
16 hours
2x N3-OSu
4x DIEA
DMF
24 hours

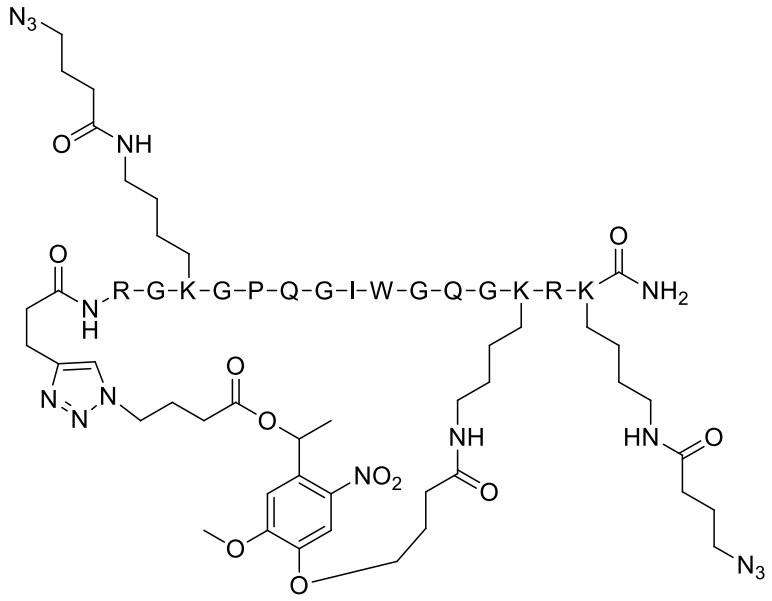

The resin-bound peptide H-RGKGPQGIWGQGK(Dde)RK-NH_2 was synthesized by microwave-assisted Fmoc SPPS (Method A4) on Rink amide resin (0.5 mmol scale). 4-pentynoic acid (0.196 g, 2.0 mmol, 4x) was pre-activated upon reaction with HATU (0.751 g, 1.975 mmol, 3.95x) and DIEA (0.517 g, 4.0 mmol, 8x) in minimal DMF for 5 minutes and then reacted with the resin for 90 minutes to functionalize the N-terminus with an alkyne. The resin was treated with hydrazine monohydrate (2%) in DMF (3 x 10 min) to remove the Dde protecting group. Resin was subsequently treated with N_3-*o*NB-OSu (Method A2, 0.65 mmol, 330 mg) and DIEA (2.0 mmol, 258 mg) in minimal DMF to introduce *o*NB functionality to the ε-amino group of the unprotected lysine. The peptide was simultaneously deprotected and cleaved from resin upon treatment with TFA/TIS/dH_2O (95:2.5:2.5, 30 mL) for 2 hours, and the crude peptide was precipitated in and washed with ice-cold diethyl ether (2x). The crude peptide was purified using RP-HPLC operating with a 43.4 minute linear gradient (20–100%) of acetonitrile in water containing TFA (0.1%); lyophilization yielded the pure intermediate (yne-RGKGPQGIWGQGK(*o*NB-N_3)RK-NH_2) as a yellow solid (116 mg, 0.0546 mmol). To induce CuAAC-mediated intramolecular stapling (copper(I)-catalyzed azide-alkyne cycloaddition), pure linear peptide (1 mM) was dissolved in nitrogen-purged DMSO (55 mL) containing copper(I) bromide (7.8 mg, 0.055 mmol, 1x), sodium ascorbate (10.8 mg, 0.055 mmol, 1x) in water (550 µL), 2,6 lutidine (55.8 mg, 0.546 mmol, 10x), and DIEA (70.6 mg, 0.546 mmol, 10x). This mixture was allowed to react under nitrogen at room temperature for 16 hours. The mixture was concentrated *in vacuo*, redissolved in dH_2O, passed through an ion exchange column (Dowex M4195 resin, 5 grams), and lyophilized. Stapled product was purified using RP-HPLC operating with a 43.4 minute linear gradient (20–100%) of acetonitrile in water containing TFA (0.1%); lyophilization yielded the pure intermediate (yne-RGKGPQGIWGQGK(*o*NB-N_3)RK-NH_2 with an intramolecular staple *via* a triazole linkage between the alkyne and *o*NB-N_3 side chains) as a yellow solid (36 mg, 0.017 mmol). To introduce azide functionalities requisite for hydrogel crosslinking, N_3-OSu (Method A1, 15.4 mg, 0.068 mmol, 2x) was dissolved in minimal DMF with DIEA (17.6 mg, 0.69 mmol, 4x) and reacted with the peptide overnight at room temperature. The stapled peptide was purified using RP-HPLC operating with a 43.4 minute linear gradient (20–100%) of acetonitrile in water containing TFA (0.1%); lyophilization yielded the final product (yne-RGK(N_3)GPQGIWGQGK(*o*NB-N_3)RK(N_3)-

NH_2 with an intramolecular staple *via* a triazole linkage between the alkyne and *o*NB-N_3 side chains, denoted EΛP) as a yellow solid (11.2 mg, 0.00477 mmol, 0.95% overall yield). Peptide purity was confirmed using MALDI-TOF: calculated for $C_{108}H_{166}N_{41}O_{30}^{+}$ $[M + {}^{1}H]^{+}$, 2346.2; observed 2346.2.

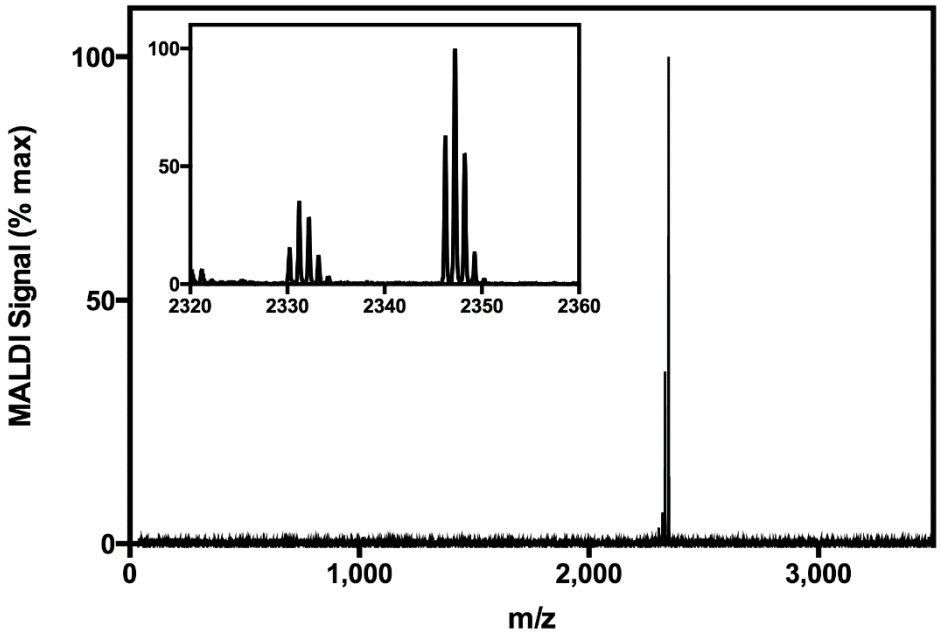

Method A13: Reductive "AND" Photo degradable crosslinker synthesis (RΛP)

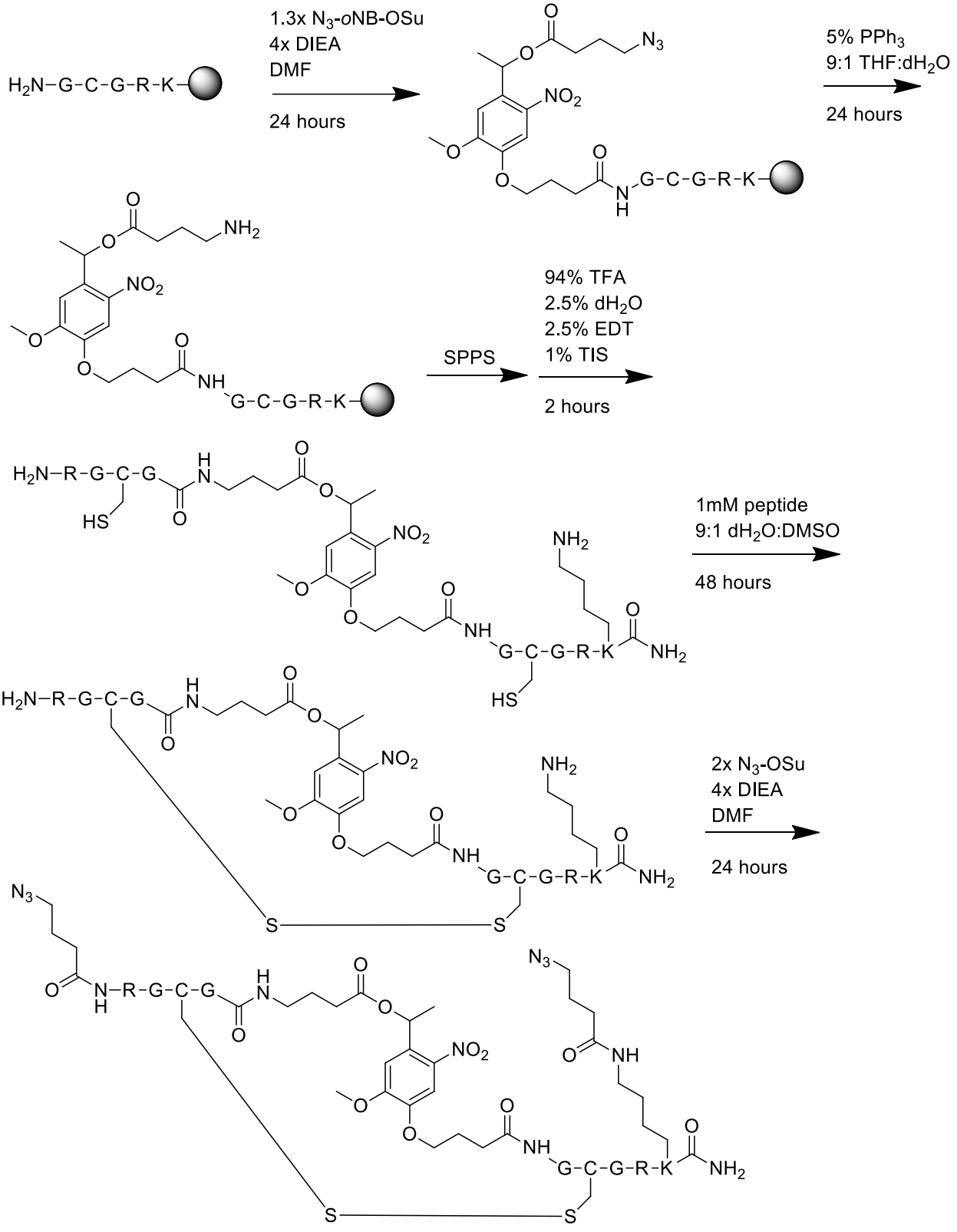

The resin-bound peptide H-GCGRK-NH_2 was synthesized by microwave-assisted Fmoc SPPS (Method A4) on Rink amide resin (0.5 mmol scale). Resin was subsequently treated with N_3-*o*NB-OSu (Method A2, 0.65 mmol, 330 mg) and DIEA (2.0 mmol, 258 mg) in minimal DMF to introduce *o*NB functionality to the N-terminus. The N-terminal azide was reduced to an amine by a Staudinger reduction; resin was washed with THF/H_2O (90:10, 3 x 20 mL), followed by reaction with 5 wt% triphenylphosphine in THF/H_2O (90:10, 30 mL) for 18 hours. The peptide sequence H-RGCG was appended to the N-terminus by standard microwave-assisted Fmoc SPPS (Method A4). The peptide was simultaneously deprotected and cleaved from resin upon treatment with TFA/dH_2O/EDT/TIS (94:2.5:2.5:1, 30 mL) for 2 hours, and the crude peptide was precipitated in and washed with ice-cold diethyl ether (2x). The crude peptide was purified using RP-HPLC operating with a 55 minute linear gradient (5–100%) of acetonitrile in water containing TFA (0.1%) lyophilization yielded the pure intermediate (H-RGCG-*o*NB-GCGRK-NH_2) as a yellow solid (119 mg, 0.0946 mmol). To promote disulfide-mediated intramolecular stapling, the purified peptide was dissolved at 0.5 mM in a dH_2O/DMSO (90:10) solution (200 mL) and reacted at room temperature with no agitation for 48 hours. Stapled product was concentrated *in vacuo* and purified using RP-HPLC operating with a 55 minute linear gradient (5–100%) of acetonitrile in water containing TFA (0.1%); lyophilization yielded the intermediate (H-RG<u>C</u>G-*o*NB-G<u>C</u>GRK-NH_2 with intramolecular stapling *via* cysteine-cysteine <u>disulfide bond</u>) as a yellow solid (101 mg, 0.0807 mmol). To introduce azide functionalities requisite for hydrogel crosslinking, N_3-OSu (Method A1, 73.0 mg, 0.323 mmol, 2x) was dissolved in minimal DMF with DIEA (83.4 mg, 0.646 mmol, 4x) and reacted with the peptide overnight at room temperature. The stapled peptide was purified using RP-HPLC operating with a 55 minute linear gradient (5–100%) of acetonitrile in water containing TFA (0.1%); lyophilization yielded the final product (N_3-RG<u>C</u>G-*o*NB-G<u>C</u>GRK(N_3)-NH_2 with intramolecular stapling *via* cysteine-cysteine <u>disulfide bond</u>, denoted R∧P) as a yellow solid (20.0 mg, 0.0135 mmol, 2.7% overall yield). Peptide purity was confirmed using MALDI-TOF: calculated for $C_{57}H_{92}N_{25}O_{18}S_2^+$ $[M + {}^1H]^+$, 1478.6; observed 1478.8.

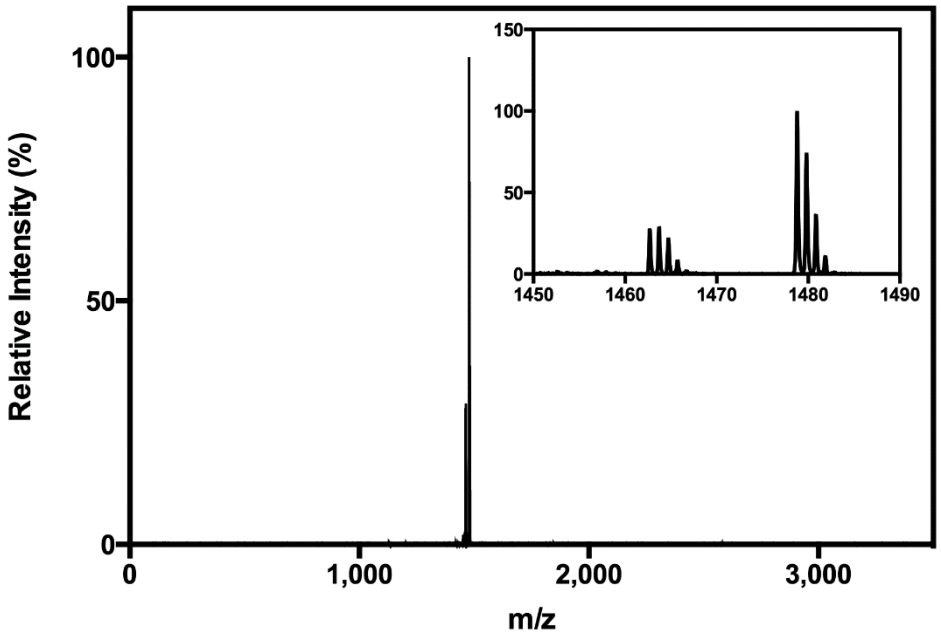

Method A14: Enzymatic “OR” Reductive “OR” Photo degradable crosslinker synthesis [R∨E∨P]

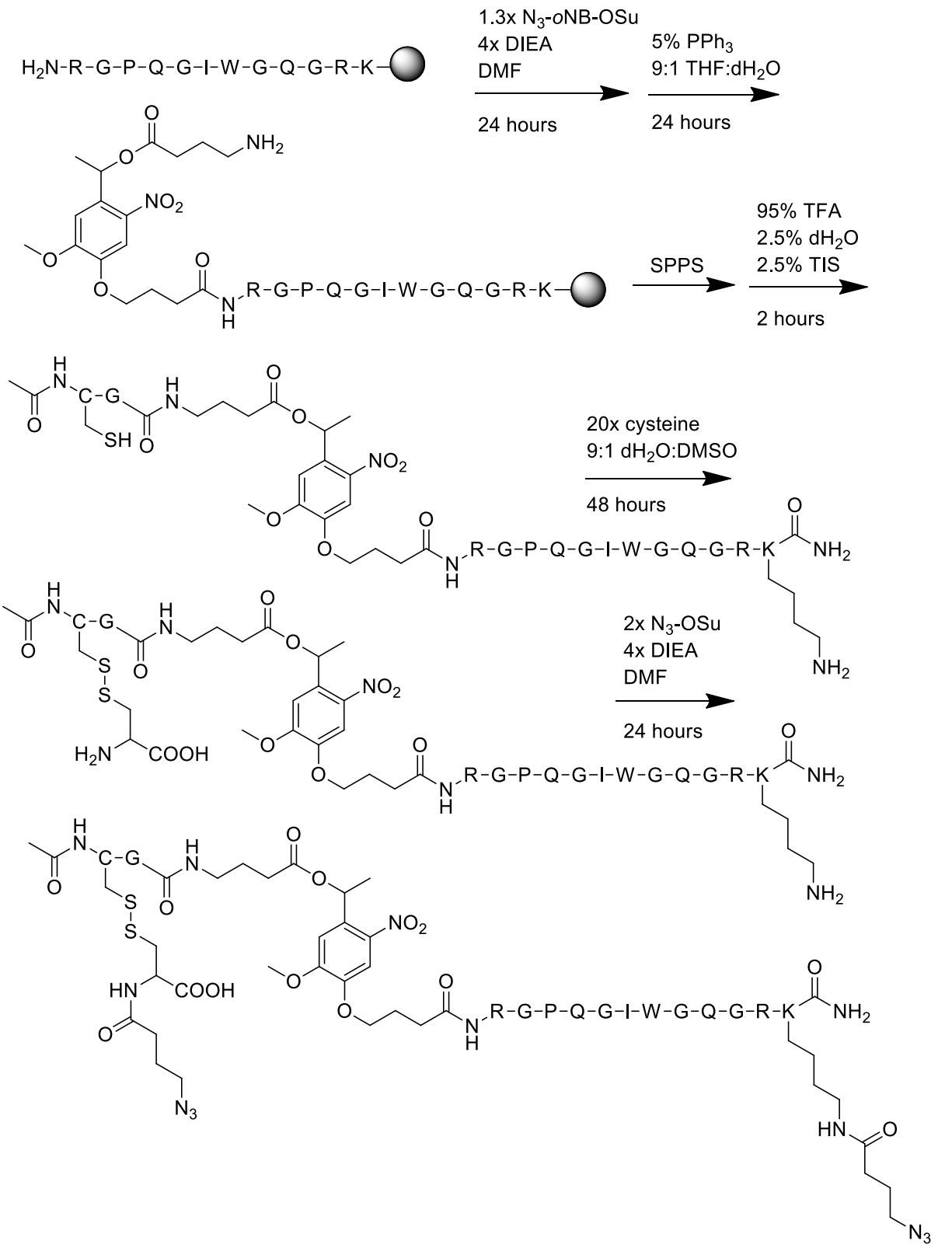

The resin-bound peptide H-RGPQGIWGQGRK-NH_2 was synthesized by microwave-assisted Fmoc SPPS (Method A4) on Rink amide resin (0.5 mmol scale). Resin was subsequently treated

with N_3-*o*NB-OSu (Method A2, 0.65 mmol, 330 mg) and DIEA (2.0 mmol, 258 mg) in minimal DMF to introduce *o*NB functionality to the N-terminus. The N-terminal azide was reduced to an amine by a Staudinger reduction; resin was washed with THF/H_2O (90:10, 3 x 20 mL), followed by reaction with 5 wt% triphenylphosphine in THF/H_2O (90:10, 30 mL) for 18 hours. The peptide sequence Ac-CG was appended to the N-terminus by standard microwave-assisted Fmoc SPPS. The peptide was simultaneously deprotected and cleaved from resin upon treatment with TFA/TIS/dH_2O (95:2.5:2.5, 30 mL) for 2 hours, and the crude peptide was precipitated in and washed with ice-cold diethyl ether (2x). The crude peptide was purified using RP-HPLC operating with a 43.4 minute linear gradient (20–100%) of acetonitrile in water containing TFA (0.1%); lyophilization yielded the pure intermediate (Ac-CG-*o*NB-RGPQGIWGQGRK-NH_2) as a yellow solid (81 mg, 0.0425 mmol). The purified peptide and cysteine (103 mg, 0.850 mmol, 20x) were dissolved in a dH_2O/DMSO (90:10) solution (100 mL) and stirred at room temperature for 48 hours. The peptide was filtered, concentrated *in vacuo*, and purified using RP-HPLC operating with a 43.4 minute linear gradient (20–100%) of acetonitrile in water containing TFA (0.1%); lyophilization yielded the pure intermediate (Ac-C(H-C-OH)G-*o*NB-RGPQGIWGQGRK-NH_2 with cysteines linked *via* disulfide bond) as a yellow solid (30.9 mg, 0.0152 mmol). To introduce azide functionalities requisite for hydrogel crosslinking, N_3-OSu (Method A1, 13.8 mg, 0.0608 mmol, 2x) was dissolved in minimal DMF with DIEA (15.7 mg, 0.122 mmol, 4x) and reacted with the peptide overnight at room temperature. The peptide was purified using RP-HPLC operating with a 43.4 minute linear gradient (20–100%) of acetonitrile in water containing TFA (0.1%); lyophilization yielded the final product (Ac-C(N_3-C-OH)G-*o*NB-RGPQGIWGQGRK(N_3)-NH_2 with cysteines linked *via* disulfide bond, denoted RV[EVP]) as a yellow solid (32.2 mg, 0.0257 mmol, 5.1% overall yield). Peptide purity was confirmed using MALDI-TOF: calculated for $C_{93}H_{143}N_{34}O_{28}S_2^+$ $[M + {}^1H]^+$, 2248.0; observed 2248.6.

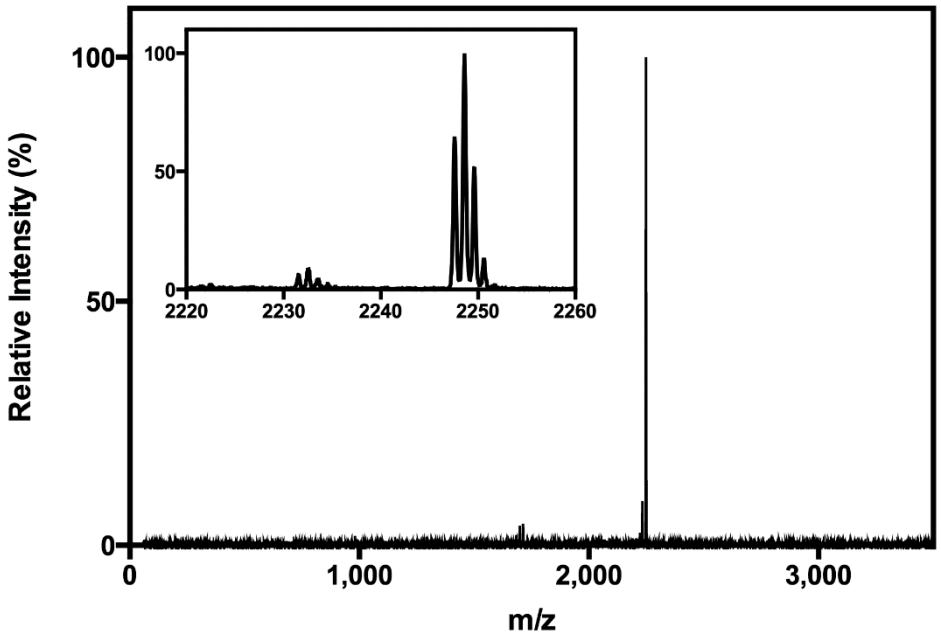

Method A15: Enzymatic "AND" Reductive "AND" Photo degradable crosslinker synthesis [RΛEΛP]

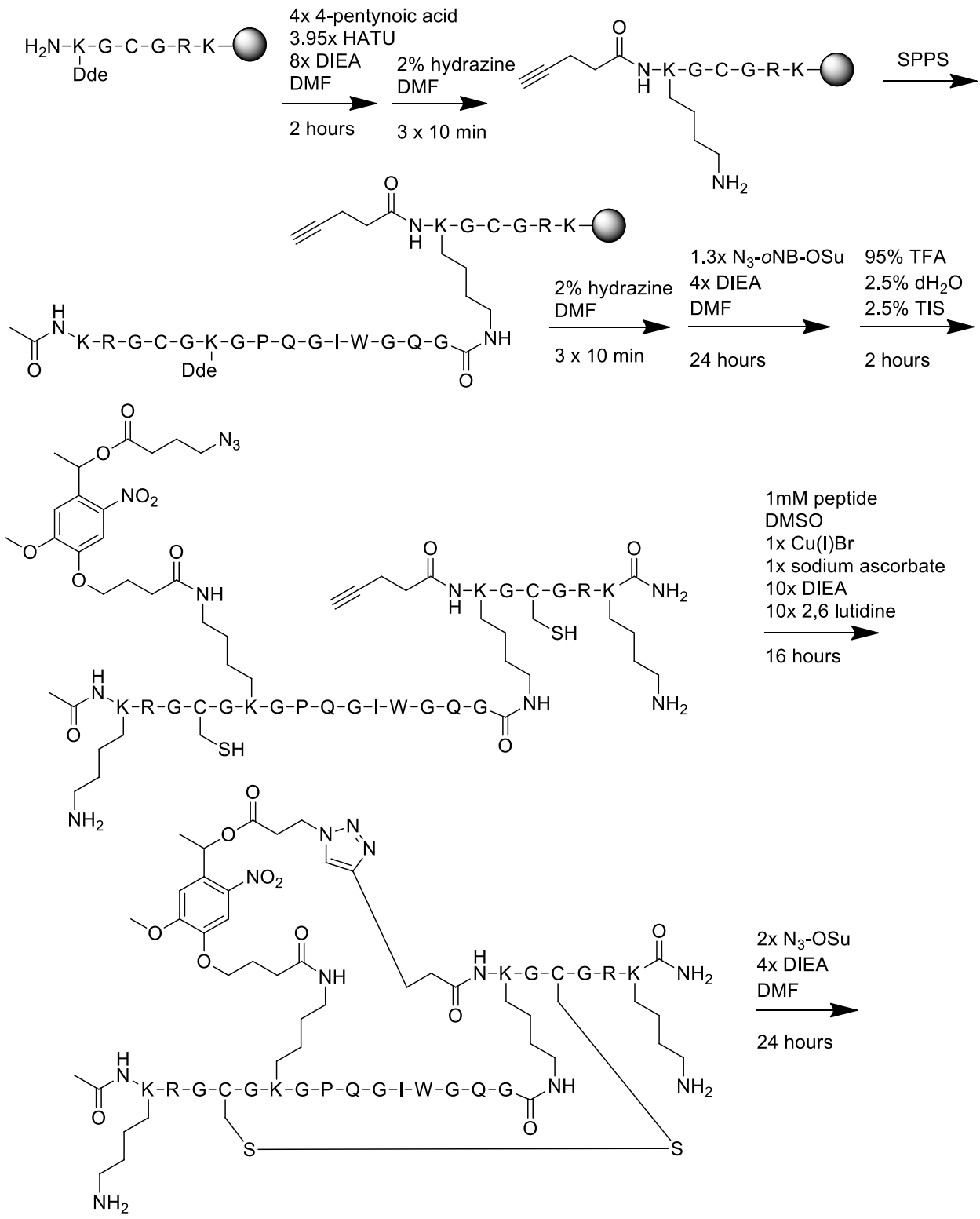

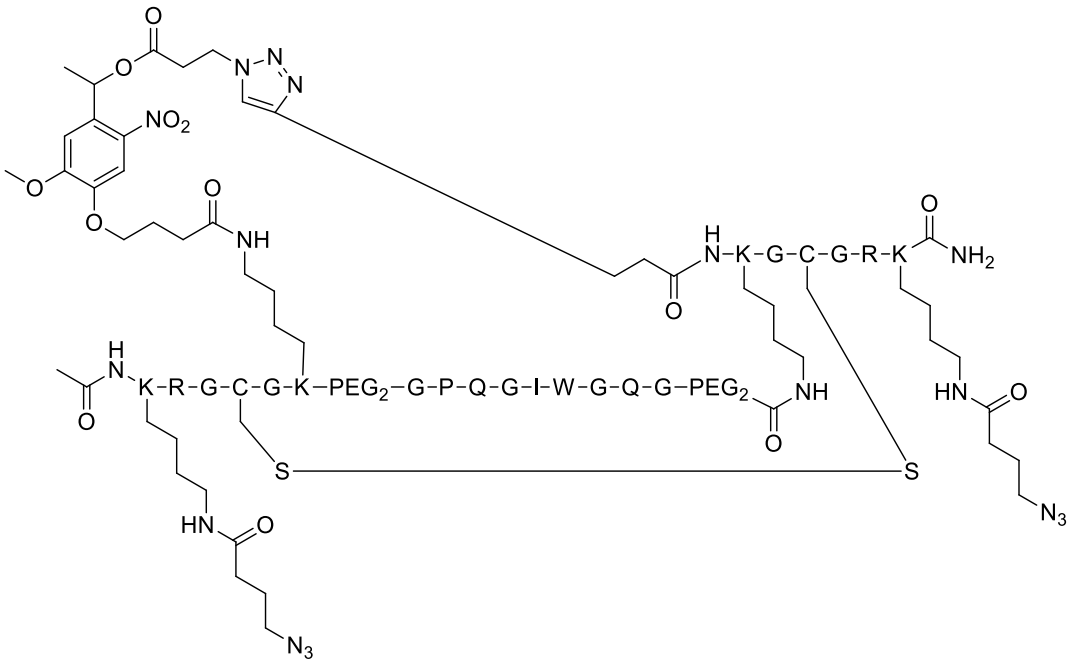

The resin-bound peptide H-K(Dde)GCGRK-NH_2 was synthesized by microwave-assisted Fmoc SPPS (Method A4) on Rink amide resin (0.5 mmol scale). 4-pentynoic acid (0.196 g, 2.0 mmol, 4x) was pre-activated upon reaction with HATU (0.751 g, 1.975 mmol, 3.95x) and DIEA (0.517 g, 4.0 mmol, 8x) in minimal DMF for 5 minutes and then reacted with the resin for 90 minutes to functionalize the N-terminus with an alkyne. The resin was treated with hydrazine monohydrate (2%) in DMF (3 x 10 min) to remove the Dde protecting group. Fmoc-8-amino-3,6-dioxaoctanoic acid (residue denoted PEG_2) was incorporated into the peptide sequence Ac-KRGCGK(Dde)-PEG_2-GPQGIWGQG-PEG_2, which was appended to the ε-amino group of the unprotected lysine by standard microwave-assisted Fmoc SPPS. The resin was again treated with hydrazine monohydrate (2%) in DMF (3 x 10 min) to remove the second Dde protecting group. Resin was subsequently treated with N_3-*o*NB-OSu (Method A2, 0.65 mmol, 330 mg) and DIEA (2.0 mmol, 258 mg) in minimal DMF to introduce *o*NB functionality to the ε-amino group of the unprotected lysine. The peptide was simultaneously deprotected and cleaved from resin upon treatment with TFA/TIS/dH_2O (95:2.5:2.5, 30 mL) for 2 hours, and the crude peptide was precipitated in and washed with ice-cold diethyl ether (2x). The crude peptide was purified using RP-HPLC operating with a 43.4 minute linear gradient (20–100%) of acetonitrile in water containing TFA (0.1%); lyophilization yielded the pure intermediate (Ac-KRGCGK(*o*NB-N_3)-PEG_2-GPQGIWGQG-PEG_2-K(yne)GCGRK-NH_2) as a yellow solid (88 mg, 0.030 mmol). To induce CuAAC-mediated intramolecular stapling, pure linear peptide (1 mM) was dissolved in nitrogen-purged DMSO (30 mL) containing copper(I) bromide (4.3 mg, 0.030 mmol, 1x), sodium ascorbate (5.8 mg, 0.030 mmol, 1x) in water (300 μL), 2,6 lutidine (31.4 mg, 0.35 mmol, 10x), and DIEA (38.3 mg, 0.35 mmol, 10x). This mixture was allowed to react under nitrogen at room temperature for 16 hours. The mixture was concentrated *in vacuo*, redissolved in dH_2O, passed through an ion exchange column (Dowex M4195 resin, 5 grams), and lyophilized. Double-stapled product was purified using RP-HPLC operating with a 43.4 minute linear gradient (20–100%) of acetonitrile in water containing TFA (0.1%); lyophilization yielded the pure intermediate (Ac-KRG<u>C</u>GK(*o*NB-<u>N_3</u>)-PEG_2-GPQGIWGQG-PEG_2-K(<u>yne</u>)G<u>C</u>GRK-NH_2 with an intramolecular staple *via* a <u>triazole</u>

linkage between the alkyne and *o*NB-N_3 side chains and a second intramolecular staple *via* cysteine-cysteine disulfide bond) as a yellow solid (20.0 mg, 0.0068 mmol). To introduce azide functionalities requisite for hydrogel crosslinking, N_3-OSu (Method A1, 6.2 mg, 0.027 mmol, 2x) was dissolved in minimal DMF with DIEA (7.1 mg, 0.54 mmol, 4x) and reacted with the peptide overnight at room temperature. The double-stapled product was purified using RP-HPLC operating with a 43.4 minute linear gradient (20–100%) of acetonitrile in water containing TFA (0.1%); lyophilization yielded the final product [Ac-K(N_3)RGCGK(*o*NB-N_3)-PEG_2-GPQGIWGQG-PEG_2-K(yne)GCGRK(N_3)-NH_2 with an intramolecular staple *via* a triazole linkage between the alkyne and *o*NB-N_3 side chains and a second intramolecular staple *via* cysteine-cysteine disulfide bond, denoted R∧(E∧P)] as a yellow solid (4.2 mg, 0.0013 mmol, 0.26% overall yield). Peptide purity was confirmed using HRMS: calculated for $C_{134}H_{210}N_{47}O_{40}S_2^+$ $[M + 3\ ^1H]^{3+}$, 1061.181; observed 1061.185.

Method A16: Enzymatic "AND" (Reductive "OR" Photo) degradable crosslinker synthesis [E∧(R∨P)]

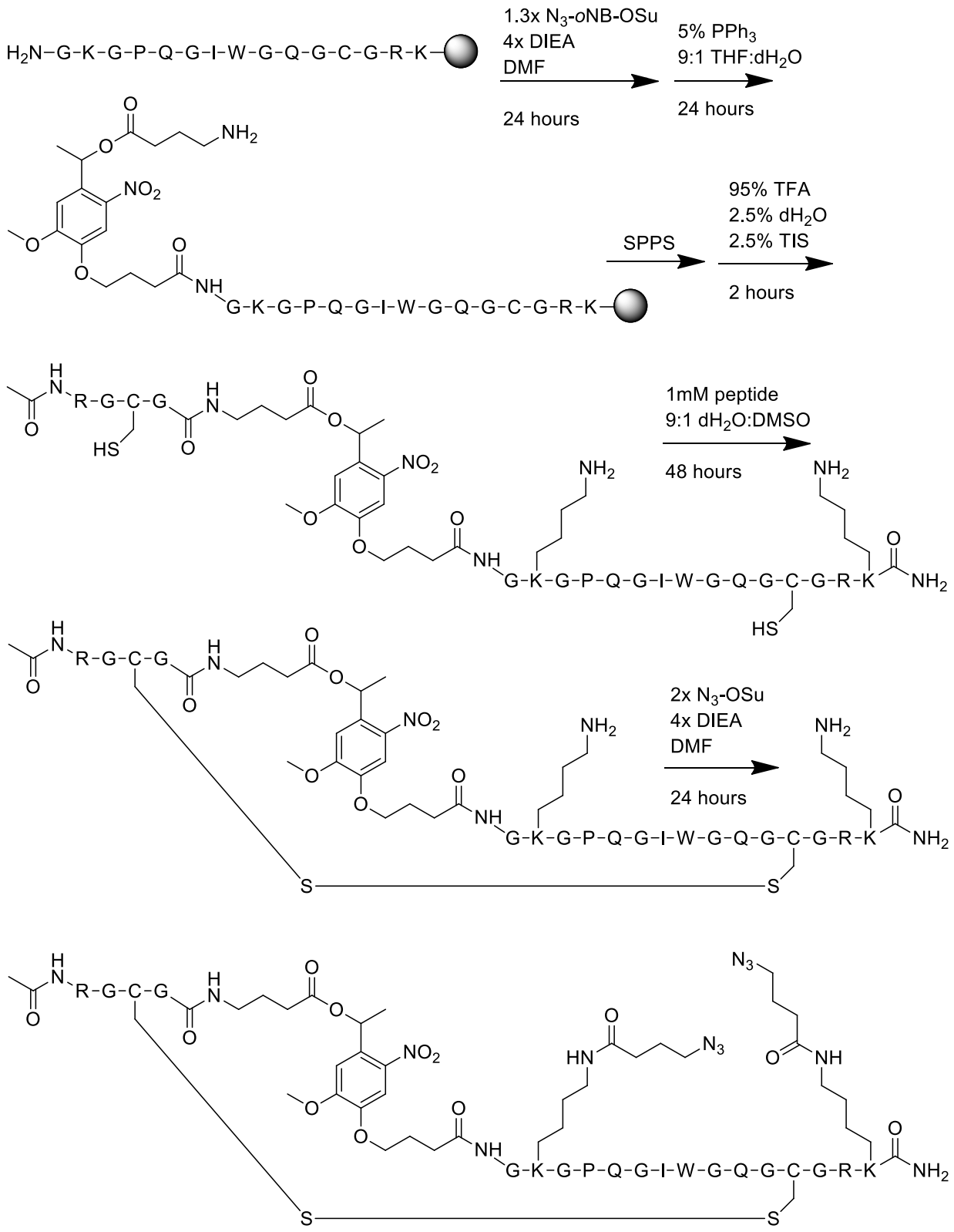

The resin-bound peptide H-GKGPQGIWGQGCGRK-NH_2 was synthesized by microwave-assisted Fmoc SPPS (Method A4) on Rink amide resin (0.5 mmol scale). Resin was subsequently treated with N_3-*o*NB-OSu (Method A2, 0.65 mmol, 330 mg) and DIEA (2.0 mmol, 258 mg) in minimal DMF to introduce *o*NB functionality to the N-terminus. The N-terminal azide was reduced to an amine by a Staudinger reduction; resin was washed with THF/H_2O (90:10, 3 x 20 mL), followed by reaction with 5 wt% triphenylphosphine in THF/H_2O (90:10, 30 mL) for 18 hours. The peptide sequence Ac-RGCG was appended to the N-terminus by standard microwave-assisted Fmoc SPPS. The peptide was simultaneously deprotected and cleaved from resin upon treatment with TFA/TIS/dH_2O (95:2.5:2.5, 30 mL) for 2 hours, and the crude peptide was precipitated in and washed with ice-cold diethyl ether (2x). The crude peptide was purified using RP-HPLC operating with a 55 minute linear gradient (5–100%) of acetonitrile in water containing TFA (0.1%); lyophilization yielded the pure intermediate (Ac-RGCG-*o*NB-GKGPQGIWGQGCGRK-NH_2) as a yellow solid (57.9 mg, 0.0251 mmol). To promote disulfide-mediated intramolecular stapling, the purified peptide was dissolved at 0.5 mM in a dH_2O/DMSO (90:10) solution (50 mL) and reacted at room temperature with no agitation for 48 hours. Stapled product was concentrated *in vacuo* and purified using RP-HPLC operating with a 55 minute linear gradient (5–100%) of acetonitrile in water containing TFA (0.1%); lyophilization yielded the pure intermediate (Ac-RGCG-*o*NB-GKGPQGIWGQGCGRK-NH_2 with intramolecular stapling *via* cysteine-cysteine disulfide bond) as a yellow solid (38.5 mg, 0.0167 mmol). To introduce azide functionalities requisite for hydrogel crosslinking, N_3-OSu (Method A1, 15.1 mg, 0.0668 mmol, 2x) was dissolved in minimal DMF with DIEA (17.3 mg, 0.134 mmol, 4x) and reacted with the peptide overnight at room temperature. The stapled peptide was purified using RP-HPLC operating with a 55 minute linear gradient (5–100%) of acetonitrile in water containing TFA (0.1%); lyophilization yielded the final product [Ac-RGCG-*o*NB-GK(N_3)GPQGIWGQGCGRK(N_3)-NH_2 with intramolecular stapling *via* cysteine-cysteine disulfide bond, denoted E∧(R∨P)] as a yellow solid (14.0 mg, 0.0055 mmol, 1.1% overall yield). Peptide purity was confirmed using MALDI-TOF: calculated for $C_{105}H_{162}N_{39}O_{31}S_2^+$ $[M + {}^1H]^+$, 2529.2; observed 2529.4.

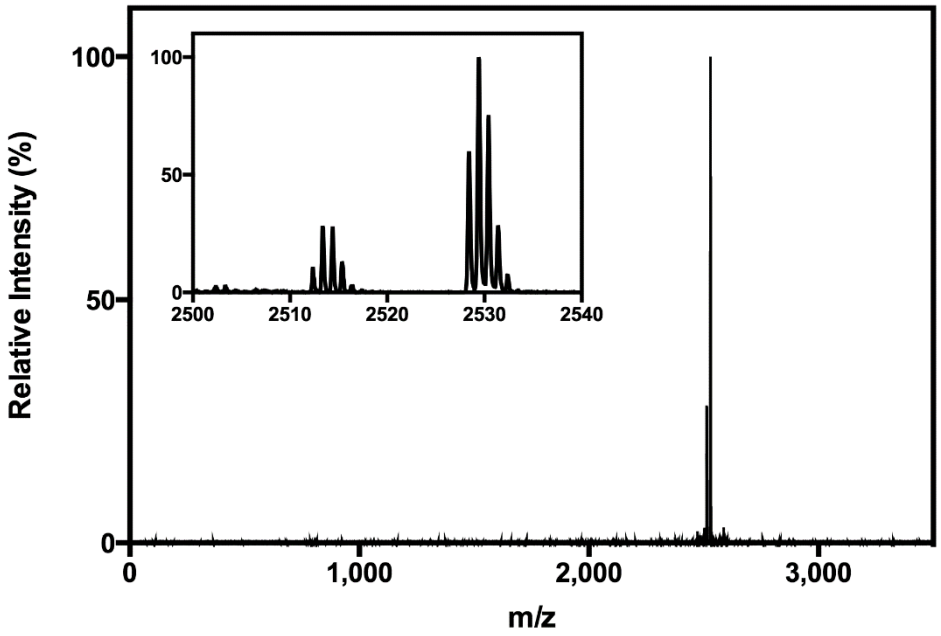

Method A17: Reductive “AND” (Enzymatic “OR” Photo) degradable crosslinker synthesis [R∧(E∨P)]

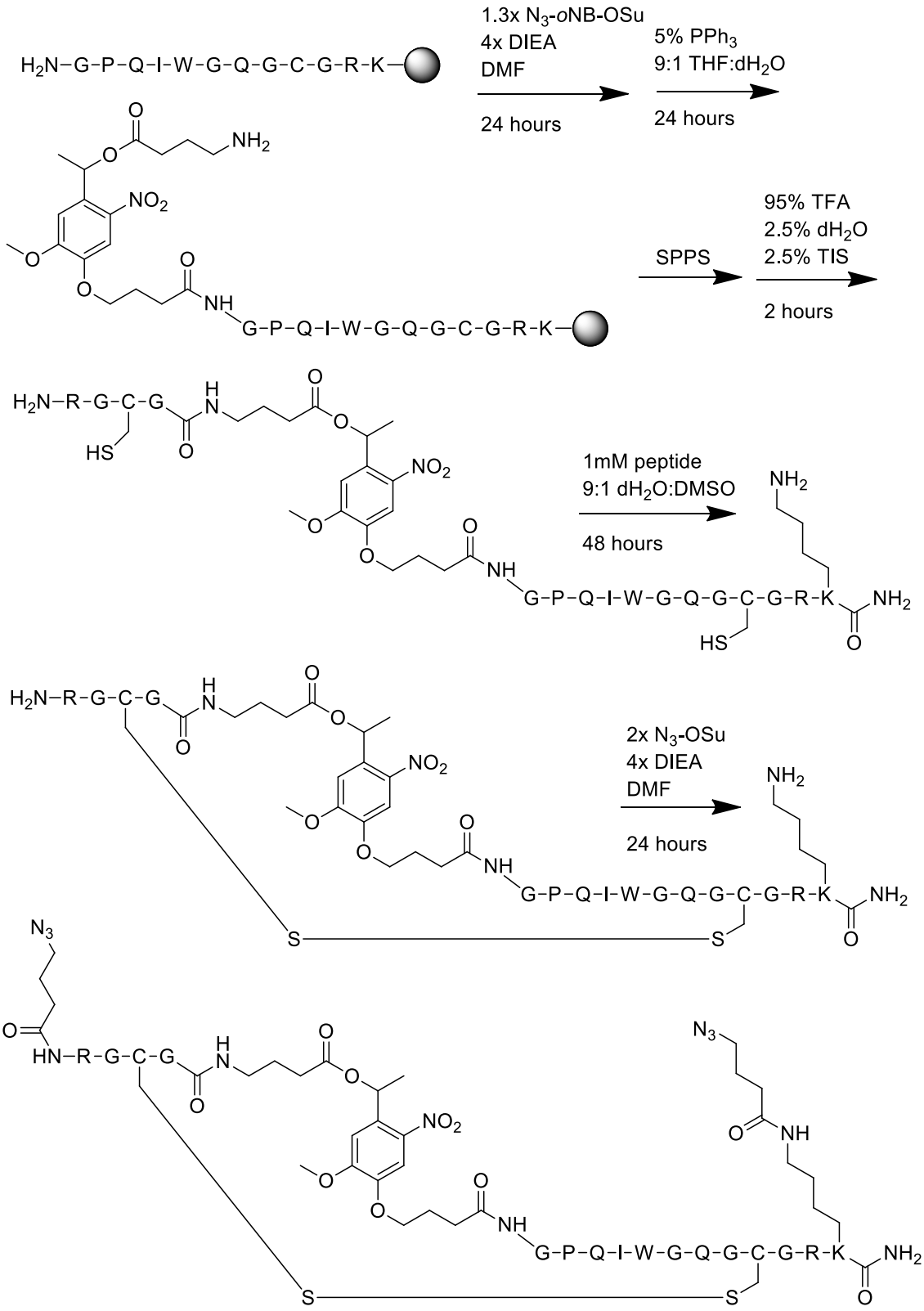

The resin-bound peptide H-GPQGIWGQGCGRK-NH_2 was synthesized by microwave-assisted Fmoc SPPS (Method A4) on Rink amide resin (0.5 mmol scale). Resin was subsequently treated

with N_3-*o*NB-OSu (Method A2, 0.65 mmol, 330 mg) and DIEA (2.0 mmol, 258 mg) in minimal DMF to introduce *o*NB functionality to the N-terminus. The N-terminal azide was reduced to an amine by a Staudinger reduction; resin was washed with THF/H_2O (90:10, 3 x 20 mL), followed by reaction with 5 wt% triphenylphosphine in THF/H_2O (90:10, 30 mL) for 18 hours. The peptide sequence H-RGCG was appended to the N-terminus by standard microwave-assisted Fmoc SPPS. The peptide was simultaneously deprotected and cleaved from resin upon treatment with TFA/TIS/dH_2O (95:2.5:2.5, 30 mL) for 2 hours, and the crude peptide was precipitated in and washed with ice-cold diethyl ether (2x). The crude peptide was purified using RP-HPLC operating with a 55 minute linear gradient (5–100%) of acetonitrile in water containing TFA (0.1%); lyophilization yielded the pure intermediate (H-RGCG-*o*NB-GPQGIWGQGCGRK-NH_2) as a yellow solid (58 mg, 0.028 mmol). To promote disulfide-mediated intramolecular stapling, the purified peptide was dissolved at 0.5 mM in a dH_2O/DMSO (90:10) solution (55 mL) and reacted at room temperature with no agitation for 48 hours. Stapled product was concentrated *in vacuo* and purified using RP-HPLC operating with a 55 minute linear gradient (5–100%) of acetonitrile in water containing TFA (0.1%); lyophilization yielded the pure intermediate (H-RGCG-*o*NB-GPQGIWGQGCGRK-NH_2 with intramolecular stapling *via* cysteine-cysteine disulfide bond) as a yellow solid (23.5 mg, 0.0113 mmol). To introduce azide functionalities requisite for hydrogel crosslinking, N_3-OSu (Method A1, 10.2 mg, 0.0452 mmol, 2x) was dissolved in minimal DMF with DIEA (11.7 mg, 0.0904 mmol, 4x) and reacted with the peptide overnight at room temperature. The stapled peptide was purified using RP-HPLC operating with a 55 minute linear gradient (5–100%) of acetonitrile in water containing TFA (0.1%); lyophilization yielded the final product [N_3-RGCG-*o*NB-GPQGIWGQGCGRK(N_3)-NH_2 with intramolecular stapling *via* cysteine-cysteine disulfide bond, denoted R∧(E∨P)] as a yellow solid (11.2 mg, 0.0049 mmol, 1.0% overall yield). Peptide purity was confirmed using MALDI-TOF: calculated for $C_{95}H_{145}N_{36}O_{28}S_2^+$ $[M + {}^1H]^+$, 2302.0; observed 2302.5.

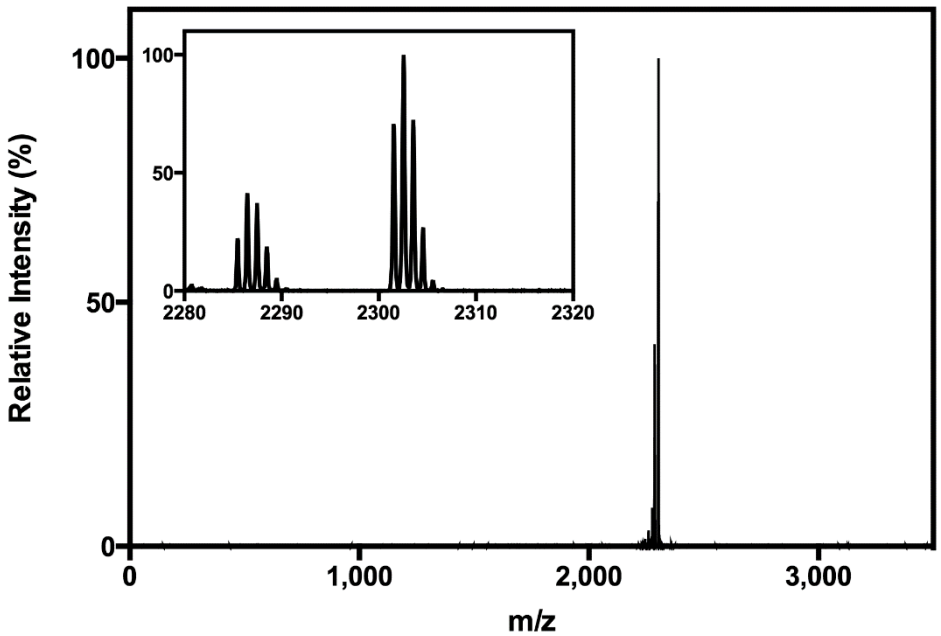

Method A18: Photo "AND" (Reductive "OR" Enzymatic) degradable crosslinker synthesis [P∧(R∨E)]

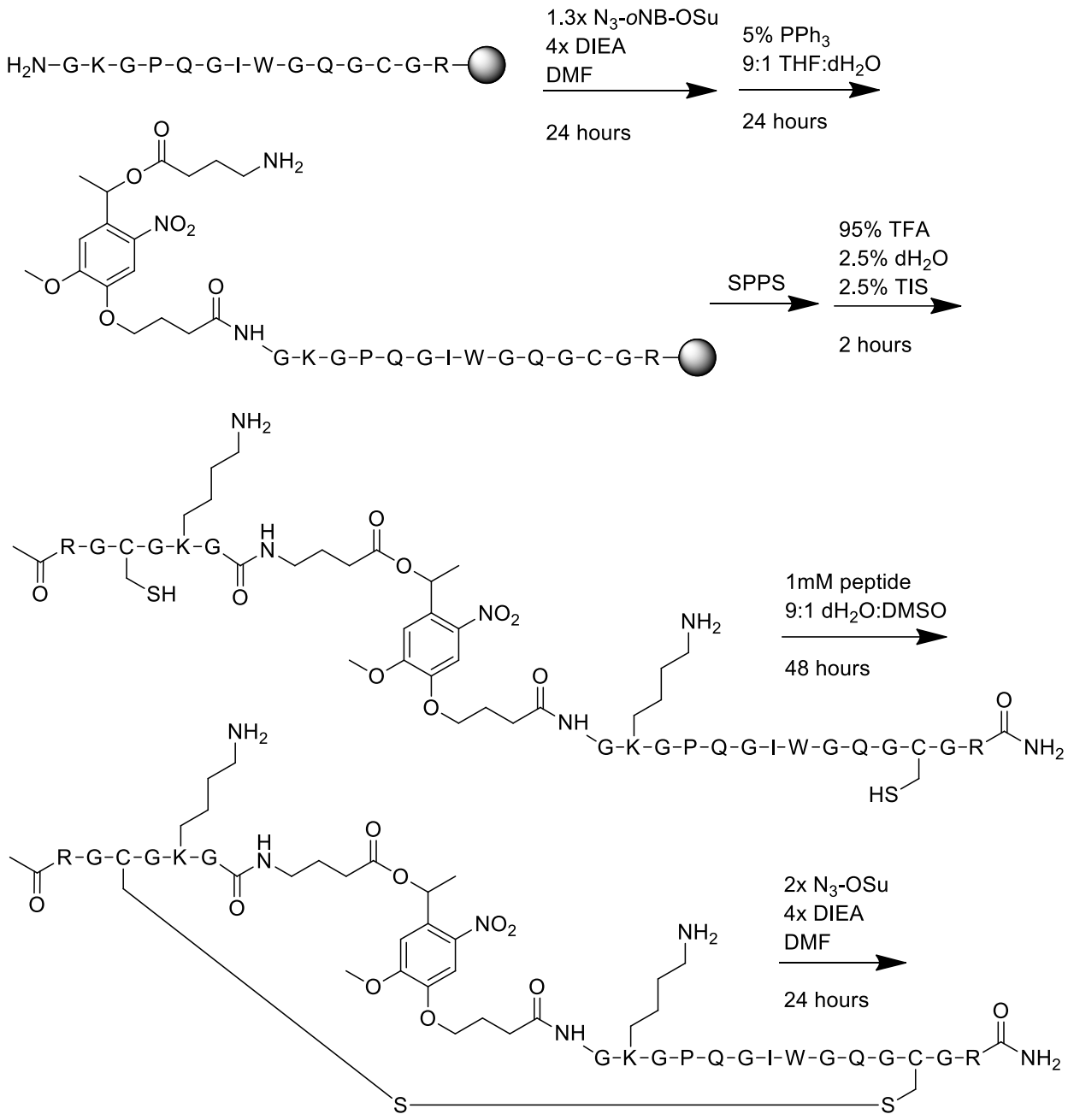

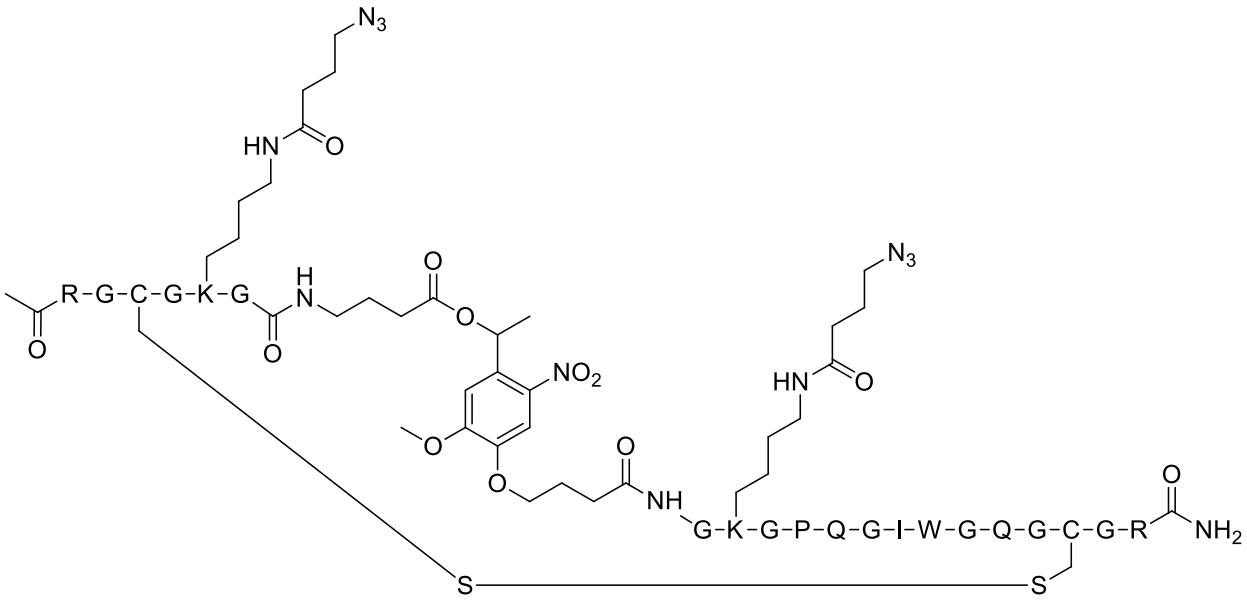

The resin-bound peptide H-GKGPQGIWGQGCGR-NH_2 was synthesized by microwave-assisted Fmoc SPPS (Method A4) on Rink amide resin (0.5 mmol scale). Resin was subsequently treated with N_3-*o*NB-OSu (Method A2, 0.65 mmol, 330 mg) and DIEA (2.0 mmol, 258 mg) in minimal DMF to introduce *o*NB functionality to the N-terminus. The N-terminal azide was reduced to an amine by a Staudinger reduction; resin was washed with THF/H_2O (90:10, 3 x 20 mL), followed by reaction with 5 wt% triphenylphosphine in THF/H_2O (90:10, 30 mL) for 18 hours. The peptide sequence Ac-RGCGKG was appended to the N-terminus by standard microwave-assisted Fmoc SPPS. The peptide was simultaneously deprotected and cleaved from resin upon treatment with TFA/TIS/dH_2O (95:2.5:2.5, 30 mL) for 2 hours, and the crude peptide was precipitated in and washed with ice-cold diethyl ether (2x). The crude peptide was purified using RP-HPLC operating with a 55 minute linear gradient (5–100%) of acetonitrile in water containing TFA (0.1%); lyophilization yielded the pure intermediate (Ac-RGCGKG-*o*NB-GKGPQGIWGQGCGR-NH_2) as a yellow solid (93.1 mg, 0.0393 mmol). To promote disulfide-mediated intramolecular stapling, the purified peptide was dissolved at 0.5 mM in a dH_2O/DMSO (90:10) solution (80 mL) and reacted at room temperature with no agitation for 48 hours. Stapled product was concentrated *in vacuo* and purified using RP-HPLC operating with a 55 minute linear gradient (5–100%) of acetonitrile in water containing TFA (0.1%); lyophilization yielded the pure intermediate (Ac-RGCGKG-*o*NB-GKGPQGIWGQGCGR-NH_2 with intramolecular stapling *via* cysteine-cysteine disulfide bond) as a yellow solid (55.3 mg, 0.0234 mmol). To introduce azide functionalities requisite for hydrogel crosslinking, N_3-OSu (Method A1, 21.2 mg, 0.0936 mmol, 2x) was dissolved in minimal DMF with DIEA (24.2 mg, 0.187 mmol, 4x) and reacted with the peptide overnight at room temperature. The stapled peptide was purified using RP-HPLC operating with a 55 minute linear gradient (5–100%) of acetonitrile in water containing TFA (0.1%); lyophilization yielded the final product [Ac-RGCGK(N_3)G-*o*NB-GK(N_3)GPQGIWGQGCGR-NH_2 with intramolecular stapling *via* cysteine-cysteine disulfide bond, denoted P∧(R∨E)] as a yellow solid (11.0 mg, 0.0043 mmol, 0.9% overall yield). Peptide purity was confirmed using MALDI-TOF: calculated for $C_{107}H_{165}N_{40}O_{32}S_2^+$ $[M + {}^1H]^+$, 2586.2; observed 2586.4.

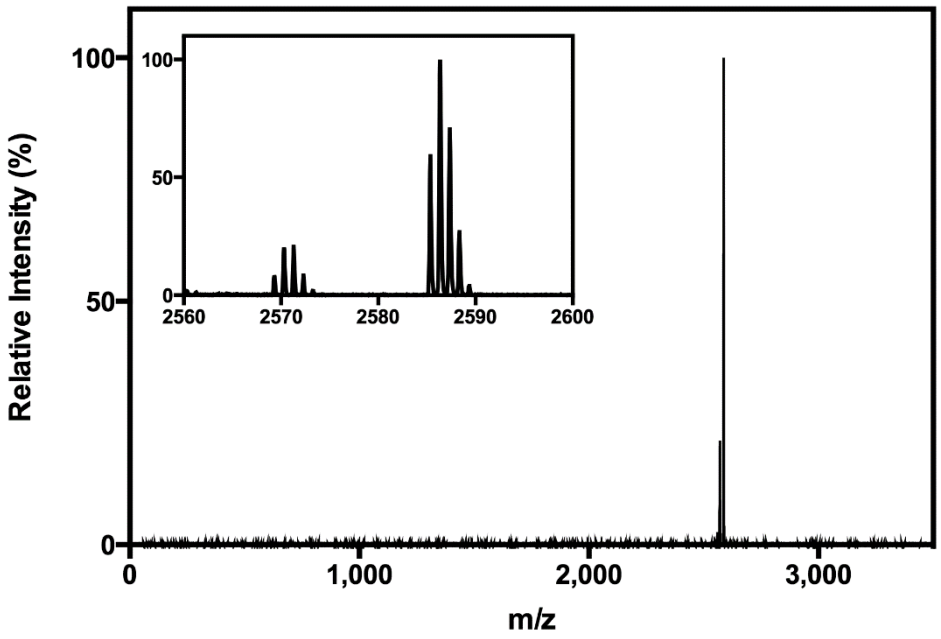
Relative Intensity (%)
100
50
0
0
1,000
2,000
3,000
m/z
100
50
0
2560
2570
2580
2590
2600

Method A19: Enzymatic “OR” (Reductive “AND” Photo) degradable crosslinker synthesis [E∨(R∧P)]

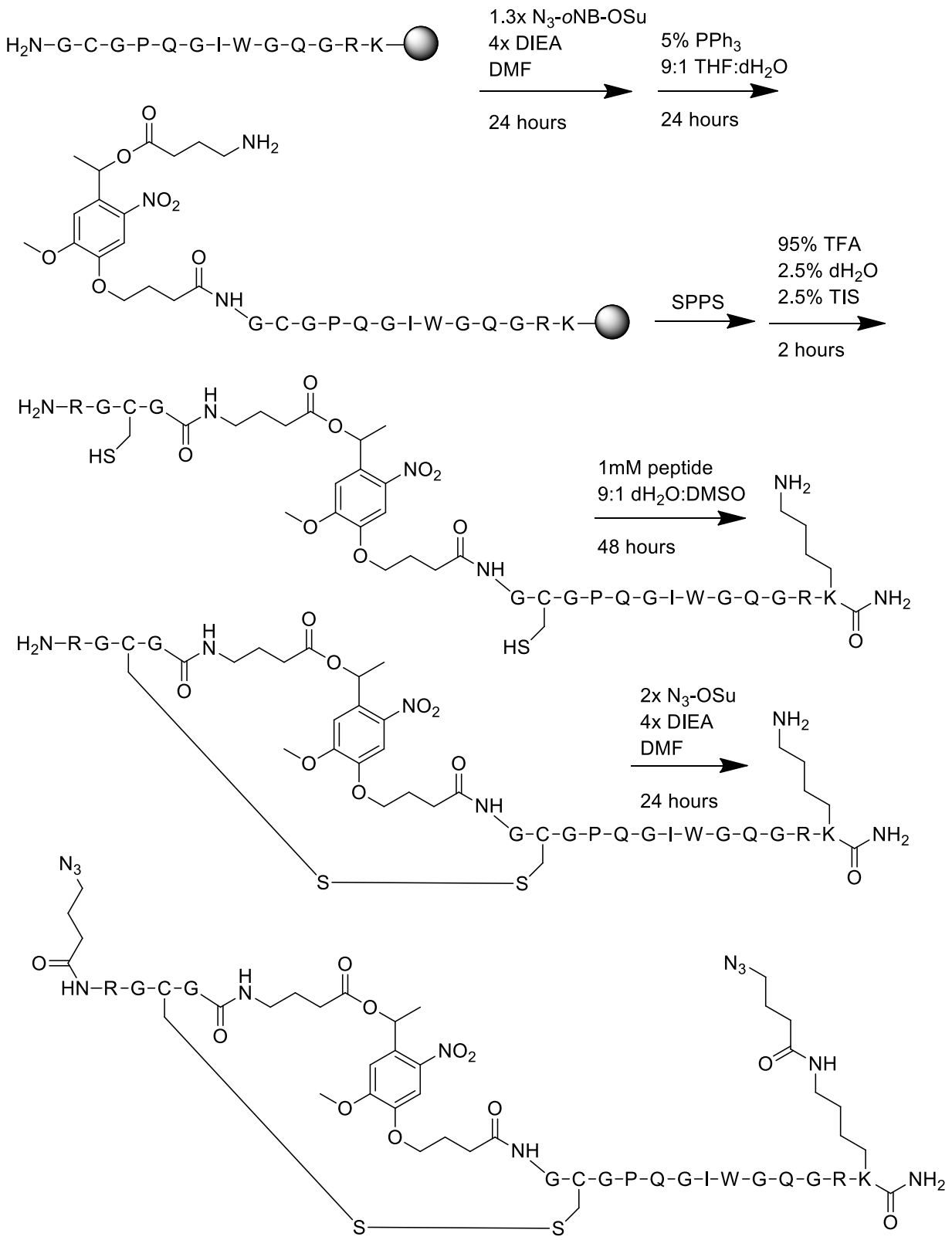

The resin-bound peptide H-GCGPQGIWGQGRK-NH_2 was synthesized by microwave-assisted Fmoc SPPS (Method A4) on Rink amide resin (0.5 mmol scale). Resin was subsequently treated

with N_3-*o*NB-OSu (Method A2, 0.65 mmol, 330 mg) and DIEA (2.0 mmol, 258 mg) in minimal DMF to introduce *o*NB functionality to the N-terminus. The N-terminal azide was reduced to an amine by a Staudinger reduction; resin was washed with THF/H_2O (90:10, 3 x 20 mL), followed by reaction with 5 wt% triphenylphosphine in THF/H_2O (90:10, 30 mL) for 18 hours. The peptide sequence H-RGCG was appended to the N-terminus by standard microwave-assisted Fmoc SPPS. The peptide was simultaneously deprotected and cleaved from resin upon treatment with TFA/TIS/dH_2O (95:2.5:2.5, 30 mL) for 2 hours, and the crude peptide was precipitated in and washed with ice-cold diethyl ether (2x). The crude peptide was purified using RP-HPLC operating with a 43.4 minute linear gradient (20–100%) of acetonitrile in water containing TFA (0.1%); lyophilization yielded the pure intermediate (H-RGCG-*o*NB-GCGPQGIWGQGRK-NH_2) as a yellow solid (85 mg, 0.0408 mmol). To promote disulfide-mediated intramolecular stapling, the purified peptide was dissolved at 0.5 mM in a dH_2O/DMSO (90:10) solution (80 mL) and reacted at room temperature with no agitation for 48 hours. Stapled product was concentrated *in vacuo* and purified using RP-HPLC operating with a 43.4 minute linear gradient (20–100%) of acetonitrile in water containing TFA (0.1%); lyophilization yielded the pure intermediate (H-RGCG-*o*NB-GCGPQGIWGQGRK-NH_2 with intramolecular stapling *via* cysteine-cysteine disulfide bond) as a yellow solid (33.9 mg, 0.0163 mmol). To introduce azide functionalities requisite for hydrogel crosslinking, N_3-OSu (Method A1, 14.7 mg, 0.0652 mmol, 2x) was dissolved in minimal DMF with DIEA (16.9 mg, 0.130 mmol, 4x) and reacted with the peptide overnight at room temperature. Stapled product was purified using RP-HPLC operating with a 43.4 minute linear gradient (20–100%) of acetonitrile in water containing TFA (0.1%); lyophilization yielded the final product [N_3-RGCG-*o*NB-GCGPQGIWGQGRK(N_3)-NH_2 with intramolecular stapling *via* cysteine-cysteine disulfide bond, denoted E∨(R∧P)] as a yellow solid (14.9 mg, 0.0065 mmol, 1.3% overall yield). Peptide purity was confirmed using MALDI-TOF: calculated for $C_{95}H_{145}N_{36}O_{28}S_2^+$ $[M + {}^1H]^+$, 2302.0; observed 2303.0.

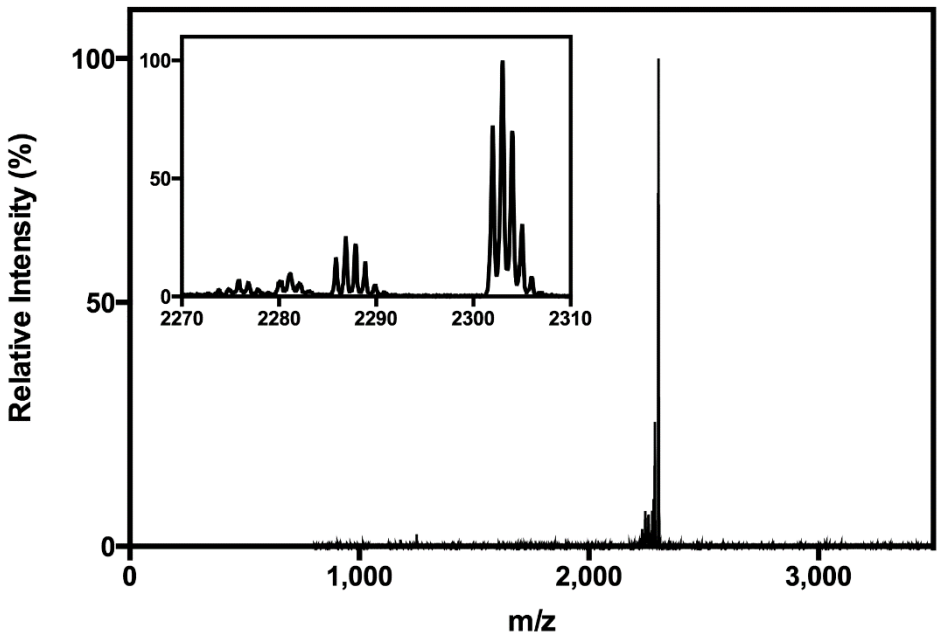

Method A20: Reductive “OR” (Enzymatic “AND” Photo) degradable crosslinker synthesis [R∨(E∧P)]

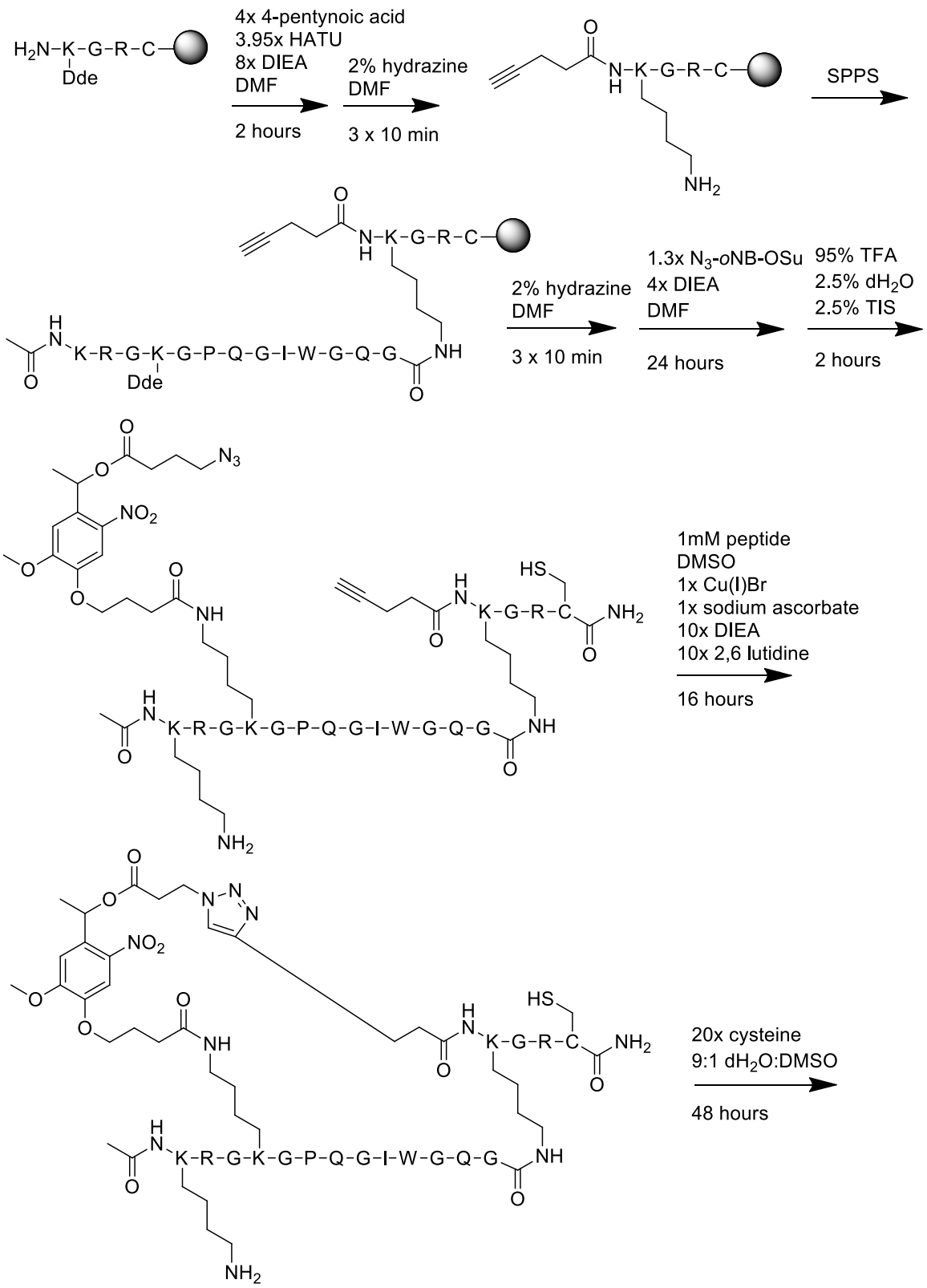
4x 4-pentynoic acid
3.95x HATU
8x DIEA
DMF
2 hours
2% hydrazine
DMF
3 x 10 min
SPPS
2% hydrazine
DMF
3 x 10 min
1.3x N3-oNB-OSu
4x DIEA
DMF
24 hours
95% TFA
2.5% dH2O
2.5% TIS
2 hours
1mM peptide
DMSO
1x Cu(I)Br
1x sodium ascorbate
10x DIEA
10x 2,6 lutidine
16 hours
20x cysteine
9:1 dH2O:DMSO
48 hours

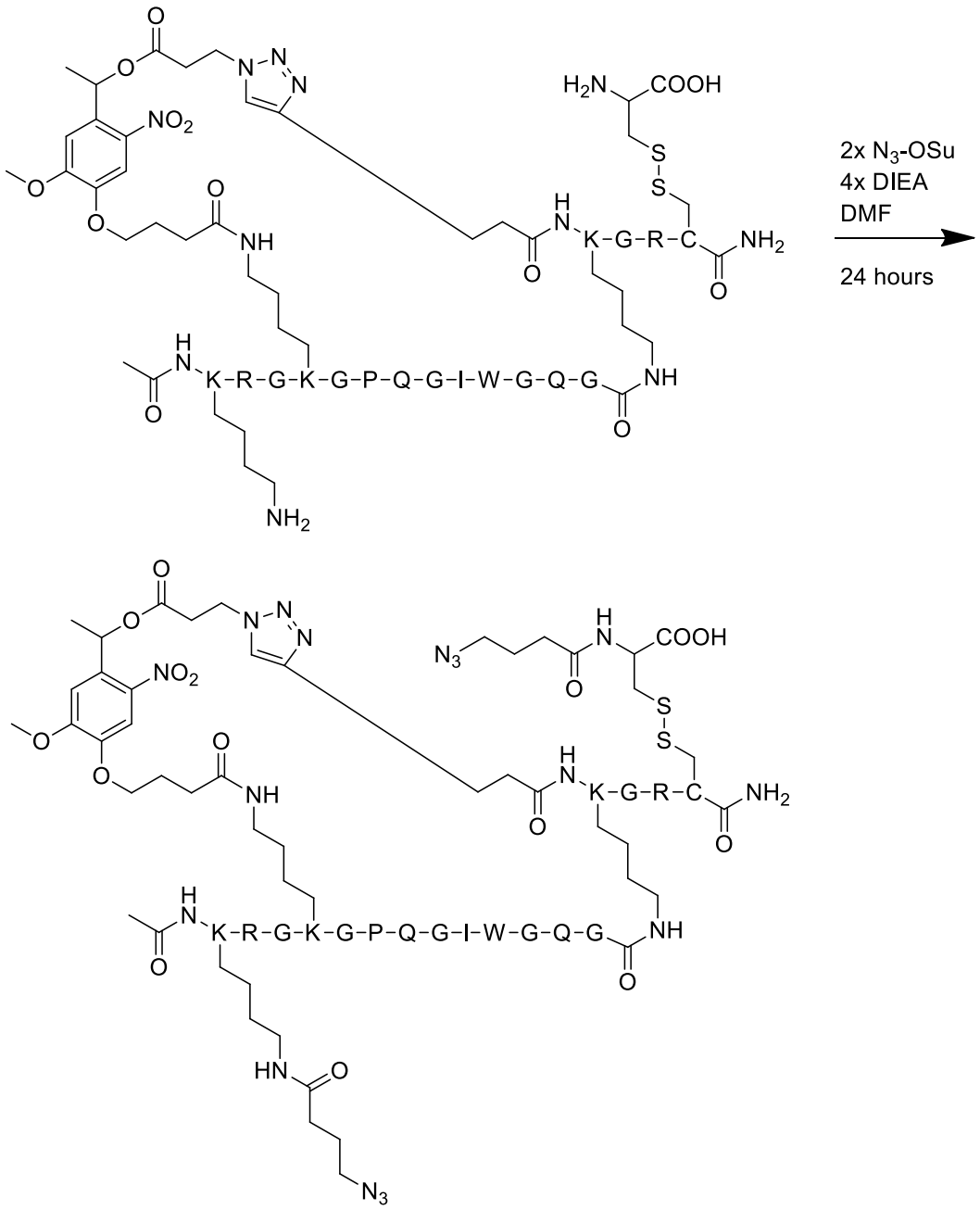

The resin-bound peptide H-K(Dde)GRC-NH_2 was synthesized by microwave-assisted Fmoc SPPS (Method A4) on Rink amide resin (0.5 mmol scale). 4-pentynoic acid (0.196 g, 2.0 mmol, 4x) was pre-activated upon reaction with HATU (0.751 g, 1.975 mmol, 3.95x) and DIEA (0.517 g, 4.0 mmol, 8x) in minimal DMF for 5 minutes and then reacted with the resin for 90 minutes to functionalize the N-terminus with an alkyne. The resin was treated with hydrazine monohydrate (2%) in DMF (3 x 10 min) to remove the Dde protecting group. The peptide sequence Ac-KRGK(Dde)GPQGIWGQG was appended to the ε-amino group of the unprotected lysine by standard microwave-assisted Fmoc. The resin was again treated with hydrazine monohydrate (2%) in DMF (3 x 10 min) to remove the second Dde protecting group. Resin was subsequently treated with N_3-*o*NB-OSu (Method A2, 0.65 mmol, 330 mg) and DIEA (2.0 mmol, 258 mg) in minimal

DMF to introduce *o*NB functionality to the ε-amino group of the unprotected lysine. The peptide was simultaneously deprotected and cleaved from resin upon treatment with TFA/TIS/dH_2O (95:2.5:2.5, 30 mL) for 2 hours, and the crude peptide was precipitated in and washed with ice-cold diethyl ether (2x). The crude peptide was purified using RP-HPLC operating with a 43.4 minute linear gradient (20–100%) of acetonitrile in water containing TFA (0.1%); lyophilization yielded the pure intermediate (Ac-KRGK(*o*NB-N_3)GPQGIWGQGK(yne)GRC-NH_2) as a yellow solid (115 mg, 0.0494 mmol). To induce CuAAC-mediated intramolecular stapling, pure linear peptide (1 mM) was dissolved in nitrogen-purged DMSO (50 mL) containing copper(I) bromide (7.1 mg, 0.049 mmol, 1x), sodium ascorbate (9.8 mg, 0.049 mmol, 1x) in water (480 μL), 2,6 lutidine (52.9 mg, 0.494 mmol, 10x), and DIEA (63.8 mg, 0.494 mmol, 10x). This mixture was allowed to react under nitrogen at room temperature for 16 hours. The mixture was concentrated *in vacuo*, redissolved in dH_2O, passed through an ion exchange column (Dowex M4195 resin, 5 grams), and lyophilized. Stapled product was purified using RP-HPLC operating with a 43.4 minute linear gradient (20–100%) of acetonitrile in water containing TFA (0.1%); lyophilization yielded the pure intermediate (Ac-KRGK(*o*NB-$\underline{\underline{N_3}}$)GPQGIWGQGK(yne)GRC-$NH_2$ with an intramolecular staple *via* a triazole linkage between the alkyne and *o*NB-N_3 side chains) as a yellow solid (55 mg, 0.0236 mmol). The purified peptide and cysteine (57 mg, 0.47 mmol, 20x) were dissolved in a dH_2O/DMSO (90:10) solution (20 mL) and stirred at room temperature for 48 hours. The stapled peptide was filtered, concentrated *in vacuo*, and purified using RP-HPLC operating with a 43.4 minute linear gradient (20–100%) of acetonitrile in water containing TFA (0.1%); lyophilization yielded the pure intermediate (Ac-KRGK(*o*NB-$\underline{\underline{N_3}}$)GPQGIWGQGK(yne)GR$\underline{C}$(H-$\underline{C}$-OH)-$NH_2$ with an intramolecular staple *via* a triazole linkage between the alkyne and *o*NB-N_3 side chains and cysteines linked *via* disulfide bond) as a yellow solid (30.0 mg, 0.0123 mmol). To introduce azide functionalities requisite for hydrogel crosslinking, N_3-OSu (Method A1, 11.1 mg, 0.049 mmol, 2x) was dissolved in minimal DMF with DIEA (12.7 mg, 0.098 mmol, 4x) and reacted with the peptide overnight at room temperature. The stapled peptide was purified using RP-HPLC operating with a 43.4 minute linear gradient (20–100%) of acetonitrile in water containing TFA (0.1%); lyophilization yielded the final product [Ac-K(N_3)RGK(*o*NB-$\underline{\underline{N_3}}$)GPQGIWGQGK(yne)GR$\underline{C}$($N_3$-$\underline{C}$-OH)-$NH_2$ with an intramolecular staple *via* a triazole linkage between the alkyne and *o*NB-N_3 side chains and cysteines linked *via* disulfide bond, denoted R∨(E∧P)] as a yellow solid (27.1 mg, 0.0102 mmol, 2.0% overall yield). Peptide purity was confirmed using MALDI-TOF: calculated for $C_{112}H_{172}N_{41}O_{32}S_2^+$ $[M + {}^1H]^+$, 2667.3; observed 2667.9.

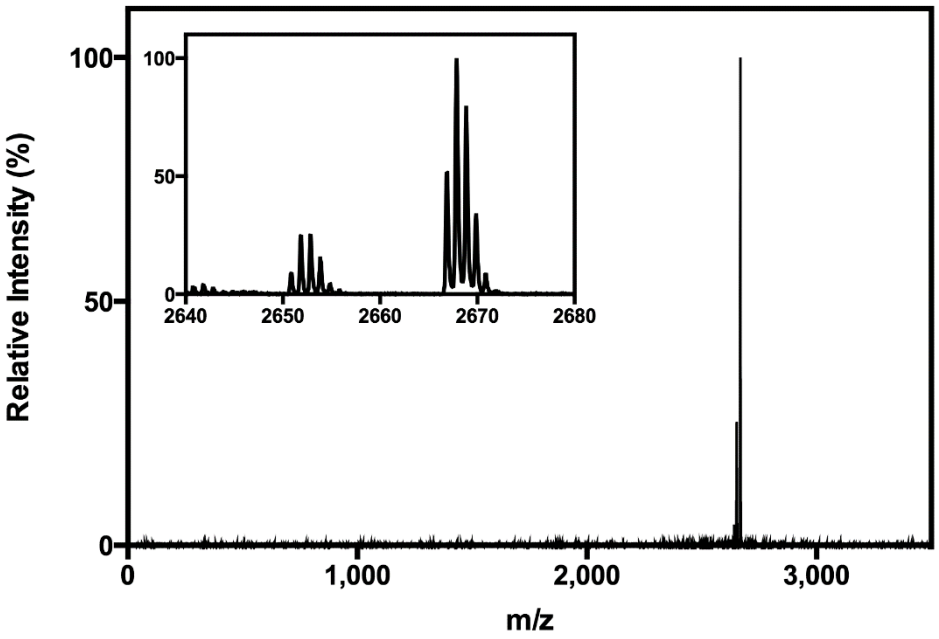
Relative Intensity (%)
100
50
0
0
1,000
2,000
3,000
m/z
100
50
0
2640
2650
2660
2670
2680

Method A21: Photo "OR" (Reductive "AND" Enzymatic) degradable crosslinker synthesis [P∨(R∧E)]

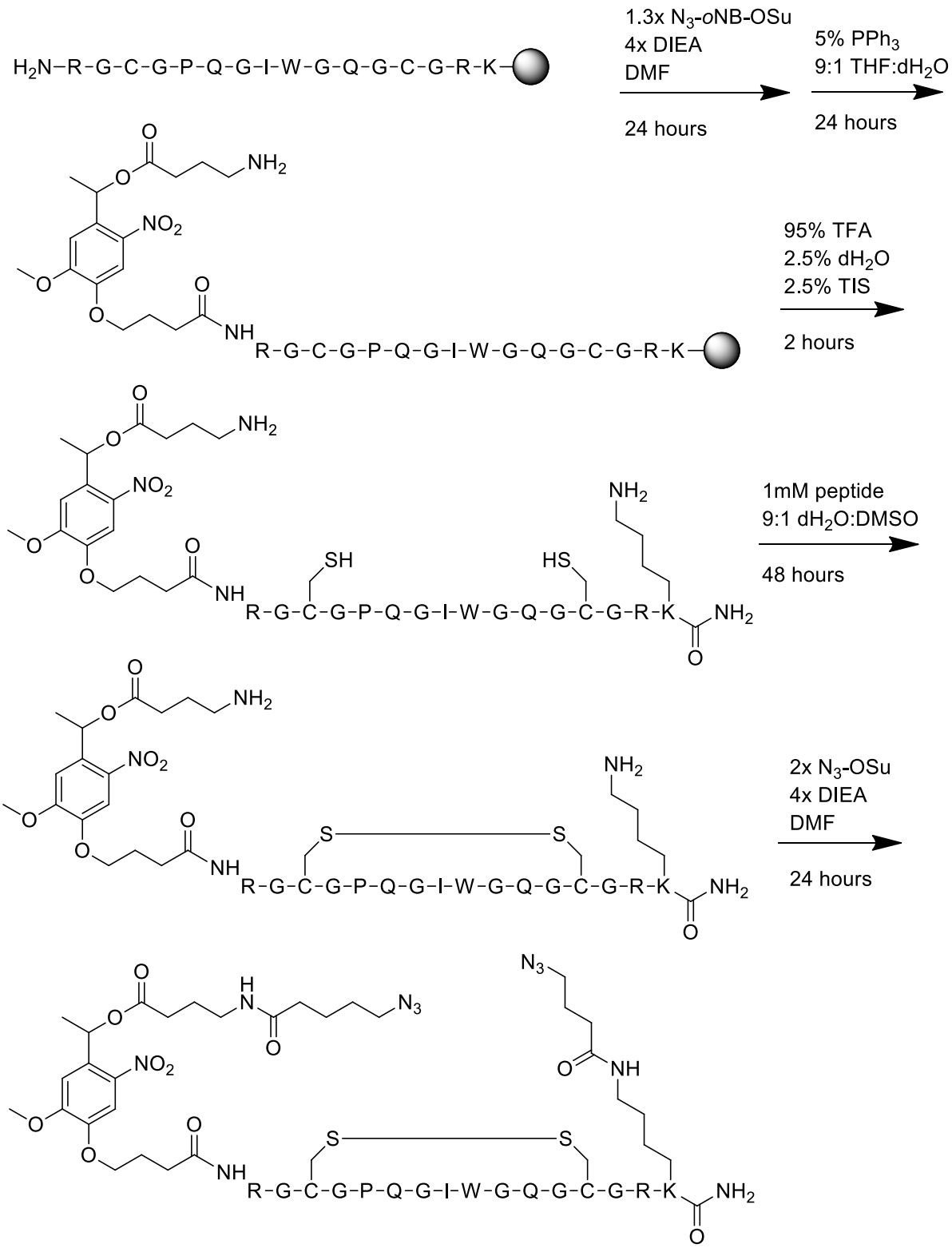

The resin-bound peptide H-RGCGPQGIWGQGCGRK-NH_2 was synthesized by microwave-assisted Fmoc SPPS (Method A4) on Rink amide resin (0.5 mmol scale). Resin was subsequently treated with N_3-*o*NB-OSu (Method A2, 0.65 mmol, 330 mg) and DIEA (2.0 mmol, 258 mg) in minimal DMF to introduce *o*NB functionality to the N-terminus. The N-terminal azide was reduced to an amine by a Staudinger reduction; resin was washed with THF/H_2O (90:10, 3 x 20 mL), followed by reaction with 5 wt% triphenylphosphine in THF/H_2O (90:10, 30 mL) for 18 hours. The peptide was simultaneously deprotected and cleaved from resin upon treatment with TFA/TIS/dH_2O (95:2.5:2.5, 30 mL) for 2 hours, and the crude peptide was precipitated in and washed with ice-cold diethyl ether (2x). The crude peptide was purified using RP-HPLC operating with a 43.4 minute linear gradient (20–100%) of acetonitrile in water containing TFA (0.1%); lyophilization yielded the pure intermediate (H_2N-*o*NB-RGCGPQGIWGQGCGRK-NH_2) as a yellow solid (99 mg, 0.0489 mmol). To promote disulfide-mediated intramolecular stapling, the purified peptide was dissolved at 0.5 mM in a dH_2O/DMSO (90:10) solution (100 mL) and reacted at room temperature with no agitation for 48 hours. Stapled product was concentrated *in vacuo* and purified using RP-HPLC operating with a 43.4 minute linear gradient (20–100%) of acetonitrile in water containing TFA (0.1%); lyophilization yielded the pure intermediate (H_2N-*o*NB-RGCGPQGIWGQGCGRK-NH_2 with intramolecular stapling *via* cysteine-cysteine disulfide bond) as a yellow solid (33.7 mg, 0.0167 mmol). To introduce azide functionalities requisite for hydrogel crosslinking, N_3-OSu (Method A1, 15.1 mg, 0.0668 mmol, 2x) was dissolved in minimal DMF with DIEA (17.2 mg, 0.133 mmol, 4x) and reacted with the peptide overnight at room temperature. The stapled peptide was purified using RP-HPLC operating with a 43.4 minute linear gradient (20–100%) of acetonitrile in water containing TFA (0.1%); lyophilization yielded the final product [N_3-*o*NB-RGCGPQGIWGQGCGRK(N_3)-NH_2 with intramolecular stapling *via* cysteine-cysteine disulfide bond, denoted P⋎(R⋏E)] as a yellow solid (10.0 mg, 0.0045 mmol, 0.9% overall yield). Peptide purity was confirmed using MALDI-TOF: calculated for $C_{93}H_{142}N_{35}O_{27}S_2^+$ $[M + {}^1H]^+$, 2245.0; observed 2245.5.

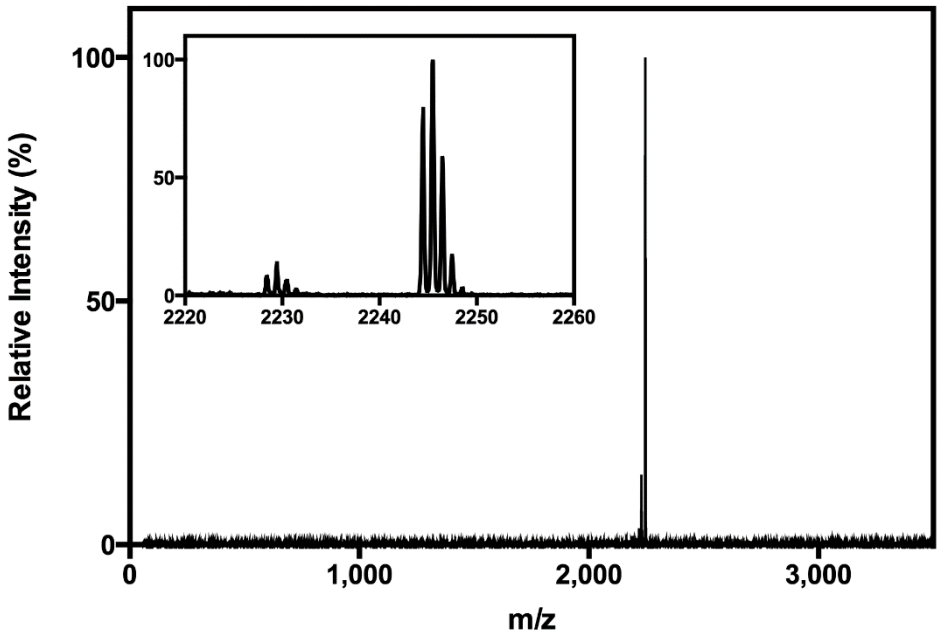

Method A22: Synthesis of 4-arm-PEG$_{20kDa}$-tetrabicyclononyne (PEG-tetraBCN) and fluorescent variants (PEG-tetraBCN-AF568, PEG-tetraBCN-FAM, PEG-tetraBCN-Cyanine5)

(1*R*,8*S*,9*s*)-bicyclo[6.1.0]non-4-yn-9-ylmethyl (2,5-dioxopyrrolidin-1-yl) carbonate (BCN-OSu) was synthesized from *(1R,8S,9s)-bicyclo[6.1.0]non-4-yn-9-ylmethanol* (BCN-OH)[179] following a published synthetic route[62].

Synthesis of (1*R*,8*S*,9*s*,*Z*)-ethyl bicyclo[6.1.0]non-4-ene-9-carboxylate (endo):

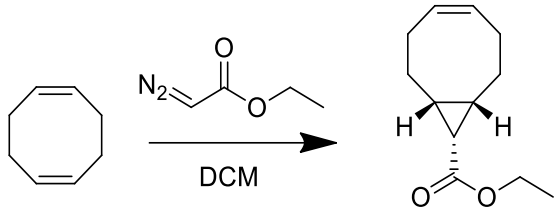

Ethyl diazoacetate (7.56 g, 7.0 mL, 66 mmol) in DCM (35 mL) was added dropwise to a 0°C solution of 1,5-cyclooctadiene (44.1 g, 50 mL, 408 mmol), rhodium(II) acetate dimer catalyst (1.0 g), and DCM (30 mL). The mixture was reacted at room temperature for 72 hours, filtered to remove the catalyst, and concentrated *in vacuo*. The product was purified on a silica column (0-1% ethyl acetate in hexanes) and concentrated to give both the exo (5.62 g, 28.9 mmol, 43.8% yield) and desired endo product (3.70 g, 19.0 mmol, 28.9% yield). Endo: ^{1}H NMR (500 MHz, $CDCl_3$) δ 5.64 (m, 2H), 4.14 (q, J=7.1 Hz, 2H), 2.53 (m, 2H), 2.23 (m, 2H), 2.08 (m, 2H), 1.86 (m, 2H), 1.73 (t, J=8.8 Hz, 1H), 1.42 (m, 2H), 1.29 (t, J=7.1 Hz, 3H).

Synthesis of (1*R*,8*S*,9*s*)-bicyclo[6.1.0]non-4-yn-9-ylmethanol:

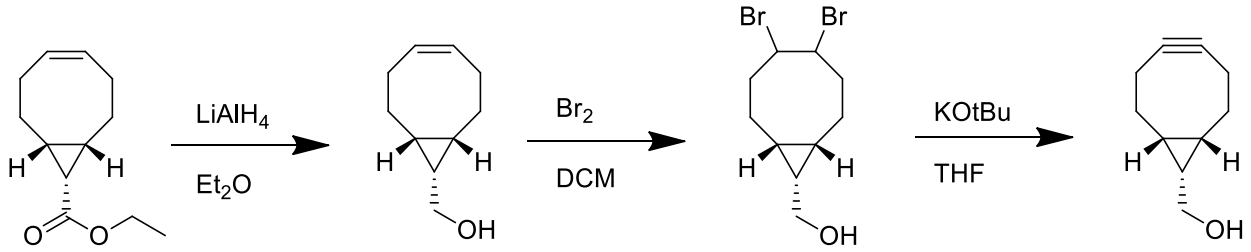

The endo intermediate, (1*R*,8*S*,9*s*,*Z*)-ethyl bicyclo[6.1.0]non-4-ene-9-carboxylate (3.70 g, 19.0 mmol), was dissolved in 0°C anhydrous ether (65 mL). Lithium aluminum hydride (750 mg, 19.8 mmol, 1.04x) in 0°C anhydrous ether (130 mL) was added dropwise to the ester over 15 minutes and the reaction was stirred at room temperature for 20 minutes. Minimal water was added to quench the solution and induced the formation of a grey precipitate. The solution was dried over $MgSO_4$, filtered, and concentrated *in vacuo* to yield the crude alcohol intermediate (1*R*,8*S*,9*s*,*Z*)-bicyclo[6.1.0]non-4-en-9-ylmethanol (2.91 g, 19.1 mmol, quantitative yield).

A solution of bromine (3.1g, 1.0 mL, 19 mmol) in DCM (13 mL) and added dropwise to a 0°C solution of the crude hydroxyl intermediate dissolved in anhydrous DCM (140 mL) until a yellow color persisted. The reaction was quenched with aqueous sodium thiosulfate (10 wt %, 50 mL). The product was extracted into DCM (2 x 70 mL), dried over $MgSO_4$, filtered, and concentrated

in vacuo to yield the crude dibromide intermediate ((1*R*,8*S*,9*s*)-4,5-dibromobicyclo[6.1.0]nonan-9-yl)methanol (5.8 g, 19 mmol, quantitative yield).
The dibromide intermediate was dissolved in 0°C anhydrous THF (120 mL) to which a solution of potassium tert-butoxide (1 M in THF, 50 mL) was added dropwise. The reaction mixture was stirred while refluxing at 75°C for 2.5 hours. The solution was cooled to room temperature and quenched with saturated aqueous ammonium chloride (150 mL). THF was removed *in vacuo* and the product was extracted into DCM (3 x 70 mL), dried over $MgSO_4$, filtered, and concentrated. The product was purified on a silica column (0-20% ethyl acetate in hexanes) and concentrated to yield pure (1*R*,8*S*,9*s*)-bicyclo[6.1.0]non-4-yn-9-ylmethanol as a yellow oil (1.48 g, 9.85 mmol, 52% yield over 3 steps). ^{1}H NMR (500 MHz, $CDCl_3$) δ 3.62 (d, J=7.7 Hz, 2H), 2.59 (br s, 1H), 2.16 (m, 6H), 1.50 (m, 2H), 1.22 (m, 1H), 0.84 (m, 1H).

Synthesis of [(1*R*,8*S*,9*S*)-bicyclo[6.1.0]non-4-yn-9-yl]methyl 2,5-dioxopyrrolidin-1-yl carbonate (BCN-OSu):

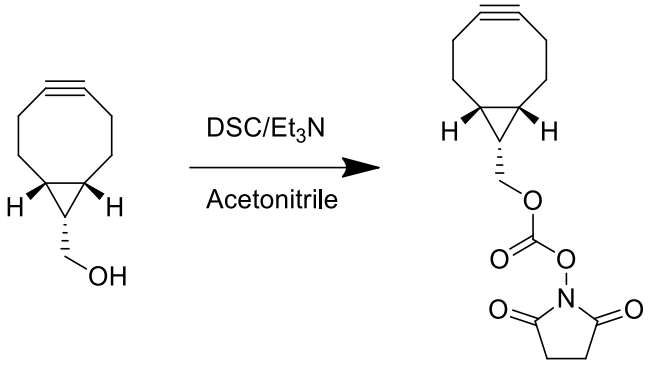

(1*R*,8*S*,9*s*)-bicyclo[6.1.0]non-4-yn-9-ylmethanol (1.48 g, 9.9 mmol) and *N,N'*-Disuccinimidyl carbonate (5.1 g, 19.9 mmol, 2x) were dissolved in acetonitrile (75 mL) under a nitrogen atmosphere. Triethylamine (3.3g, 4.5 mL, 32 mmol) was added and the reaction was stirred overnight at room temperature. The reaction was diluted with 1:1 ethyl acetate:ether (200 mL) and washed with water (6 x 100 mL) and brine (2 x 50 mL). The organic layer was dried over $MgSO_4$, filtered, and concentrated *in vacuo*. The product was purified on a silica flash column (3:1 hexanes:ethyl acetate) to yield the product [(1R,8S,9S)-bicyclo[6.1.0]non-4-yn-9-yl]methyl 2,5-dioxopyrrolidin-1-yl carbonate (denoted BCN-OSu) as a white solid (1.72 g, 5.9 mmol, 60% yield). ^{1}H NMR (500 MHz, $CDCl_3$): δ 4.48 (d, J=8.4 Hz, 2H), 2.87 (s, 4H), 2.30 (m, 6H), 1.57 (m, 3H), 1.09 (m, 2H). These spectral data matched those previously reported[62].

Synthesis of 4-arm-PEG$_{20kDa}$-tetrabicyclononyne (PEG-tetraBCN):
4-arm-PEG$_{20kDa}$-tetrabicyclononyne was synthesized following a known synthetic route[62].

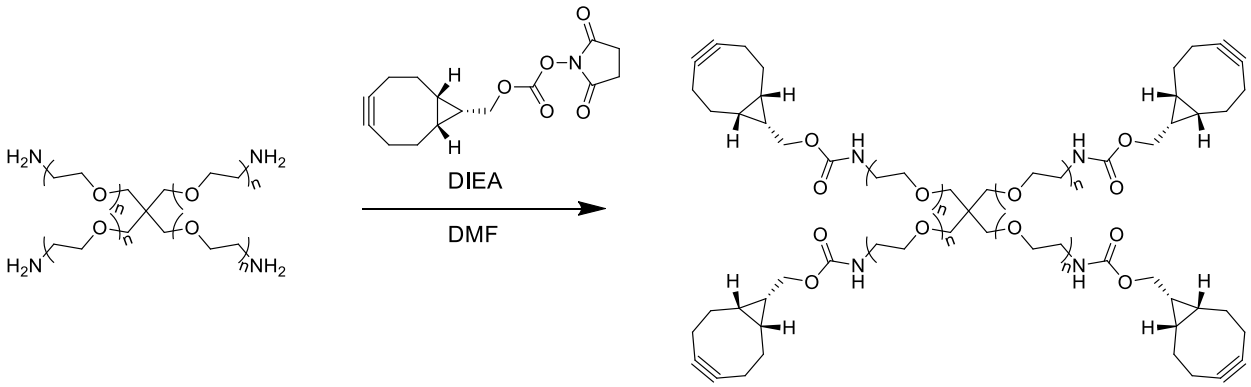

Four-arm poly(ethylene glycol) (PEG) tetraamine (M_n ~ 20 kDa, n ~ 113, 1.00 g, 0.050 mmol PEG, 0.200 mmol NH_2) and BCN-OSu (87.5 mg, 0.300 mmol, 1.5x) were dissolved in minimal DMF (10 mL) with DIEA (103.4 mg, 0.80 mmol, 4x) and stirred at room temperature overnight. The reaction mixture was diluted with water, dialyzed [molecular weight cut-off (MWCO) ~ 1 kDa, SpectraPor® 7], and lyophilized to yield the product (denoted PEG-tetraBCN) as a white powder (0.964 g, 0.0466 mmol, 93% yield). ^{1}H NMR (300 MHz, $CDCl_3$) δ 5.23 (s, 4H), 4.13 (d, J = 8.0 Hz, 8H), 3.76 – 3.71 (m, 3.3 Hz, 8H), 3.63 – 3.61 (m, 1818H), 2.34 – 2.14 (m, 24H), 1.65 – 1.48 (m, 8H), 1.40 – 1.27 (m, 4H), 0.99 – 0.87 (m, 8H). Integral values of the ^{1}H NMR peaks characteristic of BCN (δ 2.24, 1.57, 1.34, 0.93) were compared to the PEG backbone (δ 3.62) to confirm that functionalization of amines with BCN exceeded 95%.

Synthesis of Alexa Fluor® 568 functionalized PEG-tetraBCN (PEG-tetraBCN-AF568):
Alexa Fluor® 568 cadavarine (0.963 mg, 1.19 μmol, 1x) and N_3-OSu (Method A1, 0.536 mg, 2.38 μmol, 2x) were dissolved in minimal DMF (1 mL) with DIEA (0.615 mg, 4.76 μmol, 4x) and stirred at room temperature overnight. The reaction mixture was added directly to a solution of 4-arm-PEG$_{20kDa}$-tetraBCN (0.964 g, 0.0466 mmol, 40x) in phosphate-buffered saline (PBS, 30 mL) and stirred at room temperature for 3 hours. The reaction mixture was then dialyzed (MWCO ~ 10 kDa, SnakeSkin™) and lyophilized to give the product (denoted PEG-tetraBCN-AF568) as a pink powder (0.896 g, 0.0433 mmol, 93% yield).

Synthesis of FAM functionalized PEG-tetraBCN (PEG-tetraBCN-FAM):
5-FAM azide (AAT Bioquest, 20 μL of 100 mM in DMSO, 0.0020 mmol) and 4-arm-PEG$_{20kDa}$-tetraBCN (0.202 g, 0.0101 mmol) was dissolved in PBS (2 mL) and stirred for 2 hours at room temperature. The reaction mixture was diluted with water, dialyzed (MWCO 1kDa, SpectraPor® 7), and lyophilized to yield the product (denoted PEG-tetraBCN-FAM) as a yellow solid (0.204 g, 0.101 mmol, quantitative yield).

Synthesis of Cyanine5 functionalized PEG-tetraBCN (PEG-tetraBCN-Cyanine5):
Cyanine5 azide (Lumiprobe, 20 nmol) in DMSO (2 μL) was added to a solution of PEG-tetraBCN (2 μmol, 100x) in PBS (200 μL). The solution was mixed and reacted at room temperature for 2 hours. The blue product (denoted PEG-tetraBCN-Cyanine5) was used without further purification and kept as a 10 mM stock solution in PBS.

Method A23: Recombinant expression and purification of matrix metalloproteinase-8 (MMP-8)

The MMP-8 gene was lifted from pCMV-Tag4A-MMP8 Wt (a gift from Yardena Samuels[180], Addgene plasmid # 29545), adding a C-terminal 6xHis purification tag and appropriate restriction enzyme cut sites (*Nde*I and *Xho*I) using PCR, placed into pET-28a (+) (EMD Biosciences), and expressed in BL21(DE3)pLysS (Promega Corporation). Cells were lysed *via* sonication, and the 6xHis-tagged protein was solubilized in 6 M urea prior to standard polyhistidine affinity purification using Ni-NTA (Fisher Pierce).

The purified protein was denatured and solubilized in MMP buffer (200 mM sodium chloride, 50 mM tris, 5 mM calcium chloride, 1 μM zinc chloride, pH adjusted to 7.5 with hydrochloric acid) containing 6 M urea and placed into dialysis tubing (MWCO ~3.5 kDa, SpectraPor® 7). The protein was dialyzed against MMP buffer containing progressively lower urea concentrations (4 M → 0 M) over the course of 48 hours at 4 °C, and then concentrated on a spin column (10 kDa MWCO) to yield the purified, refolded MMP-8.

Protein purity was assessed by SDS-PAGE analysis (12% Bis-Tris gel), and a single band corresponding to the expected molecular weight (43.2 kDa) was observed by Coumassie staining.

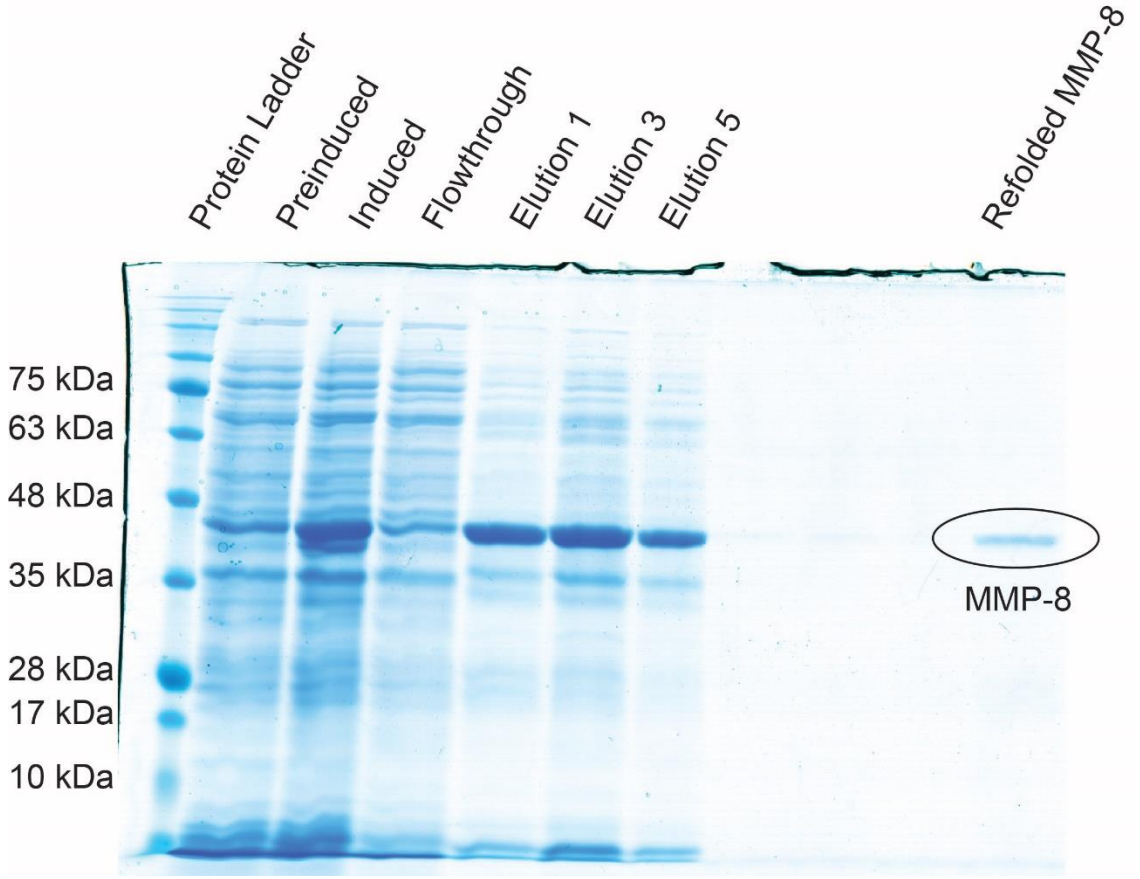

Method A24: Assessing solution-based crosslinker degradation in response to external stimuli

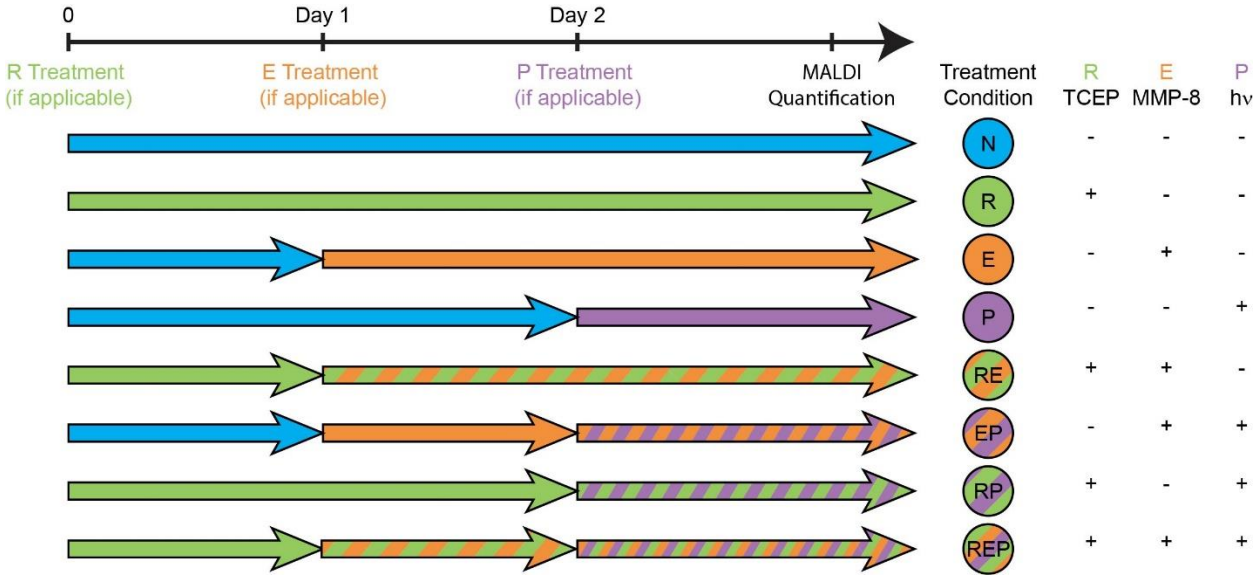

To assess crosslinker fragmentation in response to different combinations of external stimuli, a series of solution-based studies were performed on nine of the synthesized peptides: E, R, P, R∨E, E∨P, R∨P, R∧E, E∧P, and R∧P. Peptide crosslinkers (40 nmol) were dissolved in MMP buffer (110 μL) and exposed to a unique input combination of enzyme, reductive, and light treatments (outlined in further detail below). In each study, degradation products for distinct crosslinker/treatment combinations were identified by MALDI mass spectrometry; observed cleavage products were compared with those expected to assess degradation modalities of the engineered crosslinker species.

Samples receiving the reductive input ($_R$) were treated with tris(2-carboxyethyl)phosphine hydrochloride (TCEP·HCl, 2 μL, 100 mM in MMP buffer) and incubated overnight at 37 °C. To quench any unreached TCEP, these samples were further treated with hydroxyethyl disulfide (HEDS, 5 μL, 100 mM in MMP buffer) prior to incubation (4 hr, 37 °C). Samples not receiving reductive input were maintained at 37 °C.

Samples receiving the enzyme input ($_E$) were subsequently treated with MMP-8 (Method A23, 5 μL, 0.2 mg mL^{-1} in MMP buffer) and all samples were incubated (20 hr, 37 °C).

Samples receiving the light input ($_P$) were subsequently exposed to UV light (λ = 365 nm, 10 mW cm^{-2} incident light, 60 minute exposure).

All samples were diluted with acetonitrile/water (80:20, 100 μL) containing 0.1% TFA and characterized by MALDI-TOF as shown in Figures A1-A9. In these figures, green bars represent expected products that were observed while yellow bars represent expected products that were not observed. Treatment conditions are referenced using the crosslinker logical notation with a subscript indicating the inputs. For example, P_E corresponds to the "photo YES" crosslinker treated

with enzyme; $(R\wedge E)_{REP}$ corresponds to the "reductive AND enzymatic" crosslinker (R∧E) treated with every cue ($_{REP}$). Peptide fragments are referenced using the crosslinker logical notation with a subscript indicating the cues required to generate the product. If a crosslinker generates multiple fragments when treated with a set of cues, the products are differentiated by a numerical subscript. For example, $(R\wedge E)_{RE1}$ and $(R\wedge E)_{RE2}$ represent the two distinct products generated when the "reductive AND enzymatic" crosslinker (R∧E) is exposed to both reductive and enzymatic treatment.

There are inherent limitations in using MALDI to identify low-mass molecules due to interferance of the matrix molecules[181]; only molecules larger than 600 Da are within the MALDI range of detection (ROD). Additionally, molecules analyzed by MALDI that contain an *o*NB moiety generate the parent molecular ion as well as -16, -30, and -32 Da peaks corresponding to the laser-induced photodecomposition of the nitro (NO_2) group into nitroso (NO), amino (NH_2), and triplet nitrene (N:) groups, respectively[182,183]. When peptides were treated with reducing conditions, mass shifts of -26 and -52 Da were observed, correspond to a single and double reduction of an azide group (N_3) to an amino group (NH_2), respectively[184]. Free thiols (-SH) oxidized in the presence of reduced HEDS generated mass shifts of +76 Da, corresponding to the disulfide-containing species ($-SSCH_2CH_2OH$).

Figure A1: Characterization of E crosslinker degradation in solution

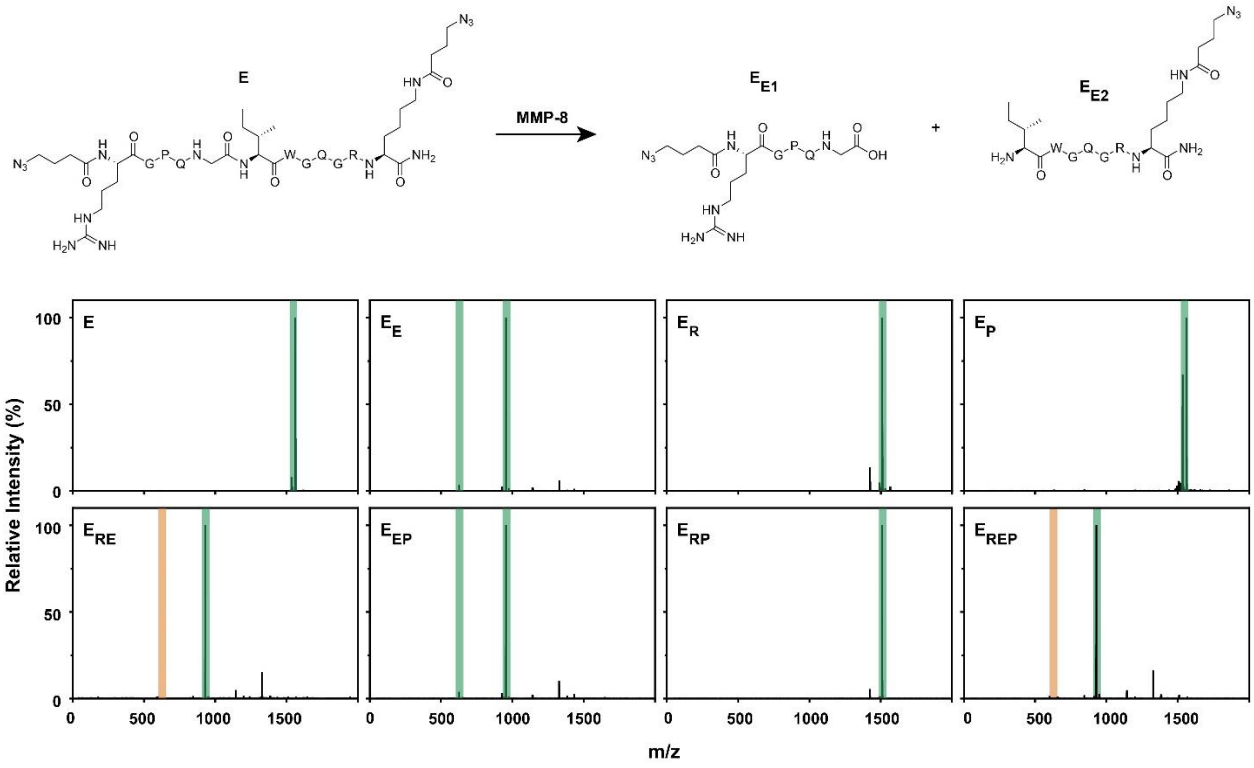

Treatment	Expected Peptides	m/z (Da)	
		Calculated	Measured
E	E	$[M+H]^+$ = 1560.8; $[M+H: -N_3 \rightarrow -NH_2]^+$ = 1534.8	1560.8; 1534.8
E_E	E_{E1}	$[M+H]^+$ = 625.3	625.5
	E_{E2}	$[M+H]^+$ = 954.5	954.6
E_R	E	$[M+H]^+$ = 1560.8; $[M+H: 2\ -N_3 \rightarrow 2\ -NH_2]^+$ = 1508.8	1509.0
E_P	E	$[M+H]^+$ = 1560.8; $[M+H: -N_3 \rightarrow -NH_2]^+$ = 1534.8	1560.8; 1533.7
E_{RE}	E_{E1}	$[M+H]^+$ = 625.3; $[M+H: -N_3 \rightarrow -NH_2]^+$ = 599.3	Below ROD
	E_{E2}	$[M+H]^+$ = 954.5; $[M+H: -N_3 \rightarrow -NH_2]^+$ = 928.5	928.7
E_{EP}	E_{E1}	$[M+H]^+$ = 625.3	625.4
	E_{E2}	$[M+H]^+$ = 954.5	954.6
E_{RP}	E	$[M+H]^+$ = 1560.8; $[M+H: 2\ -N_3 \rightarrow 2\ -NH_2]^+$ = 1508.8	1508.9
E_{REP}	E_{E1}	$[M+H]^+$ = 625.3; $[M+H: -N_3 \rightarrow -NH_2]^+$ = 599.3	Below ROD
	E_{E2}	$[M+H]^+$ = 954.5; $[M+H: -N_3 \rightarrow -NH_2]^+$ = 928.5	928.6

Expected products were identified in all treatment conditions except product E_{E1}, presumably due to being below the MALDI range of detection (m/z > 600). Products were of good purity in all cases.

Figure A2: Characterization of R crosslinker degradation in solution

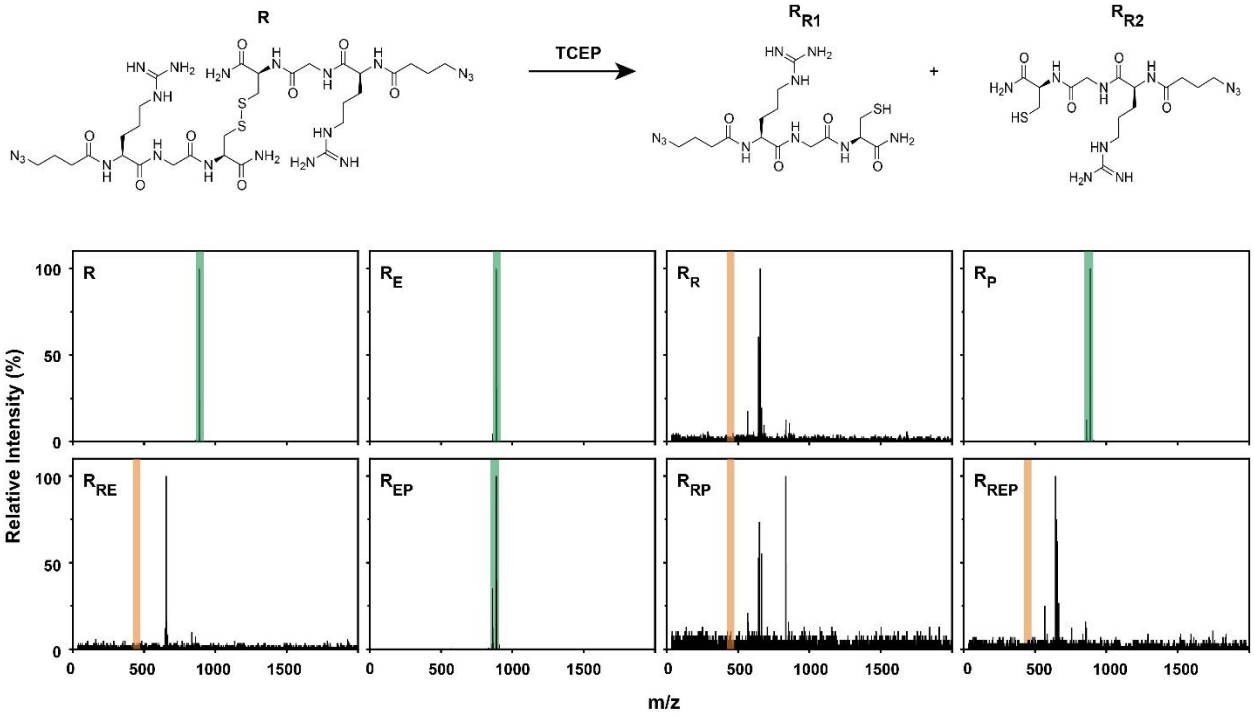

Treatment	Expected Peptides	m/z (Da)	
		Calculated	Measured
R	R	$[M+H]^+$ = 887.4	887.4
R_E	R	$[M+H]^+$ = 887.4	887.4
R_R	R_{R1}	$[M+H]^+$ = 445.2	Below ROD
	R_{R2}	$[M+H]^+$ = 445.2	Below ROD
R_P	R	$[M+H]^+$ = 887.4; $[M+H: -N_3 \rightarrow -NH_2]^+$ = 861.4	887.6; 861.6
R_{RE}	R_{R1}	$[M+H]^+$ = 445.2	Below ROD
	R_{R2}	$[M+H]^+$ = 445.2	Below ROD
R_{EP}	R	$[M+H]^+$ = 887.4; $[M+H: -N_3 \rightarrow -NH_2]^+$ = 861.4	887.5; 860.4
R_{RP}	R_{R1}	$[M+H]^+$ = 445.2	Below ROD
	R_{R2}	$[M+H]^+$ = 445.2	Below ROD
R_{REP}	R_{R1}	$[M+H]^+$ = 445.2	Below ROD
	R_{R2}	$[M+H]^+$ = 445.2	Below ROD

Expected products were identified in all treatment conditions except R_{R1} and R_{R2}, presumably due to the products being below the MALDI range of detection (m/z > 600). In treatments R_R, R_{RE}, R_{RP}, and R_{REP}, the noisy background signal is likely because no expected products were in MALDI ROD.

Figure A3: Characterization of P crosslinker degradation in solution

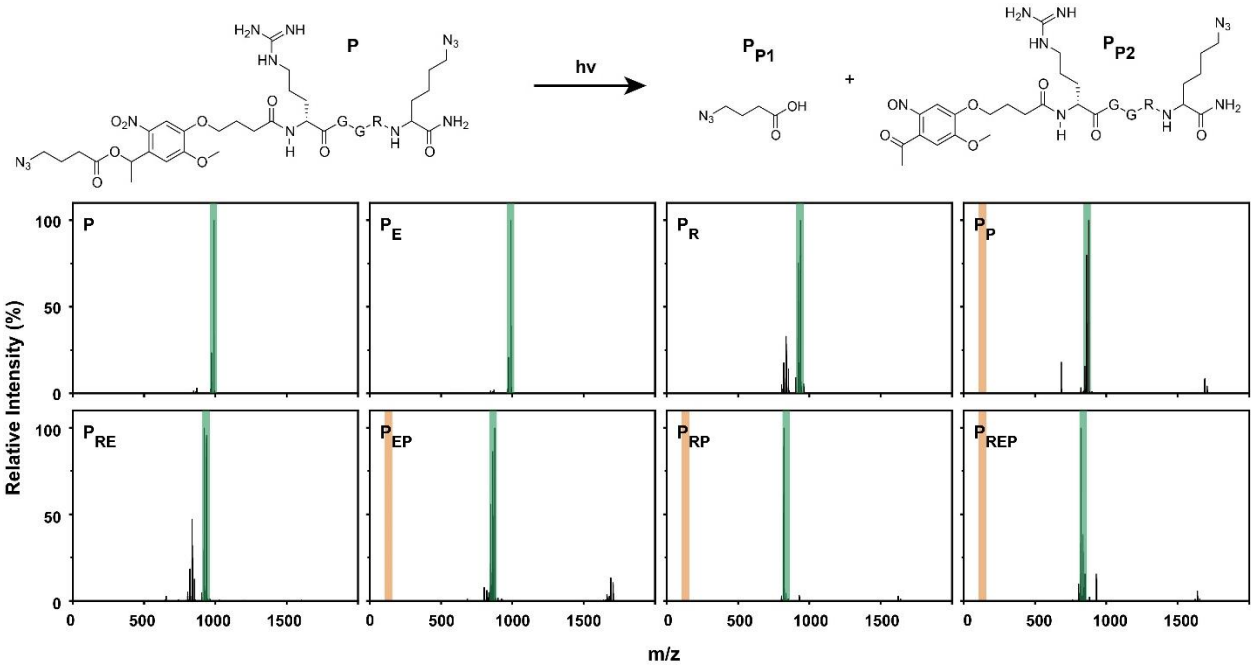

Treatment	Expected Peptides	m/z (Da)	
		Calculated	Measured
P	P	$[M+H]^+$ = 990.5; [M+H: $-NO_2 \rightarrow -NO]^+$ = 974.5	990.6; 974.6
P_E	P	$[M+H]^+$ = 990.5; [M+H: $-NO_2 \rightarrow -NO]^+$ = 974.5	990.6; 974.6
P_R	P	$[M+H]^+$ = 990.5; [M+H: 2 $-N_3 \rightarrow$ 2 $-NH_2]^+$ = 938.5; [M+H: 2 $-N_3 \rightarrow$ 2 $-NH_2$ & $-NO_2 \rightarrow -NO]^+$ = 922.5; [M+H: 2 $-N_3 \rightarrow$ 2 $-NH_2$ & $-NO_2 \rightarrow -N]^+$ = 906.5	938.6; 922.6; 906.5
P_P	P_{P1}	$[M+H]^+$ = 130.1	Below ROD
	P_{P2}	$[M+H]^+$ = 861.4; [M+H: $-NO_2 \rightarrow -NH_2]^+$ = 847.4	861.6; 847.6
P_{RE}	P	$[M+H]^+$ = 990.5; [M+H: 2 $-N_3 \rightarrow$ 2 $-NH_2]^+$ = 938.5; [M+H: 2 $-N_3 \rightarrow$ 2 $-NH_2$ & $-NO_2 \rightarrow -NO]^+$ = 922.5; [M+H: 2 $-N_3 \rightarrow$ 2 $-NH_2$ & $-NO_2 \rightarrow -N]^+$ = 906.5	938.6; 922.5; 906.5
P_{EP}	P_{P1}	$[M+H]^+$ = 130.1	Below ROD
	P_{P2}	$[M+H]^+$ = 861.4; [M+H: $-NO_2 \rightarrow -NH_2]^+$ = 847.4	861.6; 847.5
P_{RP}	P_{P1}	$[M+H]^+$ = 130.1	Below ROD
	P_{P2}	$[M+H]^+$ = 861.4; [M+H: $-N_3 \rightarrow -NH_2]^+$ = 835.4; [M+H: -N3 → -NH2 & -NO → -NH2]+ = 821.5	835.5; 821.5
P_{REP}	P_{P1}	$[M+H]^+$ = 130.1	Below ROD
	P_{P2}	$[M+H]^+$ = 861.4; [M+H: $-N_3 \rightarrow -NH_2]^+$ = 835.4; [M+H: $-N_3 \rightarrow -NH_2$ & $-NO \rightarrow -NH_2]^+$ = 821.5	835.6; 821.5

Expected products were identified in all treatment conditions except P_{P1}, presumably due to being below the MALDI range of detection (m/z > 600). Products were of good purity in all cases except for treatments P_R and P_{RE}.

Figure A4: Characterization of RVE crosslinker degradation in solution

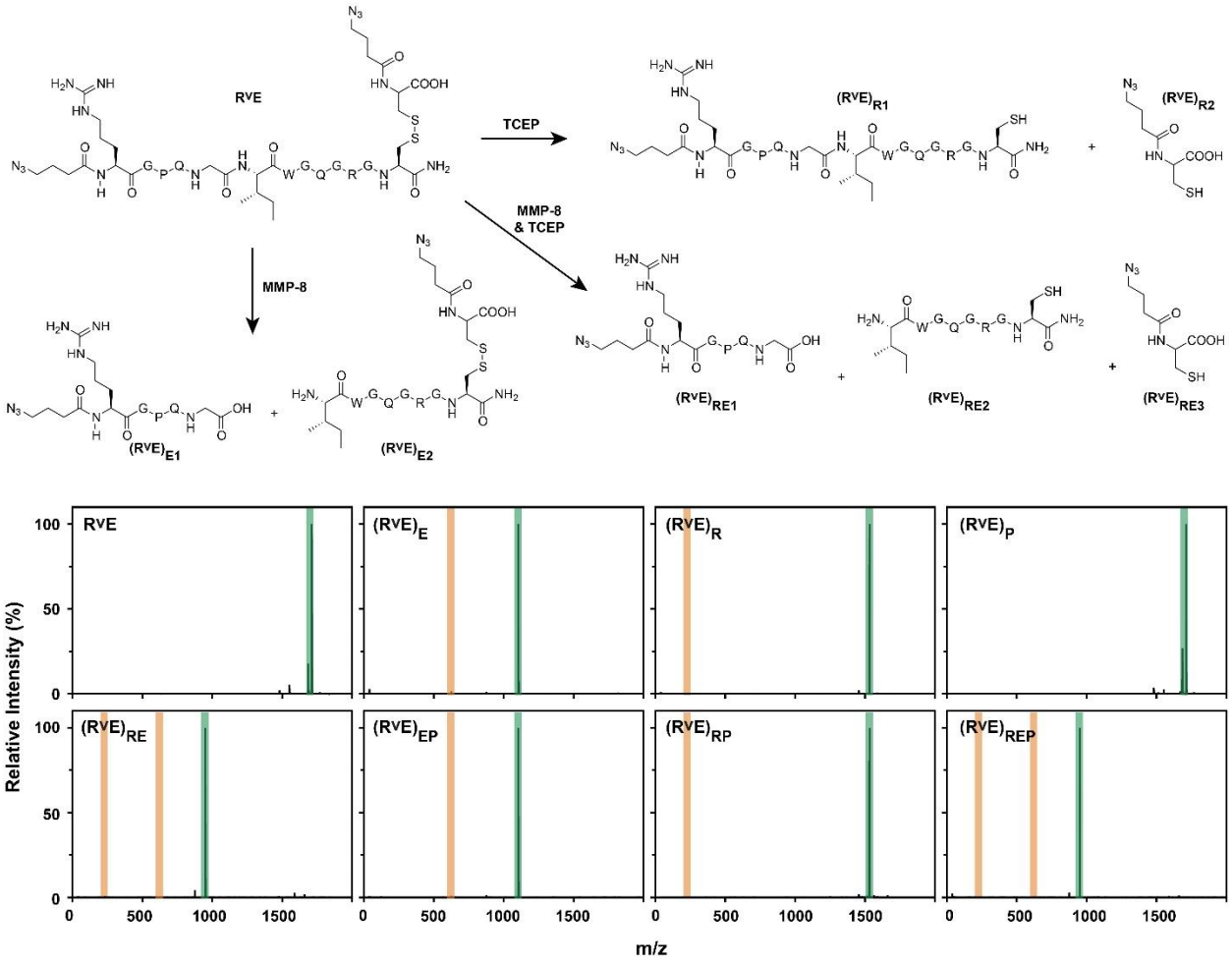

Treatment	Expected Peptides	m/z (Da)	
		Calculated	Measured
RVE	RVE	$[M+H]^+$ = 1711.8; [M+H: $-N_3 \rightarrow -NH_2]^+$ = 1685.8	1711.5; 1685.4
$(RVE)_E$	$(RVE)_{E1}$	$[M+H]^+$ = 625.3; [M+H: $-N_3 \rightarrow -NH_2]^+$ = 599.3	Below ROD
	$(RVE)_{E2}$	$[M+H]^+$ = 1105.5	1105.4
$(RVE)_R$	$(RVE)_{R1}$	$[M+H]^+$ = 1481.7; [M+H: $-N_3 \rightarrow -NH_2$ & $-SH \rightarrow -SSCH_2CH_2OH]^+$ = 1531.8	1531.6
	$(RVE)_{R2}$	$[M+H]^+$ = 233.1; [M+H: $-N_3 \rightarrow -NH_2$ & $-SH \rightarrow -SSCH_2CH_2OH]^+$ = 283.2	Below ROD
$(RVE)_P$	RVE	$[M+H]^+$ = 1711.8; [M+H: $-N_3 \rightarrow -NH_2]^+$ = 1685.8	1711.6; 1685.6
$(RVE)_{RE}$	$(RVE)_{RE1}$	$[M+H]^+$ = 625.3; [M+H: $-N_3 \rightarrow -NH_2]^+$ = 599.3	Below ROD
	$(RVE)_{RE2}$	$[M+H]^+$ = 875.4; [M+H: $-N_3 \rightarrow -NH_2$ & $-SH \rightarrow -SSCH_2CH_2OH]^+$ = 950.4	951.4
	$(RVE)_{RE3}$	$[M+H]^+$ = 233.1; [M+H: $-N_3 \rightarrow -NH_2$ & $-SH \rightarrow -SSCH_2CH_2OH]^+$ = 283.2	Below ROD
$(RVE)_{EP}$	$(RVE)_{E1}$	$[M+H]^+$ = 625.3; [M+H: $-N_3 \rightarrow -NH_2]^+$ = 599.3	Below ROD
	$(RVE)_{E2}$	$[M+H]^+$ = 1105.5	1105.4
$(RVE)_{RP}$	$(RVE)_{R1}$	$[M+H]^+$ = 1481.7; [M+H: $-N_3 \rightarrow -NH_2$ & $-SH \rightarrow -SSCH_2CH_2OH]^+$ = 1531.8	1531.7
	$(RVE)_{R2}$	$[M+H]^+$ = 233.1	Below ROD
$(RVE)_{REP}$	$(RVE)_{RE1}$	$[M+H]^+$ = 625.3; [M+H: $-N_3 \rightarrow -NH_2]^+$ = 599.3	Below ROD
	$(RVE)_{RE2}$	$[M+H]^+$ = 875.4; [M+H: $-N_3 \rightarrow -NH_2$ & $-SH \rightarrow -SSCH_2CH_2OH]^+$ = 950.4	951.4
	$(RVE)_{RE3}$	$[M+H]^+$ = 233.1; [M+H: $-N_3 \rightarrow -NH_2$ & $-SH \rightarrow -SSCH_2CH_2OH]^+$ = 283.2	Below ROD

Expected products were identified in all treatment conditions except products $(RVE)_{E1}$, $(RVE)_{R2}$, $(RVE)_{RE1}$, and $(RVE)_{RE3}$, presumably due to being below the MALDI range of detection (m/z > 600). Products were of good purity in all cases.

Figure A5: Characterization of EVP crosslinker degradation in solution

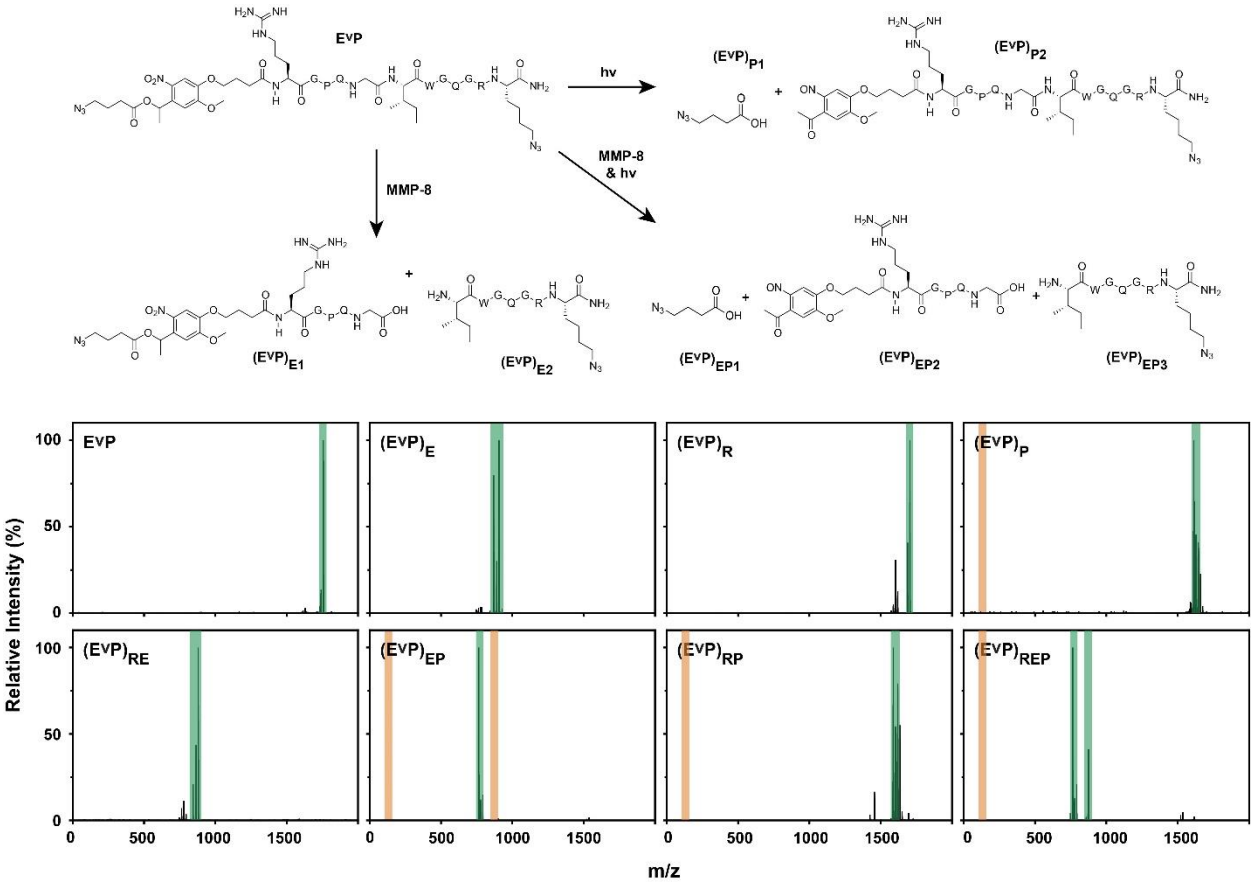

Treatment	Expected Peptides	m/z (Da)	
		Calculated	Measured
EVP	EVP	$[M+H]^+$ = 1756.9; $[M+H: -NO_2 \rightarrow -NO]^+$ = 1740.9	1756.8; 1740.8
$(EVP)_E$	$(EVP)_{E1}$	$[M+H]^+$ = 906.4; $[M+H: -NO_2 \rightarrow -NO]^+$ = 890.4	906.5; 860.5
	$(EVP)_{E2}$	$[M+H]^+$ = 869.5	869.5
$(EVP)_R$	EVP	$[M+H]^+$ = 1756.9; $[M+H: 2\ -N_3 \rightarrow 2\ -NH_2]^+$ = 1704.9; $[M+H: 2\ -N_3 \rightarrow 2\ -NH_2$ & $-NO_2 \rightarrow -NO]^+$ = 1688.9	1704.8; 1688.8
$(EVP)_P$	$(EVP)_{P1}$	$[M+H]^+$ = 130.1	Below ROD
	$(EVP)_{P2}$	$[M+H]^+$ = 1627.8; $[M+H: -NO \rightarrow -NH_2]^+$ = 1613.8	1627.6; 1613.5
$(EVP)_{RE}$	$(EVP)_{E1}$	$[M+H]^+$ = 906.4; $[M+H: -N_3 \rightarrow -NH_2]^+$ = 880.4; $[M+H: -N_3 \rightarrow -NH_2$ & $-NO_2 \rightarrow -NO]^+$ = 864.4	880.6; 864.6
	$(EVP)_{E2}$	$[M+H]^+$ = 869.5; $[M+H: -N_3 \rightarrow -NH_2]^+$ = 843.5	843.7
$(EVP)_{EP}$	$(EVP)_{EP1}$	$[M+H]^+$ = 130.1	Below ROD
	$(EVP)_{EP2}$	$[M+H]^+$ = 777.4; $[M+H: -NO \rightarrow -NH_2]^+$ = 763.4	777.5; 763.4
	$(EVP)_{EP3}$	$[M+H]^+$ = 869.5; $[M+H: -N_3 \rightarrow -NH_2]^+$ = 843.5	Not observed
$(EVP)_{RP}$	$(EVP)_{P1}$	$[M+H]^+$ = 130.1	Below ROD
	$(EVP)_{P2}$	$[M+H]^+$ = 1627.8; $[M+H: -N_3 \rightarrow -NH_2]^+$ = 1601.8; $[M+H: -N_3 \rightarrow -NH_2$ & $-NO \rightarrow -NH_2]^+$ = 1587.8	1601.7; 1587.7
$(EVP)_{REP}$	$(EVP)_{EP1}$	$[M+H]^+$ = 130.1	Below ROD
	$(EVP)_{EP2}$	$[M+H]^+$ = 777.4; $[M+H: -NO \rightarrow -NH_2]^+$ = 763.4	777.4; 763.4
	$(EVP)_{EP3}$	$[M+H]^+$ = 869.5; $[M+H: -N_3 \rightarrow -NH_2]^+$ = 843.5	Not observed

Expected products were identified in all treatment conditions except products $(EVP)_{P1}$, $(EVP)_{EP1}$, $(EVP)_{EP1}$, and $(EVP)_{EP3}$, presumably due to being below the MALDI range of detection (m/z > 600) or relative differences in ionization propensity with other species present. Products were of good purity in all cases except for treatment $(EVP)_R$.

Figure A6: Characterization of RVP crosslinker degradation in solution

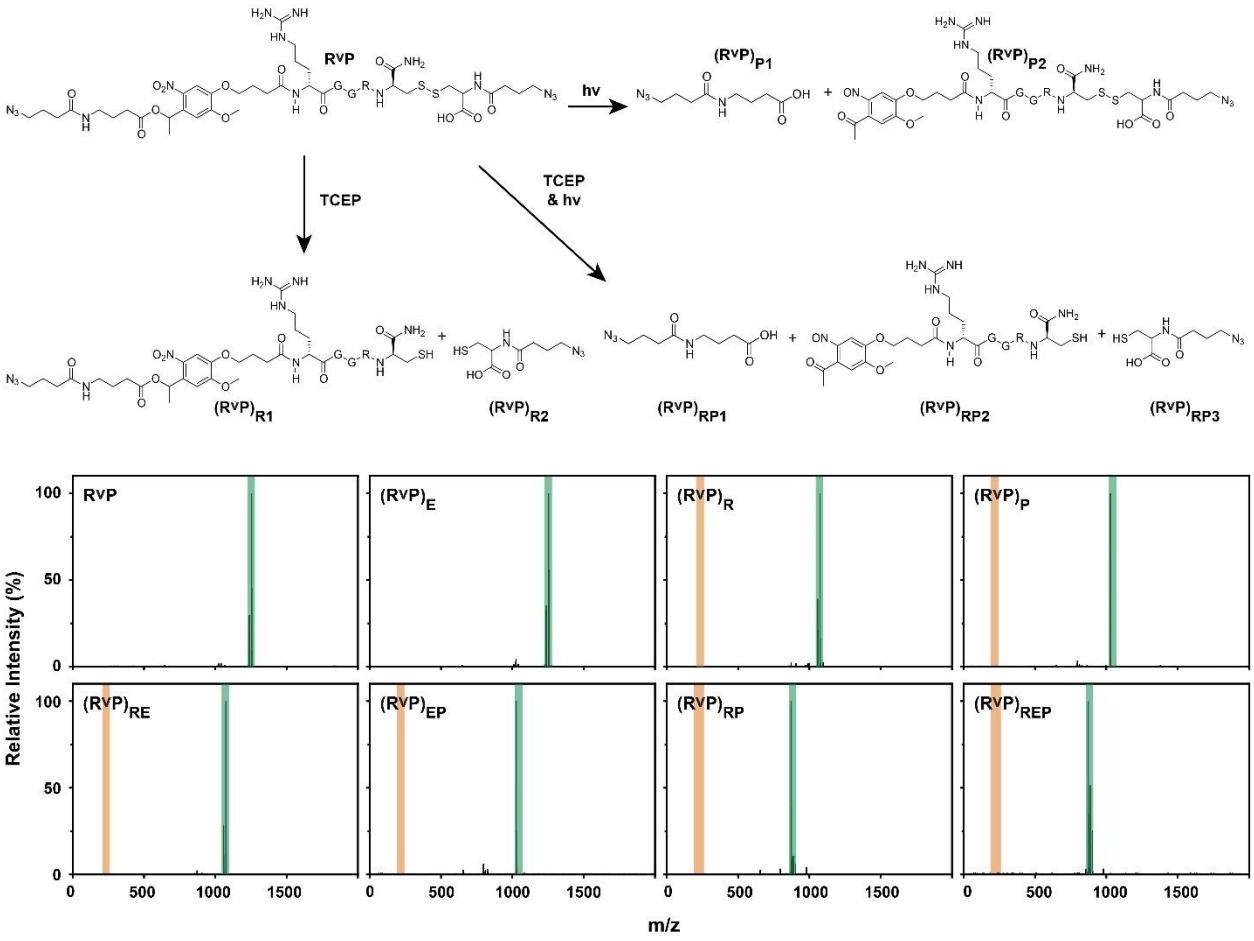

Treatment	Expected Peptides	m/z (Da)	
		Calculated	Measured
RVP	RVP	$[M+H]^+$ = 1254.5; $[M+H: -NO_2 \rightarrow -NO]^+$ = 1238.5	1254.6; 1238.6
$(RVP)_E$	RVP	$[M+H]^+$ = 1254.5; $[M+H: -NO_2 \rightarrow -NO]^+$ = 1238.5	1254.6; 1238.5
$(RVP)_R$	$(RVP)_{R1}$	$[M+H]^+$ = 1024.5; $[M+H: -N_3 \rightarrow -NH_2$ & $-SH \rightarrow -SSCH_2CH_2OH]^+$ = 1074.6; $[M+H: -N_3 \rightarrow -NH_2$ & $-SH \rightarrow -SSCH_2CH_2OH$ & $-NO_2 \rightarrow -NO]^+$ = 1058.6	1074.5; 1058.5
	$(RVP)_{R2}$	$[M+H]^+$ = 233.1	Below ROD
$(RVP)_P$	$(RVP)_{P1}$	$[M+H]^+$ = 215.1	Below ROD
	$(RVP)_{P2}$	$[M+H]^+$ = 1040.4; $[M+H: -NO_2 \rightarrow -NH_2]^+$ = 1026.4	1026.5
$(RVP)_{RE}$	$(RVP)_{R1}$	$[M+H]^+$ = 1024.5; $[M+H: -N_3 \rightarrow -NH_2$ & $-SH \rightarrow -SSCH_2CH_2OH]^+$ = 1074.6; $[M+H: -N_3 \rightarrow -NH_2$ & $-SH \rightarrow -SSCH_2CH_2OH$ & $-NO_2 \rightarrow -NO]^+$ = 1058.6	1074.6; 1058.5
	$(RVP)_{R2}$	$[M+H]^+$ = 233.1	Below ROD
$(RVP)_{EP}$	$(RVP)_{P1}$	$[M+H]^+$ = 215.1	Below ROD
	$(RVP)_{P2}$	$[M+H]^+$ = 1040.4; $[M+H: -NO_2 \rightarrow -NH_2]^+$ = 1026.4	1026.5
$(RVP)_{RP}$	$(RVP)_{RP1}$	$[M+H]^+$ = 215.1	Below ROD
	$(RVP)_{RP2}$	$[M+H]^+$ = 810.4; $[M+H: -SH \rightarrow -SSCH_2CH_2OH]^+$ = 886.5; $[M+H: -SH \rightarrow -SSCH_2CH_2OH$ & $-NO_2 \rightarrow -NH_2]^+$ = 872.5	886.5; 872.5
	$(RVP)_{RP3}$	$[M+H]^+$ = 233.1	Below ROD
$(RVP)_{REP}$	$(RVP)_{RP1}$	$[M+H]^+$ = 215.1	Below ROD
	$(RVP)_{RP2}$	$[M+H]^+$ = 810.4; $[M+H: -SH \rightarrow -SSCH_2CH_2OH]^+$ = 886.5; $[M+H: -SH \rightarrow -SSCH_2CH_2OH$ & $-NO_2 \rightarrow -NH_2]^+$ = 872.5	886.5; 872.5
	$(RVP)_{RP3}$	$[M+H]^+$ = 233.1	Below ROD

Expected products were identified in all treatment conditions except products $(RVP)_{R2}$, $(RVP)_{P1}$, $(RVP)_{RP1}$, and $(RVP)_{RP3}$, presumably due to being below the MALDI range of detection (m/z > 600). Products were of good purity in all cases.

Figure A7: Characterization of RΛE crosslinker degradation in solution

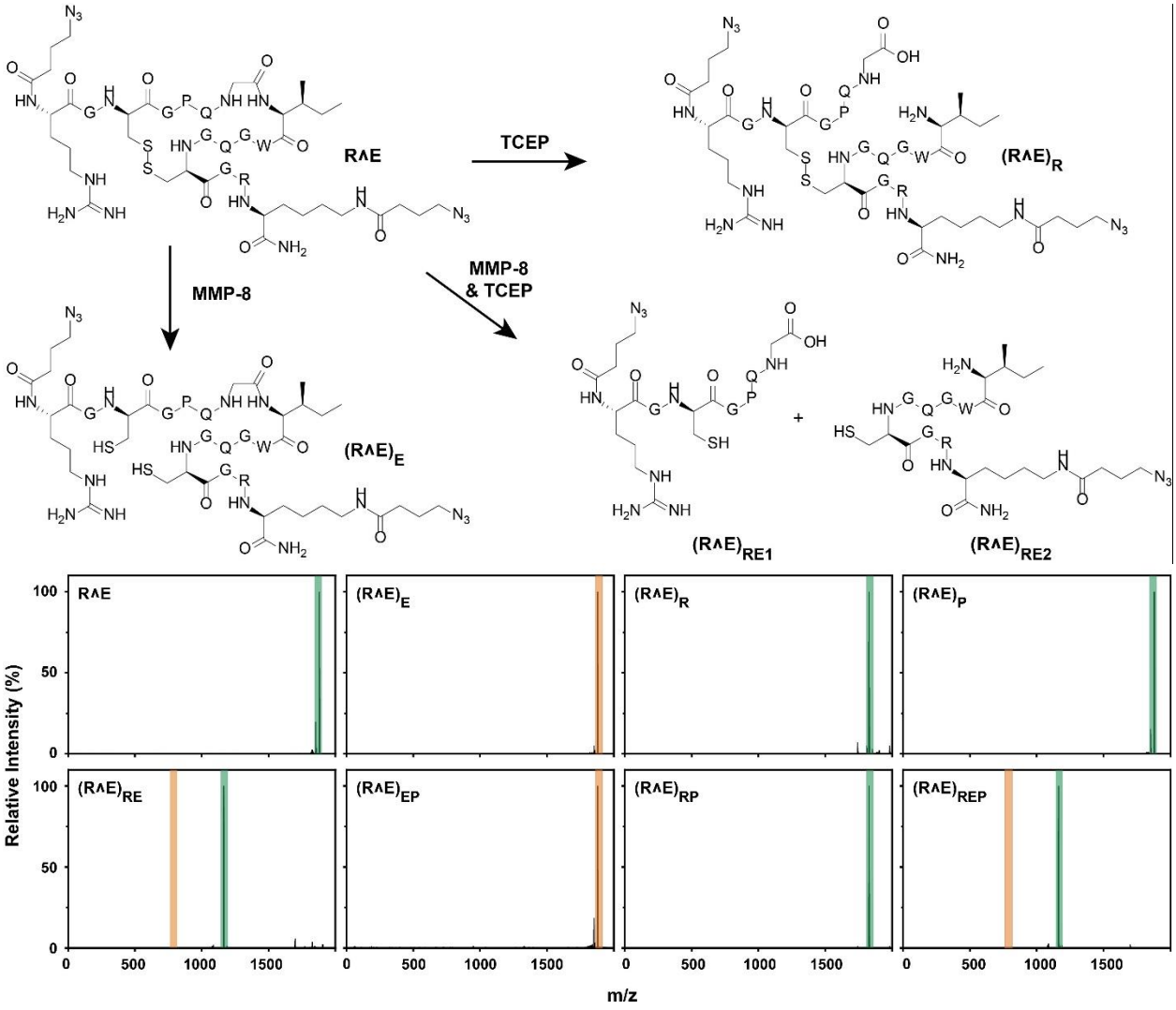

Treatment	Expected Peptides	m/z (Da)	
		Calculated	Measured
RΛE	RΛE	$[M+H]^+$ = 1878.9; $[M+H: -N_3 \rightarrow -NH_2]^+$ = 1852.9	1878.6; 1852.6
$(RΛE)_E$	$(RΛE)_E$	$[M+H]^+$ = 1896.9; $[M+H: -N_3 \rightarrow -NH_2]^+$ = 1870.9	Not observed
$(RΛE)_R$	$(RΛE)_R$	$[M+H]^+$ = 1880.9; $[M+H: -N_3 \rightarrow -NH_2]^+$ = 1854.9; $[M+H: 2\ -N_3 \rightarrow 2\ -NH_2]^+$ = 1828.9	1826.6
$(RΛE)_P$	RΛE	$[M+H]^+$ = 1878.9; $[M+H: -N_3 \rightarrow -NH_2]^+$ = 1852.9	1878.9; 1852.8
$(RΛE)_{RE}$	$(RΛE)_{RE1}$	$[M+H]^+$ = 785.3; $[M+H: -N_3 \rightarrow -NH_2$ & $-SH \rightarrow -SSCH_2CH_2OH]^+$ = 835.4	Not observed
	$(RΛE)_{RE2}$	$[M+H]^+$ = 1114.6; $[M+H: -N_3 \rightarrow -NH_2$ & $-SH \rightarrow -SSCH_2CH_2OH]^+$ = 1164.7	1164.4
$(RΛE)_{EP}$	$(RΛE)_E$	$[M+H]^+$ = 1896.9; $[M+H: -N_3 \rightarrow -NH_2]^+$ = 1870.9	Not observed
$(RΛE)_{RP}$	$(RΛE)_R$	$[M+H]^+$ = 1880.9; $[M+H: -N_3 \rightarrow -NH_2]^+$ = 1854.9; $[M+H: 2\ -N_3 \rightarrow 2\ -NH_2]^+$ = 1828.9	1826.8
$(RΛE)_{REP}$	$(RΛE)_{RE1}$	$[M+H]^+$ = 785.3; $[M+H: -N_3 \rightarrow -NH_2$ & $-SH \rightarrow -SSCH_2CH_2OH]^+$ = 835.4	Not observed
	$(RΛE)_{RE2}$	$[M+H]^+$ = 1114.6; $[M+H: -N_3 \rightarrow -NH_2$ & $-SH \rightarrow -SSCH_2CH_2OH]^+$ = 1164.7	1164.5

Expected products were identified in all treatment conditions except product $(RΛE)_{RE1}$, presumably due relative differences in ionization propensity with other species present. In conditions expected to produce $(RΛE)_E$, only the starting material was observed. Products were of good purity in all cases.

Figure A8: Characterization of EΛP crosslinker degradation in solution

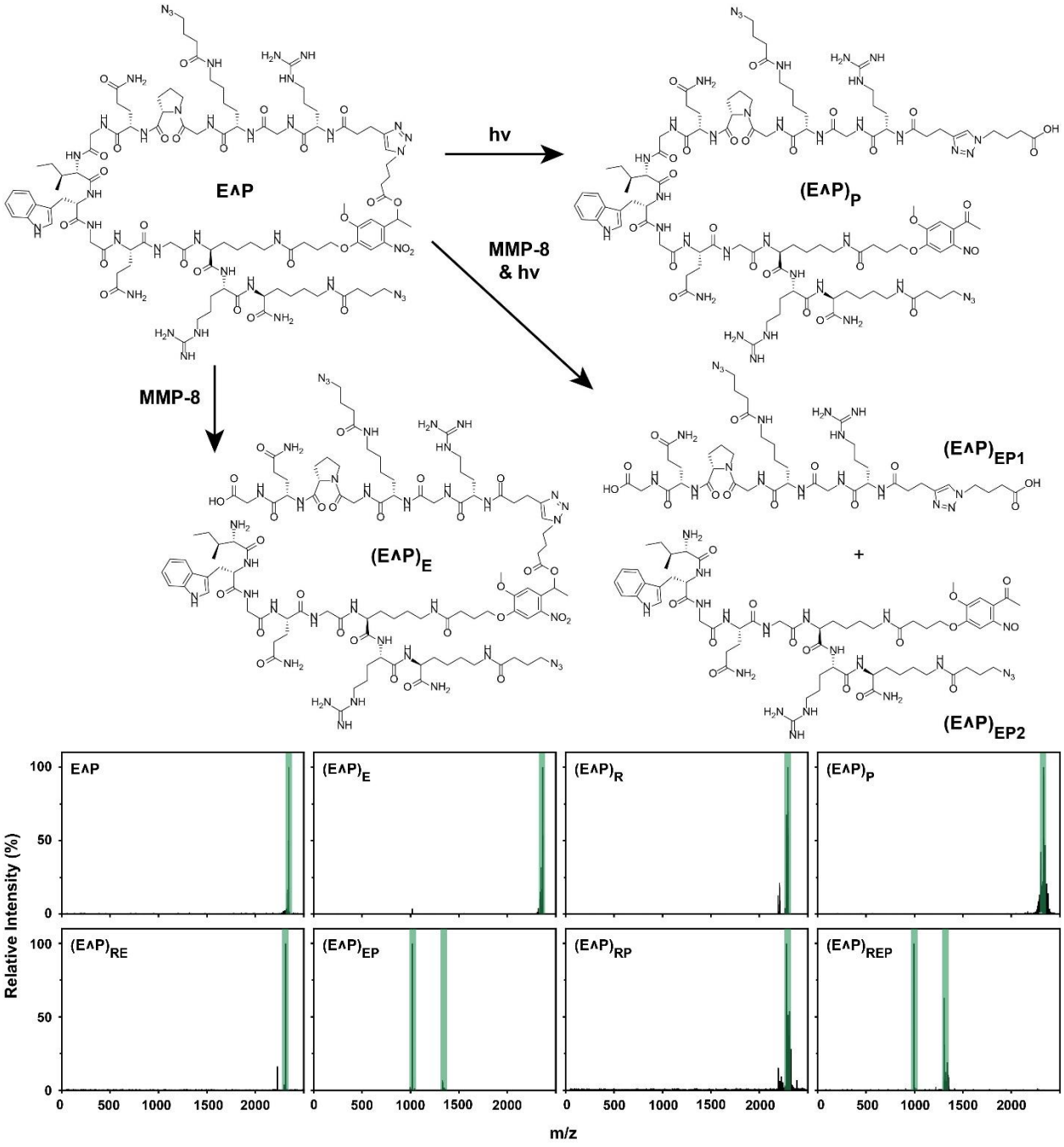

Treatment	Expected Peptides	m/z (Da)	
		Calculated	Measured
EΛP	EΛP	$[M+H]^+$ = 2346.2; [M+H: $-NO_2 \rightarrow -NO]^+$ = 2330.2	2346.0; 2330.0
$(EΛP)_E$	$(EΛP)_E$	$[M+H]^+$ = 2364.2; [M+H: $-NO_2 \rightarrow -NO]^+$ = 2348.2	2364; 2348.1
$(EΛP)_R$	EΛP	$[M+H]^+$ = 2346.2; [M+H: 2 $-N_3 \rightarrow$ 2 $-NH_2]^+$ = 2294.2; [M+H: 2 -N3 → 2 -NH2 & -NO2 → -NO]+ = 2278.2	2294.2; 2278.1
$(EΛP)_P$	$(EΛP)_P$	$[M+H]^+$ = 2346.2; [M+H: $-NO \rightarrow$ -N or $-NH_2]^+$ = 2330.2/2332.2; [M+H: $-N_3 \rightarrow -NH_2]^+$ = 2320.2; [M+H: $-N_3 \rightarrow -NH_2$ & $-NO \rightarrow$ -N or $-NH_2]^+$ = 2304.6/2306.2	2346.2; 2332.1; 2330.2; 2320.1; 2306.1; 2304.1
$(EΛP)_{RE}$	$(EΛP)_E$	$[M+H]^+$ = 2364.2; [M+H: 2 $-N_3 \rightarrow$ 2 $-NH_2]^+$ = 2312.2; [M+H: 2 $-N_3 \rightarrow$ 2 $-NH_2$ & $-NO_2 \rightarrow -NO]^+$ = 2296.2	2312.2; 2296.2
$(EΛP)_{EP}$	$(EΛP)_{EP1}$	$[M+H]^+$ = 1345.7; [M+H: $-NO \rightarrow -N]^+$ = 1329.7	1329.8
	$(EΛP)_{EP2}$	$[M+H]^+$ = 1019.5; [M+H: $-N_3 \rightarrow -NH_2]^+$ = 993.5	1019.6
$(EΛP)_{RP}$	$(EΛP)_P$	$[M+H]^+$ = 2346.2; [M+H: 2 $-N_3 \rightarrow$ 2 $-NH_2]^+$ = 2294.2; [M+H: 2 $-N_3 \rightarrow$ 2 $-NH_2$ & $-NO \rightarrow -NH_2]^+$ = 2280.2	2294.2; 2280.3
$(EΛP)_{REP}$	$(EΛP)_{EP1}$	$[M+H]^+$ = 1019.5; [M+H: $-N_3 \rightarrow -NH_2]^+$ = 993.5	993.6
	$(EΛP)_{EP2}$	$[M+H]^+$ = 1345.7; [M+H: $-N_3 \rightarrow -NH_2]^+$ = 1319.7; [M+H: $-N_3 \rightarrow -NH_2$ & $-NO \rightarrow -NH_2]^+$ = 1305.7	1319.7; 1305.8

Expected products were identified in all treatment. Products were of good purity in all cases.

Figure A9: Characterization of RΛP crosslinker degradation in solution

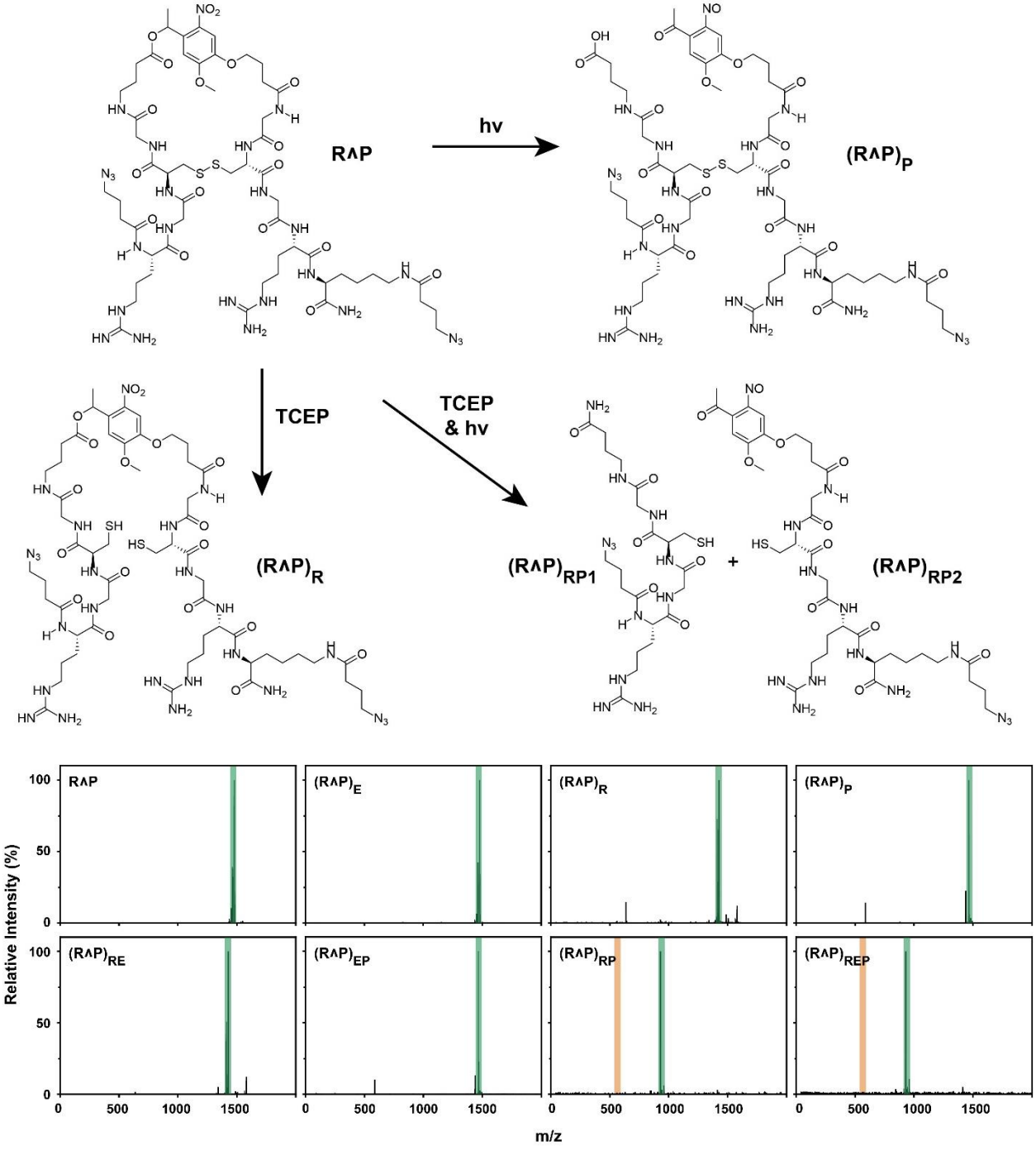

Treatment	Expected Peptides	m/z (Da)	
		Calculated	Measured
RΛP	RΛP	$[M+H]^+$ = 1478.6; $[M+H: -NO_2 \rightarrow -NO]^+$ = 1462.6; $[M+H: -N_3 \rightarrow -NH_2]^+$ = 1452.6	1478.7; 1462.5; 1452.5
$(RΛP)_E$	RΛP	$[M+H]^+$ = 1478.6; $[M+H: -NO_2 \rightarrow -NO]^+$ = 1462.6; $[M+H: -N_3 \rightarrow -NH_2]^+$ = 1452.6	1478.7; 1462.6; 1452.6
$(RΛP)_R$	$(RΛP)_R$	$[M+H]^+$ = 1480.6; $[M+H: 2\ -N_3 \rightarrow 2\ -NH_2]^+$ = 1428.6; $[M+H: 2\ -N_3 \rightarrow 2\ -NH_2$ & $-NO_2 \rightarrow -NO]^+$ = 1412.6	1428.7; 1412.7
$(RΛP)_P$	$(RΛP)_P$	$[M+H]^+$ = 1478.6; $[M+H: -NO \rightarrow -NH_2]^+$ = 1464.6; $[M+H: -N_3 \rightarrow -NH_2$ & $-NO \rightarrow -NH_2]^+$ = 1438.6	1465.8; 1439.8
$(RΛP)_{RE}$	$(RΛP)_R$	$[M+H]^+$ = 1480.6; $[M+H: 2\ -N_3 \rightarrow 2\ -NH_2]^+$ = 1428.6; $[M+H: 2\ -N_3 \rightarrow 2\ -NH_2$ & $-NO_2 \rightarrow -NO]^+$ = 1412.6	1428.0; 1412.0
$(RΛP)_{EP}$	$(RΛP)_P$	$[M+H]^+$ = 1478.6; $[M+H: -NO \rightarrow -NH_2]^+$ = 1464.6; $[M+H: -N_3 \rightarrow -NH_2$ & $-NO \rightarrow -NH_2]^+$ = 1438.6	1465.5; 1439.5
$(RΛP)_{RP}$	$(RΛP)_{RP1}$	$[M+H]^+$ = 587.3; $[M+H: -N_3 \rightarrow -NH_2]^+$ = 561.3	Below ROD
	$(RΛP)_{RP2}$	$[M+H]^+$ = 894.4; $[M+H: -N_3 \rightarrow -NH_2$ & $-SH \rightarrow -SSCH_2CH_2OH$ & $-NO \rightarrow -NH_2]^+$ = 944.5	930.6
$(RΛP)_{REP}$	$(RΛP)_{RP1}$	$[M+H]^+$ = 587.3; $[M+H: -N_3 \rightarrow -NH_2]^+$ = 561.3	Below ROD
	$(RΛP)_{RP2}$	$[M+H]^+$ = 894.4; $[M+H: -N_3 \rightarrow -NH_2$ & $-SH \rightarrow -SSCH_2CH_2OH$ & $-NO \rightarrow -NH_2]^+$ = 944.5	930.5

Expected products were identified in all treatment conditions except product $(RΛE)_{RP1}$, presumably due to being below the MALDI range of detection (m/z > 600). Products were of good purity in all cases.

Method A25: *In situ* rheology of hydrogel formation

Strain and frequency sweeps:
Oscillatory rheology was performed on an Anton Paar MCR301 rheometer equipped with a cone and plate geometry (25 mm diameter, 1° cone) at 25 °C. Strain and frequency sweeps were used to determine the linear viscoelastic region (LVR), the set of imposed conditions from which the elastic modulus is independent[139].

A solution of PEG-tetraBCN (Method A22, 2 mM) and the R crosslinker (Method A6, 4 mM) in PBS was reacted *in situ* for 120 minutes to form a hydrogel network. For the strain sweep, the frequency was fixed at 25 Hz, and the storage (G') and loss (G") moduli were measured at various strains (0.01 – 10%). For the frequency sweep, the strain was fixed at 1%, and G' and G'' were measured at various frequencies (0.1 – 100 Hz). The sweeps demonstrate that at 25 Hz and 1% strain, the hydrogel networks are in the LVR because a perturbation to either the frequency or strain does not change the value of G'. These conditions were used for future rheological analyses.

Strain sweep:

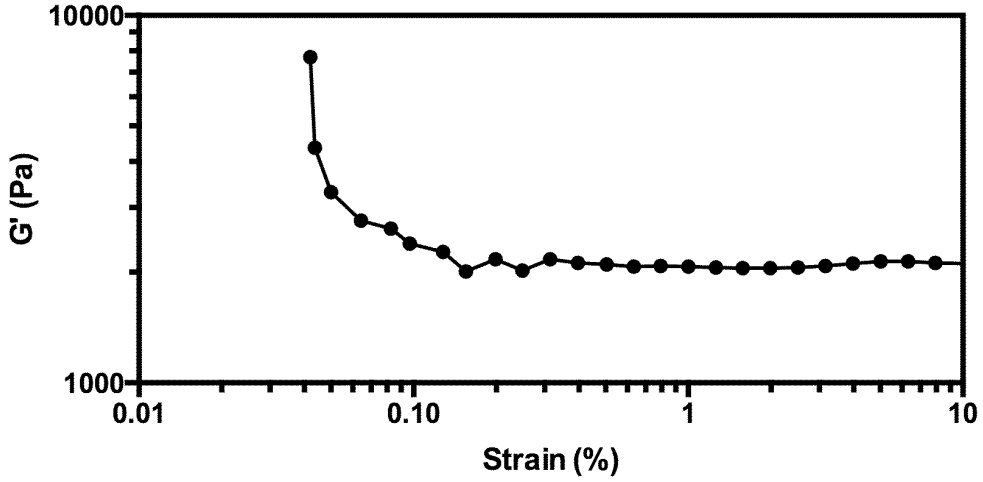

Frequency sweep:

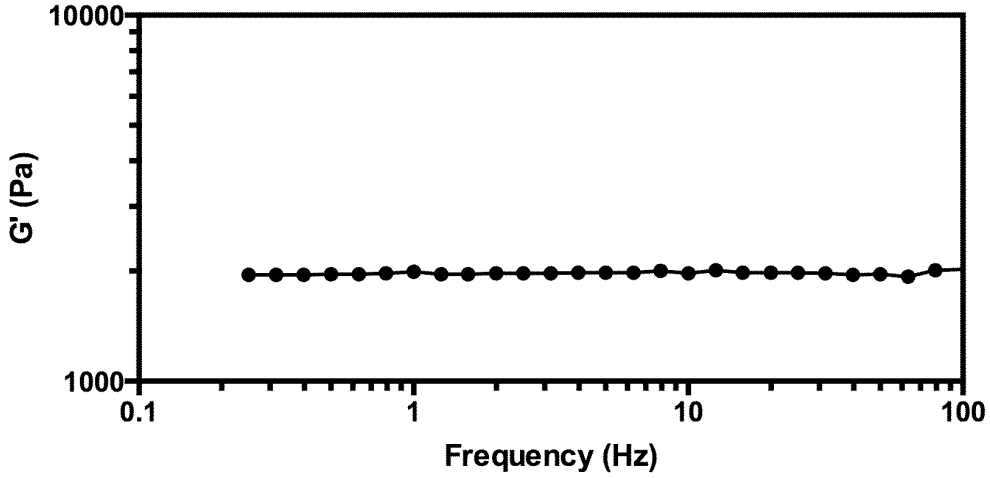

In situ hydrogel rheology:

Oscillatory rheology was performed on an Anton Paar MCR301 rheometer equipped with a cone and plate geometry (25 mm diameter, 1° cone) at 25 °C and 25 Hz with a 1% strain. A solution of PEG-tetraBCN (3 mM, Method A22) and the E∧P crosslinker (6 mM, Method A12) in MMP buffer was reacted *in situ*, while G' and G" were measured as a function of time over the course of two hours. Peptide crosslinkers were pre-treated with MMP and/or light as described in Method A24 in experimental triplicate. Hydrogels with similar stiffnesses formed when the E∧P crosslinker was untreated (G' = 1660 ± 170 Pa), exposed to just light (G' = 1580 ± 130 Pa), or exposed to just enzyme (G' = 1540 ± 110 Pa). When the crosslinker was treated with both enzyme and light, a hydrogel did not form (G' = 200 ± 30 Pa). All samples had a final loss modulus (G") of ~ 50 Pa.

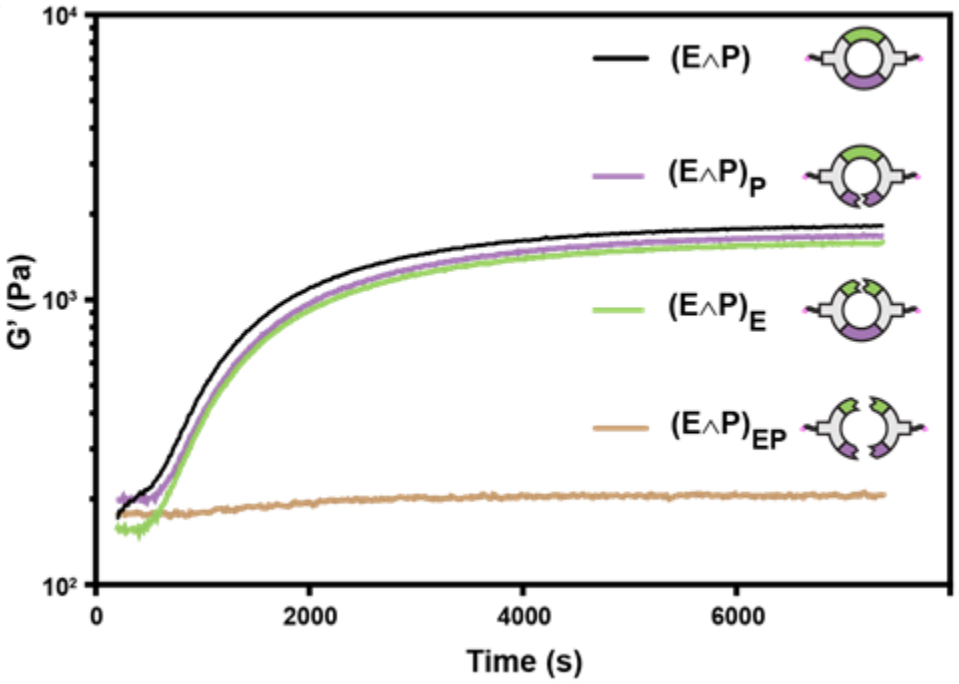

Method A26: Assessing network relaxation following partial cleavage of AND-gate crosslinkers

To estimate the effect of partial AND-gate linker cleavage on bulk material properties, we compared the average number of elastically active covalent bonds between network branch points before and after a single degradation event. As these bonds contributed by the 4-arm PEG represent the overwhelming majority of those between crosslinks (>90%), minimal structural relaxation is predicted following the cleavage of a single stimuli-labile moiety (<3% for all AND-gated crosslinkers). This is consistent with rheology data, where AND-gate crosslinker treatment with a single input does not produce a significant change in final material stiffness (Method A25).

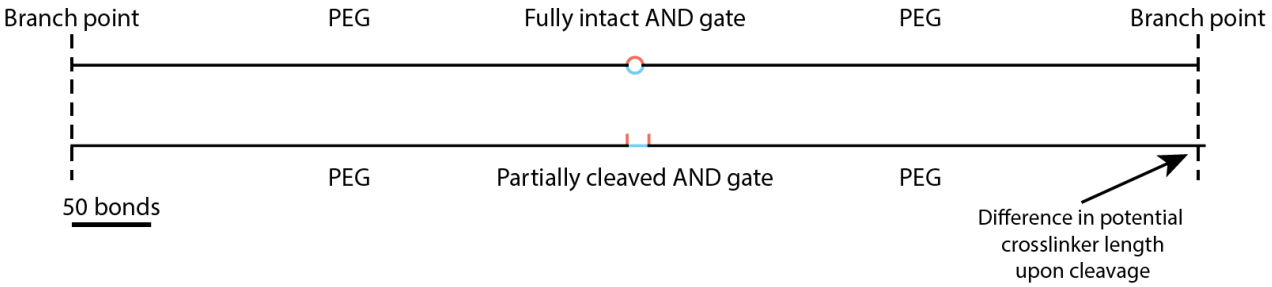

E∧P Crosslinker
Bonds from PEG macromer = 702
Bonds shared by both arms of peptide linker = 26
Bonds through E-arm = 30
Bonds through P-arm = 34
758 vs 762 indicates a **0.5% difference**

E∧R Crosslinker
Bonds from PEG macromer = 702
Bonds shared by both arms of peptide linker = 30
Bonds through E-arm = 30
Bonds through R-arm = 5
737 vs 762 is a **3.3% difference**

R∧P Crosslinker
Bonds from PEG macromer = 702
Bonds shared by both arms of peptide linker = 31
Bonds through R-arm = 5
Bonds through P-arm = 25
738 vs 758 is a **2.6% difference**

Method A27: Logic-based hydrogel degradation in response to sequential stimuli

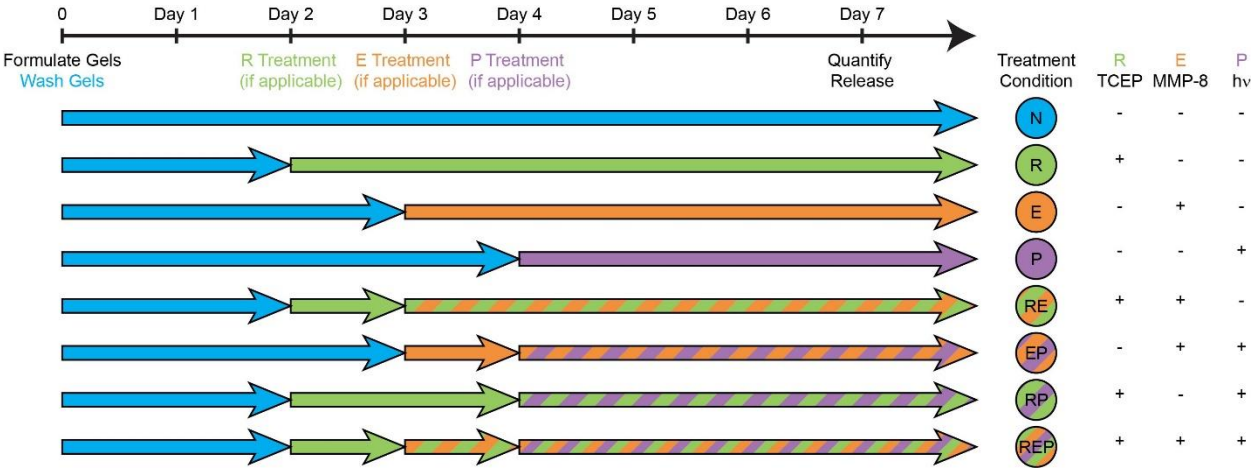

Fluorescent hydrogels were formulated from a precursor solution of PEG-tetraBCN-AF568 (2 mM) and a diazide peptide crosslinker (4 mM) in MMP buffer. Immediately upon addition of all components (65 μL total), the solution was vortexed and centrifuged. The precursor solution was transferred *via* a positive displacement pipette into microcentrifuge tubes (6 x 10 μL), centrifuged, and reacted at room temperature for 1 hour. To remove any fluorescent sol fraction, hydrogels were washed in MMP buffer (1 mL, 2 x 24 hours, 37 °C) prior to treatment. A total of 24 hydrogels were synthesized from each crosslinker (8 input combinations in experimental triplicate).

Samples receiving the reductive input ($_R$) were treated with tris(2-carboxyethyl)phosphine hydrochloride (TCEP·HCl, 2 μL, 100 mM in MMP buffer) and incubated overnight (22 hr) at 37 °C. To quench any unreacted TCEP, these samples were further treated with hydroxyethyl disulfide (5 μL, 100 mM in MMP buffer) prior to incubation (4 hr, 37 °C). Samples not receiving reductive input were maintained at 37 °C.

Samples receiving the enzyme input ($_E$) were subsequently treated with MMP-8 (Method A23, 5 μL, 0.2 mg mL^{-1} in MMP buffer) and all samples were incubated (20 hr, 37 °C).

Samples receiving the light input ($_P$) were subsequently exposed to UV light (λ = 365 nm, 10 mW cm^{-2} incident light, 60 minute exposure) prior to incubation (72 hr, 37 °C).

After 8 total days of experimental treatment, the extent of gel degradation was assessed by quantifying supernatant fluorescence (excitation: 570 nm, emission: 610 nm, emission cut-off filter: 590 nm).

Method A28: Characterization of PEG-tetraBCN-AF568 fluorescence

AF568 photobleaching study:

To assess the level of AF568 fluorophore photobleaching that occurs during light treatment conditions used in the hydrogel release studies (Method A27), AF568 was dissolved in PBS (10 μM) and exposed to UV light (λ = 365 nm, 10 mW cm^{-2}) in experimental triplicate. Sample fluorescence (100 μL, 1 μM, excitation wavelength 570 nm, emission wavelength 610 nm) was measured following 10-minute intervals of light exposure. One-way analysis of variance (ANOVA) failed to reject the null hypothesis that fluorescence does not change upon light exposure (p-value = 0.82). This suggests that AF568 does not undergo significant photobleaching under light treatment conditions used in the hydrogel degradation studies.

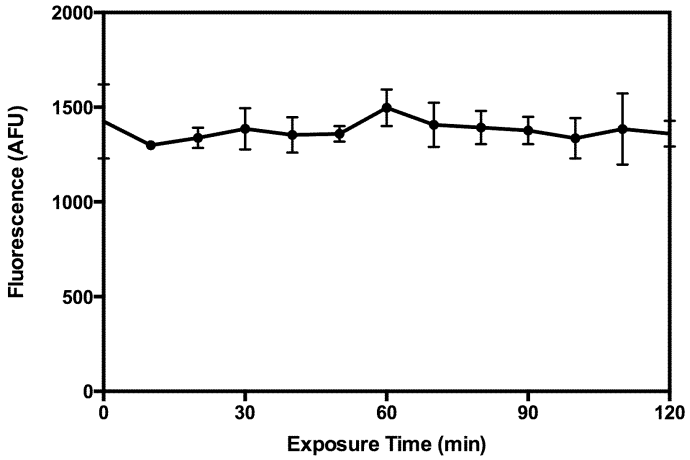

Quantification of PEG-tetraBCN-AF568 concentrations using fluorescence:

Fluorescence was used to determine the concentration of PEG-tetraBCN-AF568 in solution, and thus to quantify the extent of gel degradation in response to each combination of external stimuli. PEG-tetraBCN-AF568 fluorescence was significantly altered both in the presence of *o*NB, and in the presence of photocleaved *o*NB (*o*NB spectral properties change upon photodecomposition [134]). Therefore, three different calibration curves are required to correlate fluorescent signal with PEG-tetraBCN-AF568 concentration for crosslinkers that: 1) do not contain *o*NB; 2) contain *o*NB but have not been exposed to light; 3) contain photocleaved *o*NB.

A calibration curve (shown below, black) was generated using pure PEG-tetraBCN-AF568 in MMP buffer, and was used for constructs that do not contain *o*NB. A second calibration curve (shown below, blue) was generated using PEG-tetraBCN-AF568 and P crosslinker (Method A7, 1:2 molar ratio) in MMP buffer, and was used for systems that contain *o*NB but have not been exposed to light. The final calibration curve (shown below, red) was generated using PEG-tetraBCN-AF568 and P crosslinker (1:2 molar ratio) treated by the light condition used in the release studies (λ = 365 nm, 10 mW cm^{-2}, 60 minutes) in MMP buffer, and was used for systems that contain *o*NB and have been exposed to light.

Sample fluorescence was found to be scale with PEG-AF568 concentration for all cases, enabling the extent of hydrogel degradation to be quantified for each crosslinker system in response to different input combinations.

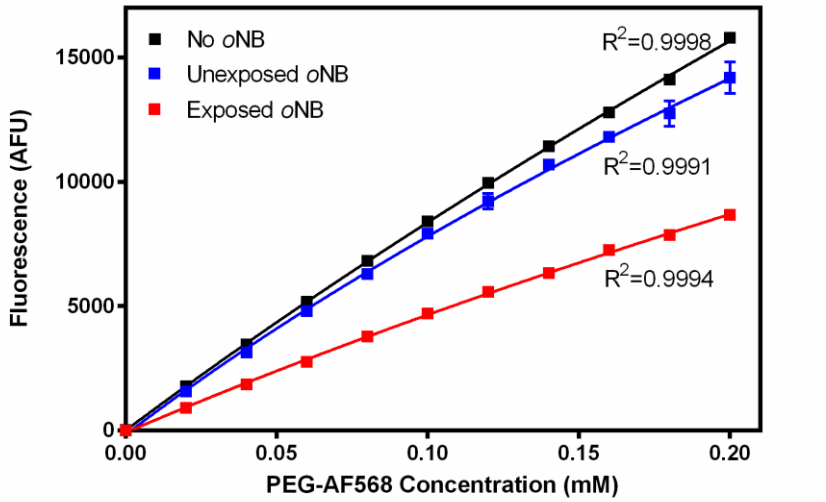

Figure A10: Gel photographs following logic-based degradation

Fluorescent hydrogels were prepared and treated as described in Method A27. Following complete degradative treatment, samples were photographed with a digital camera. Treatments that did not result in material degradation retained a hydrogel (pink). The expected degradation behavior is indicated by a colored dot in each condition; a pink dot denotes conditions that are expected to keep the material intact while a white dot denotes those expected to yield gel degradation.

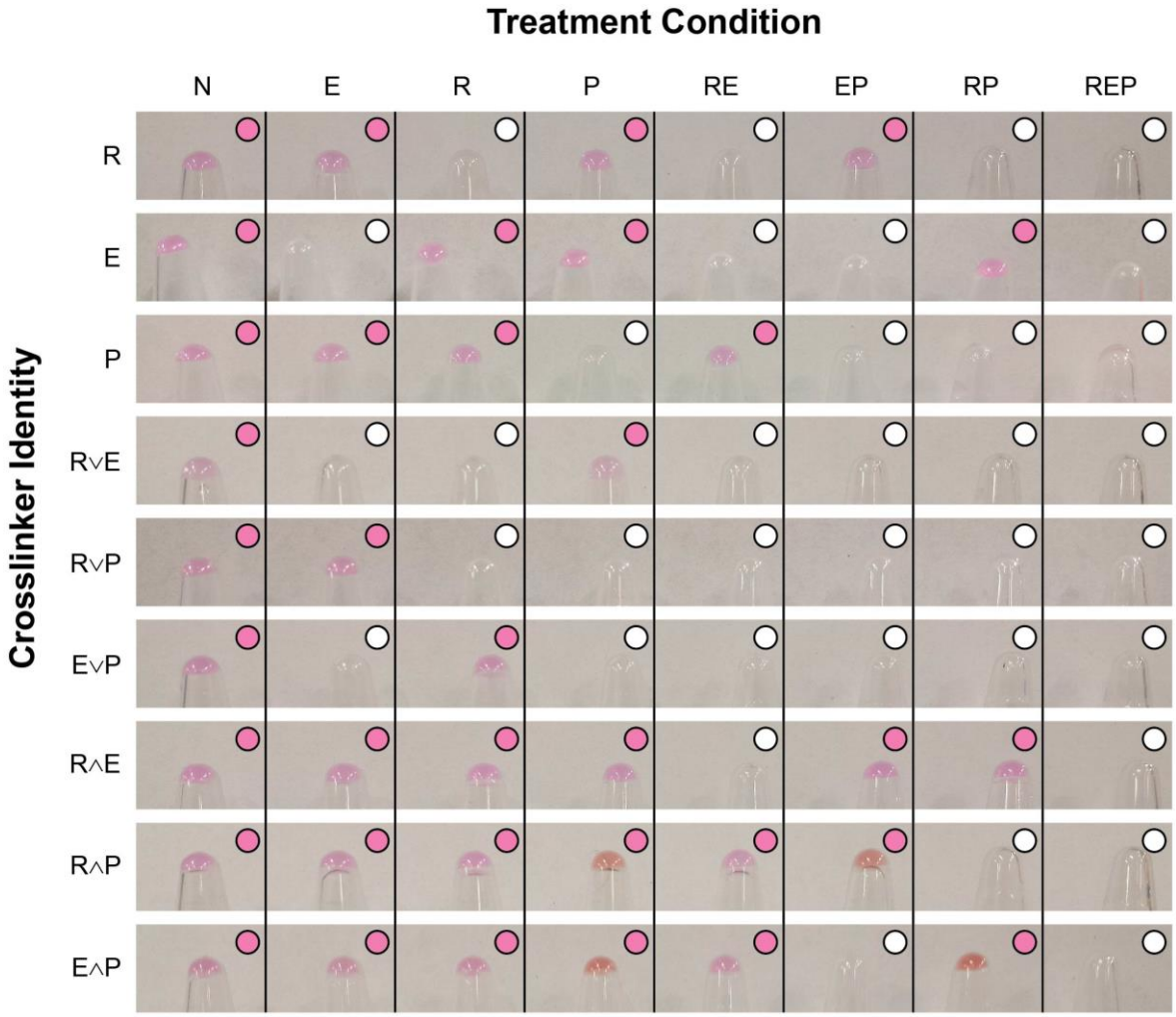

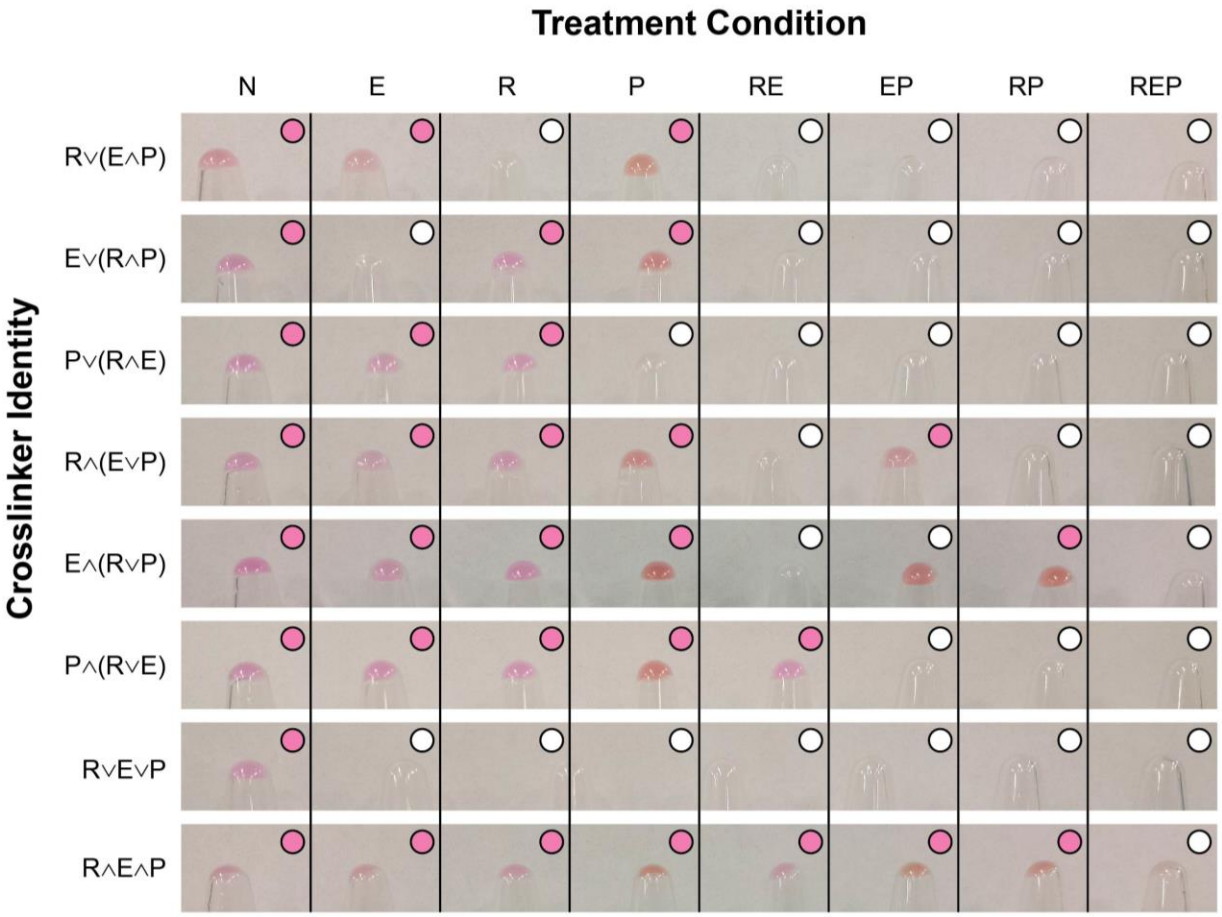
Treatment Condition
N
E
R
P
RE
EP
RP
REP
Crosslinker Identity
R∨(E∧P)
E∨(R∧P)
P∨(R∧E)
R∧(E∨P)
E∧(R∨P)
P∧(R∨E)
R∨E∨P
R∧E∧P

Figure A11: Degradation kinetics of single-input hydrogels

To assess the kinetics of hydrogel degradation, we examined the influence of input intensity and time on the response of single-input, YES-gated materials (R, E, and P). Fluorescent hydrogels were formulated as before (10 μL, Method A27) in two different geometries: 1) as a bulk gel in a microcentrifuge tube, and 2) as a thin gel (~50 μm thickness) in a 24-well plate. Hydrogels were washed with MMP buffer (1 mL, 2 x 24 hours, 37 °C) prior to treatment. At each timepoint, the extent of gel degradation was assessed by quantifying supernatant fluorescence (excitation: 570 nm, emission: 610 nm, emission cut-off filter: 590 nm), in experimental triplicate.

Reductively degradable hydrogels (R) were treated with TCEP·HCl (8.3 mM, 1.8 mM, or 0.90 mM in MMP buffer) at 37 °C.

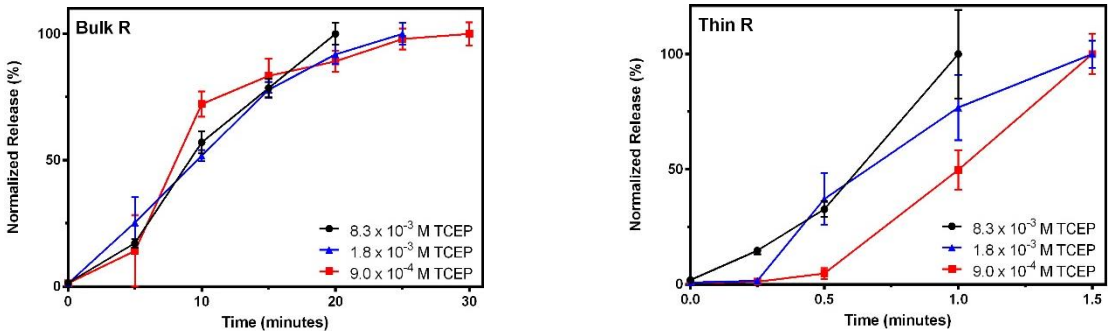

Enzymatically degradable hydrogels (E) were treated with MMP-8 (0.86 nM, 0.42 nM, 0.20 nM, or 0.042 nM in MMP buffer) at 37 °C.

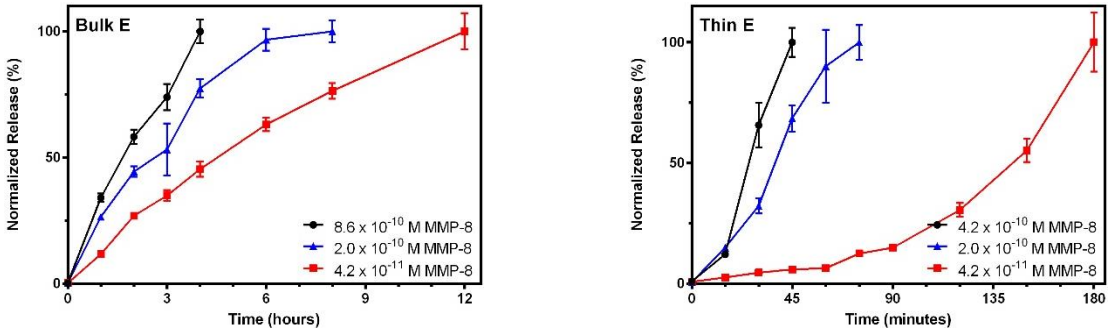

Photolytically degradable hydrogels (P), were treated with UV light (λ = 365 nm, 20 mW cm^{-2}, 10 mW cm^{-2}, or 5 mW cm^{-2}) in MMP buffer.

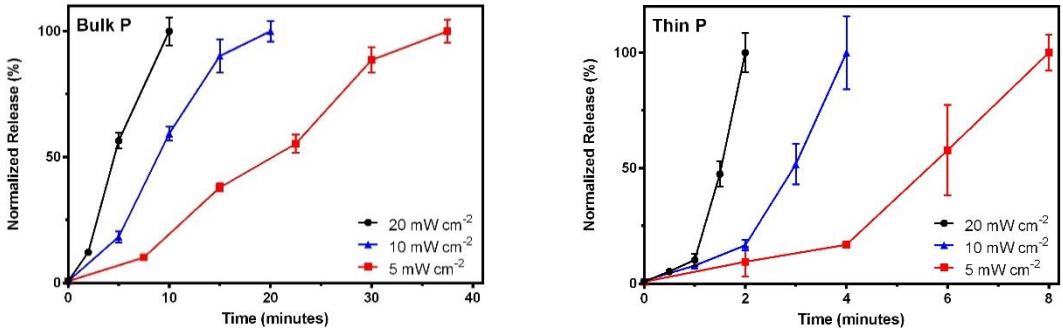

These experiments highlight that the timescale of logic-based material response is dictated, in part, by construct geometry. As each single-input gel/treatment combination yielded full degradation in <1.5 hours for thin gels or <12 hours for bulk gels, the experimental timeline outlined in Method A27 was deemed appropriate to examine biocomputational responses of higher-ordered logical systems.

Method A29: Logic-based delivery of functional doxorubicin from hydrogels

Synthesis of (1R,8S,9s)-bicyclo[6.1.0]non-4-yn-9-ylmethyl ((2S,3S,4S,6R)-3-hydroxy-2-methyl-6-(((1S,3S)-3,5,12-trihydroxy-3-(2-hydroxyacetyl)-10-methoxy-6,11-dioxo-1,2,3,4,6,11-hexahydrotetracen-1-yl)oxy)tetrahydro-2H-pyran-4-yl)carbamate (DOX-BCN):

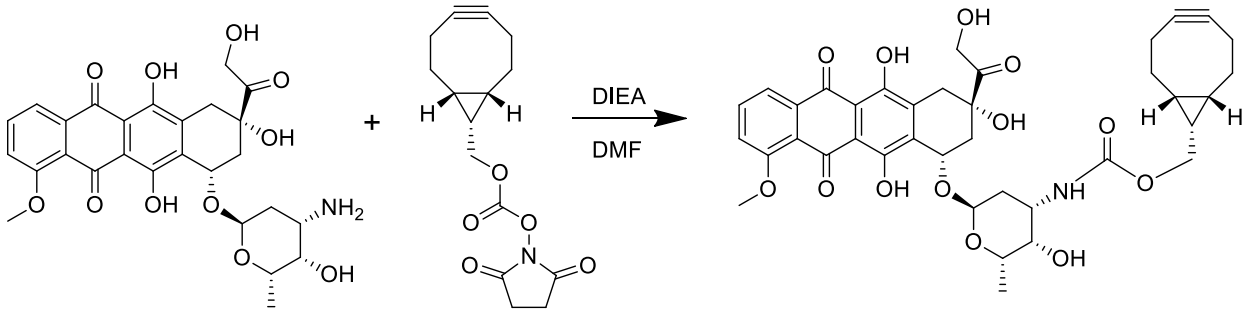

Doxorubicin hydrochloride (DOX, 6.0 mg, 10 µmol), BCN-OSu (Method A22, 6.0 mg, 21 µmol, 2x), and DIEA (5.3 mg, 41 µmol, 4x) were dissolved in minimal DMF and reacted overnight to functionalize doxorubicin with BCN. Complete functionalization of doxorubicin was confirmed *via* HPLC. The product (DOX-BCN) was used without any further purification.

Synthesis of RΛE-DOX crosslinker:
DOX-BCN (0.8 µmol) and RΛE crosslinker (4 µmol, 5x) were reacted in a mixture of DMF/PBS (300 µL) for 2 hours, whereby roughly 10% of RΛE-presented azides were modified with DOX. The product (RΛE-DOX) was used without any further purification.

DOX-loaded hydrogel treatments:
DOX-loaded hydrogels were formulated from a precursor solution of PEG-tetraBCN (2 mM) and either RΛE (4 mM, control group) or RΛE-DOX linker (4 mM, experimental group) in a 4-(2-hydroxyethyl)-1-piperazineethanesulfonic acid) (HEPES) buffer (5 mM HEPES, 3 mM $CaCl_2$, 5 µM $ZnCl_2$). Immediately upon addition of all components (95 µL total), the solution was vortexed and centrifuged. The precursor solution was transferred *via* a positive displacement pipette into microcentrifuge tubes (6 x 15 µL), centrifuged, and reacted at room temperature for 1 hour. To remove any unconjugated DOX, hydrogels were washed with HEPES buffer (1 mL, 4 x 24 hours, 37 °C) prior to treatment. A total of twelve hydrogels were synthesized (four input combinations in experimental triplicate).

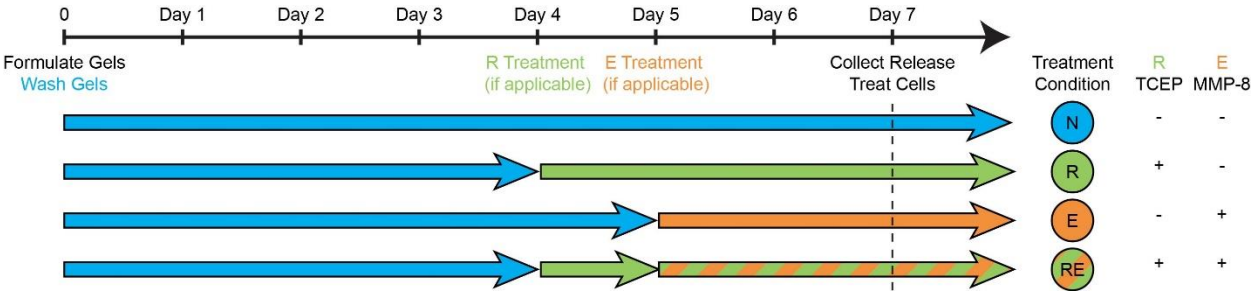

Samples receiving the reductive input ($_R$) were treated with glutathione (GSH, 2 mM) and incubated overnight (24 hr) at 37 °C. Samples not receiving reductive input were maintained at 37 °C.

Samples receiving the enzyme input ($_E$) were subsequently treated with MMP-8 (Method A23, 10 µL, 0.2 mg mL^{-1} in MMP buffer) and all samples were incubated (24 hr, 37 °C).

After experimental treatment, hydrogel supernatant (85 µL) was collected and combined with Dulbecco's Modified Eagle's Medium [DMEM, 85 µL, 2x containing 20% fetal bovine serum (FBS, Corning) and 2% Penicillin Streptomycin (PS, ThermoFisher)].

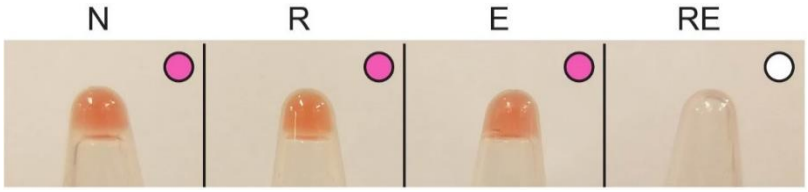

Biological response to DOX-hydrogel supernatant:
HeLa cells were seeded on a 96-well plate (2 x 10^3 cells per well) and cultured in DMEM supplemented with 10% FBS and 1% PS for 24 hours. The cells were then incubated in the DOX-hydrogel release solution (as described above), or in that from R∧E gels lacking DOX, for an additional 48 hours. A PicoGreen® dsDNA Assay (ThermoFisher) was performed to quantify the DNA concentration as a proxy for cell density.

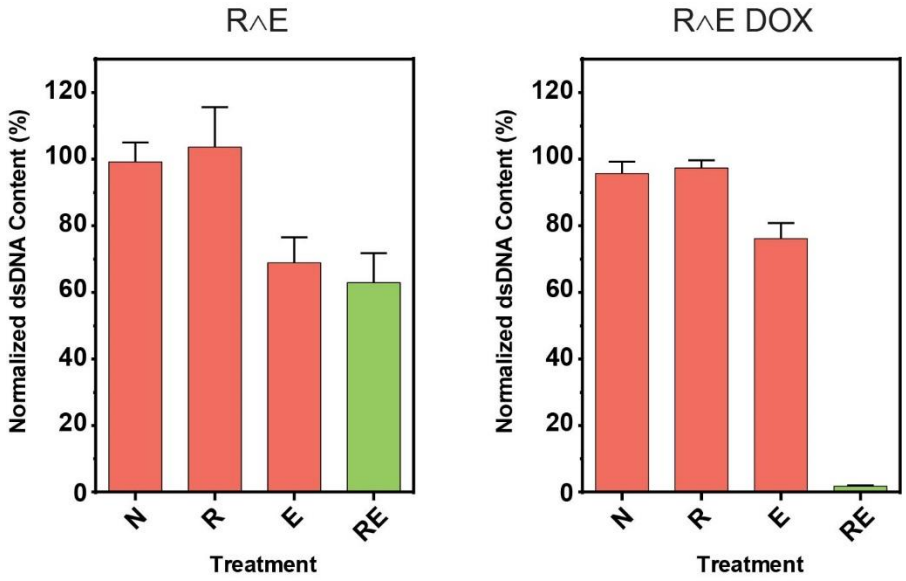

Dose-response curve for doxorubicin construct:
HeLa cells were seeded on a 96-well plate (2 x 10^3 cells per well) and cultured in DMEM supplemented with 10% FBS and 1% PS for 24 hours. The media was replaced with R∧E-DOX in a mixture of HEPES buffer and 2x media (1:1) and incubated for 48 hours prior to quantification of dsDNA by PicoGreen® analysis.

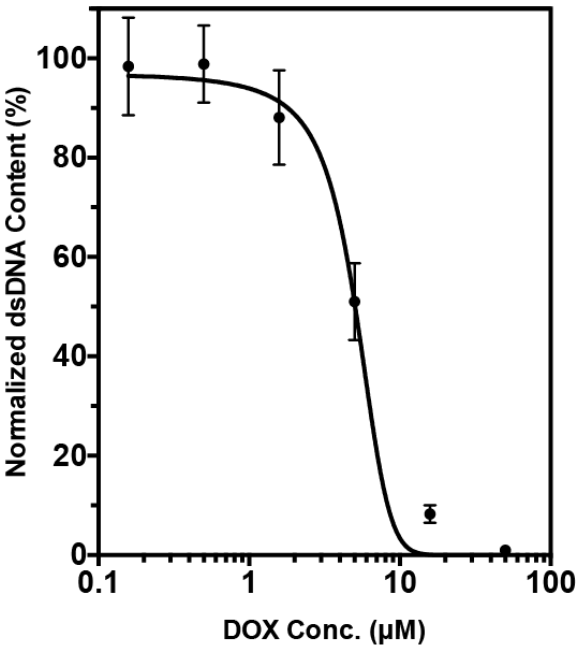
Normalized dsDNA Content (%)
100
80
60
40
20
0
0.1
1
10
100
DOX Conc. (μM)

Method A30: Multi-logic hydrogel treatment and microscopy

Azide-functionalized glass slides were synthesized following a published route[62] based on a silanization procedure was derived from the work by Walba, *et al.*[185].

Synthesis of (3-azidopropyl)trimethoxysilane:

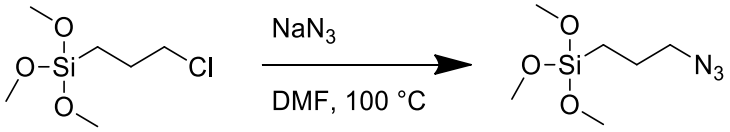

Anhydrous DMF (40 mL) was added to an oven-dried round bottom flask containing 3-chloropropyltrimethoxysilane (12 mL, 65.3 mmol, 1x) and sodium azide (6.38 g, 98.1 mmol, 1.5x) under a nitrogen atmosphere. The reaction was stirred overnight at 100 ºC, cooled to room temperature, and diluted with diethyl ether:dH_2O (1:1, 150 mL). The organic layer was washed with water (3x) and brine (1x), dried over $MgSO_4$, and concentrated *in vacuo* to yield a clear oil (12.74 g, 62.1 mmol, 95% yield). ^{1}H NMR (500 MHz, $CDCl_3$) δ 3.57 (s, 9H), 3.26 (t, *J* = 6.9 Hz, 2H), 1.75 – 1.66 (m, 2H), 0.73 – 0.66 (m, 2H); ^{13}C NMR (126 MHz, $CDCl_3$) δ 53.86, 50.72, 22.58, 6.46. These spectral data matched those previously reported[186].

Treatment of glass slides:
Plain glass slides were cleaned in piranha solution (50% sulfuric acid, 35% dH_2O, 15% hydrogen peroxide) for 30 minutes at room temperature. The slides were rinsed with water, acetone (3x) and then dried. The slides were incubated for 90 minutes in a solution of (3-azidopropyl)trimethoxysilane (70 mM) and n-butylamine (70 mM) in toluene. The slides were subsequently rinsed with toluene, wiped dry with a Kimwipe™, and baked overnight at 80 ºC. Functionalized slides were stable when stored at room temperature under ambient conditions for several weeks.

Preparation of three-region hydrogels differently sensitive to light and reductant:
Hydrogels were formed sandwiched between an azide-functional glass slide and a Rain-X®-treated glass slide separated by two 0.005" thick silicone spacers (McMaster-Carr). A precursor solution containing PEG-tetraBCN-FAM (Method A22, 2 mM) and the P crosslinker (Method A7, 4 mM) was injected between the silicone spacers (0.005 inches) and reacted for one hour. Subsequently, a precursor solution of PEG-tetraBCN-Cyanine5 (Method A22, 2 mM) and the R∨P crosslinker (Method A10, 4 mM) was injected between the FAM functionalized region and a silicone spacer and reacted for one hour. This was repeated on the other side of the FAM functionalized region with PEG-tetraBCN-AF568 (Method A22, 2 mM) and R∧P crosslinker (Method A13, 4 mM). Hydrogels were equilibrated and stored in PBS.

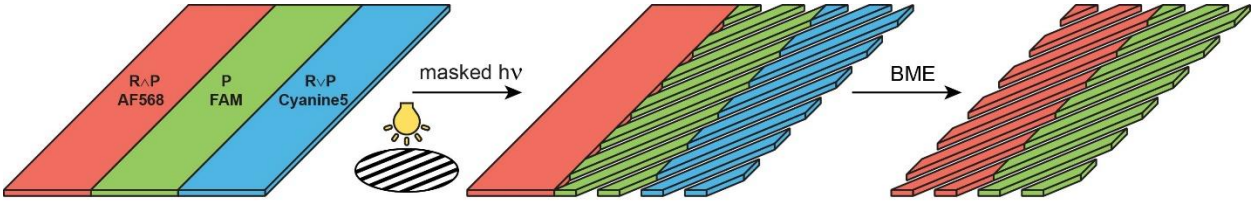

Treatment of three-region hydrogels sensitive to light and reductant:

Preformed tri-color gels were exposed to UV light (λ = 365 nm, 10 mW cm^{-2} incident light, 10 minute exposure) through a slitted photomask (200 μm wide lines separated by 200 μm spaces), inducing degradation of the P- and R∨P-based gels in the UV-exposed regions. Following light treatment, gels were soaked in 2-mercaptoethanol (BME, 0.25 mM in 50 mL PBS) for 45 minutes at room temperature, yielding full degradation of the R∨P-based gel portion while leaving the P-based volume fully intact. The R∧P-based material degraded to reveal the original photopatterned exposure, demonstrating that both inputs are required for material degradation.

Preparation of four-region hydrogels differently sensitive to reductant and enzyme:
Hydrogels containing four regions, each with a distinct logical crosslinker and fluorophore, were prepared using the method described above. The regions from left to right were: 1) R crosslinker/FAM (Methods S6, S22), 2) R∧E crosslinker/AF568 (Methods S11, S22), 3) E crosslinker/FAM (Methods S5, S22), and 4) R∨E crosslinker/Cyanine5 (Methods S8, S22).

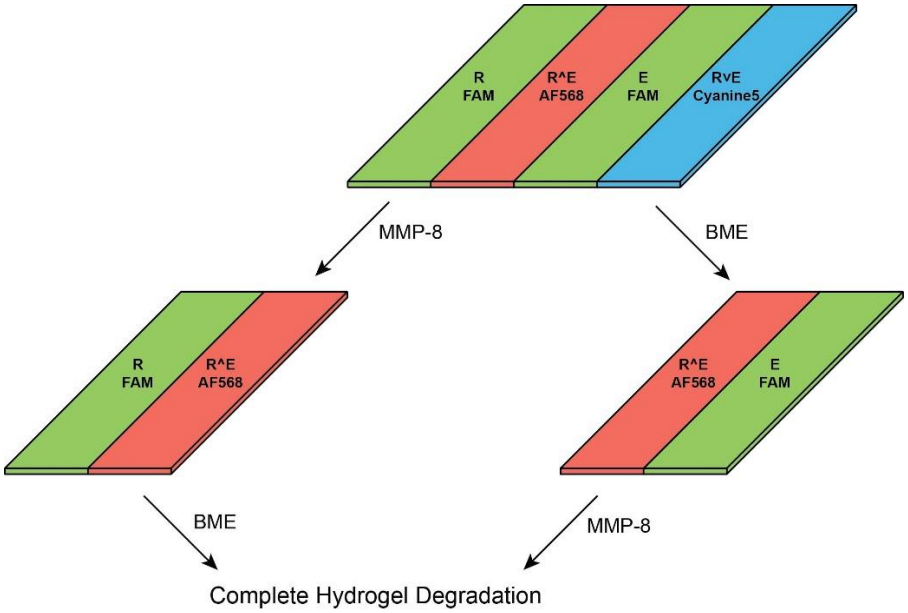

Treatment of four-region hydrogels sensitive to reductant and enzyme:
Preformed four-color gels were sequentially exposed to reducing conditions (0.25 mM BME, 45 minutes) and MMP-8 (0.20 nM, 2 hours, Method A23), in either order. In response to the initial

treatment, two regions of the hydrogel degraded (R∨E and the relevant single-input region). Exposure to the second input induced full degradation on the remainder of the hydrogel.

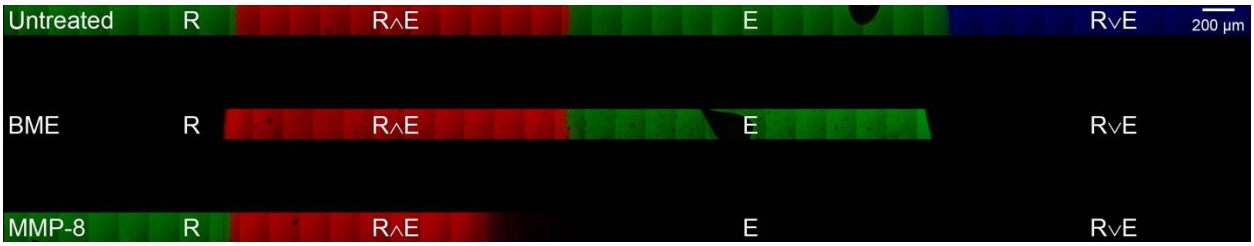

Hydrogel microscopy:

Hydrogels were imaged using fluorescent confocal microscopy. Three channels – one for each fluorophore – were simultaneously monitored. For visualization, fluorescence corresponding to AF568 (excitation 578 nm, emission 594-627 nm), FAM (excitation 515 nm, emission 520-569 nm), and Cyanine5 (excitation 646 nm, emission 663-675 nm) were false colored as red, green, and blue, respectively.

Method A31: Hydrogel-encapsulated cell release studies

Four human bone marrow-derived stromal cell lines [hS5, a gift from the Ying Zheng and Beverly Torok-Storb labs at the University of Washington and the Fred Hutchinson Cancer Research Center, respectively[187]], including one non-fluorescent control and three each stably transfected to express a single fluorescent protein [mCherry, green fluorescent protein (GFP), or blue fluorescent protein (BFP)], were cultured at 37 °C in Roswell Park Memorial Institute medium 1640 (RPMI-1640, Corning) supplemented with 10% FBS and 1% PS.

Cell-laden multi-colored hydrogel preparation for microscopy:
Hydrogels were formed sandwiched between an azide-functional glass slide and a Rain-X®-treated glass slide separated by two 0.005" thick silicone spacers (McMaster-Carr). A precursor solution containing PEG-tetraBCN (Method A22, 2 mM), the P crosslinker (Method A7, 4 mM), and hS5-GFP^+ (40×10^6 cells mL^{-1}) was injected between the silicone spacers and reacted for one hour. Subsequently, a precursor solution of PEG-tetraBCN (2 mM), the R∨P crosslinker (Method A10, 4 mM), and hS5-BFP^+ (40×10^6 cells mL^{-1}) was injected between the hS5-GFP^+ encapsulated region and a silicone spacer. Immediately afterwards, a precursor solution of PEG-tetraBCN (2 mM), R∧P crosslinker (Method A13, 4 mM), and hS5-$mCherry^+$ (40×10^6 cells mL^{-1}) was injected between the other side of the hS5-GFP^+ encapsulated region and a silicone spacer. The hS5-$mCherry^+$ and hS5-BFP^+ encapsulated regions were simultaneously reacted for one hour. Hydrogels were stored in media overnight.

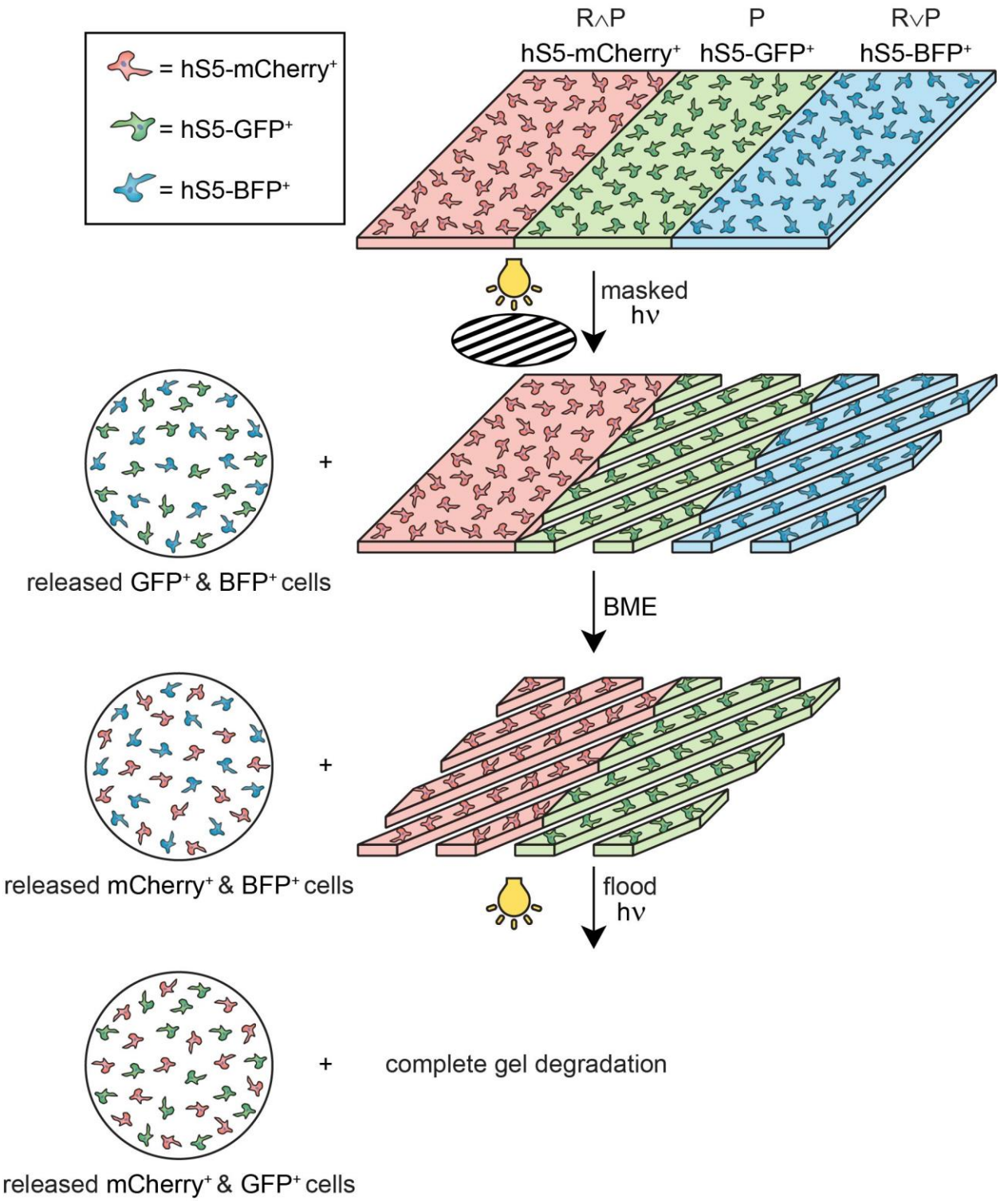
= hS5-mCherry+
= hS5-GFP+
= hS5-BFP+
R∧P
hS5-mCherry+
P
hS5-GFP+
R∨P
hS5-BFP+
masked
hν
+
released GFP+ & BFP+ cells
BME
+
released mCherry+ & BFP+ cells
flood
hν
+
complete gel degradation
released mCherry+ & GFP+ cells

Cell-laden hydrogel treatments for microscopy:
Preformed tri-color cell-laden gels were exposed to UV light (λ = 365 nm, 10 mW cm^{-2} incident light, 10 minute exposure) through a slitted photomask (200 μm wide lines separated by 200 μm spaces), inducing degradation of the P- and R∨P-based gels in the exposed regions and associated release of hS5-GFP^+ and hS5-BFP^+ cells. Following light treatment, gels were soaked in 2-mercaptoethanol (BME, 0.25 mM in 50 mL PBS) at 37 °C for 45 minutes, yielding full degradation of the R∨P-based gel portion (including hS5-BFP^+ release) while leaving the P-based gel fully intact. The R∧P-based gel degraded to match the original photopatterned exposure (causing release of hS5-$mCherry^+$ cells), demonstrating that both inputs are required for material degradation. Finally, gels were exposed to unmasked light to induce complete degradation of any remaining material and to release an equal number of hS5-GFP^+ and hS5-$mCherry^+$ cells.

Cell-laden hydrogel microscopy:
Following each degradative step, cells that remained encapsulated in the intact gel were imaged using fluorescent confocal microscopy. Three channels – one for each fluorescent protein – were simultaneously monitored. For visualization, fluorescence corresponding to mCherry (excitation 587 nm, emission 626-703 nm), GFP (excitation 489 nm, emission 499-570 nm), and BFP (excitation 405 nm, emission 413-494 nm) were false colored as red, green, and blue, respectively.

Quantifying cell release by flow cytometry:
Following each degradative step, released cells were harvested though successive gel rinsing with PBS and centrifugation. For each treatment condition, released cells were fixed using a solution of 4% formaldehyde in PBS (37 °C, 10 minutes), chilled on ice (1 minute), concentrated by centrifugation, and resuspended in PBS. Flow cytometry was performed on released cell populations using a BD Biosciences LSR II Flow Cytometer. Forward scattering (FS), side scattering (SS), and the fluorescence corresponding to BFP (405 nm and 100 mW laser line, 450/50 nm bandpass filter), GFP (488 nm and 100 mW laser line, 530/30 nm bandpass filter), and mCherry (561 nm and 150 mW laser line, 610/20 nm bandpass filter) were measured for each event. Flow cytometry was performed on standards of each cell line (non-fluorescent, mCherry, GFP, and BFP) and cells released from each treatment.

Analysis of flow cytometry data:
To account for spectral overlap of fluorescent proteins, compensation controls were calculated from the standards using automatic compensation in FACSDiva software. The gating tree was set as follows (shown below for GFP standard). *A:* FSC/SSC (the distribution of cell size and intracellular complexity, respectively, from light scatter) to *B:* FSC/pulse width (to isolate events corresponding to single cells) to *C:* histograms of each fluorescent channel. Gating for *A* and *B* was performed using non-fluorescent hS5 cells. Gating for *C* was performed for red, green, and blue fluorescence using hS5-$mCherry^+$, hS5-GFP^+, hS5-BFP^+ standards, respectively.

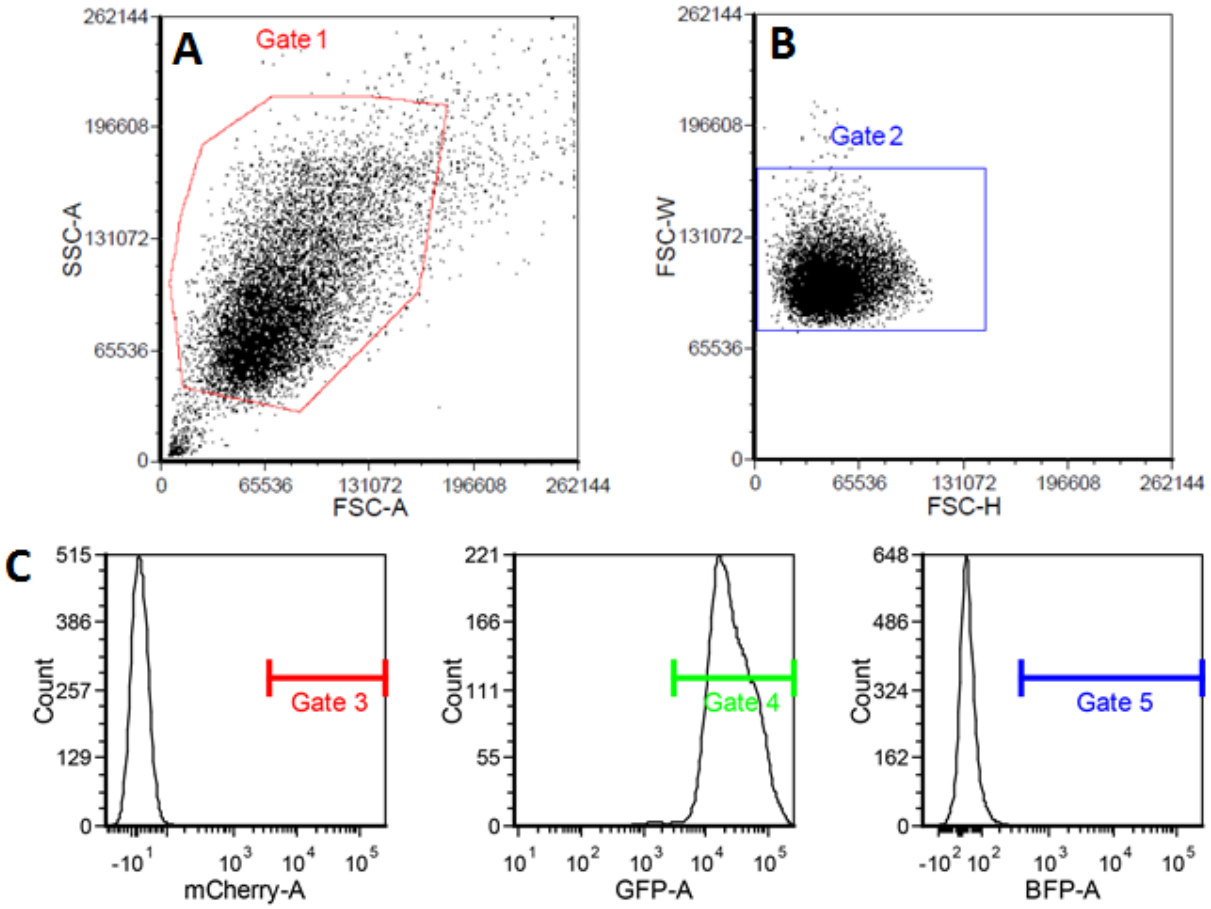
A
Gate 1
SSC-A
FSC-A
262144
196608
131072
65536
0
B
Gate 2
FSC-W
FSC-H
C
Gate 3
Count
mCherry-A
515
386
257
129
Gate 4
GFP-A
221
166
111
55
Gate 5
BFP-A
648
486
324
162

Figure A12: Cell viability following hydrogel encapsulation and triggered release

Cell-laden hydrogel preparation for viability studies:
Single-input responsive hydrogels were formed sandwiched between an azide-functional glass slide and a Rain-X®-treated glass slide separated by two 0.005" thick silicone spacers (McMaster-Carr). A precursor solution containing PEG-tetraBCN (2 mM), a YES crosslinker (either R, E, or P; 4 mM), and hS5 (40×10^6 cells mL^{-1}) was injected between the silicone spacers and reacted for one hour. Hydrogels were stored in media for one hour prior to treatments. Each material was generated and assayed in experimental triplicate.

Cell-laden hydrogel degradation for viability studies:
Gels were degraded and the viability of the released cells was assessed. To induce gel degradation, R gels were treated with BME (0.25 mM in PBS) at 37 °C for 45 minutes; P gels were exposed to UV light (λ = 365 nm, 10 mW cm^{-2} incident light) at 25 °C for 10 minutes; E gels were treated with MMP-8 (0.20 nM in RPMI) at 37 °C for 60 minutes. All treatments yielded complete hydrogel degradation. Released cells were collected and isolated *via* centrifugation prior to Live/Dead® staining (Invitrogen).

Viability analysis:
Cells released from the gels and stained with the Live/Dead® assay were imaged on a Nikon Eclipse TE2000-U microscope using filter cubes corresponding to both live (excitation 480/40 nm filter, emission 535/50 nm filter) and dead (excitation 560/20 nm filter, emission 630/60 nm filter) staining. Viability was determined for each treatment by standard image analysis. Average cell viability and representative images for each treatment condition are presented below. For each release treatment, representative fluorescent images of live and dead cells are false colored green and red, respectively.

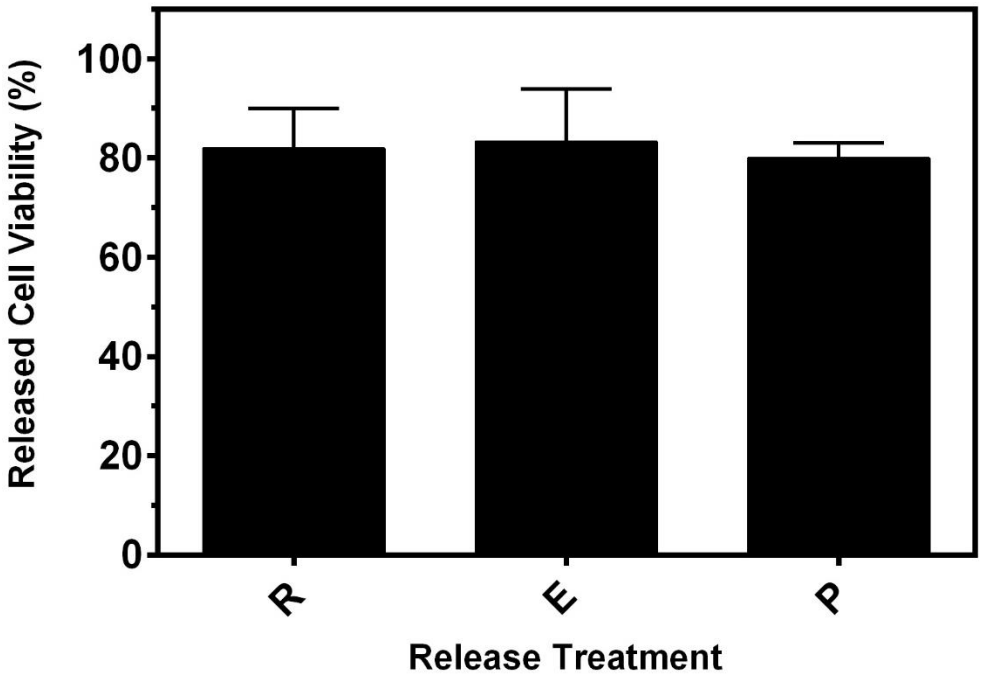

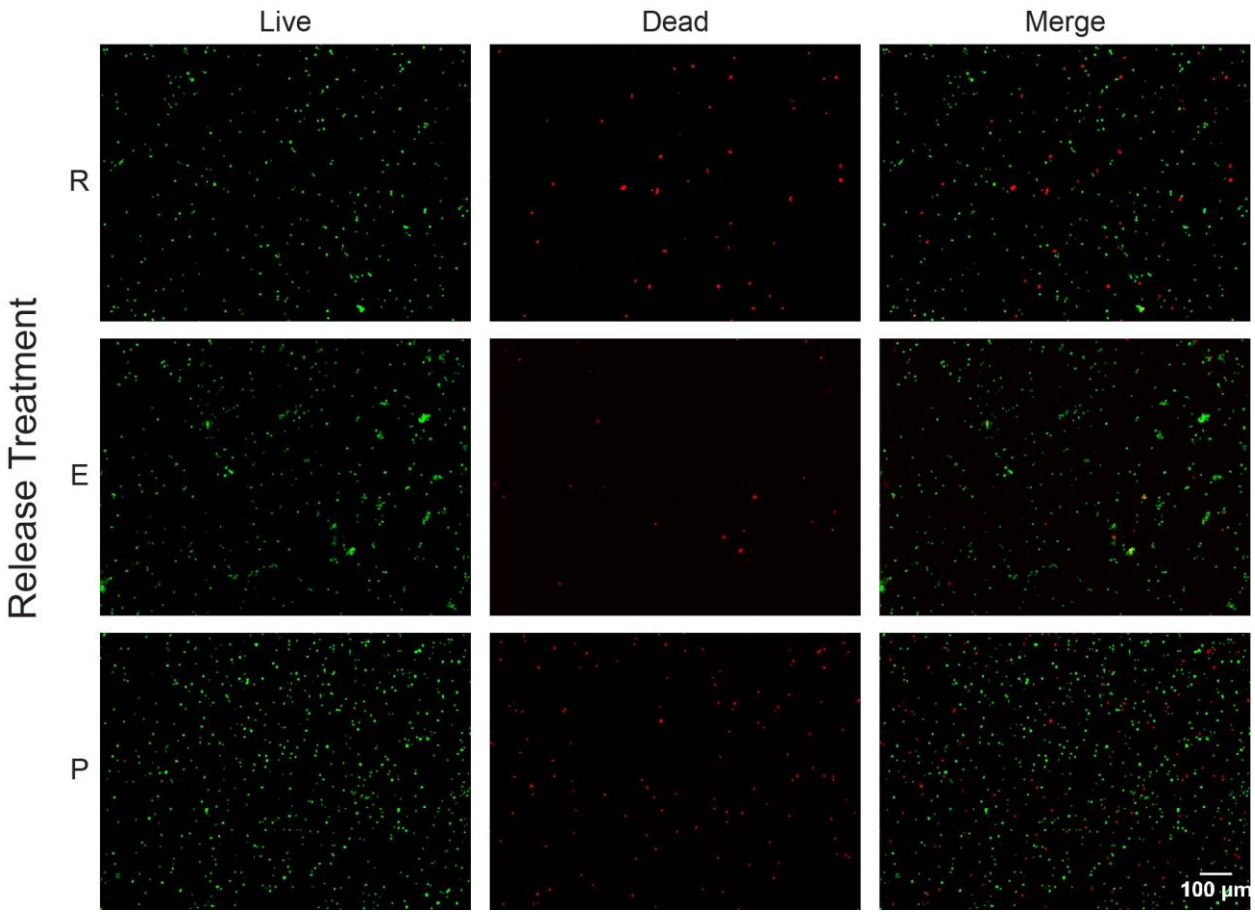
Live
Dead
Merge
Release Treatment
R
E
P
100 µm

APPENDIX B: SUPPLEMENTARY INFORMATION FOR CHAPTER 4

General synthetic information

Chemical reagents and solvents were purchased from either Sigma-Aldrich or Fisher Scientific and used as received. Peptide synthesis reagents were purchased from either ChemPep or Chem-Impex and used as received. Deionized water (dH_2O) was generated by a U.S. Filter Corporation Reverse Osmosis System with a Desal membrane. Synthetic chemical reactions were performed under a nitrogen atmosphere in oven-dried glassware and stirred with a Teflon-coated magnetic stir bar unless otherwise noted. Solvents were removed *in vacuo* with a Büchi Rotovapor R-3 equipped with a V-700 vacuum pump and V-855 vacuum controller and a Welch 1400 DuoSeal Belt-Drive high vacuum pump. Nuclear magnetic resonance (NMR) data was collected at 298 K on Bruker instruments and chemical shifts are reported relative to tetramethylsilane (TMS, $\delta = 0$). Microwave-assisted peptide synthesis was performed on a CEM Liberty 1. Semi-preparative reversed-phase high-pressure liquid chromatography (RP-HPLC) was performed on a Dionex Ultimate 3000 equipped with a variable multiple wavelength detector, automated fraction collector, and Thermo 5 µm Synchronis silica 250 x 21.2 mm C18 column. Lyophilization was performed on a LABCONCO FreeZone 2.5 Plus freeze-dryer equipped with a LABCONCO rotary vane 117 vacuum pump. Matrix-assisted laser desorption/ionization time of flight (MALDI-TOF) mass spectrometry was performed in reflectron negative ion mode on a Bruker AutoFlex II using a matrix of α-cyano-4-hydroxycinnamic acid:2,5-dihydroxy benzoic acid (2:1). Mass spectrometry of proteins was performed on a Waters SYNAPT G2-Si equipped with a liquid chromatography tandem mass spectrometer (LC-MS/MS). The light source for the photochemical cleavage was a Lumen Dynamics OmniCure S1500 Spot UV Curing system with an internal 365 nm filter and an external 360 nm cut-on longpass filter. Light intensity was measured using a Cole-Parmer Radiometer (Series 9811-50, $\lambda = 365$ nm). Fluorescence and absorbance readings were acquired on a SpectraMax M5 spectrometer using Thermo Scientific Nunc polypropylene 96-well plates. Confocal microscopy was performed at the University of Washington Keck Microscopy Center on a Leica SP8X. Polymerase chain reaction (PCR) was performed in a Bioer LifeECO thermal cycler. Protein expression was performed in a Thermo Scientific MaxQ 4000 shaker incubator. Cells were lysed using a Fisher Scientific Model 505 Sonic Dismembrator. Mammalian cell culture was performed in a NuAire LabGard ES NU-437 Class II Type A2 Biosafety Cabinet. Cells were maintained in a Sanyo inCu saFe® MCO-17AC incubator at 37 °C and 5% CO_2.

Method B1: Construction of Plasmids for Protein Expression

sfGFP-R$_9$-LPETG-6xHis

sfGFP-R$_9$-LPETG-6xHis was constructed using PCR to add on 5' NdeI and 3' XhoI cut sites, sortase recognition sequence, and polyarginine domain. pET-21a (+) plasmid and PCR products were digested (4 hr, 37 °C) with NdeI and XhoI restriction enzymes (New England BioLabs) and purified by extraction following electrophoretic separation (0.8% agarose). The digested pET-21a (+) and protein insert were ligated (T4 DNA ligase, 16 hr, 16 °C), transformed into chemically competent Top10 *E. coli* (Thermo Fisher) by heat shock, and plated onto agar plates (10 g Tryptone, 5 g Yeast Extract, 10 g NaCl, 15 g agar, 1 L dH_2O) containing ampicillin (100 μg mL^{-1}). Colonies were subsequently grown overnight in Miller's Lysogeny Broth (LB, 5 mL) containing ampicillin (100 μg mL^{-1}). Plasmids were purified using a QIAprep Spin Miniprep Kit (Qiagen), and sequenced using a SimpleSeq DNA Sequencing Kit (Thermo Fisher). Plasmids corresponding to the construct of interest were purified and subsequently transformed into chemically competent BL21(DE3) *E. coli* (Promega) for expression.

sfGFP-R$_9$-LPETG-6xHis forward primer:
5' ATATGATACATATGCGTAAAGGCGAAGAG 3'
sfGFP-R$_9$-LPETG-6xHis reverse primer:
5' GTCGTCGTCGTCGTCTGCCGGAAACCGGTGGTGGTCTCGAGGATTATAA 3'

The DNA sequence of the expressed sfGFP-R$_9$-LPETG-6xHis was:
ATGCGTAAAGGCGAAGAGCTGTTCACTGGTGTCGTCCCTATTCTGGTGGAACTGGATGGTGATGTCAACGGTCATAA
GTTTTCCGTGCGTGGCGAGGGTGAAGGTGACGCAACTAATGGTAAACTGACGCTGAAGTTCATCTGTACTACTGGTA
AACTGCCGGTACCTTGGCCGACTCTGGTAACGACGCTGACTTATGGTGTTCAGTGCTTTGCTCGTTATCCGGACCAC
ATGAAGCAGCATGACTTCTTCAAGTCCGCCATGCCGGAAGGCTATGTGCAGGAACGCACGATTTCCTTTAAGGATGA
CGGCACGTACAAAACGCGTGCGGAAGTGAAATTTGAAGGCGATACCCTGGTAAACCGCATTGAGCTGAAAGGCATTG
ACTTTAAAGAAGACGGCAATATCCTGGGCCATAAGCTGGAATACAATTTTAACAGCCACAATGTTTACATCACCGCC
GATAAACAAAAAAATGGCATTAAAGCGAATTTTAAAATTCGCCACAACGTGGAGGATGGCAGCGTGCAGCTGGCTGA
TCACTACCAGCAAAACACTCCAATCGGTGATGGTCCTGTTCTGCTGCCAGACAATCACTATCTGAGCACGCAAAGCG
TTCTGTCTAAAGATCCGAACGAGAAACGCGATCACATGGTTCTGCTGGAGTTCGTAACCGCAGCGGGCATCACGCAT
GGTATGGATGAACTGTACAAACGTCGTCGTCGTCGTCGTCGTCGTCGTCTGCCGGAAACCGGTGGTGGTCTCGAGCA
CCACCACCACCACCACTGA

10xHis-Dsb-Apoptin-R$_9$-LPETG

10xHis-Dsb-Apoptin-R$_9$-LPETG was constructed using Gibson assembly to add on consensus sequences with a disulfide bond isomerase C (DsbC)-containing plasmid (pCDB364, a gift from the Baker Lab, University of Washington), sortagging sequence, and polyarginine domain. pCDB364 plasmid and was digested (4 hr, 37 °C) with the BamHI restriction enzyme (New England BioLabs) and purified by extraction following electrophoretic separation (0.8% agarose). The digested pCDB364 and protein insert were Gibson Assembled (Gibson Assembly Master Mix NEB, 1 hr, 50 °C), and transformed into chemically competent Top10 *E. coli* (Thermo Fisher) by heat shock, and plated onto agar plates (10 g Tryptone, 5 g Yeast Extract, 10 g NaCl, 15 g agar, 1 L dH_2O) containing kanamycin (100 μg mL^{-1}). Colonies were subsequently grown overnight in LB (5 mL) containing kanamycin (100 μg mL^{-1}). Plasmids were purified using a QIAprep Spin Miniprep Kit (Qiagen), and sequenced using a SimpleSeq DNA Sequencing Kit (Thermo Fisher).

Plasmids corresponding to the construct of interest were purified and subsequently transformed into chemically competent BL21(DE3) *E. coli* (Promega) for expression.

10xHis-Dsb-Apoptin-R_9-LPETG forward primer:
5’ GCGAAAACCTGTATTTTCAGATGAACGCTCTGCAGG 3’
10xHis-Dsb-Apoptin-R_9-LPETG reverse primer:
5’ GAAACCGGTGGTGGTTAATGACGGCTGCTAACAAAGCCCGA 3’

The DNA sequence of the expressed 10xHis-Dsb-Apoptin-R_9-LPETG was:
ATGGGTCACCATCATCACCACCATCACCATCACCACGGTAGCGCGGCAATTCAACAAACGTTAGCCAAAATGGGCAT
CAAAAGCAGCGATATTCAGCCCGCGCCCGTAGCTGGCATGAAGACAGTTCTGACTAACAGCGGCGTGTTGTACATCA
CCGATGATGGTAAACATATCATTCAGGGGCCAATGTATGACGTTAGCGGCACGGCTCCGGTCAATGTCACCAATAAG
ATGCTGTTAAAGCAGTTGAATGCGCTTGAAAAAGAGATGATCGTTTATAAAGCGCCGCAGGAAAAACACGTCATCAC
CGTGTTTACTGATATTACCTGTGGTTACTGCCACAAACTGCATGAGCAAATGGCAGACTATAACGCGCTGGGGATCA
CCGTGCGTTATCTTGCTTTCCCGCGCCAGGGGCTGGACAGCGATGCAGAGAAAGAAATGAAAGCTATCTGGTGTGCG
AAAGATAAAAACAAAGCGTTTGATGATGTGATGGCAGGTAAAAGCGTCGCACCAGCCAGCTGCGACGTGGATATTGC
CGACCATTACGTACTTGGCGTCCAGCTTGGCGTTAGCGGTACTCCGGCAGTTGTGCTGAGCAATGGCACACTTGTTC
CGGGTTACCAGCCGCCGAAAGAGATGAAAGAATTCCTCGACGAACACCAAAAAATGACCAGCGGTAAAGGTAGCGAA
AACCTGTATTTTCAGGTGAACGCTCTGCAGGAAGACACCCCGCCGGGTCCGTCTACCGTTTTCCGTCCGCCGACCTC
TTCTCGTCCGCTGGAAACCCCGCACTGCCGTGAAATCCGTATCGGTATCGCTGGTATCACCATCACCCTGTCTCTGT
GCGGTTGCGCTAACGCTCGTGCTCCGACCCTGCGTTCTGCTACCGCTGACAACTCTGAATCTACCGGTTTCAAAAAC
GTTCCGGACCTGCGTACCGACCAGCCGAAACCGCCGTCTAAAAAACGTTCTTGCGACCCGTCTGAATACCGTGTTTC
TGAACTGAAAGAATCTCTGATCACCACCACCCCGTCTCGTCCGCGTACCGCTCGTCGTTGCATCCGTCTGCGTCGTC
GTCGTCGTCGCCGTCGCCGTCTGCCGGAAACCGGTGGTGGTTAA

MMP-8-6xHis

The active domain of MMP-8 was lifted from pCMV-Tag4A-MMP8 Wt (a gift from Yardena Samuels[180], Addgene plasmid # 29545) using PCR to add a 5’ NdeI and 3’ XhoI restriction site for cloning. Pet28a+ plasmid and PCR products were digested (4 hr, 37 °C) with NdeI and XhoI restriction enzymes (New England BioLabs) and purified by extraction following electrophoretic separation (0.8% agarose). The digested pET28a(+) and protein insert were ligated (T4 DNA ligase, 16 hr, 16 °C), and transformed into chemically competent Top10 *E. coli* (Thermo Fisher) by heat shock, and plated onto agar plates (10 g Tryptone, 5 g Yeast Extract, 10 g NaCl, 15 g agar, 1 L dH_2O) containing kanamycin (100 μg mL^{-1}). Colonies were subsequently grown overnight in LB (5 mL) containing kanamycin (100 μg mL^{-1}). Plasmids were purified using a QIAprep Spin Miniprep Kit (Qiagen), and sequenced using a SimpleSeq DNA Sequencing Kit (Thermo Fisher). Plasmids corresponding to the construct of interest were purified and subsequently transformed into chemically competent BL21(DE3) *E. coli* (Promega) for expression.

MMP-8-6xHis forward primer:
5’ CACAAACATATGTTAACCCCAGGAAAC 3’
MMP-8-6xHis reverse primer:
5’ CTTAACTGTAGATATGGCCTCGAGAATTAC 3’

The DNA sequence of the expressed MMP-8-6xHis was:
ATGTTAACCCCAGGAAACCCCAAGTGGGAACGCACTAACTTGACCTACAGGATTCGAAACTATACCCCACAGCTGTC
AGAGGCTGAGGTAGAAAGAGCTATCAAGGATGCCTTTGAACTCTGGAGTGTTGCATCACCTCTCATCTTCACCAGGA
TCTCACAGGGAGAGGCAGATATCAACATTGCTTTTTACCAAAGAGATCACGGTGACAATTCTCCATTTGATGGACCC
AATGGAATCCTTGCTCATGCCTTTCAGCCAGGCCAAGGTATTGGAGGAGATGCTCATTTTGATGCCGAAGAAACATG

GACCAACACCTCCGCAAATTACAACTTGTTTCTTGTTGCTGCTCATGAATTTGGCCATTCTTTGGGGCTCACTCACT
CCTCTGACCCTGGTGCCTTGATGTATCCCAACTATGCTTTCAGGGAAACCAGCAACTACTCACTCCCTCAAGATGAC
ATCGATGGCATTCAGGCCATCTATGGACTTTCAAGCAACCCTATCCAACCTACTGGACCAAGCACACCCAAACCCTG
TGACCCCAGTTTGACATTTGATGCTATCACCACACTCCGTGGAGAAATACTTTTCTTTAAAGACAGGTACTTCTGGA
GAAGGCATCCTCAGCTACAAAGAGTCGAAATGAATTTTATTTCTCTATTCTGGCCATCCCTTCCAACTGGTATACAG
GCTGCTTATGAAGATTTTGACAGAGACCTCATTTTCCTATTTAAAGGCAACCAATACTGGGCTCTGAGTGGCTATGA
TATTCTGCAAGGTTATCCCAAGGATATATCAAACTATGGCTTCCCCAGCAGCGTCCAAGCAATTGACGCAGCTGTTT
TCTACAGAAGTAAAACATACTTCTTTGTAAATGACCAATTCTGGAGATATGATAACCAAAGACAATTCATGGAGCCA
GGTTATCCCAAAAGCATATCAGGTGCCTTTCCAGGAATAGAGAGTAAAGTTGATGCAGTTTTCCAGCAAGAACATTT
CTTCCATGTCTTCAGTGGACCAAGATATTACGCATTTGATCTTATTGCTCAGAGAGTTACCAGAGTTGCAAGAGGCA
ATAAATGGCTTAACTGTAGATATGGCCTCGAGCACCACCACCACCACCACTGA

SrtA-7M

The sequence for heptamutant SrtA *(*P94R, E105K, E108Q, D160N, D165A, K190E, K196T) pet30b-7M SrtA was a gift from Hidde Ploegh (Addgene plasmid # 51141 ; http://n2t.net/addgene:51141 ; RRID:Addgene_51141).

Method B2: Protein expression and purification

Sortase 7M:

LB (500 mL) supplemented with kanamycin (100 μg mL^{-1}) was inoculated with an overnight cell culture (10 mL) and incubated (37 °C) with agitation (250 rev min^{-1}). After reaching an optical density at λ = 600 nm of 0.6, isopropyl β-D-1-thiogalactopyranoside was added (final concentration of 0.5 mM) and expression was continued overnight under reduced temperature (18 °C).

Cells were harvested *via* centrifugation (7,000 g, 10 min). The cell pellet was resuspended in lysis buffer (40 mL, 20 mM Tris, 50 mM NaCl, 10 mM imidazole, 1 mM phenylmethylsulfonyl fluoride) and sonicated on ice (6 cycles of 3 minutes at 30% amplitude 33% duty cycle and 3 min resting). Soluble and insoluble fractions were separated *via* centrifugation (5,000 g, 20 min).

Clarified lysate was applied to Ni-NTA resin (2.5 mL) and incubated under mild agitation (4 °C, 1 hr). The flow-through was discarded, and the resin was washed with wash buffer (20 mM Tris, 50 mM NaCl, 20 mM imidazole, 20 mL, 5x) and eluted in elution buffer (20 mM Tris, 50 mM NaCl, 25 mM imidazole 1 mL, 20x). The protein solution was dialyzed against Tris buffer (20 mM Tris, 50 mM NaCl, pH 7.5) using ThermoFisher SnakeSkin Dialysis Tubing (molecular weight cut-off, MWCO ~ 10 kDa) to remove any unconjugated peptide and concentrated using an Amicon centrifugal spin column (MWCO ~ 10 kDa).

Protein purity was assessed by LC-MS/MS, and a single peak corresponding to the expected molecular weight (17.8 kDa) was observed.

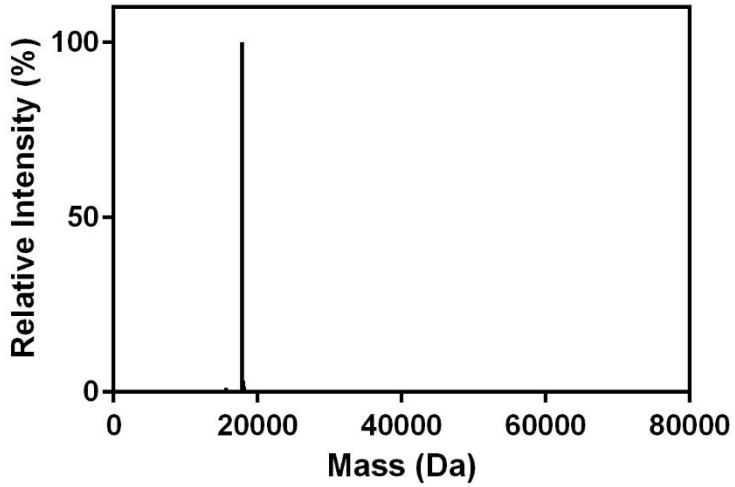

R_9 Containing Proteins (sfGFP and apoptin):

Autoinduction media (500 mL, 3g Na_2HPO4, 1.5g KH_2PO_4, 10g Tryptone, 2.5g Yeast Extract, 2.5g NaCl, 5 mL 60% v/v Glycerol, 2.5 mL 10% w/v Glucose, 12.5 mL 8% w/v Lactose)

supplemented with kanamycin or ampicillin (100 μg mL^{-1}) was inoculated from a glycerol stock and incubated (37 °C) with agitation (250 rev min^{-1}) overnight. After 16 hours, the temperature was reduced to 18 °C and expression was continued for an additional overnight step.

Cells were harvested *via* centrifugation (7,000 g, 10 min). The cell pellet was resuspended in lysis buffer (40 mL, 20 mM Tris, 50 mM NaCl, 10 mM imidazole, 1 mM phenylmethylsulfonyl fluoride) and sonicated on ice (6 cycles of 3 minutes at 30% amplitude 33% duty cycle and 3 min resting). Soluble and insoluble fractions were separated *via* centrifugation (5,000 g, 20 min).

Clarified lysate was applied to Ni-NTA resin (2.5 mL) and incubated under mild agitation (4 °C, 1 hr). The flow-through was discarded, and the resin was washed with wash buffer (20 mM Tris, 50 mM NaCl, 20 mM imidazole, 20 mL, 5x) and eluted in elution buffer (20 mM Tris, 50 mM NaCl, 25 mM imidazole 1 mL, 20x). The protein solution was dialyzed against Tris buffer (20 mM Tris, 50 mM NaCl, pH 7.5) using ThermoFisher SnakeSkin Dialysis Tubing (molecular weight cut-off, MWCO ~ 10 kDa) to remove any unconjugated peptide and concentrated using an Amicon centrifugal spin column (MWCO ~ 10 kDa).

sfGFP protein purity was assessed by LC-MS/MS, and a single peak corresponding to the expected molecular weight (28.8 kDa) was observed.

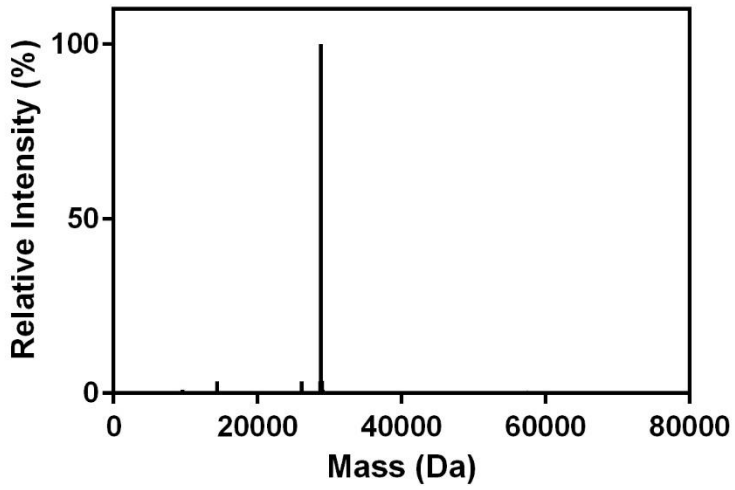

MMP-8:

LB (500 mL) supplemented with kanamycin (100 μg mL^{-1}) was inoculated with an overnight cell culture (10 mL) and incubated (37 °C) with agitation (250 rev min^{-1}). After reaching an optical density at λ = 600 nm of 0.6, isopropyl β-D-1-thiogalactopyranoside was added (final concentration of 0.5 mM) and expression was continued overnight under reduced temperature (18 °C).

Cells were harvested *via* centrifugation (7,000 g, 10 min). The cell pellet was resuspended in lysis buffer (40 mL, 20 mM Tris, 50 mM NaCl, 10 mM imidazole, 1 mM phenylmethylsulfonyl fluoride) and sonicated on ice (6 cycles of 3 minutes at 30% amplitude 33% duty cycle and 3 min resting). Soluble and insoluble fractions were separated *via* centrifugation (5,000 g, 20 min).

The insoluble fraction was dissolved in denaturation lysis buffer (40 mL, 8M urea, 200 mM sodium chloride, 50 mM tris, 5 mM calcium chloride, 1 μM zinc chloride, 10 mM imidazole, pH 7.5) overnight at room temperature with mild agitation. The denatured protein was applied to Ni-NTA resin (2.5 mL) and incubated under mild agitation (room temperature, 1 hr). The flow-through was discarded, and the resin was washed with denaturation wash buffer (8M urea, 200 mM sodium chloride, 50 mM tris, 5 mM calcium chloride, 1 μM zinc chloride, 20 mM imidazole, pH 7.5, 20 mL, 5x) and eluted in denaturation elution buffer (1 mL, 8M urea, 200 mM sodium chloride, 50 mM tris, 5 mM calcium chloride, 1 μM zinc chloride, 250 mM imidazole, pH 7.5, 20x). The protein solution was refolded via stepwise dialysis against MMP buffer (4L, 200 mM sodium chloride, 50 mM tris, 5 mM calcium chloride, 1 μM zinc chloride, pH 7.5) containing decreasing concentrations of Urea (6M, 4M, 2M, 1M, 0M Urea, 4 hours for each step at 4°C) using ThermoFisher SnakeSkin Dialysis Tubing (molecular weight cut-off, MWCO ~ 10 kDa). The refolded protein was separated from aggregates via centrifugation (5,000g, 20 minutes), and concentrated using an Amicon centrifugal spin column (MWCO ~ 10 kDa).

Protein purity was assessed by SDS-PAGE analysis (12% Bis-Tris gel), and a single band corresponding to the expected molecular weight (43.2 kDa) was observed by Coumassie staining.

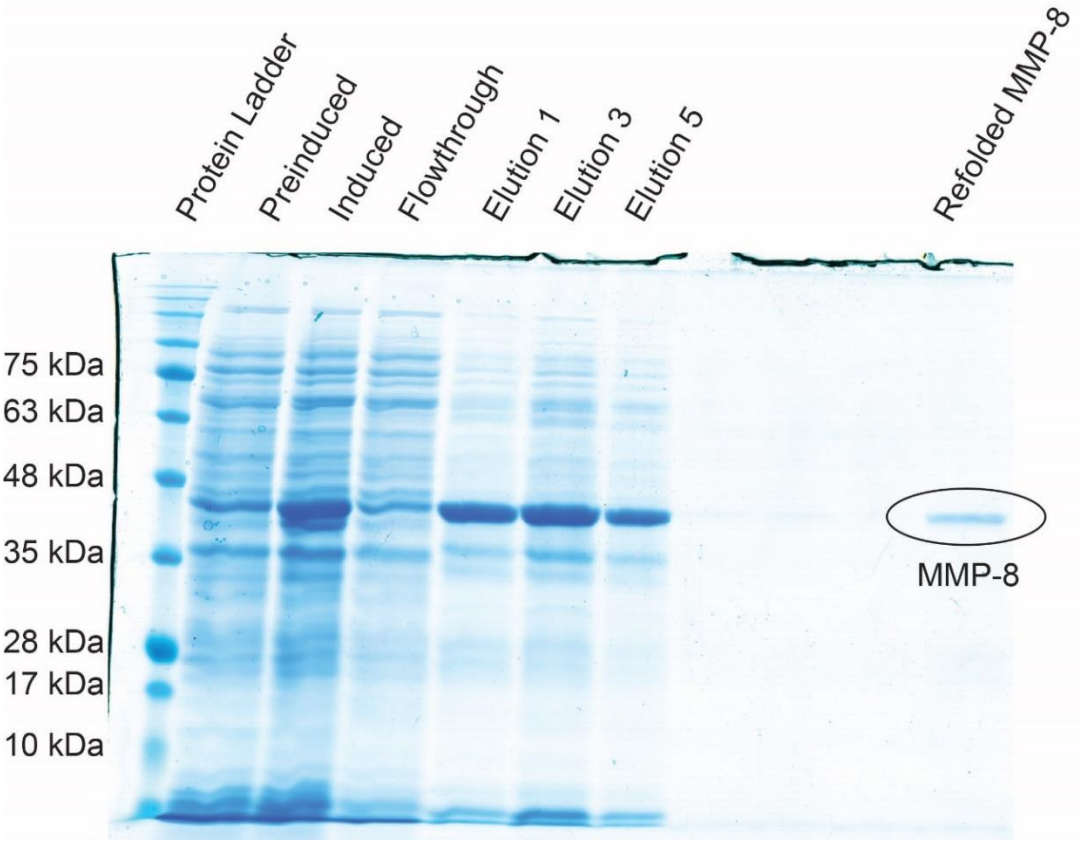
Protein Ladder
Preinduced
Induced
Flowthrough
Elution 1
Elution 3
Elution 5
Refolded MMP-8
75 kDa
63 kDa
48 kDa
35 kDa
28 kDa
17 kDa
10 kDa
MMP-8

Method B3: Synthesis of 2,5-dioxopyrrolidin-1-yl 4-(4-(1-((4-azidobutanoyl)oxy)ethyl)-2-methoxy-5-nitrophenoxy)butanoate (N_3-*o*NB-OSu)

The synthesis of 2,5-dioxopyrrolidin-1-yl 4-(4-(1-((4-azidobutanoyl)oxy)ethyl)-2-methoxy-5-nitrophenoxy)butanoate (denoted N_3-*o*NB-OSu) was performed as described previously following a known synthetic route[123].

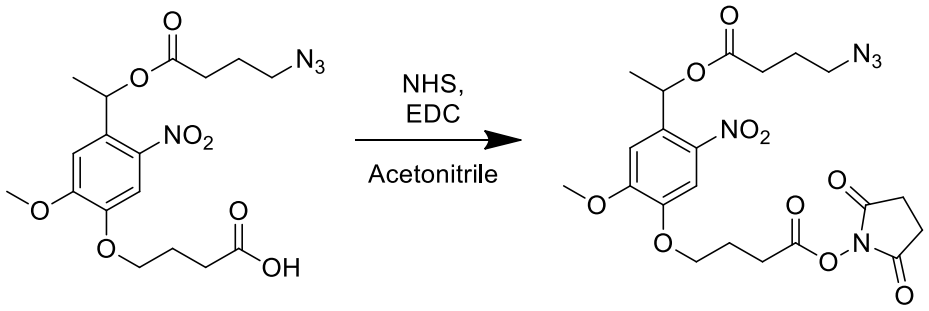

^{1}H NMR (500 MHz, $CDCl_3$) δ 7.62 (s, 1H), 7.03 (s, 1H), 6.52 (q, J = 6.4 Hz, 1H), 4.20 (t, J = 6.0 Hz, 2H), 4.00 (s, 3H), 3.42 – 3.31 (m, 2H), 2.91 (t, J = 7.3 Hz, 2H), 2.88 (s, 4H), 2.55 – 2.42 (m, 2H), 2.32 (p, J = 6.7 Hz, 2H), 1.93 (p, J = 6.9 Hz, 2H), 1.65 (d, J = 6.4 Hz, 3H). The spectral data matched those previously reported[123].

Method B4: Fmoc solid-phase peptide synthesis

Automated microwave-assisted Fmoc solid-phase peptide synthesis was performed on a CEM Liberty 1 (0.5 mmol scale). Fmoc deprotections were performed in 20% piperidine (v/v) in DMF with 0.1 M 1-hydroxybenzotriazole (HOBt) at 90 ^{o}C for 90 seconds. Amino acids were coupled to resin-bound peptides upon treatment (75 ^{o}C for 5 minutes) with Fmoc-protected amino acid (2 mmol, 4x), 2-(1H-benzotriazol-1-yl)-1,1,3,3-tetramethyluronium hexafluorophosphate (HBTU, 2 mmol, 4x), and *N*,*N*-diisopropylethylamine (DIEA, 2 mmol, 4x) in a mixture of DMF (9 mL) and *N*-Methyl-2-pyrrolidone (NMP, 2 mL).

Method B5: Synthesis of sortaggable Photo "YES" cleavable polyanionic domain (G_4-P-E_9)

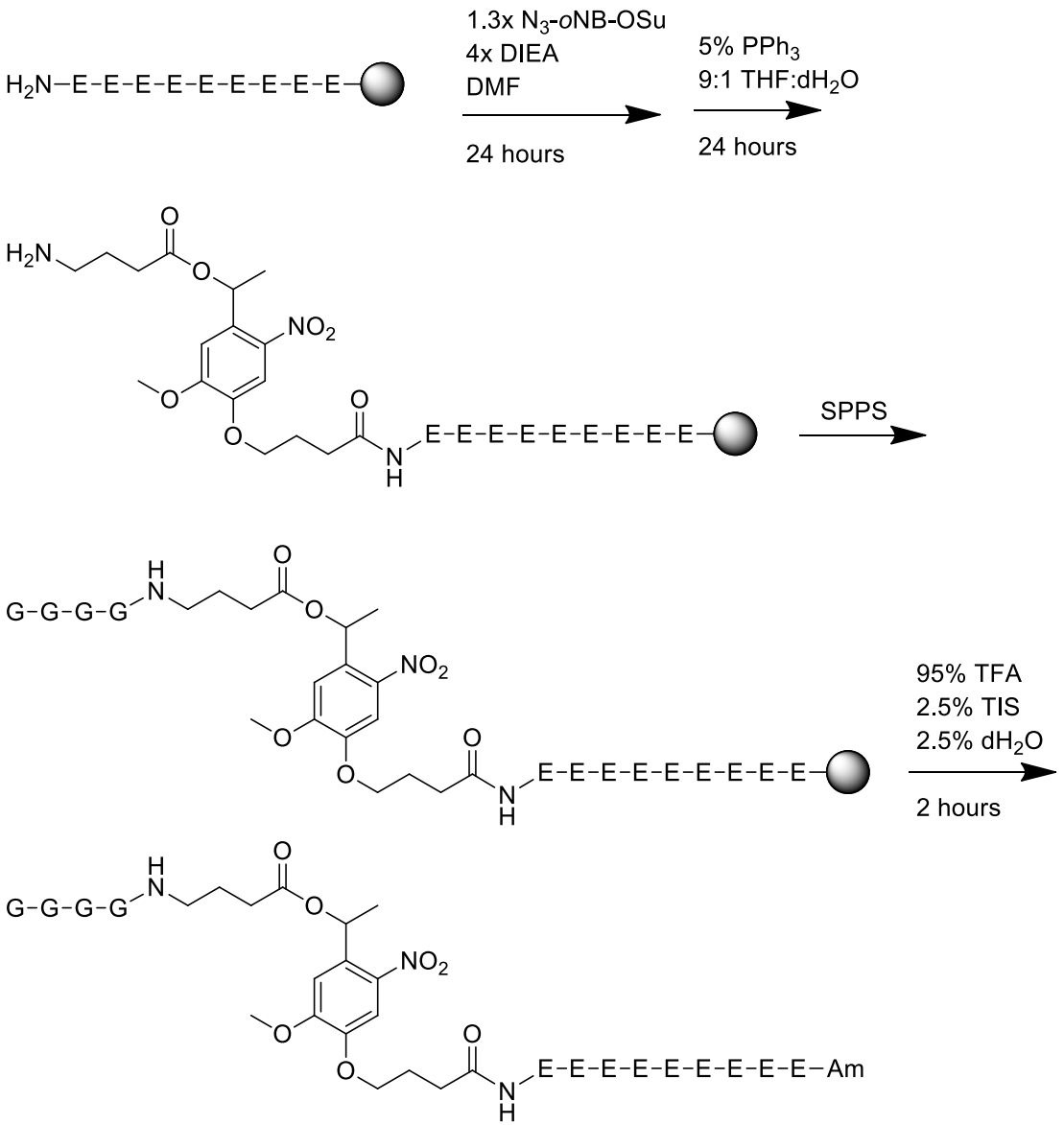

The resin-bound peptide H-EEEEEEEEE-Am was synthesized by microwave-assisted Fmoc SPPS (Method B4) on Rink amide resin (0.25 mmol scale). The resin was subsequently treated with N_3-*o*NB-OSu (Method B3, 0.33 mmol, 165 mg) and DIEA (1.0 mmol, 130 mg) in minimal DMF to introduce *o*NB functionality to the N-terminus. The N-terminal azide was reduced to an amine by a Staudinger reduction; resin was washed with THF/H_2O (90:10, 3 x 20 mL), followed by reaction with 5 wt% triphenylphosphine in THF/H_2O (90:10, 30 mL) for 18 hours. The peptide sequence H-GGGG was appended to the N-terminus by standard microwave-assisted Fmoc SPPS. The peptide was simultaneously deprotected and cleaved from resin upon treatment with TFA/TIS/dH_2O (95:2.5:2.5, 20 mL) for 2 hours, and the crude peptide was precipitated in and washed with ice-cold diethyl ether (2x). The crude peptide was purified using RP-HPLC operating with a 40 minute linear gradient of acetonitrile (5–50%) in 25 mM phosphate buffer (pH = 7.5).

The peptide was desalted and lyophilized to yield the final product (GGGG-*o*NB-EEEEEEEEE-Am, denoted G_4-P-E_9) as a yellow solid (145 mg, 0.0818 mmol, 32.7% overall yield). Peptide purity was confirmed using MALDI-TOF: calculated for $C_{70}H_{101}N_{16}O_{38}^-$ $[M]^-$, 1773.6; observed 1773.3.

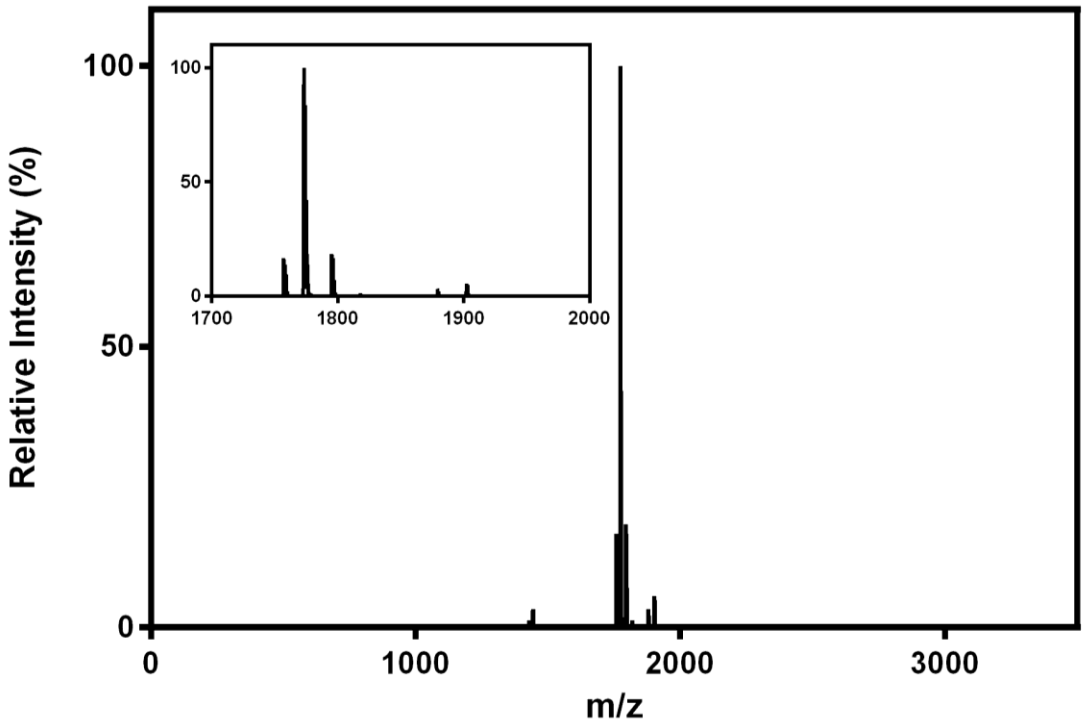

Method B6: Synthesis of sortaggable MMP "YES" cleavable polyanionic domain (G_4-M-E_9)

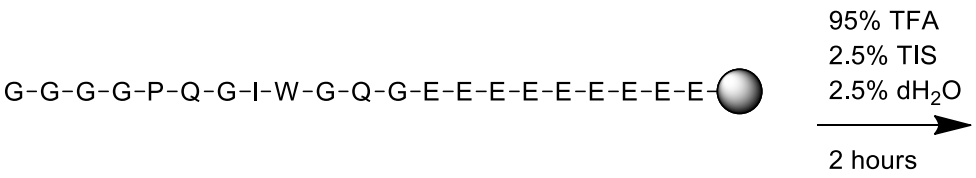

G-G-G-G-P-Q-G-I-W-G-Q-G-E-E-E-E-E-E-E-E-E-Am

The resin-bound peptide H-GGGGPQGIWGQGEEEEEEEEE-Am was synthesized by microwave-assisted Fmoc SPPS (Method B4) on Rink amide resin (0.25 mmol scale). The peptide was simultaneously deprotected and cleaved from resin upon treatment with TFA/TIS/dH_2O (95:2.5:2.5, 20 mL) for 2 hours, and the crude peptide was precipitated in and washed with ice-cold diethyl ether (2x). The crude peptide was purified using RP-HPLC operating with a 40 minute linear gradient of acetonitrile (5–50%) in 25 mM phosphate buffer (pH = 7.5). The peptide was desalted and lyophilized to yielded the final product (GGGGPQGIWGQGEEEEEEEEE-Am, denoted G_4-M-E_9) as a yellow solid (120 mg, 0.0538 mmol, 21.5% overall yield). Peptide purity was confirmed using MALDI-TOF: calculated for $C_{91}H_{131}N_{25}O_{41}^-$ $[M]^-$, 2229.9; observed 2230.4.

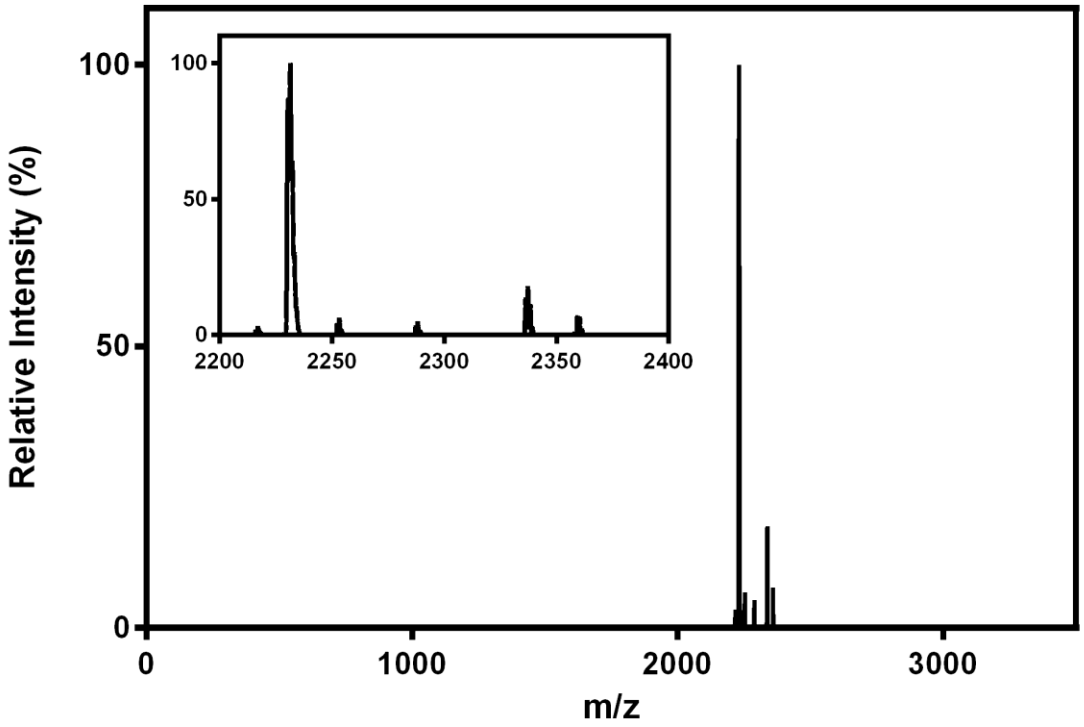

Method B7: Synthesis of sortaggable MMP "OR" Photo cleavable polyanionic domain (G_4-MVP-E_9)

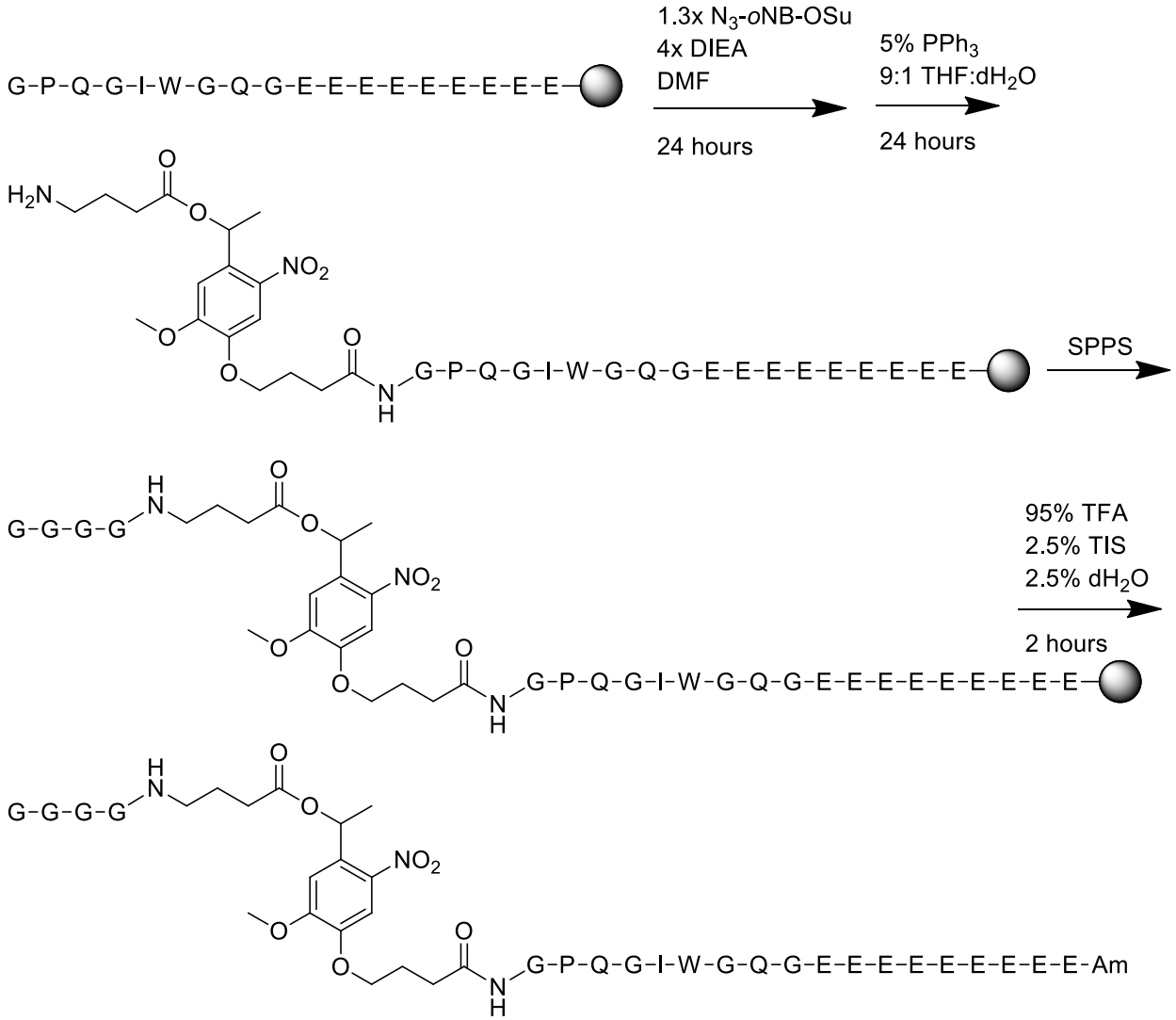

The resin-bound peptide H-GPQGIWGQGEEEEEEEEE-Am was synthesized by microwave-assisted Fmoc SPPS (Method B4) on Rink amide resin (0.5 mmol scale). The resin was subsequently treated with N_3-*o*NB-OSu (Method B3, 0.65 mmol, 330 mg) and DIEA (2.0 mmol, 260 mg) in minimal DMF to introduce *o*NB functionality to the N-terminus. The N-terminal azide was reduced to an amine by a Staudinger reduction; resin was washed with THF/H_2O (90:10, 3 x 20 mL), followed by reaction with 5 wt% triphenylphosphine in THF/H_2O (90:10, 30 mL) for 18 hours. The peptide sequence H-GGGG was appended to the N-terminus by standard microwave-assisted Fmoc SPPS. The peptide was simultaneously deprotected and cleaved from resin upon treatment with TFA/TIS/dH_2O (95:2.5:2.5, 20 mL) for 2 hours, and the crude peptide was precipitated in and washed with ice-cold diethyl ether (2x). The crude peptide was purified using RP-HPLC operating with a 40 minute linear gradient of acetonitrile (5–50%) in 25 mM phosphate

buffer (pH = 7.5). The peptide was desalted and lyophilized to yield the final product (GGGG-*o*NB-GPQGIWGQGEEEEEEEEE-Am, denoted G_4-MVP-E_9) as a yellow solid (240 mg, 0.0904 mmol, 18.1% overall yield). Peptide purity was confirmed using MALDI-TOF: calculated for $C_{110}H_{157}N_{28}O_{49}^-$ $[M]^-$, 2654.1; observed 2656.7 and 2527.0 [M - Glu].

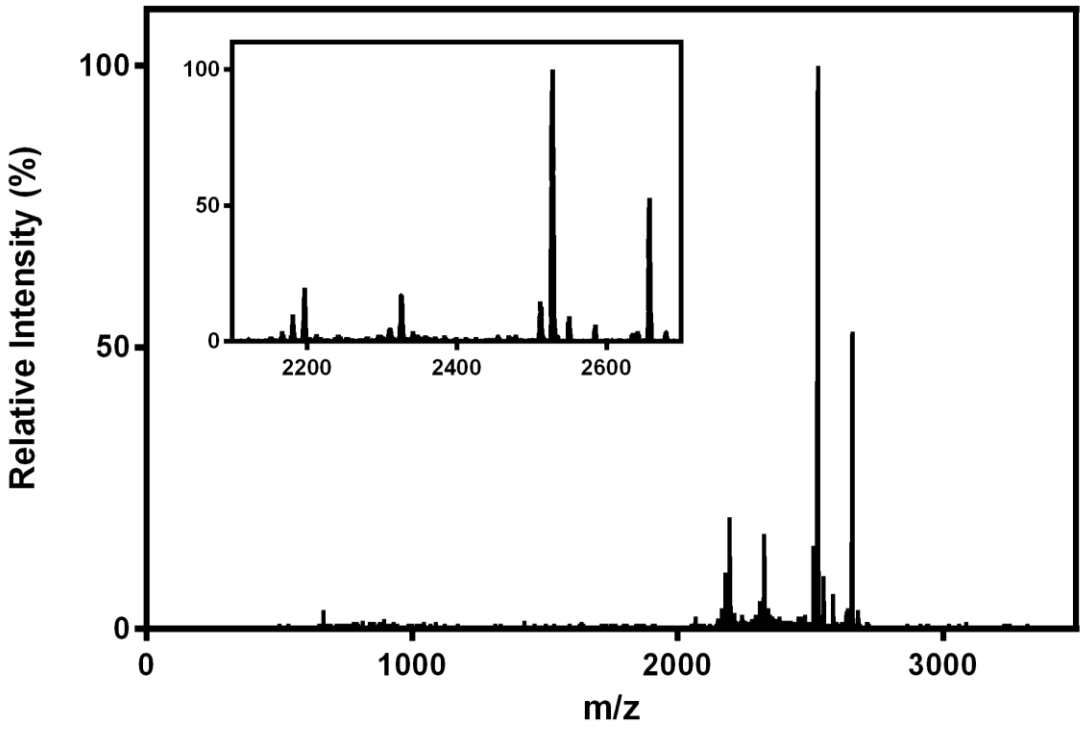

Method B8: Sortase-mediated conjugation of sfGFP-R_9-LPETG to G_4-X-E_9 & GGG

sfGFP-R_9 (Method B2, 8 mg, 275 μM), G_4-X-E_9 (Methods B5-B7, 10x, 2.8 mM) or triglycine (2.9 mM), and SrtA-7M (Method B2, 0.1x, 27.5 μM) were combined in buffer (20 mM tris, 50 mM NaCl, pH 7.5, 10 vol% DMSO) and incubated under mild agitation (1.5 hr, 37 °C).

The reaction mixture was applied to Ni-NTA resin (2 mL) to bind under mild agitation (25 °C, 2 hr). Sortagged sfGFP was eluted and combined with Ni-NTA washes with buffer (20 mM tris, 50 mM NaCl, pH 7.5). The protein solution was concentrated, separated from unconjugated peptide, and exchanged into MMP buffer (200 mM sodium chloride, 20 mM tris, 5 mM calcium chloride, 1 μM zinc chloride, pH 7.5) using and Amicon centrifugal spin column (MWCO ~ 10 kDa). Products are denoted sfGFP-ACPP(X), where X refers to the linker logical function. When triglycine was used as the probe, the product is denoted sfGFP-R_9.

Protein purity was assessed by SDS-PAGE analysis (12% Bis-Tris gel) and a single band corresponding to the expected molecular weight (29 kDa sfGFP-R_9, 32 kDa sfGFP-ACPP) was observed by Coumassie staining.

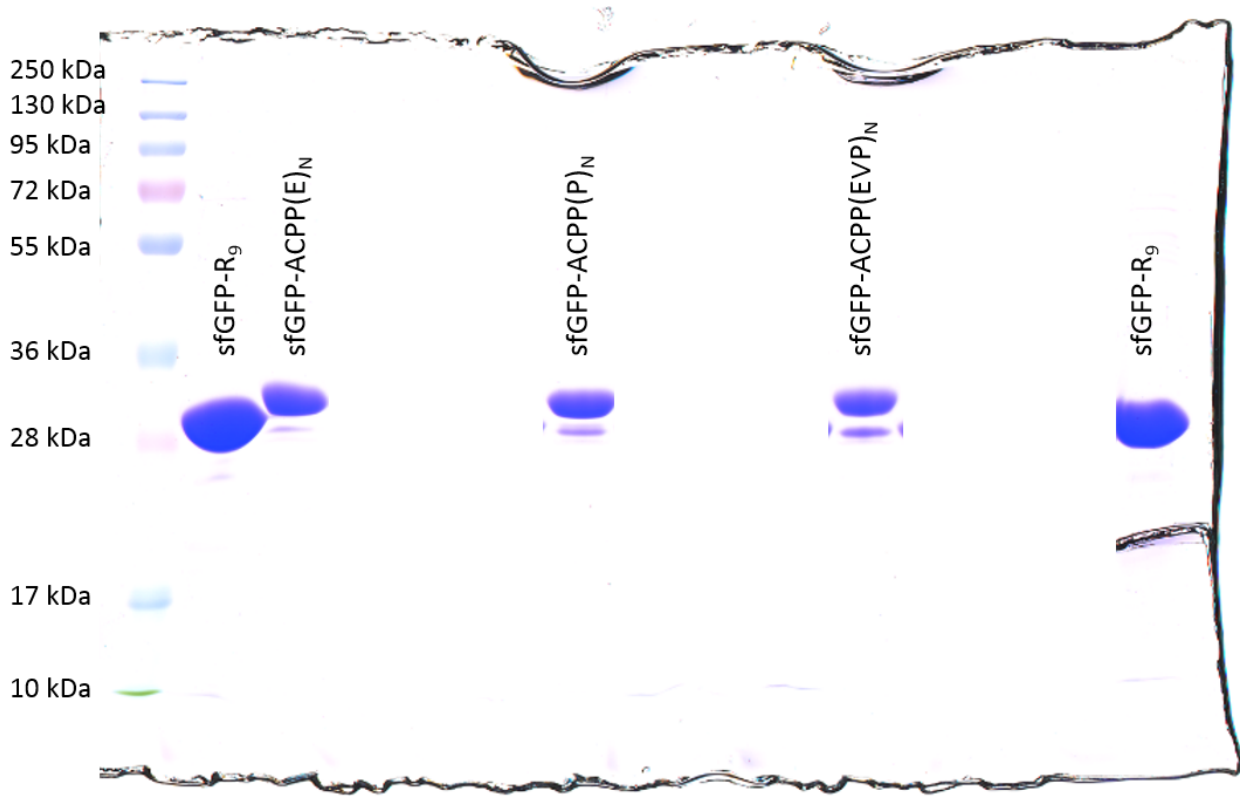

Method B9: ACPP treatments with external stimuli

To assess ACPP activation in response to combinations of external stimuli, each sfGFP-ACPP construct in MMP buffer (20 μM, 100 μL) was exposed to every input combination: null, enzyme, light, or both enzyme and light. Samples receiving enzyme were treated with MMP-8 (Method B2, 10 μL, 0.2 mg mL^{-1}) and all samples were incubated in MMP buffer (1.5 hr, 37 °C). Samples receiving the light were subsequently exposed to UV light (λ = 365 nm, 10 mW cm^{-2} incident light, 10 minute exposure).

The product of each reaction was assessed using SDS-PAGE analysis (12% Bis-Tris gel). The mass shift associated with the loss of the anionic shielding domain allowed for the comparison of the relative amounts of activated and inactivated proteins. Activated proteins were generated only when the inputs satisfied the conditions of their Boolean function.

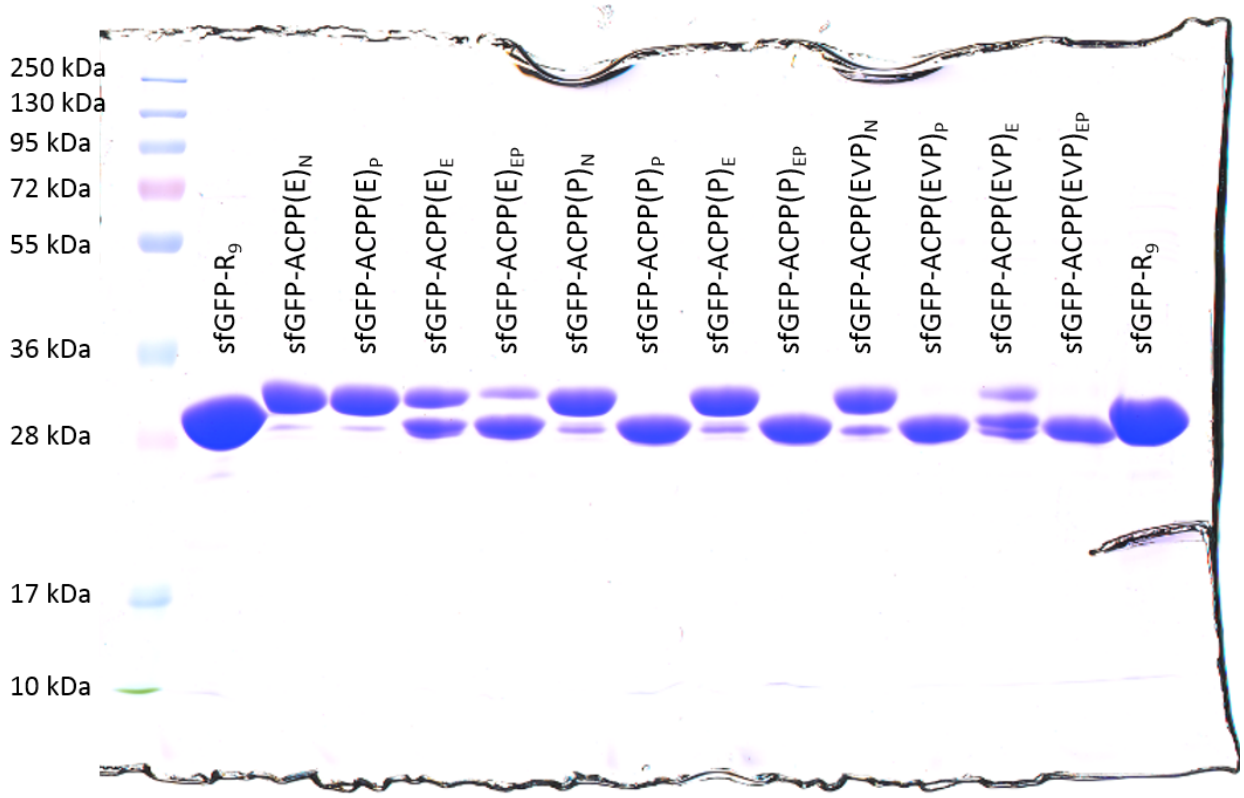

Method B10: Cell treatments with sfGFP-R_9-ACPP constructs and microscopy

Cellular uptake of sfGFP-ACPP constructs:
HeLa cells with CellTracker™ Red were seeded on 8-well chambered glass slides (7×10^3 cells per well) and cultured in DMEM supplemented with fetal bovine serum (FBS, 10%) and penicillin-streptomycin (PS, 1%) for 24 hours. Each pre-treated sfGFP-ACPP construct (Method B9) was diluted with media (70% DMEM, 5 μM) and incubated with cells (1 hr, in triplicate). Cells were washed with phosphate buffered saline (PBS), fixed (1% formaldehyde in PBS, 15 min), and stained with DAPI nuclear stain prior to imaging.

Cell microscopy:
Cells were imaged using fluorescent confocal microscopy. Three channels—one for each fluorophore—were simultaneously monitored: CellTracker™ Red (excitation 577 nm, emission 583-651 nm), sfGFP (excitation 485 nm, emission 501-548 nm), and DAPI (excitation 405 nm, emission 434-469 nm) were false colored as red, green, and blue, respectively.

Image processing and quantification of sfGFP uptake:
A Matlab script was used to process the confocal data. First, the CellTracker™ Red channel was used to identify the boundaries of cells. The average fluorescent intensity of the GFP channel was then calculated for each image. Each linker/treatment combination was performed in biological triplicate, with three images per sample. The background autofluorescence was determined from control samples and subtracted from each experimental sample. Uncertainty was reported as the standard error of mean.

Method B11: Characterization of sfGFP-R_9-LPETG photobleaching

sfGFP-R_9-LPETG photobleaching study:

To assess the level of sfGFP fluorophore photobleaching that occurs under the light treatment conditions used for protein photoactivation (Method B9), sfGFP-R_9-LPETG in MMP buffer (25 μM) was exposed to UV light (λ = 365 nm, 10 mW cm^{-2}, 0 – 60 min) in experimental triplicate. Sample fluorescence (excitation wavelength 480 nm, emission wavelength 510 nm) was measured for samples exposed to light for differing amounts of time. One-way analysis of variance (ANOVA) failed to reject the null hypothesis that fluorescence does not change upon light exposure (p-value = 0.97). This suggests that sfGFP does not undergo significant photobleaching under light treatment conditions used to activate the protein-ACPP construct.

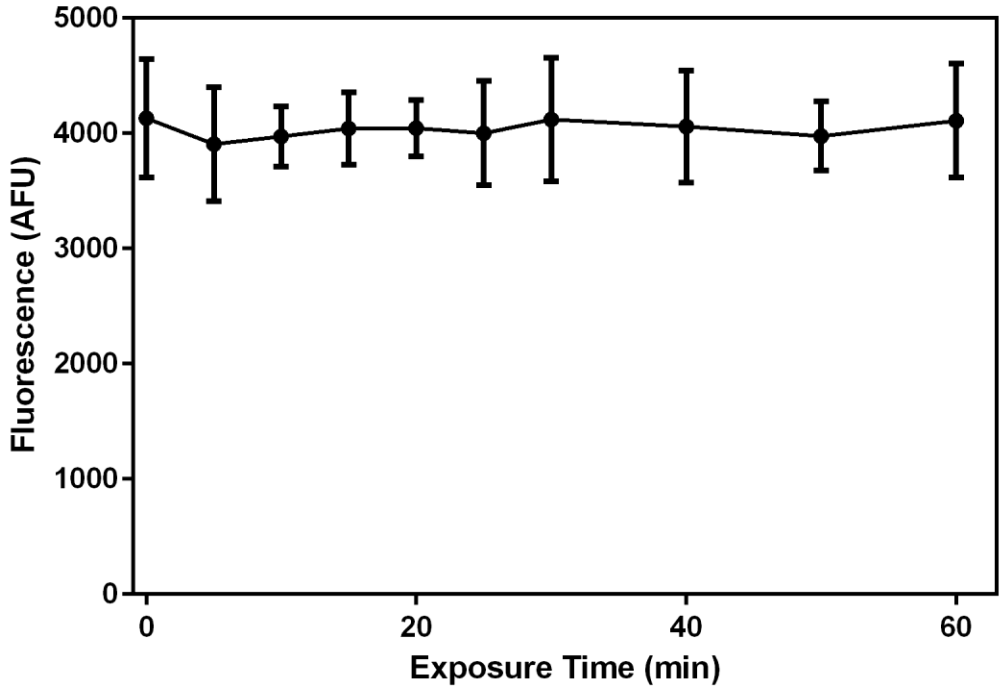

Method B12: The influence of sfGFP-R_9 and X-E_9 species on cell viability

The effect of sfGFP-R_9 and X-E_9 species on cell viability:
HeLa cells were seeded on 96-well tissue culture polystyrene (5×10^3 cells per well) and cultured in DMEM supplemented with FBS (10%) and PS (1%) for 24 hours. Cells were cultured either in sfGFP-R_9 (Method B9, 2.5 μM) or G_4-P-E_9 (Method B5, 2.5 μM) in media (24 hr, in triplicate) prior to a Crystal Violet Assay for cell viability.

Cells were washed with PBS and fixed in ice-cold methanol (10 min) prior to staining with an aqueous solution of crystal violet (0.5%, 10 min). The samples were washed with water (2x) and solubilized in acetic acid (10% in water, 20 minutes). Absorbance readings were collected at 595 nm.

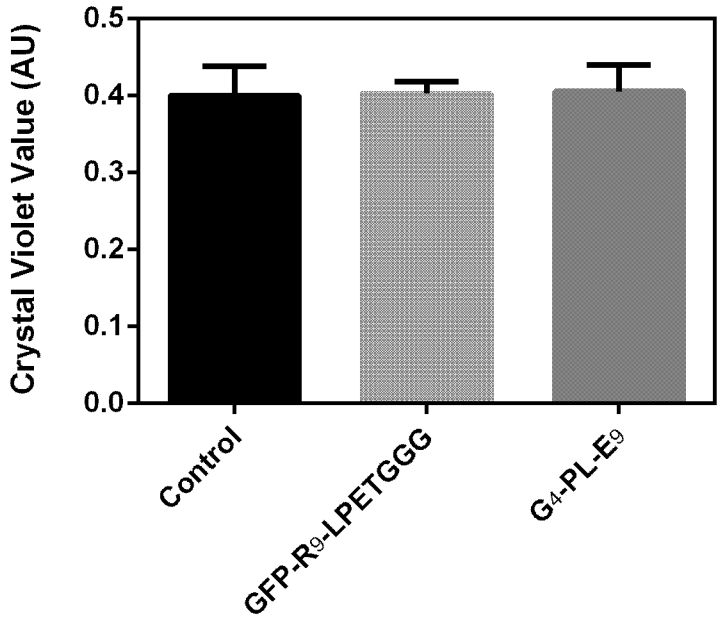

VITA

EDUCATION

2013-2019 University of Washington, *Seattle, WA*
Ph.D. in Chemical Engineering (expected 2019)
M.S. in Chemical Engineering
Cumulative GPA: 3.89/4.00

2009-2013 University of Minnesota, *Minneapolis, MN*
B.S. in Chemical Engineering
B.S. in Chemistry
Cumulative GPA: 3.66/4.00

PROFESSIONAL EXPERIENCE

2013-2019 University of Washington, *Seattle, WA*
Graduate Research Assistant, *Advisor: Cole DeForest*

- Developed a modular framework for logical biomaterials that can perform Boolean computation and be programmed to precisely respond to combinations of environmental cues. Used system for controlled delivery of cells, proteins, & drugs.
- Played an integral role in the set-up of a new lab, including purchasing, protocol development & troubleshooting, equipment maintenance & repair, and training.
- Fields of expertise: biomaterials, polymers, drug delivery, and biochemistry.
- Laboratory skills: advanced peptide synthesis & purification, organic synthesis, mammalian cell culture, photochemistry, microscopy, rheometry, protein modification, flow cytometry, spectroscopy (NMR, IR, MALDI, LC-MS).
- Delivered 30^{+} lectures and provided 400^{+} hours of in-person instruction.

2010-2013 University of Minnesota, *Minneapolis, MN*
Undergraduate Research Assistant, *Advisor: Kevin Dorfman*

- Studied and optimized microfluidic devices for DNA electrophoresis. Used sparse nanopost arrays and colloidal crystals to achieve size-based separation.

PUBLICATIONS

1) **Badeau, B. A.**, Shadish, J. A., DeForest, C.A., Boolean environmentally triggered activation of cell-penetrating peptides for targeted protein delivery, *In submission*
2) Gawade, P. G., **Badeau, B. A.** †, Shadish, J. A.†, DeForest, C. A. Logic-based delivery of site-specifically modified proteins from environmentally responsive hydrogel biomaterials, *In submission*
3) **Badeau, B. A.**, DeForest, C. A. Programming stimuli-responsive behavior into hydrogels, *Annual Reviews Biomedical Engineering* (2019)
4) Ruskowitz, E. R., Comerford M. P., **Badeau, B. A.**, DeForest, C. A. Logical stimuli-triggered delivery of small molecules from hydrogel biomaterials, *Biomaterials Science* (2019)
5) **Badeau, B. A.**, Comerford M. P., Arakawa C. K., Shadish J. A, DeForest C. A. Engineered biomaterial logic gates for environmentally triggered drug delivery, *Nature Chemistry* (2018)
6) Arakawa C. K, **Badeau, B. A.**, Zheng, Y., DeForest C. A. Multicellular vascularized engineered tissues through user-programmable biomaterial photodegradation, *Advanced Materials* (2017).

PATENT

1) **Badeau B. A.**, DeForest C. A. Molecular Logic Gates for Controlled Material Degradation, WO/2018/057941 (2018).

PRESENTATIONS

1) **Badeau B. A.**, National Institute of Materials Science & University of Washington Joint Research Symposium (August 2018).
2) **Badeau B. A.**, University of Washington Department of Chemical Engineering Faculty Lecture Award (November 2017).
3) **Badeau B. A.**, Chemical Engineering Graduate Symposium (September 2017).
4) **Badeau B. A.**, University of Washington Biomaterials Seminar (October 2016).
5) **Badeau B. A.**, Chemical Engineering Graduate Symposium, Poster (September 2016).
6) **Badeau B. A.**, University of Washington Biomaterials Seminar (January 2015).

TEACHING EXPERIENCE

Delivered over 30 lectures and provided more than 350 hours of in-person instruction to 300 students.

Spring 2018	Polymer Chemistry Laboratory, *Teaching Assistant*
Winter 2018	Transport Processes II, *Teaching Assistant*
Spring 2017	Polymer Chemistry Laboratory, *Teaching Assistant*
Fall 2015	Transport Processes III, *Teaching Assistant*
Winter 2015	Transport Processes II, *Teaching Assistant*
Spring 2014	Chemical Engineering Laboratory I, *Teaching Assistant*

LEADERSHIP EXPERIENCE

2016-2019	University of Washington Wrestling Club, *Assistant & Interim Coach, Vice President*
2013-2015	Association of Chemical Engineering Graduate Students, *Officer, Social Chair*
2009-2012	Engineers Without Borders, *Haiti Biofuels and Plastic Recycling Projects*

AWARDS AND HONORS

2019	Bonderman Graduate Travel Fellowship
2018	Academic All-American, *National Colligate Wrestling Association*
2018	National Championships Qualifier, *National Colligate Wrestling Association*
2017	Faculty Lecture Award, *University of Washington Department of Chemical Engineering* ***(Annually awarded to a single recipient based on overall scholarship and productivity)***
2012-2013	Merit Scholar, *University of Minnesota Department of Chemical Engineering*
2011-2013	Merit Scholar, *University of Minnesota College of Science and Engineering*
2009-2013	Gold Scholar, *University of Minnesota*
2009	National Merit Scholar
2008	Eagle Scout, *Boy Scouts of America*